Wireless Communications and Mobile Computing

Vehicle-to-Everything (V2X) Communication Approach Towards Advanced Intelligent Transportation

Lead Guest Editor: Zahid Khan
Guest Editors: Farhan Ullah and Sohail Jabbar

Vehicle-to-Everything (V2X) Communication Approach Towards Advanced Intelligent Transportation

Wireless Communications and Mobile Computing

Vehicle-to-Everything (V2X) Communication Approach Towards Advanced Intelligent Transportation

Lead Guest Editor: Zahid Khan
Guest Editors: Farhan Ullah and Sohail Jabbar

Chief Editor

Associate Editors

Academic Editors

Contents

Hindawi
Wireless Communications and Mobile Computing
Volume 2023, Article ID 3776815, 18 pages
https://doi.org/10.1155/2023/3776815

Research Article

A Clustering-Based Routing Protocol Using Path Pattern Discovery Method to Minimize Delay in VANET

Xiaoyun Xie[1,2] **Yahya Dorostkar Navaei**[3] **and Sajad Einy**[4]

[1]*School of Electronic Information Engineering, Gannan University of Science and Technology, Ganzhou, 341000 Jiangxi, China*
[2]*Ganzhou Key Laboratory of Cloud Computing and Big Data, Ganzhou, 341000 Jiangxi, China*
[3]*Computer and Information Technology Engineering, Qazvin Branch, Islamic Azad University, Qazvin, Iran*
[4]*Istanbul Aydin University, Department of Application and Research Center for Advanced Studies, Istanbul, Turkey*

Correspondence should be addressed to Yahya Dorostkar Navaei; y.dorostkar@qiau.ac.ir

Received 13 February 2022; Revised 22 January 2023; Accepted 28 April 2023; Published 14 June 2023

Academic Editor: Farhan Ullah

In vehicular ad hoc networks (VANETs), vehicle-to-vehicle (V2V) communications can link vehicles to each other, and vehicle-to-infrastructure (V2I) messaging and communications can link roadside infrastructure such as routers. The vehicles in these networks act as relays that transmit critical messages in the network. Due to the high-speed movement of vehicles on the road, real-time messaging and minimizing the delay in sending messages is one of the most important objectives of VANET developers. On the other hand, the high mobility of vehicles causes communication interruptions and decreases the data delivery rate in VANET. To overcome this issue, predicting the path of vehicles can play an important role in sending data from the source to the destination. When an accident occurs on the road, the messages that are sensed by the imbedded sensors in the vehicles need to be sent, and if they are sent by the vehicles that change their route, these messages will not be sent to the destination and the performance of the network will be disturbed. Previous methods in the literature for data transmission in intervehicular networks have focused more on reliability and trust, and little attention has been paid to the prediction of vehicle movement paths in these types of networks. Therefore, for fast and reliable data transmission in VANET, accurate prediction of vehicle movement and creation of movement patterns can be effective in message transmission delay and data delivery rate. In this paper, we present an approach using a combination of cluster-based routing protocols and pattern discovery methods to minimize latency in VANETs. The outline of the proposed method has four modules: primary data collection and analysis, primary data preparation and analysis, pattern extraction and vehicle route discovery, and vehicle clustering and data/information transmission routing. The simulation results show that the proposed method with a delivery rate of 88.56% has significantly improved compared to the previous methods in terms of package delivery rate. Also, the proposed method with a total delay of 24.566 ms has a shorter delay than the previous methods in terms of message sending delay in the network.

1. Introduction

With the increasing usage of wireless communications, today we are witnessing the emergence of new types of wireless networks. The vehicular ad hoc network (VANET) is one of these new networks that enables wireless connections between vehicle nodes and roadside infrastructure. VANETs are a decentralized, self-organized communication network in which nodes consist of high-speed vehicles that are automatically routed between adjacent devices, without the use of any infrastructure (such as routers and servers). Thus, vehicles can effectively transmit a message from one source node to other nodes, through their adjacent vehicle to vehicle (V2V) or even with communicate with some existing infrastructure (V2I), such as roadside units, in the same geographic area to create a better environment for safer driving [1, 2].

The use of VANETs has expanded rapidly in recent years due to its diverse and useful applications, but there are several challenges in using this technology. For example,

the high speed of vehicles in this network causes frequent changes in the network topology, and as a result, the communication link between vehicles will be unstable or may even be cut off. To establish route between source and destination in a VANET, we need to use routing protocols. Transferring packets from the node that is the source of the message to another node in the neighborhood of the source vehicle involves transferring packets across the network. In fact, in VANETs, unlike fixed networks, there is no clear connection between nodes, and this has made it difficult to route and transmit packets. Every vehicle in the network, when it receives data packets, must also send these packets to its neighboring vehicles, which is called VANET message retrieval. Routing in VANETs is done by sending data packets between the sender and receiver in the network until all the vehicles in the network receive the desired packets. Therefore, the use of machine learning in improving routing in VANET can provide an effective solution. The application of machine learning methods has been proven in various fields of science such as wireless networks [3, 4], social networks [5], network security [6–8], and pattern recognition [9–14]. One of the most important challenges in VANET is the delay in sending and receiving messages between vehicles.

The main purpose of VANETs is to effectively transmit a message from one source node to other nodes located in the same geographical area and to create a suitable environment for safer, more efficient, and easier driving [15, 16]. This platform has warning programs to warn other vehicles, weather and traffic conditions, the exchange of multimedia files between vehicles (for example, songs and movies) and road units (TV, radio, or news), and so on [3]. For example, information about traffic areas can be sent from one vehicle to another, or drivers can be notified of potential accidents or traffic jams. In addition, it is possible to introduce alternative routes in the VANET in order to avoid possible or delayed accidents in high-traffic areas. Similarly, a vehicle through its built-in sensors can detect potential accidents such as a frozen road and notify other vehicles [17].

The motivation of this paper is to find the vehicles that aligned with the vehicle carrying the message and extracting the movement pattern of these vehicles according to the movements of the previous similar vehicles. In the proposed method, vehicle information is received based on moment-to-moment location changes and their instantaneous and average speed as a time series. Then, according to the frequent patterns in the movement of vehicles in the time series, a fixed pattern for the movement of vehicles is found according to their speed and direction. Then, based on the change of location of the vehicles, it is determined whether these cars are aligned with the car carrying the message or not. On the other hand, according to the current location of the vehicles, the network is clustered and neighboring cars are identified. Then, according to the movement patterns of the vehicles, the next path is predicted for the neighboring cars. A vehicle that meets the following three conditions is determined as the cluster head vehicle that is able to receive the message:

(1) Be in the middle of the cluster based on your distance with other cars

(2) Be in line with the vehicle carrying the message

(3) Match the predicted movement pattern

After determining the cluster head vehicles, the message can be transferred to the destination through the cluster head vehicles. The proposed method uses the extraction of the movement pattern of cars based on the information of the vehicles in the form of time series as an innovation, which has been given less attention in previous articles.

The main contributions of this paper are as follows:

(i) Using the decision tree classification method to classify vehicles in aligned and not aligned vehicles

(ii) Using sequential pattern mining to discover vehicle movement patterns

(iii) Clustering vehicles in the network based on the current position to detect neighbor vehicles

(iv) Finding best cluster head to transfer messages using combination of above three steps

This article is organized in 6 sections. In the second section, we will have an overview of the background of researches in the field of VANET. In the third part, we will explain the proposed method, and in the fourth part, we will bring the simulation results of the proposed method, and in the fifth part, we will explain the evaluation results of the proposed method. In the sixth section, we will have a conclusion.

2. Related Works

Kakkasageri and Manvi [18] used regression mechanism and proposed a method for collecting information and disseminating critical information based on cognitive factor in VANET. The regression-based cognitive approach effectively aggregates the critical information collected and minimizes the dissemination of transmitted data. The proposed scheme works on cluster vehicles using a set of static and moving agents. The scheme has steps including (1) validating and filtering the critical information collected, (2) generating knowledge based on important and critical information filtered, (3) gathering knowledge to motivate using regression techniques, (4) increasing motivation for better quality of information aggregation, and (5) disseminating the collected information to neighboring clusters.

Rehman et al. [19] proposed a scheme for selecting bidirectional stable communication (BDSC) for multistep broadcast protocols on a wide range of vehicles. The selection of relay nodes based on the quantitative representation of link characteristics for single-step neighboring nodes is proposed using a link quality estimation algorithm. The BDSC scheme is designed to improve packet delivery rates and minimize delays in communicating in a high-density network with nodes distributed over a large coverage area. To achieve this goal, the proposed design in this study attempts to balance

the quality of the estimated link and the distance between the source distributor and potential senders when selecting the next nodes to transmit the sent messages.

Louazani and Sekhri [20] introduced a clustering mechanism based on connection maintenance in VANET called AODV-CV. In this research, a formal model using net Petri time as a mathematical tool to prove the properties of the protocol is presented. Also, a mobile virtual clustering protocol for VANET is proposed to improve connectivity on a highway.

Jalooli et al. [21] investigated the message propagation performance in the VANET environment and proposed a safety-based disconnected RSU replacement algorithm (S-BRP). VANETs are dramatically designed to increase road safety and traffic efficiency through vehicle-to-vehicle communications and vehicle-to-road infrastructure. Roadside units (RSUs) play an important role in terms of connectivity, routing, and data transmission latency in VANETs. However, using RSU cannot provide enough coverage for our target area. The S-BRP algorithm has been evaluated through extensive simulation. The results show that this algorithm has a good performance in terms of reducing the propagation delay and traffic flow.

Abuashour and Kadoch [22] have proposed three protocols (including Cluster-Based Life-Time Routing (CBLTR), Intersection Dynamic VANET Routing (IDVR), and Control Overhead Reduction Algorithm (CORA)). The CBLTR protocol is designed to increase path stability and average performance in a two-way road scenario. Cluster nodes (CHs) are selected based on the maximum lifespan of all vehicles within each cluster. The IDVR protocol is designed to increase path stability and average performance and reduce point-to-point latency in network topology. The selected node receives a Set of Candidate Shortest Routes (SCSRs) to the nearest intended destination from the defined software network. The IDVR protocol selects the optimal route from the SCSR based on the current location, destination location, and maximum average power. Finally, the CORA implements control overhead messages between cluster members and CH with the aim of reducing the amount of message control overhead in clusters by creating a new mechanism for calculating optimal numbers.

Shahidi and Ahmed [23] proposed an approach for the two-way multilane highway that can be efficient in both directions due to the movement of vehicles. In this approach, the possible end-to-end delay distribution is calculated and its dependence on system parameters (such as two-way speed distribution, communication range, and vehicle density) is investigated. Simulation of this approach has been used to investigate the analytical model. The good agreement between the simulation results and the analytical calculations shows the accuracy of the proposed analytical model.

Mohammed Nasr et al. [24] proposed a VANET cluster routing algorithm for desert areas and other rugged environments that provides a stable cluster structure and a reliable route between source and destination nodes. In addition, it uses vehicles equipped with mobile or satellite links to act as gateways to inaccessible destinations. A new method for selecting eclipses has also been proposed in this study and has been theoretically analyzed. During this study, numerical simulations were used to evaluate the proposed method for selecting the cluster head. The simulation results were also performed to evaluate the proposed routing algorithm in terms of packet delivery ration (PDR), terminal-to-terminal latency, and cluster stability and compare it with other options.

Ardakani [25] presented the ACR algorithm, which is a cluster-based routing protocol for transmitting network traffic in VANET. Using this protocol, each node first selects an identifier, called a LOCO, based on its location and mobility. The network is then divided into a set of clusters based on the node mobility pattern. The Hamming distance criterion is used to measure the similarity of moving nodes using LOCO values. Nodes are categorized using a lightweight clustering algorithm. Each cluster is managed by a cluster (CH) whose functionality is to communicate with RSUs.

In [26], a blockchain technique has considered the best technique that provides secrecy and protection to the control system in real-time conditions. In [27], the trust-based framework with a novel mechanism to determine DDoS attacks in VANET has developed. In [28], a secure information management scheme has proposed named Third Eye, by satisfying all the performance parameters as well as satisfying the trust metrics among the vehicles and devices. In [29], a portable VANET routing protocol that learns the optimal route by employing a fuzzy constraint Q-learning algorithm has proposed. In [30], an efficient routing solution based on a flooding technique has conceived to make the data delivery more reliable and to guarantee robust paths. In [31], a flooding scheme that automatically reacts at each topology variation while overcoming the present obstacles while exchanging data in ad hoc mode with drones that are commonly called unmanned aerial vehicles (UAVs) has designed. In [32], a routing algorithm in software-defined vehicular network (SDVN) based on the hidden Markov model (HMM) and temporal graph has introduced that considers the vehicular network as a temporal graph, in which each data transmission as an edge has its specific temporal information. In [33], a social computing inspired predictive routing scheme (SPIDER) for SDVNs has proposed to low-latency reliable data exchange under dynamic vehicular networks. In Table 1, the important evaluation parameters in the previous methods are reviewed.

As shown in Table 1, previous related methods in the literature for data transmission in VANET have focused more on reliability and trust, and little attention has been paid to the prediction of vehicle movement and path pattern discovery in these types of networks. Therefore, in order to overcome this issue, the proposed method has presented an approach based on clustering and frequent pattern discovery in predicting the movement path of vehicles.

3. Proposed Methodology

The outline of the proposed method has four modules as follows:

Module 1: initial data collection and analysis

Table 1: Evaluation parameters in related works.

Related work	Delay	Reliability	Data delivery	Trust
[18]	✓	×	✓	×
[19]	✓	✓	✓	×
[20]	✓	✓	✓	×
[21]	✓	✓	✓	×
[22]	✓		✓	×
[23]	✓	✓	×	×
[24]	✓	×	×	✓
[25]	✓	✓	×	✓
[26]	✓	×	✓	✓
[27]	×	✓	✓	×
[28]	✓	✓	×	✓
[29]	✓	×	✓	✓
[30]	×	✓	✓	×
[31]	✓	✓	×	✓
[32]	×	✓	✓	✓
[33]	✓	✓	✓	✓

Module 2: data preparation and initial analysis

Module 3: creating a pattern and discovering the path of cars

Module 4: vehicle clustering and data/information transmission routing

In the following, we will describe the modules and methods that are used in these modules. The flowchart of the proposed method is shown in Figure 1.

As shown in Figure 1, the proposed method flowchart has four modules as follows.

3.1. Initial Data Collection and Analysis. The first part of doing anything is collecting raw data. In the intelligent transportation system, the required data about the traffic on the routes and the speed of the vehicles are collected in different ways. Some of these methods include installing cameras on the road and installing sensors on the floor of the street, sensors in the body and inside the car, and so on. Some other data is collected via GPS used in vehicles, such as the exact geographical location of the vehicle.

All collected data must be stored in a single memory. The sensors themselves have a limited storage compartment, so it is necessary to connect this data to RSU roadside infrastructure using communication methods such as Wi-Fi, VANET, and Internet and send the data to the center through them for storage, analysis, and control.

The first step in the proposed intelligent system is to create and develop a sensing system. This sensing system consists of the following parts:

(i) *Environmental data collection tools/sensors*: in the method proposed in this research, a set of environmental data collection tools (such as sensors) installed on street pavement, sensors installed on cars, cameras installed on the streets, sensors installed on roadside control, and communication infrastructure is used to establish V2I communications to collect environmental data. This data can eventually be integrated together or transferred separately to control centers. In this research, the emphasis is on sensors installed under the pavement of the streets and on the car to measure the ambient temperature and identify glacial routes and GPS system to identify the location of cars and send it to the control center in line with other data. We used the collected NFCs for cases where we need to carefully monitor short but sensitive streets and routes, or we can say that the geographical area covered is less in this case. Since different sensors can be used simultaneously with these tools and sensors mentioned and considered by us, so we actually intend to use WSNs, NFC, and GPS as the main methods of collecting environmental data. In some cases, some very urgent and common operations can be performed by installing actuators in our proposed system. Like foggy air-sensitive actuators, the actuators can automatically alert the driver as soon as the environment detects that the environment is foggy, and in some smart and automatic vehicles, they automatically slow down their speed

(ii) *Communication technologies*: after collecting data, the next step is how to exploit this data. Most of our tools and sensors are not able to fully process and exploit this data, so this data must be transferred to training centers. For this purpose, some communication technologies are used depending on the use (such as VANET, Wi-Fi, Bluetooth, DSRC, and GSM)

(iii) *Communication tools/communication channel*: we use Internet communication channels as well as 5G mobile services to create communication

(iv) *Web server/data storage and initial processing*: to store the collected data and maintain it for future processing or processing in real time or to separate the data and store the data in the database, available data such as location data in the GPS database, environmental data such as temperature or frost in the Ambience DB database, or location data in the commuter DB database is saved. This data in different databases can be used by the server when processing data, and the data contained in them is updated at certain intervals

3.2. Data Preparation and Initial Analysis. Some basic analyses such as identifying high-risk routes in terms of high accident statistics, identifying congested routes, detecting congestion hours during the day, and detecting congested days during the week and year are performed in this section. Finally, the normalized and desirable data for further analysis, along with the results obtained from the initial analysis performed in this module, are stored in a special main database.

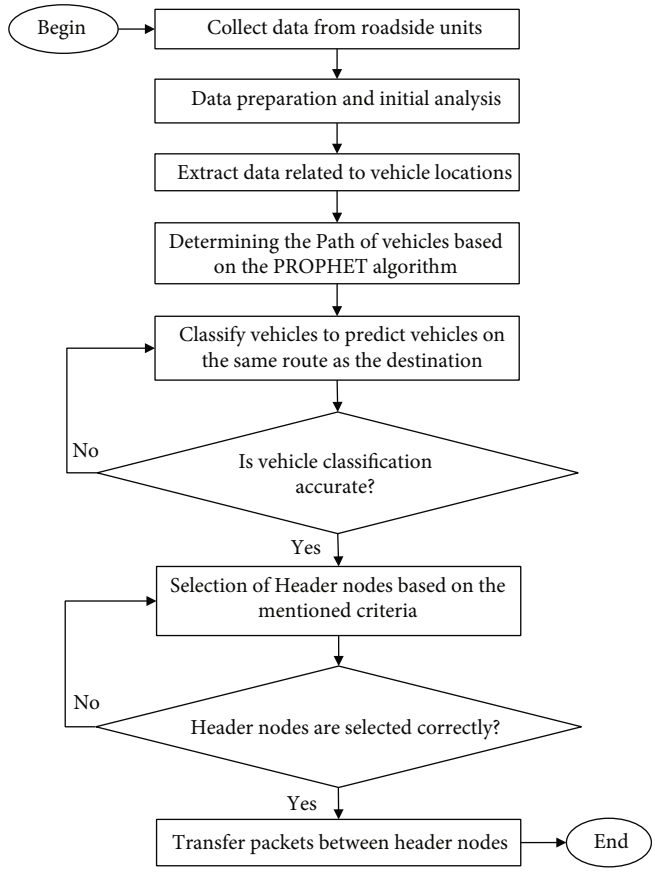

Figure 1: Flowchart of the proposed method.

Major tasks in data preparation or preprocessing performed on data include data comprehension, data cleansing, data integration, data conversion, and data size reduction.

3.3. Extraction of Pattern and Discovering the Path of Vehicles. In this module, two ways are applied to create a unique pattern for each vehicle:

(i) *Applying the classification techniques in data mining*: classification techniques, such as decision tree, Naïve Bayesian, SVM, neural networks, rough set, and random forests, try to model each vehicle using attributes like the routes traveled, average speed, type of vehicle, age and gender of the vehicle driver, and number of offenses and extract the pattern of behavior for each vehicle. Because the decision tree technique is one of the simplest methods of classifying samples and can work with different types of data, in this study, this technique has been used to determine the behavioral patterns of drivers. Also, for each of the existing routes, a pattern is extracted based on the number of vehicle on that route and traffic situation at different hours of the day and at different days of the week and months of the year. In this model, the traffic situation and congestion of vehicle at different hours, especially during rush hour congestion, are examined

(ii) *Use of protocols to create vehicle trajectories in different routes*: the number of transit packages between vehicles and RSU off-road infrastructure and between vehicles and control centers is examined, and a pattern of the number of collisions, collisions of messages, or loss of messages is examined

In this research, using the PRoPHET protocol, we have collected and created the vehicle trajectory so that we can adjust the routing tolerance with error.

3.4. Vehicle Clustering and Data/Information Transfer Routing. In this module, for all vehicles on the route, we put them in clusters based on various criteria such as the behavioral similarities or routes traveled, average speed, amount of traffic offenses, and number of accidents. Flowchart in Figure 2 is used to select the header in each cluster.

The data exchange paths will be creating from the header to the other nodes. And first, there is the priority with nodes that have a higher degree.

3.5. Complexity. Due to the fact that the movement data of vehicles collected in a certain period of time is used to

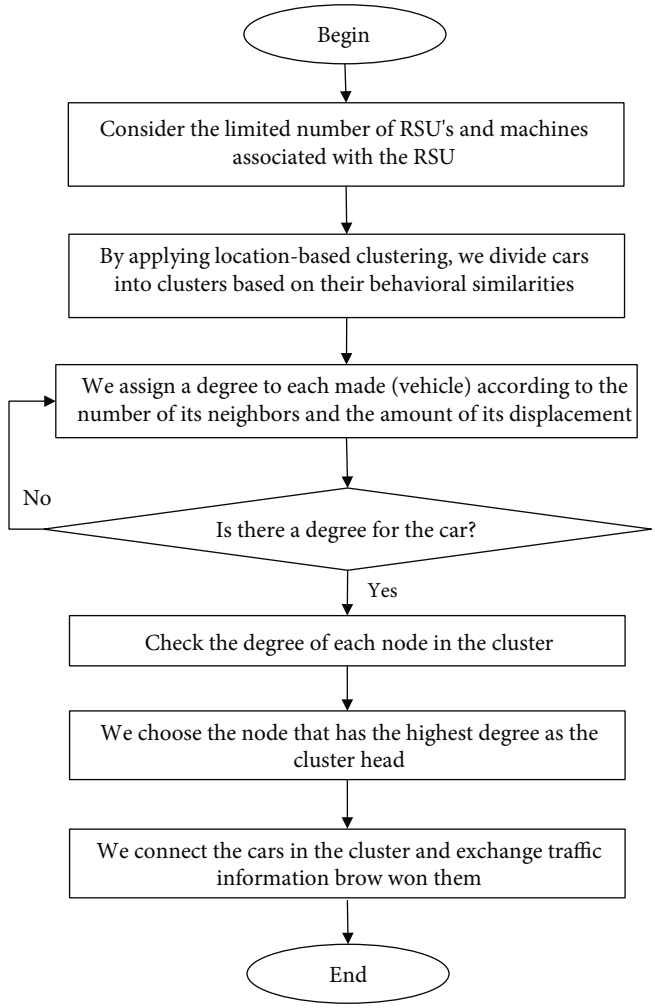

Figure 2: Flowchart of how to choose cluster head.

generate movement patterns, therefore, the generation of movement patterns will be performed offline and once during the proposed method. The time complexity of generating movement patterns based on the steps of the proposed method is $O(n)$ for clustering cars and $O(n^2)$ for comparing the movement of vehicles on the road. After generating movement patterns, to predict the movement path of new vehicles, it is enough to compare the location of the vehicles with the patterns. Due to the limited number of vehicle movement patterns, the time complexity of predicting the movement path of new vehicles can be ignored, and the time order of the proposed method is determined based on the number of vehicles in the network and of the order of $O(n)$. Finally, the total time cost of the proposed method will be of the order of $O(n^2)$.

4. Experimental Results

In order to simulate the proposed method in this research, NS-2 network simulator software version 2.35 was used. The simulation environment is a cross street with dimensions of 1000 by 1000 meters, which has four access points (AP) and two holes along the road. The street is located between two intersections, at both ends of which are points simulated as traffic lights, with a total of 29 vehicles moving on the street. Vehicles in the network vary in speed from 10 to 30 km/h. Also, the settings related to the antenna and other infrastructures in this scenario have been applied in accordance with the standard settings in the simulation of previous works. More details about the simulation scenario are shown in Table 2.

4.1. Implementation of the First Module of the Proposed Method: Data Collection. In order to implement the first module and collect data, apply the scenario mentioned in Section 3 on the NS-2 emulator software and the result of the scenario on the NS-2 emulator in two output files with extensions save * .nam and * .tr. The file with the * .nam extension is related to the scenario visualization part. This file runs on the Nam console, which is part of the NS-2 simulator, and shows how vehicles move and transmit messages between vehicles. Figure 3 shows the graphical view of Nam software.

As shown in Figure 3, the cars are moving in the street and are communicating with each other wirelessly through built-in sensors. When a vehicle becomes aware of a hazard in the network for various reasons, it sends this message to

Table 2: Scenario details of the proposed method.

Simulation details	Initial values
Simulation space	1000*1000 m
Number of vehicles	29
Speed of vehicles	10-30 km/h
Package size	50
Routing protocol	DSDV
Communication protocol	FTP, TCP
Simulation time	35 s
Neighbor selection threshold	200 m

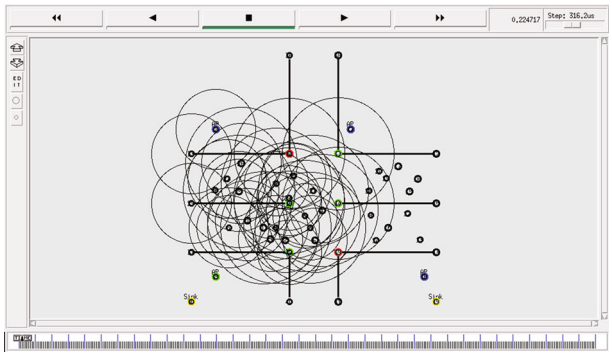

Figure 3: Appearance of street and vehicle simulation.

other vehicles within the network. According to the proposed method, before sending the message, the neighboring vehicles in the network should be identified and the message should be transmitted only between these vehicles to avoid redundancy and creating excessive duplicate messages and wasting time. For this purpose, in the event of an accident in the VANET, the originator first collects the distances of other vehicles in the network. Then, the position of each vehicle at any time relative to the starting point is calculated. Table 3 shows the values for the starting points and the speed and location of the new vehicles at different times.

As shown in Table 3, the position of each vehicle is calculated at different times. Now we transfer information in the network and collect data based on what happened in the network.

4.2. Implementation of the Second Module of Proposed Method: Data Preparation. The data collected in the first module is in the form of raw data that shows the position of vehicles in the network. In this module, we will prepare the data for presentation to the next modules. For this purpose, based on the defined scenario, we transfer information in the network between vehicles and roadside units and save the events in the trace file for later use. Hence, in Figure 4, transfer of information between vehicles present in the network is shown.

As shown in Figure 4, information is transmitted between vehicles on the network and reports the sending and receiving packets, sending and receiving times, vehicle locations, average vehicle speeds, and number of lost packets. This information is saved on the trace file. In this module, we will prepare this information for use in the next modules.

4.2.1. Data Preprocessing. In recent years, various training models have been found that, by performing an educational process on data, are able to predict and describe unknowns to the system. The important point here is the type of data used for each type of model. In fact, each model deals with a specific data type and explores a specific type of data. To use the models and benefit from the output results of the model, it is necessary to prepare the data in a specific model format. The data preparation process for each model is called data preprocessing. Data preprocessing has several steps that in this research, two types of these preprocessing steps are required that will be applied to the data extracted from the trace file in the simulation of the proposed scenario. Table 4 shows an example of the data stored in the trace file.

4.2.2. Data Cleaning. According to the set of features shown in Table 4, it can be seen that the data extracted from the trace file have many dimensions and the values of these features have been expanded in various ranges. The most important problem among data that needs to be cleaned is missing values. In order to overcome the problem of missing values, several solutions have been proposed in the sources, which are as follows:

(i) Delete the sample with the missing value

(ii) Replace the lost value with a random value

(iii) Replace the lost value with the same value

(iv) Replace the lost value with the average

(v) Replace lost value based on specific function

The most common solution is the method of replacing the lost value with the mean, which in this research has been used in order to overcome the problem of lost values. Therefore, properties that have a missing value are cleared using the method of replacing the lost value with the mean.

4.2.3. Select a Subset of Features. The second preprocessing step used in this research is the selection of a subset of attributes that are directly related to the class label. As shown in Table 4, the data extracted from the trace file has 11 properties, and this large number of attributes can complicate the training model and the path discovery protocol which is used. Therefore, some of these attributes, which have little effect on node path detection, should be removed during the preprocessing step of selecting the feature subset.

The purpose of the preprocessing step is to select a subset of features to remove unrelated features and attributes and plugins so that in addition to reducing the data dimension and reducing the operational and spatial complexity of the system, the system accuracy can be increased. In addition, selecting a subset of data can detect implicit dependencies between data and path detection patterns to easily predict the path of test nodes that will be added to the scenario in the future. Therefore, in this study, irrelevant features and attributes that do not have many changes in the samples and naturally cannot have much effect on discovering the node path pattern

Table 3: Information on vehicle locations.

Location at $t = 25$ s		Location at $t = 10$ s		Location at $t = 1$ s		Vehicle speed	$y0$	$x0$	Vehicle no.
454.448	349.448	382.015	277.015	363.955	258.955	20	330	225	1
436.893	426.893	357.217	347.217	337.3509	327.350	22	300	290	2
374.448	504.448	302.015	432.015	283.955	413.955	20	250	380	3
443.336	553.336	389.011	499.011	375.466	485.466	15	350	460	4
494.448	654.448	422.015	582.015	403.955	563.955	20	370	530	5
387.113	237.113	336.411	186.411	323.768	173.768	14	300	150	6
405.560	655.560	315.019	565.019	292.444	542.444	25	250	500	7
436.893	616.893	357.217	537.217	337.350	517.350	22	300	480	8
424.448	464.448	352.015	392.015	333.955	373.955	20	300	340	9
412.224	792.224	376.007	756.007	366.977	746.977	10	350	730	10
399.558	899.558	341.612	841.612	327.164	827.164	16	300	800	11
393.115	463.115	309.818	379.818	289.048	359.048	23	250	320	12
422.224	942.224	386.007	906.007	376.977	896.977	10	360	880	13
349.558	1029.558	291.612	971.612	277.164	957.164	16	250	930	14
368.226	868.226	299.415	799.415	282.257	782.257	19	250	750	15
524.669	964.669	481.209	921.209	470.373	910.373	12	450	890	16
624.448	1054.448	552.015	982.015	533.955	963.955	20	500	930	17
693.115	993.115	609.818	909.818	589.048	889.048	23	550	850	18
593.115	873.115	509.818	789.818	489.048	769.048	23	450	730	19
643.115	943.115	559.818	859.818	539.0486	839.048	23	500	800	20
654.448	894.448	582.015	822.015	563.955	803.955	20	530	770	21
543.336	593.336	489.011	539.011	475.466	525.466	15	450	500	22
590.891	500.891	543.810	453.810	532.070	442.070	13	510	420	23
482.224	462.224	446.007	426.007	436.977	416.977	10	420	400	24
560.891	430.891	513.810	383.810	502.070	372.070	13	480	350	25
593.115	343.115	509.818	259.818	489.048	239.048	23	450	200	26
703.115	353.115	619.818	269.818	599.048	249.048	23	560	210	27
636.893	286.893	557.217	207.217	537.350	187.350	22	500	150	28

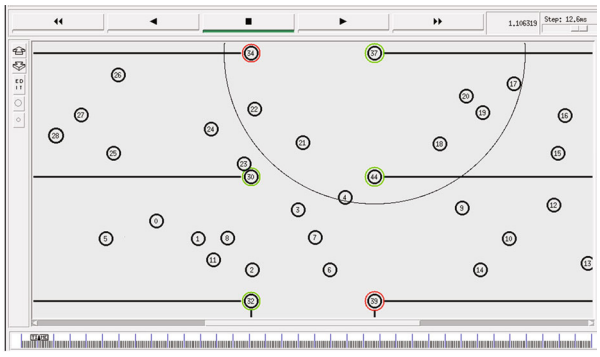

Figure 4: Transfer of information in the VANET.

Table 4: An example of the data extracted from the trace.

Description	Value
Event	r
Time	0.032237058
Sender node	28
Protocol	RTR
Packet type	Message
Receiver node	30
Communication port	[0 ffffffff 1e 800]
Communication path	[30 : 255-1 : 255 32 0]
Initial location	930,500
Final location	10,450
Node speed	20.00

are removed to impose additional complexity on the model to avoid suggested training.

Feature selection methods can be broadly divided into filter and wrapper methods. In the filter approach, the attribute selection method is independent of the training model that is applied to the selected attributes and evaluates the attribute weight only by considering the intrinsic properties of the data. In most cases, the amount of weight is calculated and the weak features are removed. The extracted features are presented as input to the training model. In this research, the filter approach is used to select features. After applying the filter method on the data obtained from the trace file, you can see that the features related to the

communication port, message type, and communication protocol are removed.

4.3. Implementation of the Third Module: Discover the Path of Vehicles and Create a Pattern. After preprocessing the data and extracting important features about the behavior of vehicles in the proposed network, in this module, we will explore the vehicle path and create patterns to identify vehicles moving on the existing route to the destination. The vehicle path refers to the direction in which the vehicle moves from the beginning of the simulation moment to the end of the simulation. This path represents the starting point of the vehicle x_0, the end point of the vehicle x_n, and the direction of the car. For this purpose, we use the data recorded in the trace file and extract the starting points and locations of the vehicles at any time. Now, using the data related to the location of the cars, we will draw the path of the cars in the proposed network. Figure 5 shows an example of the path of vehicles in the network.

As shown in Figure 5, the vehicles in the proposed network start moving from point x_0 and continue moving up to point x_n. The trajectory of each vehicle is recorded at each moment according to the location at the beginning and end of the route and the location of the vehicle, and based on this, the trajectory of that vehicle is determined. Now, according to the trajectory of vehicles and according to the average speed of vehicles and the direction of movement of each vehicle, it is possible to create patterns about vehicles in the network.

To create patterns for vehicles on the network, we first classify vehicles in order to find vehicles moving in the direction of the destination. Thus, the vehicles in the network are divided into two classes: destination-oriented vehicles and non-destination-oriented vehicles. Routine vehicles are vehicles that, due to their behavior in the network, approach the destination node along their route and can exchange information with the destination node. Therefore, we apply the behavior of vehicles in the network to the decision tree as the characteristics of the vehicles so that the decision tree classifies the vehicles and the path patterns of the vehicles are determined. These characteristics include the average difference between the distance of each vehicle to the destination node, vehicle speed, distance of vehicles at the x_n point from the destination node, and total distance of the vehicle from other vehicles on the route.

4.3.1. Implement the Decision Tree. In this research, the decision tree, which is a rule-based classifier, has been used. The important point here is to choose a feature and a condition on the feature that divides the data well, so that the leaves have the maximum degree of purity. Therefore, in this research, gain ratio criterion has been used to divide the samples based on features, so that important features can be identified and used as a condition for division. This criterion is calculated at each stage (level) of the decision tree production for all properties. Figure 6 shows the application of conditions to properties and the creation of a decision tree.

As can be seen in Figure 6, the decision tree applies conditions to the properties in the data set based on the importance of these properties and divides the entire data into subtrees that apply in these conditions. Each of these conditions represents a pattern that describes the vehicle's behavior on the road. Therefore, we make these patterns into rules in order to predict the trajectory of future vehicles. As mentioned earlier, in this study, nodes are defined in two groups of aligned and nonaligned vehicles, and all vehicles are placed in one of these two groups based on their behavioral patterns. Alignments are shown as class 1 and nonaligned vehicles as class 2. The patterns created are shown in Table 5.

As can be seen in Table 4, the patterns created based on the decision tree are based on the features in the data set, which will be used to predict the trajectory of future vehicles. After classifying the vehicles and creating patterns of vehicle behavior, we predict the trajectory of the next vehicles using the PRoPHET protocol (probable routing protocol using encounter date and transfer protocol).

In PRoPHET, the predictability of delivery between two nodes is calculated based on the date of contact between them, while the higher predictability of delivery increases the likelihood of further communication between them. In the PRoPHET protocol, a message is copied to the contact node only when the transmission prediction capability for the destination node of the contact node is greater than the transfer node. By doing so, the PRoPHET protocol is likely to deliver packets well, as well as meet latency and message overhead costs.

In this method, we use the PRoPHET protocol to predict the trajectory of vehicles within the network. Vehicle lanes are designed to transmit information and warning data within the road network to destination nodes or roadside potholes. Vehicles that have a trajectory along the hole are a good option for transmitting information, and messages can be delivered to these vehicles. For this purpose, in the proposed method, the PRoPHET protocol is used for vehicles that have been selected as aligned vehicles in the previous step through the decision tree, in which we use vehicle trajectory factors and vehicle speed to calculate delivery capability. Therefore, to calculate the deliverability, we use the proposed

$$\mathrm{DC}(i) = \left| \frac{1}{\sum_{j=1}^{t}\sum_{i=1}^{n}\left(\left(\sqrt{\left(x_{ij-}x_s\right)+\left(y_{ij}-y_s\right)^2}-\sqrt{\left(x_{(i-1)j-}x_s\right)+\left(y_{(i-1)j}-y_s\right)^2}\right)/n\right)} \right| + \left| \frac{1}{\sum_{i=1}^{n}\sqrt{\left(x_{n-}x_s\right)+\left(y_n-y_s\right)^2}} \right| + v_i, \tag{1}$$

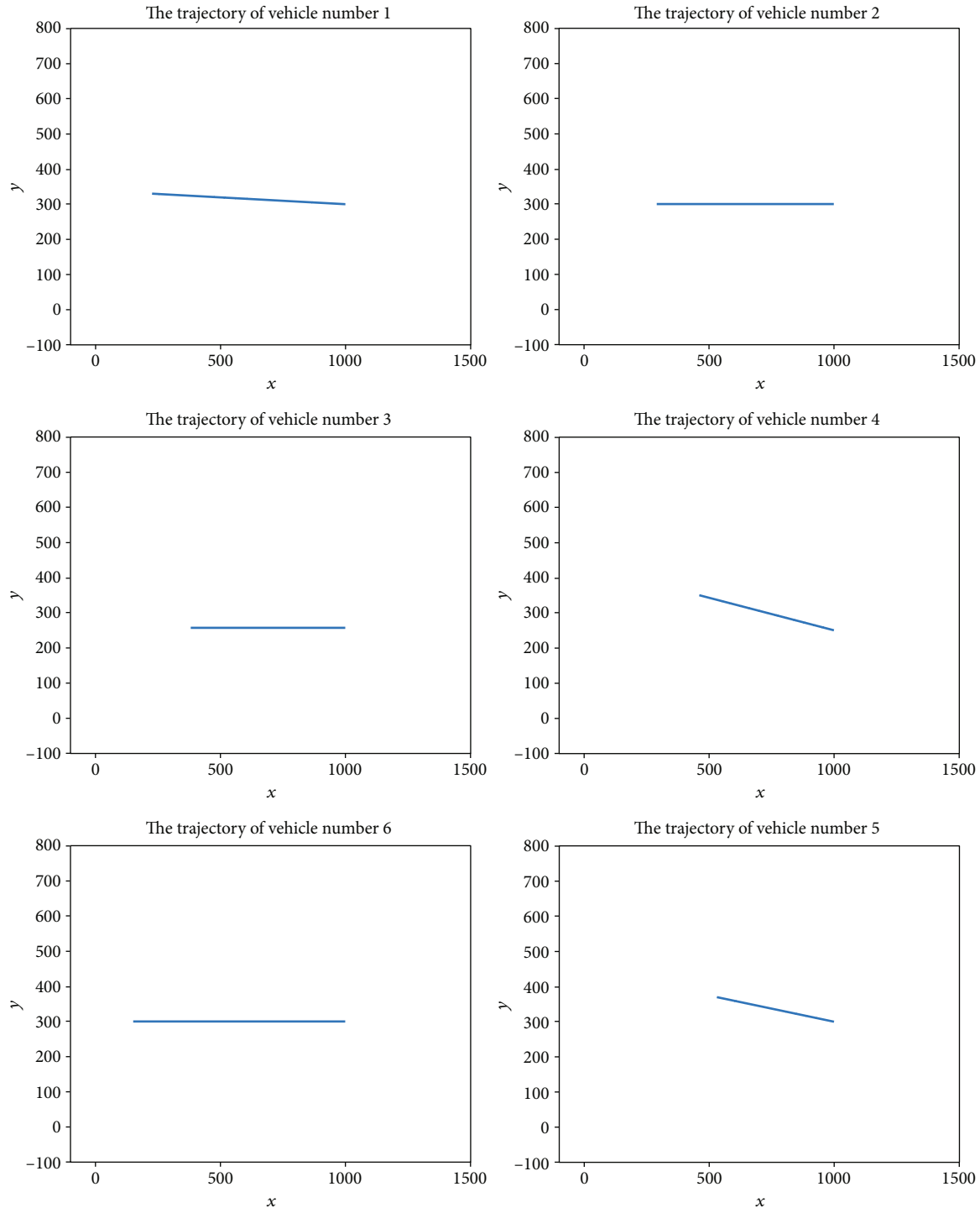

Figure 5: An example of the path of vehicles in the network (given the large number of vehicles in the network, only the path of a sample of vehicles is shown in the figure).

where x_{ij} and y_{ij} are the length and width of the i-th vehicle at the j-th moment, x_s and y_s are the length and width of the hole, n is the total vehicle number, and v_i is the average speed of each vehicle. The higher the DC value for a vehicle, the greater the delivery capacity for that vehicle, and the more likely it is to transmit data packets to the destination. Therefore, it is possible to select a vehicle with the highest amount of delivery capability among the vehicles that have been designated as aligned vehicles and send data packets to that vehicle in order to transfer it to the destination hole or node. Table 6 shows the distance of each car to the hole node over time.

As can be seen in Table 6, the distance of aligned vehicle relative to the hole node decreases over time. Therefore, it can be said that aligned vehicles will approach the hole node at the end of the route. Table 7 also shows the difference

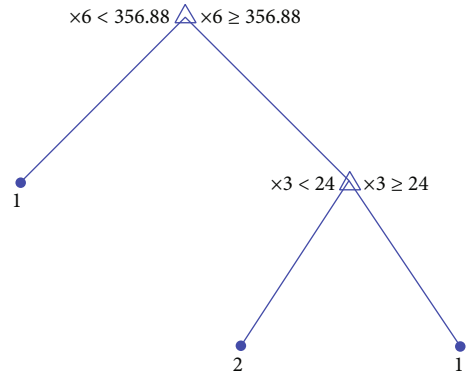

Figure 6: Steps to create a decision tree.

Table 5: Patterns created from the decision tree to discover the trajectory of vehicles.

Decision tree for classification
If "other vehicle distances" < 356.88, then class = 1
Else if "other vehicle distances" ≥ 356.88 and if "other vehicle distances" < 24, then node 4 else if $x3 \geq 24$ then class = 2
Else if "other vehicle distances" ≥ 356.88 and if "other vehicle distances" < 24, then node 4 else if $x3 < 24$ then class = 1

between the distance of each car to the hole node at each moment of its travel path. In fact, the difference between the distance of each speed shows the tendency of each car towards the hole node.

As can be seen in Table 7, the difference in distances between aligned vehicles is gradually decreasing. Therefore, it can be said that aligned vehicles will approach the hole node at the end of the route.

Alignment vehicles according to the PRoPHET protocol will most likely deliver complete and secure packets to the destination vehicle or pit with high confidence, but the transmission of the packet by one vehicle along the entire route can be very delayed. Therefore, in this research, in order to reduce the delay of message transmission, the clustering method has been used, which we will describe and implement in the fourth module in the continuation of this chapter.

4.4. Implementation of the Fourth Module: Vehicle Clustering and Data/Information Transfer Routing. After predicting the trajectory of vehicles and shaping aligned vehicles and detecting nonaligned vehicles, in the proposed method, we will cluster the aligned vehicles. Vehicle clustering is based on the distance between vehicles and the accumulation of vehicles in road areas. The presence of vehicles in the road network may be complex or scattered. When vehicles are integrated, a clustered vehicle is first selected to cluster the vehicles on the road. The vehicle is selected based on three factors: alignment, maximum accumulation of vehicles, and minimum distance to other vehicles. Therefore, the following equation can be used to select the node [12]:

$$D(i,j) = \left| \sqrt{\left(x_{i-}x_j\right) + \left(y_i - y_j\right)^2} \right|, \tag{2}$$

$$\mathrm{HC}(i) = \arg\max \left\{ (\mathrm{DC}(i) + \left(\frac{1}{D(i,j)}\right) + \mathrm{density}(i) \right\} \text{ for } i \in n_{\mathrm{dc}}, j \in C, \tag{3}$$

where $D(i, j)$ is the distance between the vehicles in the road network, $\mathrm{DC}(i)$ is the amount of convergence tendency if the vehicle is aligned with the destination vehicle, and n_{dc} of the aligned vehicles and density (i) is the density of the vehicles around the vehicle. Based on Equation (3), the vehicle with the highest amount of $\mathrm{HC}(i)$ is selected as the threaded node. When a message is sensed on the network through sensors embedded in vehicles, the message is transmitted between aligned vehicles. Because aligned vehicles are clustered on the road network, messages are transmitted to the destination via clustered vehicles. The transmission of messages through threaded nodes according to Equation (3) assures us that the messages are transmitted to the destination at the appropriate speed in the direction of the destination and these messages are sent to the vehicles that are in the middle of the other vehicles and the crowd of vehicles around it is high. Therefore, if needed, that vehicles can send PAM to other vehicles in the network with the lowest communication cost and inform other cars about what is happening in the network.

In the case of vehicles, they may be spread across the road network and there are large distances between the vehicles in the road network. In this case, based on Equation (3), the vehicles that are in the direction of the destination node and move towards the destination with the highest speed have the highest amount of HC, and the appropriate option for selecting the vehicle for routing is selected. Table 8 shows the HC values for vehicles in the network.

As shown in Table 7, the value of the evaluation function is calculated to select the threaded node for all vehicles in the network. Now, based on the accumulation of nodes in the network sections, the nodes are clustered and the clustered nodes are identified according to Table 7. The vehicle with the highest value of the evaluation function is selected as the best vehicle in the desired cluster. Figure 7 shows the clustering of vehicles in the proposed method.

As shown in Figure 7, vehicles within the network are divided into clusters due to their accumulation in the road network. After clustering the vehicles within the network, the evaluation function of selecting the clustered node for these clusters is executed, and among these clusters, for those clusters and vehicles that are in the direction of the destination node, the clustered nodes based on Equation (3) and Table 7 are selected. As shown in Figure 7, in transferring information from the source node to the destination in the first cluster of vehicle no. 1, which according to Table 7 has the highest value of the evaluation function of the cluster node among the other vehicles in the cluster, the cluster node is selected and receives the message from the source node. In the next step, in order to transmit the message to the destination, the vehicle number 4, which

Table 6: The distance of each vehicle to the hole node over time.

	$t = 0$	$t = 100$	$t = 1000$	$t = 5000$	$t = 10000$	$t = 15000$	$t = 20000$	$t = 30000$	$t = 35493$
V1	445	442.9247	424.0585	340.2086	235.3963	130.5839	25.7716	183.8532	299
V2	410	408.0223	390.0436	310.1383	210.2566	110.3750	10.4933	189.2700	299
V3	370	368.2734	352.5769	282.8147	195.6119	108.4092	21.2064	153.1991	249
V4	190	188.7755	177.6434	128.1674	66.3225	4.4776	57.3673	181.0572	249
V5	100	98.8870	88.7693	43.8014	12.4085	68.6183	124.8282	237.2479	299
V6	550	547.6318	526.1030	430.4195	310.8151	191.2107	71.6062	167.6026	299
V7	250	248.6081	235.9546	179.7165	109.4190	39.1215	31.1761	171.7711	249
V8	220	218.4129	203.9842	139.8571	59.6982	20.4607	100.6196	260.9374	349
V9	360	358.0223	340.0436	260.1383	160.2566	60.3750	39.5067	239.2700	349
V10	80	80.7503	87.5716	117.8883	155.7841	193.6800	231.5759	307.3676	349
V11	100	100.5551	105.6013	128.0289	156.0634	184.0979	212.1323	268.2013	299
V12	430	429.0795	420.7114	383.5199	337.0306	290.5412	244.0519	151.0732	100
V13	240	240.1395	241.4074	247.0424	254.0863	261.1301	268.1740	282.2616	290
V14	180	180.3319	183.3495	196.7610	213.5253	230.2897	247.0540	280.5827	299
V15	0	0.6946	7.0086	35.0713	70.1496	105.2280	140.3063	210.4629	249
V16	340	339.7462	337.4386	327.1828	314.3630	301.5432	288.7234	263.0838	249
V17	430	427.2943	402.6972	293.3768	156.7263	20.0758	116.5747	389.8757	540
V18	400	397.6569	376.3564	281.6871	163.3506	45.0141	73.3224	309.9955	440
V19	180	178.2706	162.5487	92.6738	5.3302	82.0134	169.3570	344.0443	440
V20	300	299.3027	292.9632	264.7878	229.5686	194.3494	159.1302	88.6918	50
V21	300	297.9359	279.1711	195.7720	91.5232	12.7257	116.9745	325.4722	440
V22	50	50.9512	59.5982	98.0294	146.0684	194.1074	242.1464	338.2244	391
V23	70	71.1743	81.8500	129.2973	188.6064	247.9156	307.2247	425.8430	491
V24	180	181.0042	190.1330	230.7055	281.4212	332.1368	382.8525	484.2838	540
V25	170	171.1715	181.8218	229.1564	288.3247	347.4930	406.6612	524.9977	590
V26	350	350.8089	358.1627	390.8461	431.7004	472.5547	513.4089	595.1175	640
V27	230	230.4463	234.5036	252.5358	275.0761	297.6164	320.1567	365.2372	390
V28	350	350.3905	353.9406	369.7188	389.4416	409.1643	428.8871	468.3326	490
V28	450	449.9721	449.7185	448.5915	447.1827	445.7740	444.3652	441.5477	440

has the highest value of the evaluation function of the heading node in the next cluster, is selected as the heading node and receives the message from the previous heading vehicle, which is vehicle number 1. Finally, node 10, which is located in the next cluster in the direction of the destination node (hole node), receives messages and sends them to the destination. Table 9 shows the process of selecting recruited vehicles from aligned vehicles within the road network. More about this source text is required for additional translation information.

As shown in Table 8, the nodes that have the highest value of the header node selection evaluation function are selected as header nodes in each cluster.

5. Evaluation

In the proposed method, a method is used to transfer data and information based on vehicle trajectory forecasting and routing based on vehicle clustering in line with the destination, with the aim of reducing the delay of messages sent on the network. In fact, the sending of messages in the VANET started right after the accident and received the first message due to the danger on the road by the vehicle of origin. Accordingly, by publishing messages on the network and sending sensed messages to the destination node, the number of messages sent also increases. Therefore, with increasing simulation time, the number of messages sent in the network will also increase. Figure 8 shows a diagram of messages sent over the network based on increasing time.

As shown in Figure 8, the number of messages sent on the network increases with increasing network time and sending security messages on the network to the destination node. Due to the fact that the vehicles carrying the message of the clusters in the clusters are in the road network, the transmission of information in the network takes place only between the clustered nodes until these packets are sent to the destination node reach. Therefore, the number of messages sent on the network increases at a slow pace. In fact, in the proposed method, the transfer of data packets is purposeful and sending packets in the form of all broadcasts is not an unnecessary waste of data packets.

Table 7: The difference between the distances of each vehicle at each moment of the route.

	$t = 0$	$t = 100$	$t = 1000$	$t = 5000$	$t = 10000$	$t = 15000$	$t = 20000$	$t = 30000$	$t = 35493$
V1	445	442.9247	424.0585	340.2086	235.3963	130.5839	25.7716	183.8532	299
V2	410	408.0223	390.0436	310.1383	210.2566	110.3750	10.4933	189.2700	299
V3	370	368.2734	352.5769	282.8147	195.6119	108.4092	21.2064	153.1991	249
V4	190	188.7755	177.6434	128.1674	66.3225	4.4776	57.3673	181.0572	249
V5	100	98.8870	88.7693	43.8014	12.4085	68.6183	124.8282	237.2479	299
V6	550	547.6318	526.1030	430.4195	310.8151	191.2107	71.6062	167.6026	299
V7	250	248.6081	235.9546	179.7165	109.4190	39.1215	31.1761	171.7711	249
V8	220	218.4129	203.9842	139.8571	59.6982	20.4607	100.6196	260.9374	349
V9	360	358.0223	340.0436	260.1383	160.2566	60.3750	39.5067	239.2700	349
V10	80	80.7503	87.5716	117.8883	155.7841	193.6800	231.5759	307.3676	349
V11	100	100.5551	105.6013	128.0289	156.0634	184.0979	212.1323	268.2013	299
V12	430	429.0795	420.7114	383.5199	337.0306	290.5412	244.0519	151.0732	100
V13	240	240.1395	241.4074	247.0424	254.0863	261.1301	268.1740	282.2616	290
V14	180	180.3319	183.3495	196.7610	213.5253	230.2897	247.0540	280.5827	299
V15	0	0.6946	7.0086	35.0713	70.1496	105.2280	140.3063	210.4629	249
V16	340	339.7462	337.4386	327.1828	314.3630	301.5432	288.7234	263.0838	249
V17	430	427.2943	402.6972	293.3768	156.7263	20.0758	116.5747	389.8757	540
V18	400	397.6569	376.3564	281.6871	163.3506	45.0141	73.3224	309.9955	440
V19	180	178.2706	162.5487	92.6738	5.3302	82.0134	169.3570	344.0443	440
V20	300	299.3027	292.9632	264.7878	229.5686	194.3494	159.1302	88.6918	50
V21	300	297.9359	279.1711	195.7720	91.5232	12.7257	116.9745	325.4722	440
V22	50	50.9512	59.5982	98.0294	146.0684	194.1074	242.1464	338.2244	391
V23	70	71.1743	81.8500	129.2973	188.6064	247.9156	307.2247	425.8430	491
V24	180	181.0042	190.1330	230.7055	281.4212	332.1368	382.8525	484.2838	540
V25	170	171.1715	181.8218	229.1564	288.3247	347.4930	406.6612	524.9977	590
V26	350	350.8089	358.1627	390.8461	431.7004	472.5547	513.4089	595.1175	640
V27	230	230.4463	234.5036	252.5358	275.0761	297.6164	320.1567	365.2372	390
V28	350	350.3905	353.9406	369.7188	389.4416	409.1643	428.8871	468.3326	490
V28	450	449.9721	449.7185	448.5915	447.1827	445.7740	444.3652	441.5477	440

Table 8: Evaluation function values for selecting header nodes for vehicles in the network.

Vehicle no.	The value of the header node evaluation function	Vehicle no.	The value of the header node evaluation function	Vehicle no.	The value of the header node evaluation function
1	12605.0025230644	11	11450.8443351707	21	10199.0068933721
2	9762.84175823016	12	9420.60520826243	22	8167.08652900570
3	9357.58973116927	13	12413.5949490017	23	8973.49306016971
4	18301.4087332702	14	1445.61204611270	24	8214.88333766602
5	8525.81733039176	15	11292.5886888899	25	9094.22389569419
6	12256.4692509958	16	12411.8153697601	26	11010.5772186310
7	9170.01142069164	17	12516.0434281110	27	12089.7135617565
8	8758.10006652234	18	11499.9662504847	28	12442.5178217940
9	9300.62029930559	19	9212.94159417572	29	11234.9592498159
10	14237.0772406787	20	10526.5165883803		

Therefore, another criterion that has been evaluated in the present study is the number of lost packets in the network. An ACK message has been received from the vehicle when the source vehicle sends a message to the vehicle. After receiving the confirmation message, the packets are sent to the header node. The same thing is repeated for other vehicles until the message reaches its destination. Due to the limited capacity of the queue in the vehicles, the received

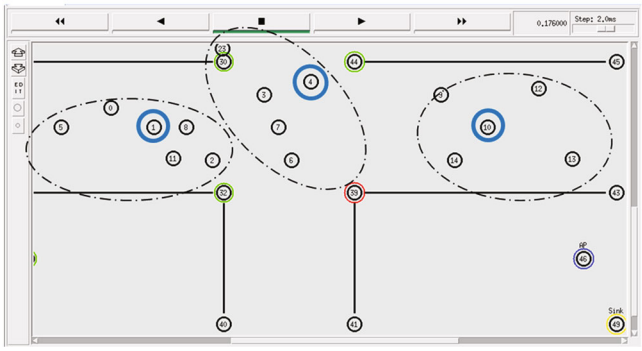

Figure 7: Clustering of vehicles within the network.

Table 9: The process of selecting header vehicles.

The cluster head in first connection is node number 4
The cluster head in second connection is node number 1
The cluster head in third connection is node number 10

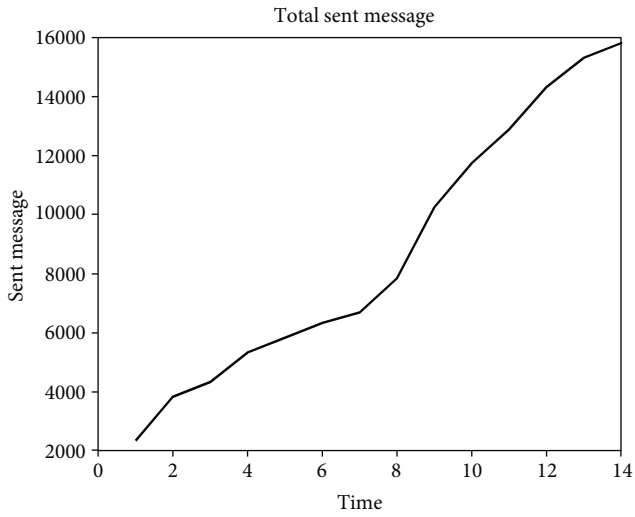

Figure 8: Graph of messages sent in the network.

messages should be stored in the queue of the vehicle to be examined in turn. When the number of these messages exceeds the queue size, the excess messages are lost and the accuracy of the information transmitted in the network may be damaged. This event will increase the number of lost packets in the VANET, which is considered as one of the weaknesses of routing methods in VANETs. Figure 9 shows the number of lost message packets as the VANET increases with time. More about this source text is required for additional translation information.

As shown in Figure 9, the number of messages lost in the proposed vehicle network increases slightly with increasing time, and finally, the total number of messages lost during the simulation of the proposed scenario only 130 messages, which is only 0.8111% of the total messages sent on the network.

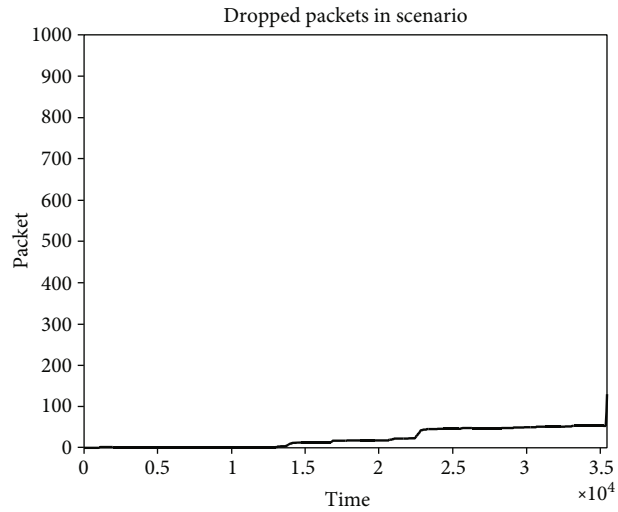

Figure 9: Number of lost message packets.

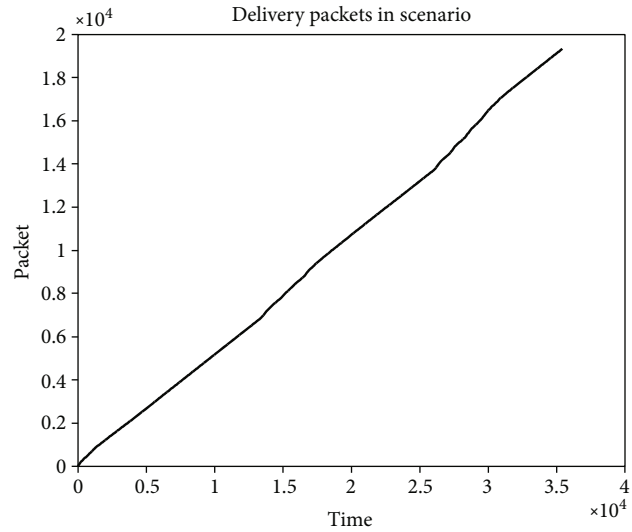

Figure 10: Diagram of delivered packages.

Due to the small number of lost packets, another criterion that has been examined in this method is the delivery rate of data packets. Package delivery rate is the ratio of the number of delivered messages to the sent messages. Figure 10 shows the diagram of packages delivered based on the proposed scenario with increasing time. Figure 11 also shows the package delivery rate in the proposed scenario.

As shown in Figures 10 and 11, a large number of healthy packages sent have been delivered to the destination and the packet delivery rate tends to be a fixed amount. By calculating the average package delivery rate over time, this amount is about 88.56%.

The last criterion that has been examined in this research is the delay of packets sent in the VANET, which is one of the most important criteria in this type of network. Due to the fact that delays in VANETs cause a loss of time for drivers to react to road accidents and disrupt real-time applications in VANETs, so any delay in less VANETs, the

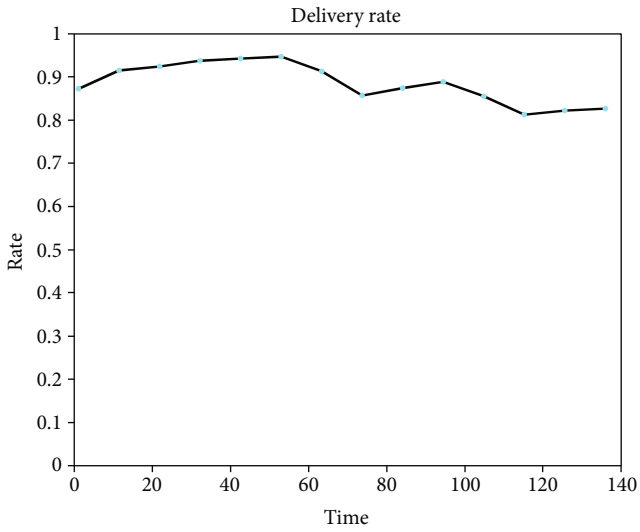

Figure 11: Package delivery rate.

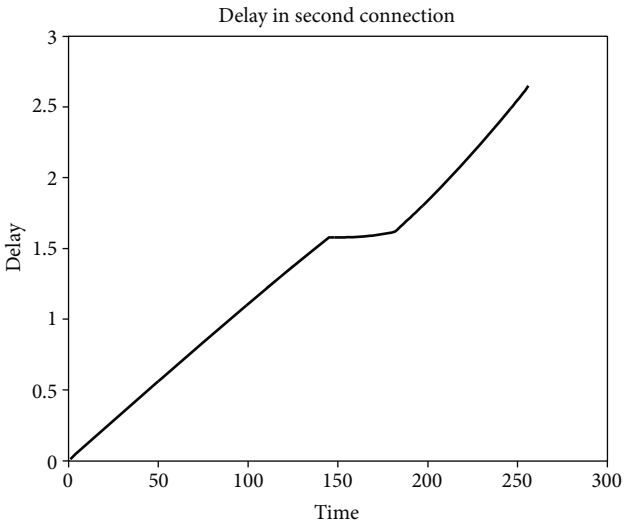

Figure 13: Delay in message transmission in the second stage of communication.

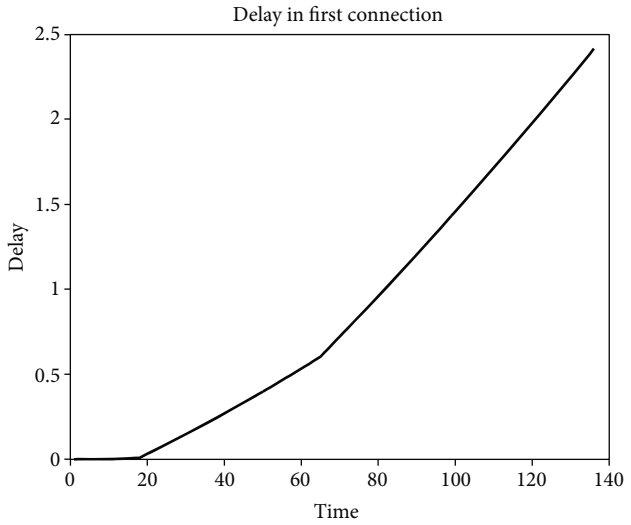

Figure 12: Message transmission delay in the first stage of communication.

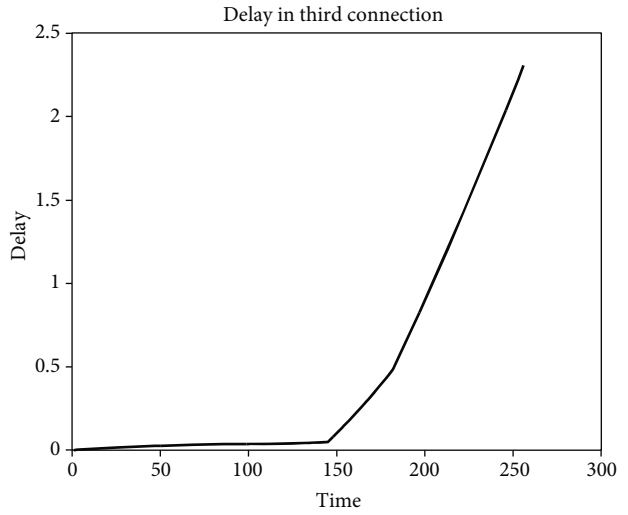

Figure 14: Delay in message transmission in the last stage of communication.

routing method used is more effective. In the proposed method, since the messages are transmitted between the node clusters, therefore, the delay of message transmission between the clusters must be calculated. Figure 12 shows the message transmission delay in the first stage, Figure 13 shows the message transmission delay in the second stage, and finally, Figure 14 shows the message transmission delay in the last stage.

As shown in Figures 12–14, the message transmission delay between threaded nodes tends to be constant. Therefore, by calculating the maximum delay during message transmission between headers, the total network message delay can be expressed as 24.566 ms.

5.1. Comparing the Proposed Method with Previous Methods. Routing methods in VANET can be evaluated and compared based on different evaluation criteria. Since reducing the delay and increasing the data delivery rate are the main goals in the proposed method, we compare the proposed method with other state-of-the-art methods based on these criteria. The proposed method tries to reduce the delay in message transmission by choosing the optimal cluster head vehicles based on density criteria and close distance to other vehicles. On the other hand, by finding aligned vehicles and predicting the movement path of neighbor vehicles, it tries to transmit messages with high reliability, which reduces the loss rate of packets and increases the data delivery rate. Therefore, in Figure 15, the data delivery rate in the proposed method is compared with previous methods, including the method based on the farthest distance (FD) [34], the expected progress distance (EPD) [35], and the two-way stable communication (BDSC) [19] .

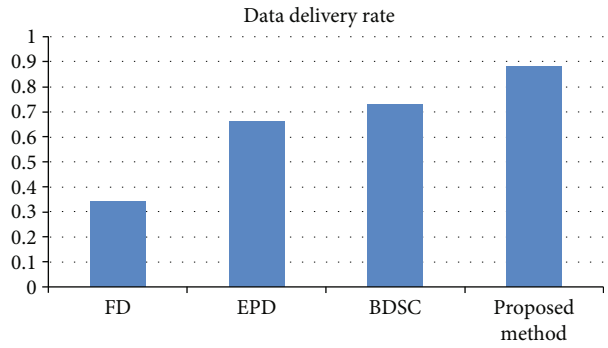

Figure 15: Comparing the delivery rate of the proposed method with previous methods.

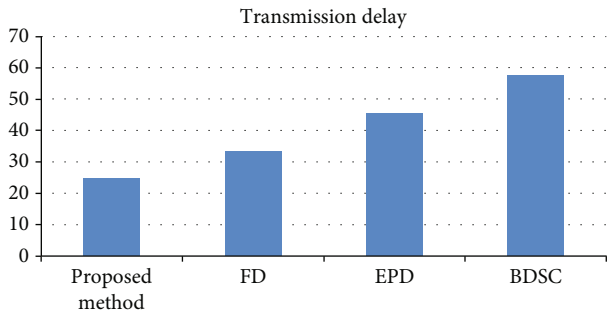

Figure 16: Comparing the delay of message transmission in the proposed method with previous methods.

As shown in Figure 15, the proposed method has a significant improvement in terms of package delivery rate compared to previous methods. Figure 16 also compares the message transmission delay in the proposed method with the previous methods included.

As shown in Figure 16, the proposed method has a lower value in terms of message transmission delay in the network compared to previous methods.

6. Conclusion and Discussion

The dissemination of real-time information in automotive case networks (VANET), due to the dynamic nature and rapid movement of vehicles, has become one of the research challenges in this field, which has attracted the attention of many researchers in this field. The data published in this network may not reach the destination in time due to changes in distances, redirects, and unforeseen movements by vehicles and may cause excessive delays. Therefore, informing the vehicles in the network quickly will be very useful in preventing accidents on the road. Therefore, in order to prevent disruption of the timely information process in automotive networks, strategies should be considered to reduce network latency. Also, previous related methods in the literature for data transmission in VANET have focused more on reliability and trust, and little attention has been paid to the prediction of vehicle movement and path pattern discovery in these types of networks. Therefore, in order to overcome this issue, the proposed method has presented an approach based on clustering and frequent pattern discovery in predicting the movement path of vehicles. In this research, a new method for data transfer and information in VANETs was proposed, which is based on discovering the trajectory of vehicles within the network and predicting the trajectory of future vehicles and sending messages based on clustering of aligned vehicles. The contributions of this paper are included, using the decision tree classification method to classify vehicles in aligned and not aligned vehicles, using sequential pattern mining to discover vehicle movement patterns, clustering vehicles in the network based on the current position to detect neighbor vehicles, and finding best cluster head to transfer messages using combination of above three steps. This research proposed a new method to discover the trajectory and clustering of vehicles, from the distance of each vehicle to the destination node at any time in order to extract the acceleration of the vehicle to the destination, vehicle speed, and vehicle distance to another vehicle, and the density of vehicles around the vehicle is used. The simulation results show that the proposed method with a delivery rate of 88.56% has significantly improved in terms of package delivery rate compared to previous methods. Also, the proposed method with a total delay of 24.566 ms in terms of message transmission delay in the network has a lower value compared to previous methods.

The limitation of the proposed method is to store the history of vehicle's movement on any type of road, and based on that, it produces movement patterns of vehicle and predicts the path of new vehicles. The proposed method stores the history of vehicle movement on any type of road, and based on that, it produces movement patterns of vehicle and predicts the path of new vehicles. It is natural that the more data related to vehicle movements in the proposed method, the more accurate in path pattern discovery. This method is more useful on busy roads where there are more vehicles than quiet roads. The accuracy of the proposed method will be lower in predicting the path pattern of the vehicles on quiet roads.

Data Availability

The simulated data used to support the findings of this study are included within the article.

Conflicts of Interest

The authors declare that they have no conflicts of interest.

Acknowledgments

This work was supported by 03 Special Project and 5G Project of Jiangxi Province under Grant 20204ABC03A18.

References

[1] B. Jarupan and E. Ekici, "Mobility management for efficient data delivery in infrastructure-to-vehicle networks," *Computer Communications*, vol. 35, no. 18, pp. 2274–2280, 2012.

[2] M. Bakhouya, J. Gaber, and P. Lorenz, "An adaptive approach for information dissemination in vehicular ad hoc networks,"

Journal of Network and Computer Applications, vol. 34, no. 6, pp. 1971–1978, 2011.

[3] Z. Peng, M. S. Jabloo, Y. D. Navaei et al., "An improved energy-aware routing protocol using multiobjective particular swarm optimization algorithm," *Wireless Communications and Mobile Computing*, vol. 2021, Article ID 6677961, 16 pages, 2021.

[4] X. Zhao, W. Zhong, and Y. D. Navaei, "A novel energy-aware routing in wireless sensor network using clustering based on combination of multiobjective genetic and cuckoo search algorithm," *Wireless Communications and Mobile Computing*, vol. 2022, Article ID 6939868, 14 pages, 2022.

[5] Z. Peng, M. Rastgari, Y. D. Navaei et al., "TCDABCF: a trust-based community detection using artificial bee colony by feature fusion," *Mathematical Problems in Engineering*, vol. 2021, Article ID 6675759, 19 pages, 2021.

[6] S. Einy, C. Oz, and Y. D. Navaei, "The anomaly- and signature-based IDS for network security using hybrid inference systems," *Mathematical Problems in Engineering*, vol. 2021, Article ID 6639714, 10 pages, 2021.

[7] S. Einy, C. Oz, and Y. D. Navaei, "Network intrusion detection system based on the combination of multiobjective particle swarm algorithm-based feature selection and fast-learning network," *Wireless Communications and Mobile Computing*, vol. 2021, Article ID 6648351, 12 pages, 2021.

[8] S. Einy, C. Oz, and Y. D. Navaei, "IoT cloud-based framework for face spoofing detection with deep multicolor feature learning model," *Journal of Sensors*, vol. 2021, Article ID 5047808, 18 pages, 2021.

[9] Y. Nanehkaran, Z. Licai, J. Chen et al., "Anomaly detection in heart disease using a density-based unsupervised approach," *Wireless Communications and Mobile Computing*, vol. 2022, Article ID 6913043, 14 pages, 2022.

[10] S. Jamali and Y. D. Navaei, "A two-level product recommender for E-commerce sites by using sequential pattern analysis," *International Journal of Integrated Engineering*, vol. 8, no. 1, 2016.

[11] Y. D. Navaei and M. Afzali, "Dihedral product recommendation system for E-commerce using data mining applications," *International Journal of Computer & Information Technologies (IJOCIT)*, vol. 3, pp. 610–631, 2015.

[12] Y. D. Navaei and M. Afzali, "A survey on product recommendation system in E-commerce," *International Journal of Computer & Information Technologies (IJOCIT)*, pp. 585–600, 2014.

[13] R. Zhang, H. Shu, and Y. D. Navaei, "Load balancing in edge computing using integer linear programming based genetic algorithm and multilevel control approach," *Wireless Communications and Mobile Computing*, vol. 2022, Article ID 6125246, 22 pages, 2022.

[14] Y. Nanehkaran, Z. Licai, J. Chen et al., "Diagnosis of chronic diseases based on patients' health records in IoT healthcare using the recommender system," *Wireless Communications and Mobile Computing*, vol. 2022, Article ID 5663001, 14 pages, 2022.

[15] H. Shahwani, S. Attique Shah, M. Ashraf, M. Akram, J. (. P.). Jeong, and J. Shin, "A comprehensive survey on data dissemination in vehicular ad hoc networks," *Vehicular Communications*, vol. 34, article 100420, 2022.

[16] T. Nadeem, P. Shankar, and L. Iftode, "A comparative study of data dissemination models for VANETs," in *2006 Third Annual International Conference on Mobile and Ubiquitous Systems: Networking & Services*, pp. 1–10, San Jose, CA, USA, 2006.

[17] M. M. Hamdi, O. A. R. Al-Dosary, O. A. S. Alrawi, A. S. Mustafa, M. S. Abood, and M. S. Noori, "An overview of challenges for data dissemination and routing protocols in VANETs," in *2021 3rd International Congress on Human-Computer Interaction, Optimization and Robotic Applications (HORA)*, pp. 1–6, Ankara, Turkey, 2021.

[18] M. Kakkasageri and S. S. Manvi, "Regression based critical information aggregation and dissemination in VANETs: a cognitive agent approach," *Vehicular Communications*, vol. 1, no. 4, pp. 168–180, 2014.

[19] O. Rehman, M. Ould-Khaoua, and H. Bourdoucen, "An adaptive relay nodes selection scheme for multi-hop broadcast in VANETs," *Computer Communications*, vol. 87, pp. 76–90, 2016.

[20] A. Louazani and L. Sekhri, "Petri net model for connectivity maintenance in VANET clustering-based routing algorithm," in *2016 International Conference on Advanced Aspects of Software Engineering (ICAASE)*, pp. 92–97, Constantine, Algeria, 2016.

[21] A. Jalooli, M. Song, and X. Xu, "Delay efficient disconnected RSU placement algorithm for VANET safety applications," in *2017 IEEE Wireless Communications and Networking Conference (WCNC)*, pp. 1–6, San Francisco, CA, USA, 2017.

[22] A. Abuashour and M. Kadoch, "Performance improvement of cluster-based routing protocol in VANET," *Ieee access*, vol. 5, pp. 15354–15371, 2017.

[23] R. Shahidi and M. H. Ahmed, "On the analytical calculation of the probability distribution of end-to-end delay in a two-way highway VANET," *IEEE access*, vol. 6, pp. 1109–1125, 2018.

[24] M. M. Mohammed Nasr, A. Abdelgader, Z. G. Wang, and L. F. Shen, "VANET clustering based routing protocol suitable for deserts," *Sensors*, vol. 16, no. 4, p. 478, 2016.

[25] S. P. Ardakani, "ACR: a cluster-based routing protocol for VANET," 2018, https://arxiv.org/abs/1805.07565.

[26] G. Rathee, A. Sharma, R. Iqbal, M. Aloqaily, N. Jaglan, and R. Kumar, "A blockchain framework for securing connected and autonomous vehicles," *Sensors*, vol. 19, no. 14, p. 3165, 2019.

[27] M. Poongodi, M. Hamdi, A. Sharma, M. Ma, and P. K. Singh, "DDoS detection mechanism using trust-based evaluation system in VANET," *IEEE Access*, vol. 7, pp. 183532–183544, 2019.

[28] A. Sharma and N. Kumar, "Third eye: an intelligent and secure route planning scheme for critical services provisions in Internet of vehicles environment," *IEEE Systems Journal*, vol. 16, no. 1, pp. 1217–1227, 2022.

[29] C. Wu, S. Ohzahata, and T. Kato, "Flexible, portable, and practicable solution for routing in VANETs: a fuzzy constraint Q-learning approach," *IEEE Transactions on Vehicular Technology*, vol. 62, no. 9, pp. 4251–4263, 2013.

[30] O. S. Oubbati, N. Chaib, A. Lakas, P. Lorenz, and A. Rachedi, "UAV-assisted supporting services connectivity in urban VANETs," *IEEE Transactions on Vehicular Technology*, vol. 68, no. 4, pp. 3944–3951, 2019.

[31] O. Sami Oubbati, N. Chaib, A. Lakas, S. Bitam, and P. Lorenz, "U2RV: UAV-assisted reactive routing protocol for VANETs," *International Journal of Communication Systems*, vol. 33, no. 10, article e4104, 2020.

[32] L. Zhao, Z. Li, A. Y. al-Dubai et al., "A novel prediction-based temporal graph routing algorithm for software-defined vehicular networks," *IEEE Transactions on Intelligent Transportation Systems*, vol. 23, no. 8, pp. 13275–13290, 2022.

[33] L. Zhao, T. Zheng, M. Lin, A. Hawbani, J. Shang, and C. Fan, "SPIDER: a social computing inspired predictive routing scheme for softwarized vehicular networks," *IEEE Transactions on Intelligent Transportation Systems*, vol. 23, no. 7, pp. 9466–9477, 2022.

[34] W. B. Jaballah, M. Conti, M. Mosbah, and C. E. Palazzi, "Fast and secure multihop broadcast solutions for intervehicular communication," *IEEE Transactions on Intelligent Transportation Systems*, vol. 15, no. 1, pp. 433–450, 2014.

[35] H. Okada, A. Takano, and K. Mase, "A Proposal of Link Metric for Next-Hop Forwarding Methods in Vehicular Ad Hoc Networks," in *2009 6th IEEE Consumer Communications and Networking Conference*, pp. 1–5, Las Vegas, NV, USA, 2009.

Hindawi
Wireless Communications and Mobile Computing
Volume 2022, Article ID 3884761, 8 pages
https://doi.org/10.1155/2022/3884761

Research Article

Jamming Attack in Vehicular Networks: Adaptively Probabilistic Channel Surfing Scheme

Anh Tuan Giang, Hoang Tung Tran, Huu Ton Le, Nhat Quang Doan, and Minh Huong Nguyen

University of Sciences and Technologies of Hanoi, Hanoi, Vietnam

Correspondence should be addressed to Anh Tuan Giang; giang-anh.tuan@usth.edu.vn

Received 8 April 2022; Accepted 29 June 2022; Published 11 July 2022

Academic Editor: Zahid Khan

Vehicular networks play a crucial role in Intelligent Transportation System (ITS), making transportation safer and more convenient. Most applications in ITS require information carried by basic safety messages (BSMs) to be exchanged periodically among vehicles. However, BSMs are vulnerable to different attacks, especially jamming attacks, due to their limited short message length and life span. In this paper, we analyze the impact of a jamming attack on BSMs and initially propose a random channel surfing scheme to attempt to react to the attack. We investigate the scheme by a simple extendible probabilistic model and simulation in NS-3. Obtained results provide a reference to design an optimal channel surfing scheme that adapts to its supported applications.

1. Introduction

Vehicular networks facilitate communication among vehicles (V2V) and between vehicles and roadside infrastructure (V2I) in the transportation network. Thanks to this communication, the network infrastructure can serve an extensive range of applications. Among these, safety applications that make transportation safer are one crucial type. They operate based on essential information included in basic safety messages (BSMs), such as position, velocity, acceleration of vehicles, and hazardous incident warnings. Due to the requirement of freshness and the compact of information, BSMs are exchanged periodically every 100ms [1, 2] and have short lengths. These characteristics make BSMs prone to be targets of many types of wireless attacks, especially attacks at the physical and medium access control layer, such as jamming attacks. Limited packet length does not allow complex cryptography. The short life span, in milliseconds, makes BSMs easily become victims of simple but effective attacks like jamming attacks, as no time is taken for the attacker to do complex computations.

Jamming is one kind of Denial-of-Service (DoS) attack. It broadcasts radio signals in the physical channel to block any communication in the same physical channel within its transmission range. Jamming can be either constant jamming or reactive jamming. In constant cases, the attacker continually emits radio signals not following any rule of communication protocol. In reactive jamming, the attacker (so-called the jammer) transmits radio signals upon sensing a transmission in the medium. Reactive jamming is more dangerous and harder to detect as it conforms to legitimate transmission [3]. The impact of jamming is graver to safety applications because of their time constraints. The consequence can be severe if the safety-related information is not delivered to the appropriate vehicles at the right time because of the interruption caused by jamming.

While the impact of a jamming attack is profound for safety applications, mitigation against them in vehicular networks encounters even more challenges. Indeed, characteristics of the vehicular environment have raised these challenges in VANETs. The main ones include issues of inherent properties of radio channels, highly dynamic oper-

ating environment, lack of centralized management, high-reliability requirements, and low latency communication and scalability.

In the case of BSMs, it becomes even more challenged because BSMs are supposed to be transmitted only in the control channel and renewed every short-time period (100 ms, as the suggestion in [1, 2]). It relates to a multichannel operation specified in the suit of standards IEEE 1609 for Wireless Ad hoc Vehicular Environments (WAVEs). According to the suit of standards, vehicles switch alternatively between one control channel (CCH) to any service channel (SCH), as illustrated in Figure 1. This working mechanism allows single-PHY devices, or vehicles in VANETs, to access high-prioritized data and management traffic in CCH during CCH intervals (CCHIs), as well as general traffic in SCH intervals (SCHI).

There are a considerable number of proposals dealing with jamming attacks, one of the most practical proposed approaches is channel surfing [4]. After detecting jamming [5] [6] (jamming detection are out of our scope), communication devices change from the current jammed channel to other available channels. The question is which channel should be chosen provided that the communication can be remained among as many devices as possible while other performance and security constraints should be satisfied. The concept of channel surfing is commonly studied in wireless and vehicular networks but is not dedicated to safety applications. This paper focuses on safety applications in vehicular networks, precisely the critical type of messages, the BSMs.

Our contributions are in both mathematical and networking aspects. Firstly, we study the integration of mitigation against jamming attacks from wireless networks into VANETs and propose an adapted channel surfing scheme to deal with jamming attacks on safety applications in VANETs. Secondly, we offer a probabilistic model in the evaluation of our works. Simulation results validated the model. Furthermore, the results allow us to choose appropriate parameters of the scheme for the delay requirement of safety applications.

The paper is organized as follows: the threat of jamming attacks on safety applications in vehicular networks is briefly described in this Section 1; Section 2 discusses related works on methods to deal with jamming attacks in wireless networks; our random channel surfing scheme is elaborated in Section 3; the analytical model to investigate our proposed scheme is defined in Section 4; the obtained numerical results are validated by simulation and also analyzed in details in Section 5; Section 6 concludes the paper.

2. Related Works

Many research efforts focus on designing defense strategies for vehicular networks, but the problem remains an open issue. Several approaches have been developed in wireless networks to defend against jamming attacks. We can classify these solutions into two types of strategies: competition strategy and retreat strategy. In the competition strategy, nodes reduce jamming effects by adjusting their physical-layer parameters such as transmit power, data rate, and carrier sensing threshold [3]. Because the radio channel substantially impacts communication in the vehicular environment, one should carefully consider the feasibility of competition strategy in vehicular networks. Besides, the retreat strategy seems more practical for communication in the vehicular environment. In retreat strategy, devices must coordinate to switch to the same new channel when jamming attacks block the current channel. However, channel coordination emerges as a problem for broadcasting, and BSM exchange has a broadcasting nature. This paper considers the feasibility of retreat strategy and channel surfing approach, particularly an attempt to deal with jamming attacks on BSMs.

In wireless networks, channel surfing approaches have been proposed [4, 7–9]. The crucial point making channel surfing feasible is how devices agree beforehand on the channel switching sequence. Based on how devices choose the channel switching sequence, channel surfing approaches can be classified into prior negotiation and without negotiation. In prior negotiation, devices must exchange information to make a channel agreement [10]. Considering Wi-Fi communication, Navda et al. [10] proposed a channel surfing scheme on which the access point generates a pseudo-random channel sequence, encrypts it, and exchanges it securely using the client's public key. In [8], the authors propose a coordinated channel-switching strategy. The devices, or nodes, detect themselves as jammed nodes, switch immediately to the orthogonal channel, and wait for chances to reconnect to the entire network. The boundary nodes who lose connectivity with their neighbors monitor available channels and connectivity to their neighbors in these channels. Finally, the boundary node selects the new channel and notifies all other nodes. Performance of channel surfing approaches also varies accordingly to the mobility of the networks because of the change in neighborhood leading to the variation of the number of neighbors [11, 12].

The prior negotiation may guarantee the channel agreement after jamming detection; however, it can be vulnerable to attackers. Negotiation data is exposed and possibly intercepted; thus, one can reveal the surfing sequence or information of the new channel. For this reason, Djuraev et al. propose a channel surfing scheme without prior negotiation. They use transmission power and received signal strength to determine the next channel in [4]. In [7], two entities, A and B, exchange packets, and B sends a data packet to A. Then, A acknowledges back to B in the following ACK. The next channel is determined based on the received signal strength indicator of the data packets and ACKs received at corresponding entities. Considering physical technology to deal with jamming, Strasser et al. propose a frequency hopping on which the two communication entities switch their channel at different rates [9]. There exist time slots that the two entities can encounter. The technique requires advanced transceivers and does not reach high channel utilization. The issue of effective coordination among vehicles to react to jamming attacks remains [3, 13].

The abovementioned approaches focus on communication between only two entities in wireless networks.

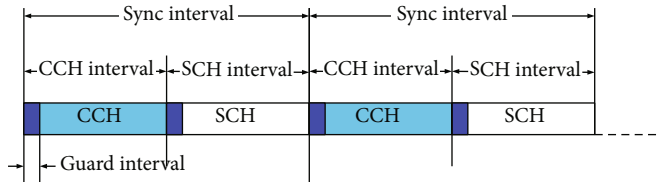

Figure 1: Multiple operation: alternating access.

Mitigating jamming attacks in vehicular networks for broadcast communication is still an open issue. There have been several works on broadcast in wireless networks. The authors in [14] utilize spreading code to cope with jamming in broadcast scenarios. The proposed protocol applies to the Code Division Multiple Access (CDMA) system. In [15], the authors propose a collaborative broadcast scheme using the uncoordinated frequency hopping technique. According to this scheme, nodes receiving a broadcast message will help forward it to other nodes. There are always opportunities for nodes to exchange messages through unjammed channels. As one of the limited number of works that consider broadcast in VANETs, [16] proposes a hideaway strategy. Vehicles stop all transmission until the jammer moves away. It means communication is interrupted for an undetermined period. Focusing on safety applications in vehicular networks, in this paper, we initially propose an adaptively probabilistic channel surfing scheme that adapts to their characteristics, such as broadcast manner, multiple channel operation, and short lifespan of BSMs. This scheme is an extended version of the one proposed in [17]. We study our scheme in a mathematical model and use simulation to validate the results. The mathematical model allows us to tune the scheme to achieve the time constraint requirements of safety applications in vehicular networks. We elaborate on the detail of the scheme in the following section.

3. Adaptively Probabilistic Channel Surfing Scheme

3.1. Assumption. This paper assumes vehicles that participated in the network have been deployed with some safety applications, and these applications always have safety information that is needed to broadcast through BSMs. Second, the jammer will attack the network at a given time. According to the standard IEEE 1604.9, vehicles alternatively switch from one CCH to one of 6 available SCHs to accommodate corresponding services. BSMs are exchanged periodically every 100 ms at CCHIs. In case of being attacked, communication in CCH is blocked by a reactive jammer that emits a noninformation radio signal whenever it senses a transmission within its sensitivity range. After detecting the attack of the jammer, vehicles will trigger our proposed random channel surfing scheme. Vehicles change their operating channel to a random one of the 6 SCHs instead of CCH during each CCHI. For SCHIs, vehicles keep their original schedule to maintain non-safety services. Every vehicle is supposed to have one safety-related information included in several BSMs that should be sent repeatedly within a certain period, provided that the number of vehicles that received the information is as high as possible. In this work, vehicles continuously transmit the safety information till the transmission times reach 100, i.e., during 10 seconds.

3.2. Random Channel Surfing Scheme. When a vehicle detects a jamming attack, the channelSurfing() procedure implemented in this vehicle is triggered. First, the vehicle chose a set of predefined probability parameters for channel assignment. The values of those parameters represent the probabilities of which SCH channels will be assigned for the next CCHI. The applications that need to broadcast their safety information must choose which set of parameters. Criteria are selected based on their designs and requirements of time constrain. In this paper, we evaluate three different sets of predefined probability parameters (Table 1). The first set corresponds to when choosing one of the available SCHs is uniformly distributed between 1 and 6. In the second and third cases, the distribution of choosing SCH is linear and geometric. Figure 2 illustrates these distributions.

Once the channel number is assigned, the vehicle switches to that channel for the next CCHI. The SCH number follows the same distribution the vehicle chooses at the beginning. The channelSurfing() procedure is detailed in Algorithm 1. After the jamming attack is confirmed and the communication fails, this procedure first calls the channelGenerator() function. This function returns the number of SCH based on the type of safety application. Each application has a corresponding set of probability parameters. Next, the application stops communication on the current SCH, and a new SCH will be used in the next CCHI. The channelSurfing() procedure will be executed until the communication is recovered (receiving BSMs).

3.3. Evaluation Metric. We can evaluate the usefulness of this random channel surfing scheme by the mean number of vehicles that can recover the communication when suffering a jamming attack after a time interval t. It means that after t CCHIs (BSMs are exchanged periodically every CCHI), the larger the mean number of vehicles that receive BSMs is, the better the performance of the proposed scheme is. The evaluation of this proposed scheme thus boils down to finding out the average number of vehicles that receive the BSMs after t CCHIs.

4. Analytical Model

Proposition 1. *We consider the random channel surfing described in the previous section. Let N be the number of vehicles receiving BSMs from a sender. Let K_t be the random variable representing the number of vehicles able to receive*

Table 1: Different sets of probability parameters.

	p_1	p_2	p_3	p_4	p_5	p_6
Uniform distribution	$\frac{1}{6}$	$\frac{1}{6}$	$\frac{1}{6}$	$\frac{1}{6}$	$\frac{1}{6}$	$\frac{1}{6}$
Linear distribution	$\frac{3}{10}$	$\frac{2.5}{10}$	$\frac{2}{10}$	$\frac{1.5}{10}$	$\frac{0.5}{10}$	$\frac{0.5}{10}$
Geometric distribution	$\frac{5}{10}$	$\frac{2}{10}$	$\frac{1.5}{10}$	$\frac{1}{10}$	$\frac{0.5}{10}$	$\frac{0.5}{10}$

BSMs after t CCHIs. Then, $K_t \sim Binomial(N, \sum_{i=1}^{t}(1-p)^{i-1}p)$ with its probability mass function:

$$\mathbb{P}(K_t = c) = \binom{N}{c}\left(\sum_{i=1}^{t}(1-p)^{i-1}p\right)^{c} \times \left(1 - \sum_{i=1}^{t}(1-p)^{i-1}p\right)^{N-c}, \tag{1}$$

where $p = \sum_{i=1}^{6} p_i^2$ is the matching probability for sender and receivers to stay in the same SCH number, p_i is the probability that SCH number i will be assigned. The mean number of vehicles that can receive BSMs after t timeslot is

$$\mathbb{E}[K_t] = N\sum_{i=1}^{t}(1-p)^{t-1}p = f(t,p). \tag{2}$$

Proof. Firstly, communication can only happen if the sender and receiver work in the same channel frequency. According to the assumption, the sender and receiver can randomly choose one of the six SCHs. The matching probability p for them to stay in the same SCH is given by:

$$\begin{aligned} p &= \mathbb{P}(\text{channel}_{\text{sender}} = \text{channel}_{\text{receiver}}) \\ &= \sum_{i=1}^{6}\mathbb{P}(\text{channel}_{\text{sender}} = i, \text{channel}_{\text{receiver}} = i) \\ &= \sum_{i=1}^{6}\mathbb{P}(\text{channel}_{\text{sender}} = i)\mathbb{P}(\text{channel}_{\text{receiver}} = i) = \sum_{i=1}^{6} p_i^2 \end{aligned} \tag{3}$$

Secondly, call T the number of CCHIs until a receiver receives the BSM message. The best scenario is $T = 1$, meaning that the receiver gets the message immediately. The worst scenario occurs when $T \longrightarrow \infty$, meaning this receiver always selects the channel differently from the sender. Indeed, T is a discrete random variable that could take any value from 1 to ∞. For instance, consider the case $T = 9$, which means that in 8 previous timeslots, this receiver did not receive the message. As mentioned above, at any given timeslot, the probability that the receiver gets the message is p, and the probability of not receiving the message is $1 - p$. Thus, the probability of $T = 9$ is given by

$$\mathbb{P}(T = 9) = \left(1 - p(1-p)^{8}p. \right. \tag{4}$$

Specifically, the random variable T follows the Geometric distribution with parameter p: $T \sim \text{Geometric}(p)$ and its probability mass function (PMF) is

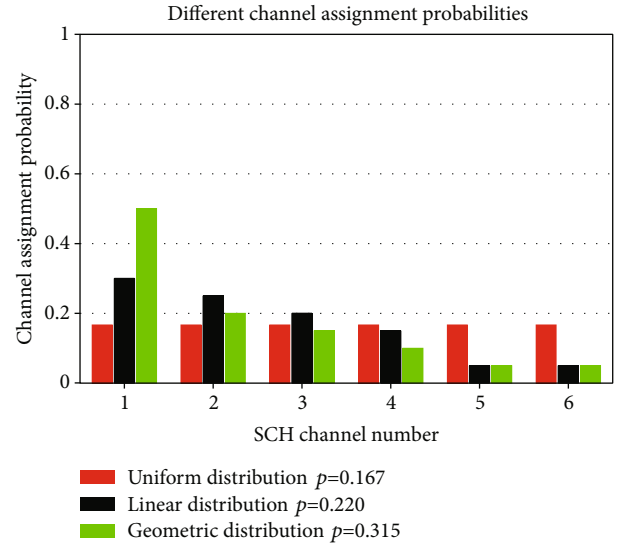

Figure 2: SCH assignment probability distributions.

$$\mathbb{P}(T = t) = (1-p)^{t-1}p. \tag{5}$$

So, the probability for the receiver to receive the message at a given timeslot $T = t$ is given by

$$\mathbb{P}(T \le t) = \sum_{i=1}^{t}\mathbb{P}(T = i) = \sum_{i=1}^{t}(1-p)^{i-1}p. \tag{6}$$

Finally, consider the number of receiver that got the message after t timeslots, K_t. Each receiver has $\sum_{i=1}^{t}(1-p)^{i-1}p$ chance to receive the message independently from other receiver, and K_t is fundamentally a Binomial random variable $K_t \sim \text{Binomial}(N, \sum_{i=1}^{t}(1-p)^{i-1}p) + .$ □

4.1. Application of Random Channel Surfing Model. One direct application of our analytical model for this random channel surfing scheme is to optimize the design of safety applications in vehicular networks. Indeed, safety applications are sensitive to time constrain. A natural way to improve the communication of safety applications when suffering jamming attacks is to adjust the matching probability. From (2), we can write

$$p = f^{-1}(t, \mathbb{E}[K_t]). \tag{7}$$

Thus, p can be computed as a function of t and $\mathbb{E}[K_t]$.

Figure 3 depicts the mean number of vehicles that can recover communication as regards time (computed from the number of CCHIs). As the analytical model showed, when p is uniformly distributed, we need almost 1 second for 80% of vehicles to recover. In case p is geometrically distributed ($p = 0.315$), only 0.5 seconds is required for 80% of vehicles to reestablish the communication. Thus, by adjusting the channel assignment probabilities, a safety application

Input: jamming alert signal
Output: new communication channel
begin
  if*a jamming attack is detected***then**
    while*communication is false***do**
      Choose a new channel for the appropriate application;
      Stop communication on the current channel;
      Start communication on the new selected channel;

Algorithm 1: ChannelSurfing() procedure.

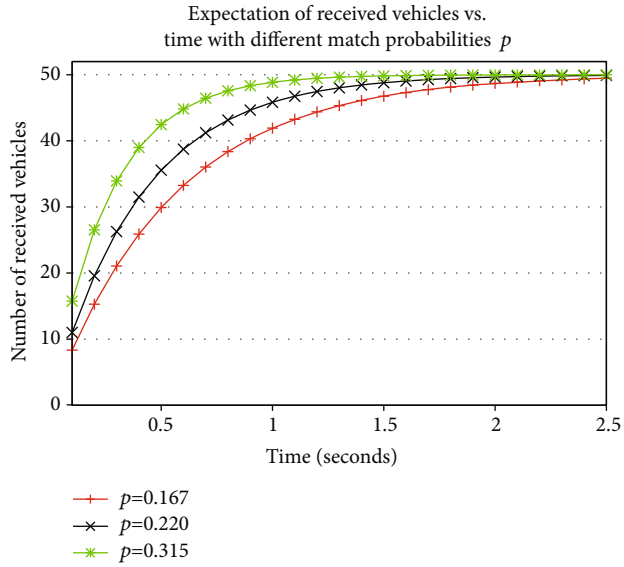

Figure 3: Comparison between theoretical results in case the choosing of SCHs is uniformly ($p = 0.167$), linearly ($p = 0.220$), and geometrically ($p = 0.315$) distributed.

can easily achieve its target of how many vehicles can be notified about safety information within a certain time slot.

5. Performance Evaluation

We evaluate our random channel surfing scheme by the number of vehicles receiving one information sent by a vehicle, called the sender, after a given time which is computed in a number of CCHIs. The analytical model and simulation allow us to study many scenarios with a different number of vehicles in the network. Due to lack of space, we present only the result for the scenario of $N + 1 = 51$ vehicles in a communication range. Among $N + 1$ vehicles, one vehicle plays the sender role. It retransmits its information in messages broadcast every CCHI. Every vehicle switches randomly to one of 6 service channels every CCHI when the jamming attack is detected. The numerical result obtained from the analytical model allows us to determine $\mathbb{E}[K_t]$, the expectation or the average number of vehicles that received the information after t CCHIs. To validate the analytical model, we run simulations in NS-3 [18] with the channelSurfing() procedure being implemented in all vehicles (nodes) and using the WAVE model that is specified for the vehicular environment. The IEEE standard 802.11p and the 1609 standard set are implemented in the simulations. All simulation results are computed at 95% confidence intervals. We evaluate our scheme with three different sets of probabilities parameters (p_1, p_2, p_3) given in Table 1 and consider two cases of mobility: constant mobility where vehicle pattern has been fixed and traffic mobility where a traffic simulator generates vehicle pattern. Parameters used in the simulation are listed in Table 2.

5.1. Constant Mobility. Firstly, we analyze our scheme by studying the average number of received vehicles after a given time. Analytical and simulation results are compared in all figures. Figures 4–6 show the increase in the average number of vehicles that receive the information; in another words, the expectation of random variable K_t as defined in the previous section. This figure also displays its corresponding standard deviation, which expresses how the real value differs from the average one. The simulation results validate the analytical results: they closely match the analytical results. At early CCHIs, the number of received vehicles increases dramatically and reaches 80%, i.e., nearly 40 vehicles at 9^{th} CCHI in case $p = 0.167$ (5^{th} and 7^{th} in case $p = 0.220$ and $p = 0.315$, respectively). After that, the number increases insignificantly. Almost vehicles, up to 48 among 49 vehicles, received information after 25 CCHIs (2.5 seconds). Matching the time requirement of ITS safety application specified in [19], approximately 80% of vehicles using our scheme can satisfy the maximum latency of a given safety application of 1 second. Depending on the use cases of applications, this performance can probably be acceptable. Thus, it raises the question of which cases this performance is reasonable. Then, in these cases, the information should be more critical to some vehicles than others. For example, vehicles close to the origin of the information about an incident may be much more impacted than vehicles at a far distance. Therefore, it is potential to extend our channel surfing scheme with the idea of prioritizing the receivers. It means that the scheme should somehow manage groups of vehicles provided that higher prioritized vehicles must be acknowledged of the safety information early, while others can loosen the time constraint.

Secondly, our analytical model also allows us to figure out the likely number of received vehicles after a certain time. Figure 7 depicts the probability distribution of the obtained value of K_t at 10^{th} CCHIs in the analytical model and so in simulation. The number of received vehicles

Table 2: Parameters used in simulations.

Parameters	Value
Number of vehicles	51
CCHI	50ms
Frequencies of channels	DSRC allocated spectrum [3]
Samples per point	100
Jamming attack event	At 2.0 seconds
SCH assignment probabilities	Uniform, linear and geometric Distribution
Message size	100 bytes
Number of retransmissions	100
Simulation time	12 seconds

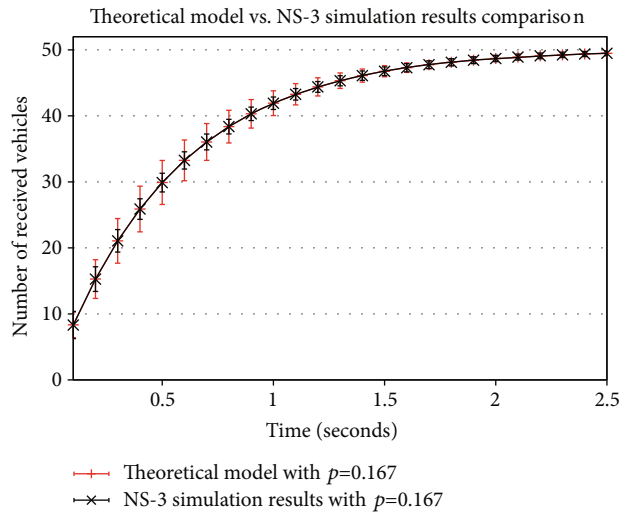

Figure 4: Comparison between simulation and theoretical results in case SCH is uniformly distributed.

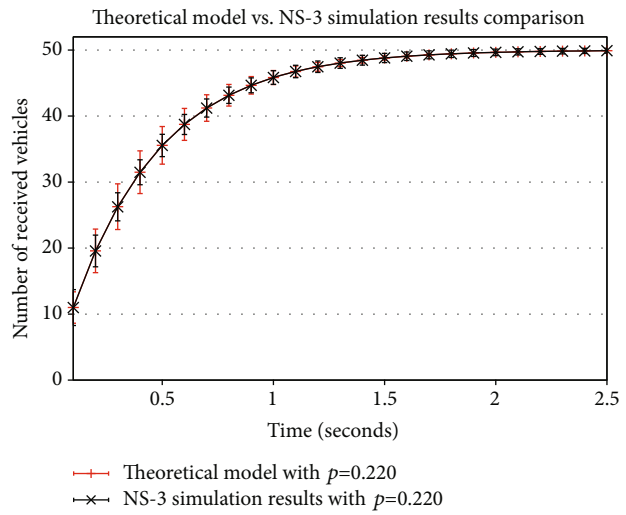

Figure 5: Comparison between simulation and theoretical results in case SCH is linearly distributed.

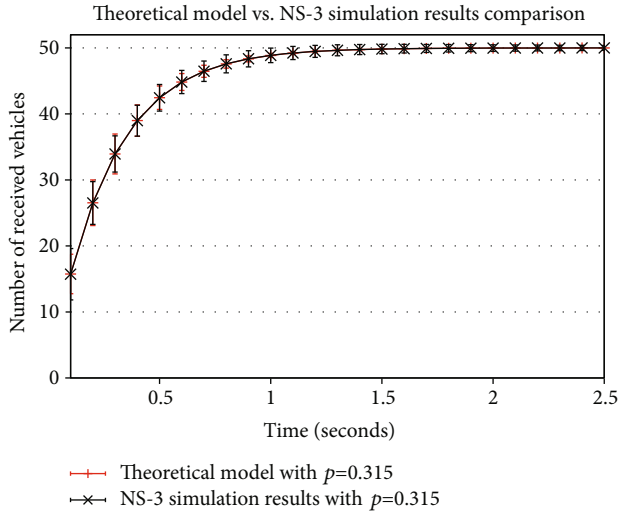

Figure 6: Comparison between simulation and theoretical results in case SCH is geometrically distributed.

approximately ranges from 34 to 46. It means that about 70% to 93% of vehicles are warned about the information after 1 second. The value has the highest probability at 41(83%) in theory and 43(88%) in simulation. The probability distribution of K_t after 5 CCHIs is illustrated in Figure 8. After 5 CCHIs, 19(39%) to 23(47%) vehicles receive the information. The results indicate the list of possible values of the number of received vehicles after a given time. It can be a reference to select the proposed scheme for suitable applications in terms of the freshness of exchanged information, expected informing scale of information, and network parameters such as the number of vehicles, density, available frequencies.

5.2. Traffic Mobility. To evaluate the impact of realistic traffic patterns, we generate vehicle locations from a traffic simulator in this scenario. This traffic simulator allows us to emulate driver behavior faithfully. On a highway, driver behavior is limited to accelerating, braking, and changing lanes. We assume that there is no off-ramp on the section of the highway. The desired speed is associated with each vehicle. It corresponds to the speed that the driver would reach if he was alone in his lane. If the driver is alone (the downstream vehicle is sufficiently far), he adapts his acceleration to reach his desired speed (free-flow regime). If he is not alone, he adapts his acceleration to the vehicles around him (car following regime). He can also change lanes if the conditions of another lane seem better. All these decisions are functions of traffic conditions (speed and distance) and random variables used to introduce a different behavior for each vehicle. This kind of simulation is called microsimulation [20], and the model we used, which has been tuned and validated with regard to real data collected on a highway, is presented in detail in [21, 22]. We simulated a road/highway with this traffic simulator with three lanes, and the simulation time was 60 minutes. The vehicle positions are then injected into NS-3 for simulation. In this

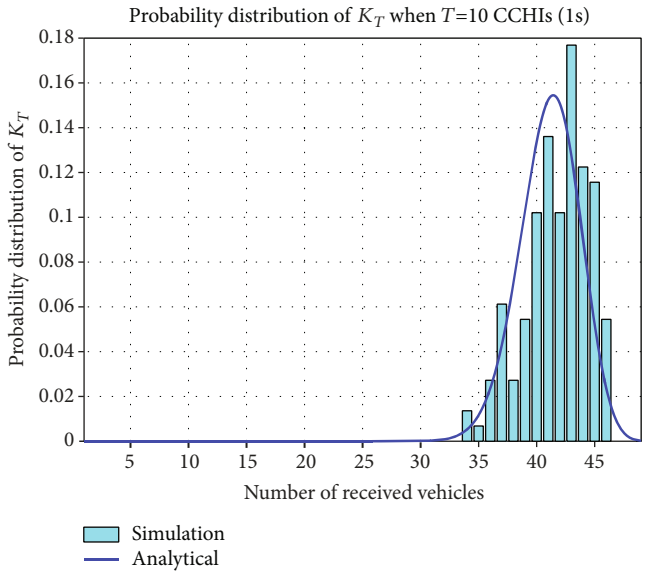

Figure 7: Probability distribution of the number of received vehicles after $t = 10$ CCHIs (1 s.)

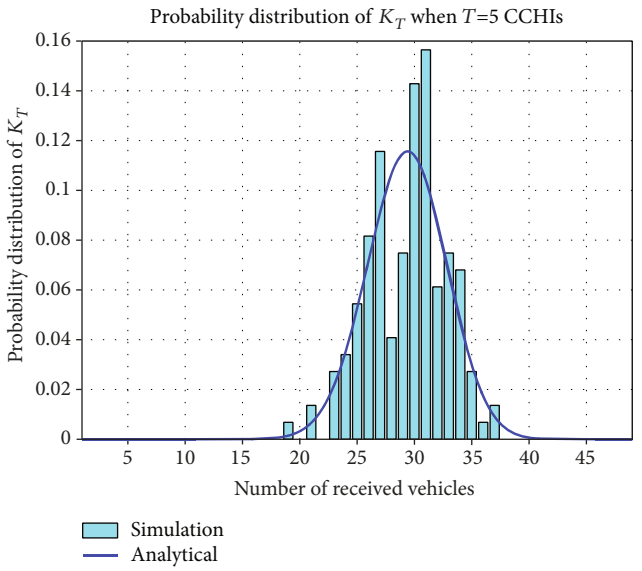

Figure 8: Probability distribution of the number of received vehicles after $t = 5$ CCHIs (0.5 s)

scenario, we also consider 50 receivers in the communication range of the sender as in the constant mobility case.

In Figure 9, we compare the simulation results performed with different traffic intensities (λ) in traffic mobility and constant mobility scenarios. For both scenarios (constant and traffic mobility), the channel assignment probability is the same and uniformly distributed ($p = 0.167$). As shown, the traffic pattern has an important impact on the performance of our proposed scheme. When the traffic intensity is high ($\lambda = 5$, the mean distance between two consecutive vehicles is 5 meters), the average number of vehicles that can be acknowledged of the information is about 10%

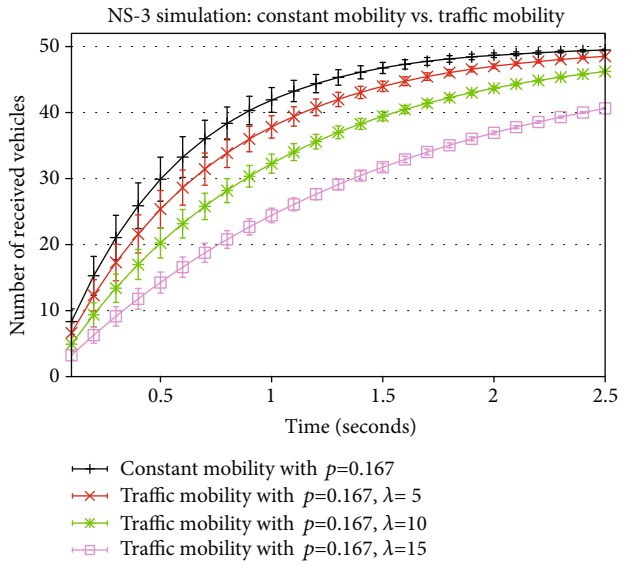

Figure 9: Comparison between constant mobility and different traffic mobility scenarios.

lower than the constant mobility case at $t = 1$ s. Moreover, we can observe a significant decrease (30% and 60%, respectively, at $t = 1$ s) in the performance of the traffic mobility scenario when considering low traffic intensities ($\lambda = 10, \lambda = 15$). This may happen due to the high frame error rate in the traffic mobility scenario. The traffic simulator mimics the real traffic pattern where vehicles are likely to form clusters. Consequently, vehicles that belong to a far cluster could not receive any message even when they chose the same SCH as the sender.

6. Conclusion

This paper investigated the feasibility of a channel surfing approach against jamming attacks in vehicular networks, especially for safety applications with strict time constraints and a broadcast nature. We initialize and implement a random channel surfing scheme in vehicular networks. A simple, extensible probabilistic model is proposed to evaluate and study the favorable use case of our scheme. This model provides the key to designing safety applications sensitive to time constrain by adjusting SCH assignment probabilities. We validate the analytical model by NS-3 simulations. The simulation results have shown that a large number of vehicles can recover their communication within an acceptable time. The real traffic pattern has an essential effect on the performance of this random channel surfing scheme. We are currently working on an extension of this model that takes into account the frame error rate to model the real testbed scenarios accurately reported in this manuscript.

Data Availability

No data were used to support this study.

Conflicts of Interest

The authors declare that they have no conflicts of interest.

Acknowledgments

The authors would like to thank the University of Sciences and Technologies of Vietnam, Vietnam Academy of Science and Technology (VAST), for funding this research in the scope of project USTH.ICT.01/21-22. The original idea about the random channel surfing scheme was partially published at the 2020 RIVF International Conference on Computing and Communication Technologies (RIVF) [17]. We would like to thank Professor Anthony BUSSON (LIP, ENS Lyon) and Professor Yacine Ghamri-Doudane (L3I, University of La Rochelle) for their enthusiastic discussions that allowed us to extend our previous work to this version.

References

[1] SAE International, *Dsrc Implementation Guide. A Guide of Users of sae j2735 Message Sets Over dsrc*, 2010.

[2] A. T. Giang, A. Lambert, A. Busson, and D. Gruyer, "Topology control in VANET and capacity estimation," in *2013 IEEE Vehicular Networking Conference*, pp. 135–142, Boston, MA, USA, December 2013.

[3] H. Nguyen-Minh, *Contribution to the Intelligent Transportation System: Security of Safety Applications in Vehicle Ad Hoc Networks*, PhD thesis, University of Avignon, 2016.

[4] S. Djuraev, J.-G. Choi, K.-S. Sohn, and S. Y. Nam, "Channel hopping scheme to mitigate jamming attacks in wireless LANS," *EURASIP Journal on Wireless Communications and Networking*, vol. 2017, no. 1, 2017.

[5] A. Benslimane and H. Nguyen-Minh, "Jamming attack model and detection method for beacons under multichannel operation in vehicular networks," *IEEE Transactions on Vehicular Technology*, vol. 66, no. 7, pp. 6475–6488, 2017.

[6] L. Wang and A. M. Wyglinski, "A combined approach for distinguishing different types of jamming attacks against wireless networks," in *Proceedings of 2011 IEEE Pacific Rim Conference on Communications, Computers and Signal Processing*, pp. 809–814, Victoria, BC, Canada, August 2011.

[7] S. Chen, K. Zeng, and P. Mohapatra, "Jamming-resistant communication: channel surfing without negotiation," in *2010 IEEE International Conference on Communications*, pp. 1–6, Cape Town, South Africa, May 2010.

[8] X. Wenyuan, W. Trappe, and Y. Zhang, "Channel surfing: defending wireless sensor networks from interference," in *2007 6th International Symposium on Information Processing in Sensor Networks*, pp. 499–508, Cambridge, MA, USA, April 2007.

[9] M. Strasser, C. Pöpper, and S. Čapkun, "Efficient uncoordinated fhss anti-jamming communication," in *Proceedings of the tenth ACM international symposium on Mobile ad hoc networking and computing - MobiHoc '09*, pp. 207–218, New Orlean, LA, USA, 2009.

[10] V. Navda, A. Bohra, S. Ganguly, and D. Rubenstein, "Using channel hopping to increase 802.11 resilience to jamming attacks," in *IEEE INFOCOM 2007 - 26th IEEE International Conference on Computer Communications*, pp. 2526–2530, Anchorage, AK, USA, May 2007.

[11] H. Nguyen-Minh, A. Benslimane, and M. Radenkovic, *Social Delay Tolerant Protocol for Safety Services in Vehicular Networks*.

[12] H. N. Minh, A. M. Vegni, V. Loscrí, and A. Benslimane, "Connectivity management in an integrated heterogeneous social networks framework in vehicular environments," in *Proceedings of the Conference on Information Technology for Social Good*, pp. 25–30, New York, NY, USA, September 2021.

[13] N. Lyamin, D. Kleyko, Q. Delooz, and A. Vinel, "Ai-based malicious network traffic detection in VANETs," *IEEE Network*, vol. 32, no. 6, pp. 15–21, 2018.

[14] J. T. Chiang and H. Yih-Chun, "Cross-layer jamming detection and mitigation in wireless broadcast networks," *IEEE/ACM Transactions on Networking*, vol. 19, no. 1, pp. 286–298, 2011.

[15] L. Xiao, H. Dai, and P. Ning, "Jamming-resistant collaborative broadcast using uncoordinated frequency hopping," *IEEE Transactions on Information Forensics and Security*, vol. 7, no. 1, pp. 297–309, 2012.

[16] I. K. Azogu, M. T. Ferreira, J. A. Larcom, and H. Liu, "A new anti-jamming strategy for VANET metrics-directed security defense," in *2013 IEEE Globecom workshops (GC Wkshps)*, pp. 1344–1349, Atlanta, GA, USA, December 2013.

[17] N.-M. Huong, T. Hoang Tung, G. Anh Tuan, and H. Thanh Tung, "Channel surfing to mitigate against jamming attacks on safety applications in vehicular networks," in *2020 RIVF International Conference on Computing and Communication Technologies (RIVF)*, pp. 1–5, Ho Chi Minh City, Vietnam, October 2020.

[18] "Network simulator 3 - ns3," http://www.nsnam.org.

[19] ETSI TS 102 637-2 V1.1.1, "Intelligent transport systems (its); vehicular communications; basic set of applications; part 2: Specification of cooperative awareness basic service," 2010.

[20] S. Druitt, "Introduction to microsimulation," *Traffic Engineering & Control*, vol. 39, no. 9, 1998.

[21] K. I. Ahmed, *Modeling Drivers' Acceleration and Lane Changing Behavior*, PhD thesis, Massachusetts Institute of Technology, 1999.

[22] A. T. Giang and A. Busson, "Modeling CSMA/CA in VANET," in *ASMTA*, Springer, 2012.

Hindawi
Wireless Communications and Mobile Computing
Volume 2022, Article ID 3909685, 13 pages
https://doi.org/10.1155/2022/3909685

Research Article

High-Capacity Data Collection Platform for Smart Cities Using IEEE 802.11ad-Based Millimeter-Wave V2X Communication

Kosei Nakano,[1] **Hiroyuki Motozuka**,[2] **Gaius Yao Huang Wee**,[3] **Masataka Irie**,[1] **Akihiro Egami**,[1] **Takenori Sakamoto**,[1] **Koji Takinami**,[1] **and Kazuaki Takahashi**[1]

[1]*Panasonic Industry, Co., Ltd., 600 Saedo-cho, Tsuzuki-ku, Yokohama City 224-8539, Japan*
[2]*Panasonic Intellectual Property Management Co., Ltd., 600 Saedo-cho, Tsuzuki-ku, Yokohama City 224-8539, Japan*
[3]*Panasonic R&D Center Singapore, Panasonic Asia Pacific Pte. Ltd., Singapore 469332*

Correspondence should be addressed to Kosei Nakano; nakano.kosei@jp.panasonic.com

Received 19 April 2022; Accepted 22 June 2022; Published 9 July 2022

Academic Editor: Zahid Khan

The collection and utilization of huge sensor data from vehicles for visualizing the city is expected to realize various enhanced services for smart cities. A next-generation gigabit vehicle-to-everything (V2X) data collection platform based on 60 GHz millimeter-wave (mmWave) small cell radio access has been proposed in the previous work for enabling efficient and high-capacity data upload from vehicles to the cloud. This paper presents further analysis of the initial link setup delay to evaluate the effectiveness of the fast initial V2X link setup method proposed, which is suitable for 60 GHz communication based on IEEE 802.11ad. This paper also presents the application programming interface (API) design based on the hypertext transport protocol (HTTP) to enable the efficient upload of hundreds of files. Combined with the buffering technique at a multiaccess edge computing (MEC) server, the proposed system successfully utilizes very high bandwidth between a vehicle and a MEC server. The proposed methods achieve a 30 times improvement in delay for establishing the initial link and an 11 times higher average throughput. A prototype system installed in Marysville, Ohio, achieved a peak throughput of 2.8 Gbps and successfully demonstrates the effectiveness of city visualization based on high-capacity data collection and analytics.

1. Introduction

With the recent advances in Advanced Driver Assistance Systems (ADAS) and autonomous driving technologies, vehicles are expected to collect huge amounts of data from onboard sensors such as cameras, sonars, and Global Positioning System (GPS)/Global Navigation Satellite System (GNSS) devices [1, 2]. By analyzing the collected data and visualizing the city, various services for smart cities can be realized, such as enhanced traffic control and expedited emergency response [3]. Demonstrations which utilize such collected data have been on the rise in various cities and countries [4], and efficient data collection of real-time high-resolution data and massive amounts of delay-tolerant data [5] via wireless communication from vehicles in the city is becoming increasingly relevant.

Existing vehicle-to-everything (V2X) communication technologies such as IEEE 802.11p-based Dedicated Short-Range Communication (DSRC) [6] and Cellular-V2X (C-V2X) [7] are not suitable for such high-capacity data collection due to their limited bandwidth. Recently, millimeter-wave (mmWave) wireless communication has been increasingly highlighted as one of the key technologies for the 5th Generation (5G) and next-generation V2X communication [8, 9]. IEEE 802.11ad, also known as WiGig, is a technical standard for mmWave wireless communications operating in the 60 GHz frequency band which is assigned as an unlicensed band in countries worldwide. The IEEE 802.11ad standard originally defined a high-speed communication mode supporting up to 6.7 Gbps and was further enhanced to support up to 8 Gbps in IEEE 802.11-2016 [10]. Due to its limited communication range and general

need for line-of-sight conditions, small cell architecture has been studied for mmWave V2X communication [11]. To fully utilize the high-throughput performance and low latency of mmWave communication, the use of mobile edge computing/multiaccess edge computing (MEC) has also been studied [12].

In V2X scenarios for a small cell environment, a vehicle establishes a wireless communication link and performs data transmission each time it enters the communication area. To ensure sufficient time for data transmission before the vehicle leaves the communication range, the establishment of the link should be completed as quickly as possible. With the conventional initial link setup process, link establishment often takes several seconds or longer. The fast initial link setup (FILS) was standardized in IEEE 802.11ai [13] and is a method for shortening initial link setup time for sub-6 GHz wireless LAN. FILS achieves a faster link setup by reducing the number of required packet exchanges. A study [14] has proposed introducing the techniques of FILS also for 60 GHz band communication based on IEEE 802.11ad. However, further study may be needed for small cell V2X scenarios because the initial link setup procedure would often be performed at the cell edge while the connecting vehicle is moving, usually resulting in the communication environment fluctuating severely. To benefit from FILS and achieve the fast initial link setup for mmWave V2X, the procedure must be able to handle increased packet loss without incurring substantial delays.

Another challenge for mmWave V2X is the reduced bandwidth due to core network delay and congestion and also cloud server response delay, which prevents full utilization of the high-throughput performance of mmWave communications. MEC is a promising technology to realize applications that require very low latency [15] but is also able to accelerate and improve the efficiency of uploading a large amount of data by using buffering at MEC/mobile edge servers. There has been research on cache size and handover between MEC servers [16, 17]; however, the application programming interface (API) suitable for high-volume data upload using MEC for multi-Gbps wireless access has yet to be presented.

In [18], the authors presented a data collection platform that enables data upload from vehicles to the cloud using IEEE 802.11ad and tackled the challenges mentioned above. This paper describes in detail the system architecture and technologies applied in the data collection platform as an extension of [18] and additionally showcases a proof-of-concept demonstration conducted in Marysville, Ohio, USA. The major contributions of this paper are listed below:

(1) Presents the proposed fast initial V2X link setup method suitable for IEEE 802.11ad that avoids large delays and extends communication time for a vehicle passing through a communication area ("pass-through communication")

(2) Presents REST (Representational State Transfer) API which uses buffering by reverse proxy in the MEC server for realizing high-speed data upload for multi-Gbps wireless access

(3) Presents a prototype platform and field evaluations that successfully demonstrate the effectiveness of the proposed methods by showing up to 30 times shorter initial link setup delay and 11 times higher average throughput for data upload during pass-through communication

The rest of this paper is organized as follows. Section 2 describes the system architecture of the data collection platform and the challenges of applying IEEE 802.11ad for V2X scenarios. Section 3 describes two proposed methods which address the technical challenges. Section 4 evaluates the performance of the proposed methods in a field test, and Section 5 shows an experimental demonstration of the data collection platform operating in a real environment. Finally, Section 6 concludes the paper.

2. System Architecture and Target Performance

This section presents the design and technical challenges of 60 GHz small cell radio access for a V2X system based on IEEE 802.11ad.

2.1. Small Cell mmWave for Pass-Through Communication. Table 1 shows the comparison of conventional sub-6 GHz and mmWave communications. Sub-6 GHz wireless communication is suitable for wide area coverage deployment, whereas mmWave wireless communication technologies, such as 5G New Radio (NR) over mmWave and IEEE 802.11ad, are excellent for providing high-throughput communication with focused coverage. This study targets the use case of uploading a large amount of delay-tolerant data from the vehicle to the cloud server. A key objective is to fully utilize the high-throughput performance of mmWave within the limited coverage. The authors assume a vehicle-to-infrastructure (V2I) communication scenario with base stations/roadside units (RSUs) installed at locations such as intersections where the vehicles pass through. Vehicles are equipped with onboard units (OBUs) that upload a large amount of stored data to the cloud via the RSU as they pass through the mmWave coverage of the RSU.

As signal propagation in the mmWave frequency band is highly directional, the RSUs and OBUs employ beamforming, which involves dynamically sweeping/steering the antenna beam direction to achieve wider coverage. Even though the beam sweep direction can be two-dimensional, a one-dimensional (vertical or horizontal) beam sweep is commonly implemented to achieve a small form factor and low cost. In this system, which uses one-dimensional beam sweeping, the antennas of the RSU and the OBU are arranged such that the beams are swept vertically. Figure 1 illustrates the beamforming configuration of the OBU and the RSU. This configuration provides improved coverage in the area below the RSU during V2I pass-through communication.

Table 1: Features of wireless communications.

	Sub-6 GHz (4G LTE, 5G NR, Wi-Fi)	mmWave (5G NR, 802.11ad)
Communication area, coverage	Wide coverage (whole area)	Focused coverage (small cell/limited)
Effective throughput performance in a typical usage scenario	Medium (<400 Mbps)	High (>1 Gbps)

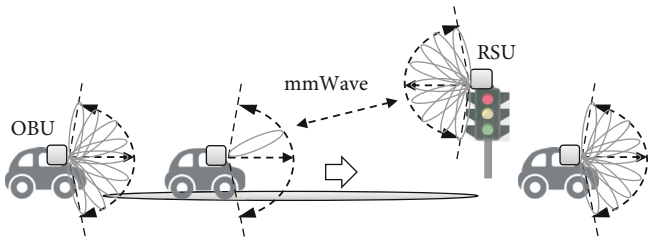

Figure 1: Beamforming configuration for V2I pass-through communication. Cited from [18].

2.2. Data Collection Platform. Figure 2 shows the system configuration of the data collection platform. While driving, the vehicle stores data, such as pictures and sensor data, in the OBU. The OBU is equipped with storage to temporarily store the data to be uploaded. The stored data is uploaded when the vehicle enters the RSU's mmWave coverage. The data is transferred to the MEC server via the RSU and from the MEC server to the cloud. The collected data is utilized for visualizing the city. During communication, the OBU takes the role of an IEEE 802.11ad station (STA) and the RSU operates as an access point (AP). The RSU also acts as a router and is connected to the MEC server by 10 GbE; therefore, the OBU gains high-speed access to the MEC server when it enters the RSU's coverage.

2.3. Target Performance. Table 2 shows the target performance of the platform. Here, it is assumed that 1 GB of data is uploaded every hour, which is based on a 1-hour update frequency for quasistatic information of a dynamic map and the approximate amount of data accumulated in a trial vehicle within 1 hour. Supposing a vehicle speed of 60 km/h and a 200 m communication area, which is based on throughput measurements conducted in a stationary state [19], the estimated duration available for communication by a vehicle during pass-through communication is 12 seconds. The 12 seconds of communication time can be broken down into 4 seconds for the delay due to the initial link setup and 8 seconds for the data transmission, which results in the target effective throughput of 1 Gbps at the application layer.

2.4. Technical Challenges. In order to achieve the target performance, two major technical challenges need to be addressed. First, IEEE 802.11ad is a wireless standard that assumes a quasistatic environment and the mobility of a pedestrian, so it can take several or more seconds to establish an initial link. This results in insufficient time for data transmission and hence failure to upload the target transfer data amount within a pass-through of the coverage area. Second, the MEC server has access to the Internet to transfer the uploaded data from the OBU to the cloud server, but the speed of the link between the MEC server and the cloud is much slower than that of the mmWave wireless link; thus, the system would not be able to fully exploit the high-throughput capability of IEEE 802.11ad. The following section addresses these two challenges.

3. Proposed Methods for mmWave V2X

In this section, a fast initial V2X link setup method and high-speed upload using the MEC server are proposed. The fast initial V2X link setup enables the vehicle/OBU to start data transmission shortly after entering the RSU's coverage, thereby increasing data transmission time during pass-through communication. The high-speed upload using the MEC server accelerates data upload by overcoming the limitation of the slower link speed between the MEC server and the cloud.

3.1. Fast Initial V2X Link Setup. This subsection describes the details of the proposed fast initial V2X link setup. The symbols used for the proposed method are given in Table 3.

3.1.1. Initial Link Breakdown Analysis. The factors that take up time in establishing an initial link have been analyzed. As illustrated in Figure 3, the initial link setup procedure consists of three sections, and Figure 4 shows an example sequence of the initial link setup procedure. The breakdown of each section is given below.

(1) PHY (Physical)/MAC (Medium Access Control) Section. The PHY/MAC delay, $T_{\text{PHY/MAC}}$, is the delay from when the first beacon is received from the RSU until the OBU establishes IEEE 802.11ad connection with the RSU. At first, scan processing is performed to search for candidate access points (RSUs) over the specified channels. Then, association processing is performed to connect to the desired access point. The section also includes Wi-Fi Pre-Shared Key (WPA-PSK) authentication processing for encrypted communication and other software processing. Therefore, the PHY/MAC delay, $T_{\text{PHY/MAC}}$, is given as

$$T_{\text{PHY/MAC}} = T_{\text{Scan}} + T_{\text{Assoc}} + T_{\text{WPA-PSK}} + T_{\text{ProcessDelay}}. \quad (1)$$

Scan processing is an active scanning procedure defined in IEEE 802.11ad, in which the OBU performs beamforming training by a sector-level sweep sequence upon reception of DMG Beacon frames transmitted by the RSU, followed by a probe exchange. The scan delay, T_{Scan}, is defined as the duration starting from the reception of the first beacon until the end of the active scanning procedure including any scan retries. A scan retry process occurs when the active scanning

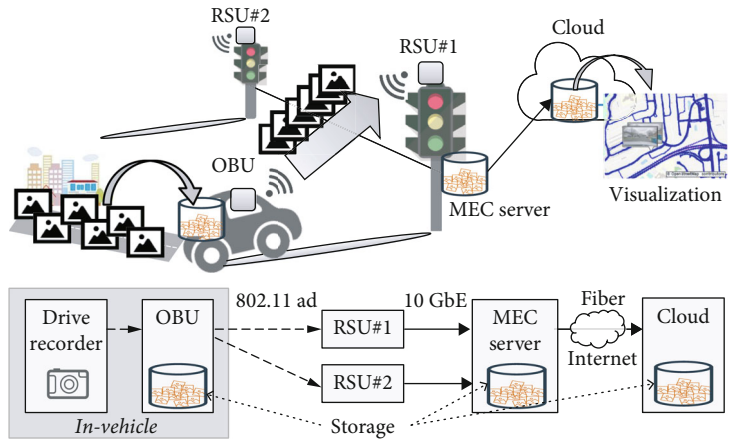

Figure 2: System configuration. Cited from [18].

Table 2: Target performance of the platform.

	Item	Value
Assumed conditions	Transfer data amount	1 GB
	Vehicle speed	60 km/h
	Communication area	200 m
	Communication time	12 s
Target values	Link setup delay	4 s
	Effective throughput	1 Gbps

time, T_{ScanTime}, expires before the OBU successfully completes the probe exchange with the RSU, which results in additional delay. The scan delay, T_{Scan}, is derived as

$$T_{\text{Scan}} = (T_{\text{ScanTime}} - T_{\text{FirstBeacon}}) + (T_{\text{ScanTime}} + T_{\text{ScanInterval}}) \times N_{\text{ScanRetry}}. \quad (2)$$

T_{ScanTime} and $T_{\text{ScanInterval}}$ are constants, while $T_{\text{FirstBeacon}}$ and $N_{\text{ScanRetry}}$ are variables that depend on the channel condition. Association processing consists of join and association frame exchange processes. Join is a process for the OBU to synchronize with the RSU by receiving DMG Beacon frame(s) from the RSU. After a successful join process, the OBU transmits an Association Request frame as part of the association exchange process. If the OBU successfully receives an Association Response frame back from the RSU, the process is completed. Otherwise, the OBU may retry join and association exchange processes after a given backoff time, $T_{\text{AssocBackOff}}(n)$. Therefore, the association delay T_{Assoc} is derived as

$$T_{\text{Assoc}} = \sum_{n=0}^{N_{\text{AssocRetry}}} \{T_{\text{AssocBackOff}}(n) + T_{\text{Join}}(n) + T_{\text{AssocExchange}}(n)\}. \quad (3)$$

The number of retry attempts, $N_{\text{AssocRetry}}$, depends on the channel condition. A poor channel condition may result in packet reception errors during join and association exchange processes. $T_{\text{Join}}(n)$ depends on the beacon interval, which is typically set to 100 time units (TUs), where 1 TU is 1.024 ms, and the number of beacon intervals until the OBU successfully receives the DMG Beacon frame(s). $T_{\text{AssocExchange}}(n)$ may increase if the channel is busy due to communication between the RSU and the other OBUs. There is no backoff time for the first attempt; i.e., $T_{\text{AssocBackOff}}(0)$ is 0. For retry attempts, backoff time, $T_{\text{AssocBackOff}}(n)$, may be set depending on the current retry count, n. This is discussed in Section 3.1.3 in detail.

(2) DHCP (Dynamic Host Configuration Protocol) Section. After establishing the IEEE 802.11ad connection, DHCP processing is performed to assign an Internet Protocol (IP) address to the OBU connected to the RSU. The process includes the negotiation with a DHCP server, duplicate check of the IP address (ping check) by the server, and software processing. The DHCP delay, T_{DHCP}, is derived as

$$T_{\text{DHCP}} = T_{\text{dhcp}} + T_{\text{PingCheck}} + T_{\text{ProcessDelay}}. \quad (4)$$

(3) HTTPS (Hypertext Transfer Protocol Secure) Section. After establishing the IP connection to the RSU, the uploader application software is immediately launched. Handshake procedures are then performed to establish Transmission Control Protocol (TCP) and Secure Sockets Layer (SSL)/Transport Layer Security (TLS) sessions between the OBU and the MEC server. After all sessions have been established, the data is transferred over HTTPS from the OBU, and an upload completion response is received from the MEC server. Since the transfer time of application data increases according to the amount of data, the delay up to the first byte will be considered the delay of the initial link setup. The section also includes Address Resolution Protocol (ARP) processing to obtain

Table 3: Symbols used in the proposed method.

Symbol	Description
$T_{\text{PHY/MAC}}$	Delay from receiving the first beacon to establishing the IEEE 802.11ad connection with the RSU
T_{Scan}	Scan delay
T_{Assoc}	Association delay
$T_{\text{WPA-PSK}}$	WPA-PSK 4-way handshake delay
$T_{\text{ProcessDelay}}$	Processing delay
T_{ScanTime}	Active scanning time
$T_{\text{FirstBeacon}}$	Delay until the first beacon received
$T_{\text{ScanInterval}}$	Scan interval
$N_{\text{ScanRetry}}$	Number of scan retries (probe exchange failures)
T_{Join}	Join delay
$T_{\text{AssocExchange}}$	Channel access time for association frame exchange
$N_{\text{AssocRetry}}$	Number of association retries (association exchange failures)
$T_{\text{AssocBackOff}}$	Association backoff delay
T_{DHCP}	Delay in assigning an IP address to the OBU connected to the RSU
T_{dhcp}	DHCP 4-way handshake delay
$T_{\text{PingCheck}}$	Ping check delay
T_{HTTPS}	Delay from launching the uploader application software to the first byte transfer by HTTPS
T_{ARP}	ARP delay
T_{TCP}	TCP 3-way handshake delay
$T_{\text{SSL/TLS}}$	SSL/TLS 4-way handshake delay
$T_{\text{FirstByte}}$	First byte data transfer delay by HTTPS
T_{Delay}	Delay of the entire initial link setup procedure

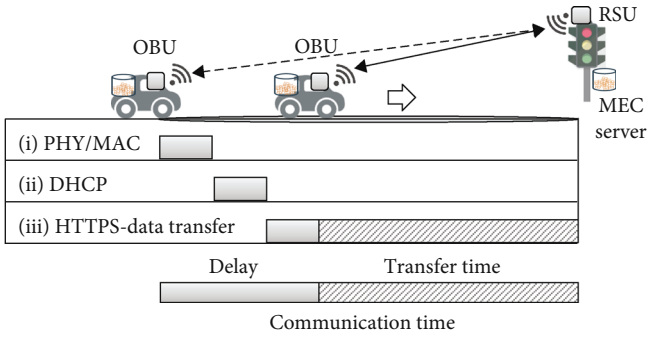

Figure 3: Time budget for V2I pass-through communication. Cited from [18].

the MAC address of the RSU and software processing. The HTTPS delay, T_{HTTPS}, is derived as

$$T_{\text{HTTPS}} = T_{\text{ARP}} + T_{\text{TCP}} + T_{\text{SSL/TLS}} + T_{\text{ProcessDelay}} + T_{\text{FirstByte}}. \quad (5)$$

In summary, the delay of the entire initial link setup procedure, T_{Delay}, is given as

$$T_{\text{Delay}} = T_{\text{PHY/MAC}} + T_{\text{DHCP}} + T_{\text{HTTPS}}. \quad (6)$$

Figure 5 shows a breakdown of the measured delays for the conventional link setup method, where delays due to (i) PHY/MAC and (ii) DHCP are observed to be dominant.

3.1.2. Fast Scan Processing and DHCP Processing. Conventionally, when scanning for APs, the scan period, which is the active scanning time, T_{ScanTime}, is set to several seconds. To analyze the impact of the scan period, the scan success rates for different scan periods were evaluated. As shown in Figure 6, the scan success rate gradually decreased as the scan period was reduced to 210 TUs and then decreased sharply when below 210 TUs. The sharp decrease in the success rate was due to the OBU not receiving a beacon at least once during the scan period. This occurred as the scan period became shorter than the beacon interval, which was set to 100 TUs, plus the operating speed of the firmware (time to start scanning the specified channel). Therefore, a scan period of 210 TUs ($=T_{\text{ScanTime}}$) was selected to minimize delay while ensuring an acceptable scan success rate. Additionally, the probe exchange performed after reception of the first beacon could fail due to packet errors depending on the channel condition. Especially if there are multiple vehicles/OBUs, collisions and carrier sense delays may occur

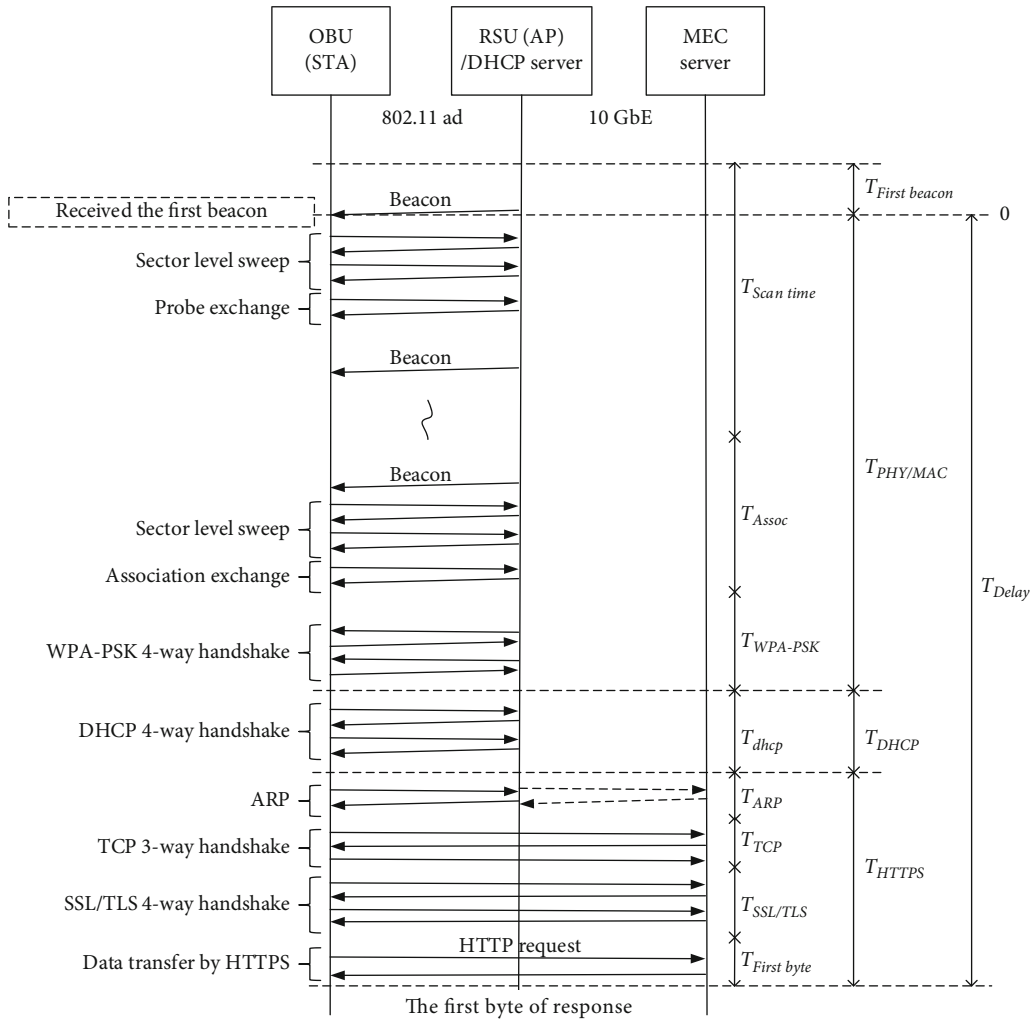

Figure 4: Initial link setup procedure example sequence with analysis.

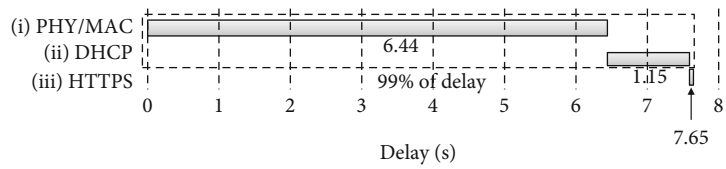

Figure 5: Delay performance with the conventional method. Cited from [18].

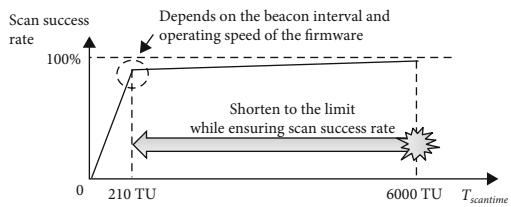

Figure 6: Relationship between the scan period and the scan success rate. Cited from [18].

due to the IEEE 802.11ad Carrier Sense Multiple Access/Collision Avoidance (CSMA/CA). Therefore, to avoid such delays, $T_{\text{ScanInterval}}$ was set to 0 to make the OBU immediately retry scan processing (rescan) after an unsuccessful scan attempt. By these configurations, the scan period was shortened by up to about 6 seconds.

Typically, the DHCP server needs to perform a duplicate check to confirm that no other OBU is using the same address to be offered before notifying the OBU of the IP address information. But in this system, the DHCP server is installed in the RSU, and the IP address is assigned only to the terminal connected to the RSU. Therefore, the duplicate check may be skipped; i.e., set $T_{\text{PingCheck}}$ to 0. By doing so, the DHCP time was shortened by about 1 second compared to the conventional implementation. Table 4 summarizes the values that were applied for configurable parameters related to PHY/MAC and DHCP processes.

Table 4: Parameters for fast scan and DHCP processing.

Section	Item	Value	
		Conventional method	Proposed method
$T_{\text{PHY/MAC}}$	T_{ScanTime}	6000 TUs	210 TUs
	$T_{\text{ScanInterval}}$	5 s	0 s
T_{DHCP}	$T_{\text{PingCheck}}$	1 s	0 s

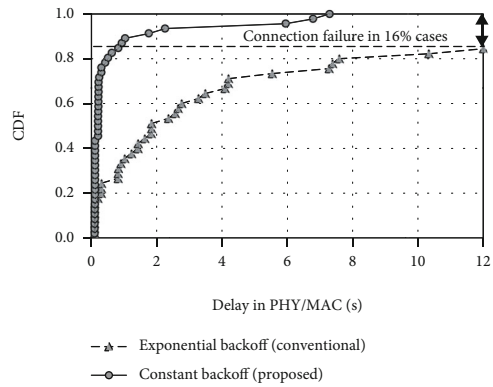

Figure 7: Comparison of PHY/MAC delay performance in a mobility environment. Cited from [18].

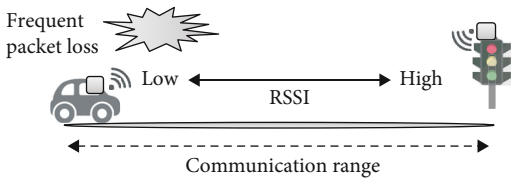

Figure 8: Wireless environment in V2I communication where frequent packet loss occurs. Cited from [18].

3.1.3. Reduction of Delay Variation due to Association Processing Failure. Figure 7 shows the cumulative distribution function (CDF) of the PHY/MAC delay in a mobility environment (at 60 km/h) after applying the improvements described in Section 3.1.2. The PHY/MAC delay in the best case has been reduced to well below 1 second as a result of applying the techniques on scan processing and DHCP described in Section 3.1.2. It can also be observed from the conventional method that large delays exceeding 8 seconds occur from 80% in the CDF, and connection failure, in which the OBU could not complete the establishment of the connection within the target 12 seconds, occurred in 5 out of the 45 test runs (16%). The large variations in delay were determined to be from the association process. In the WPA supplicant software [20], which controls the association process, exponential backoff ($T_{\text{AssocBackOff}}(n)$) is applied upon failure of the Association Request/Response frame exchange. The backoff durations configured in the WPA supplicant software for the first to fourth failures are 100, 500, 1000, and 5000 ms, respectively.

In the pass-through communication scenario, the association process is expected to be performed at the edge of the mmWave coverage as the OBU enters the RSU's communication range. As a result, packet loss for the Association Request/Response may occur frequently. This is illustrated in Figure 8. Thus, the WPA supplicant software was modified to apply a constant backoff time of 50 ms after the failure of the association exchange and the timeout of the association process was set to 240 ms so that the OBU retries the association exchange up to 4 times. In case of a timeout, the OBU restarts with scan and join processes to perform

Table 5: Parameters for the association of a mobility environment.

Section	Item	Value	
		Conventional method	Proposed method
$T_{\text{PHY/MAC}}$	$T_{\text{AssocTimeOut}}$	10 s	0.24 s
	$T_{\text{AssocBackOff}}(n)$	Exponential backoff 0.1, 0.5, 1, 5 s for $n = 1, 2, 3, 4$	0.05 s for any $n \geq 1$

Table 6: An example of a POST request for hundreds of pictures.

Endpoint: /edgeapi/v1/storage/file/_multipart
Request headers: Content-Type: multipart/form-data; boundary = *boundary* Content-Length: *Length* Request body: *–boundary* Content-Disposition: form-data; name = "metadata" Content-Type: application/json; charset = UTF-8 *<list of metadata in JSON format>* *–boundary* Content-Disposition: form-data; name = "jpgfile"; filename = "000001.jpg" Content-Type: image/jpeg *<binary content of file: 000001.jpg>* *–boundary* ... *–boundary* Content-Disposition: form-data; name = "jpgfile"; filename = "000100.*jpg*" Content-Type: image/jpeg *<binary content of file: 000100.jpg>* *–boundary*

Table 7: PC specs for performance measurement.

Component	Spec
CPU	Intel Core i7-6600U, 2.6 GHz
RAM	DDR4 2133 MHz, 16 GB
SSD	SATA III, 500 GB (OBU and RSU)/1 TB (MEC server)
OS	Ubuntu 16.04

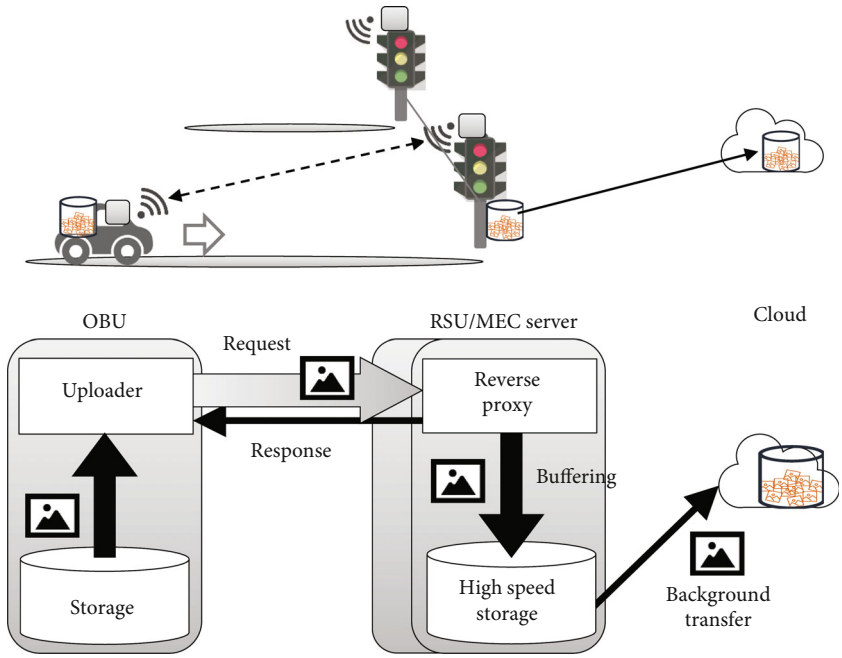

Figure 9: System configuration/protocol using the MEC server. Cited from [18].

synchronization with the RSU. This avoids harmful interference from the continuous transmission of Association Request frames by the OBU when the RSU is busy or unavailable. Table 5 summarizes the parameters for conventional and proposed methods. As shown by the solid line in Figure 7, the proposed method was able to substantially suppress the variations in delay.

3.2. High-Speed Upload System Using the MEC Server. This subsection describes the details of the proposed method of high-speed upload using the MEC server including overcoming the issue of slower link speed between the MEC server and the Internet.

3.2.1. High-Speed Upload API Design. In this subsection, a design of REST API that is suitable for high-speed upload during pass-through communication is presented. REST API is usually HTTP-based and implements CRUD (Create, Read, Update, and Delete) operations on resources on the remote server. Recently, HTTPS-based REST API is becoming widely adopted for Internet applications. REST API is also being considered to be adopted for MEC applications, and [15] describes design principles for REST MEC service APIs. While most typical applications for MEC involve offloading of tasks that require large computational cost and/or low latency which cannot be fulfilled by on-vehicle computers, upload acceleration may also be considered a class of task offloading. With REST API, the upload task is implemented as an HTTP POST request.

In the data collection platform, thousands of photo images are uploaded by a vehicle during pass-through communication. While upload time for an image, which is several hundreds of KBs, takes only several milliseconds, the response time of the server may take at least several milliseconds for each request, which causes degradation of throughput performance, especially if each image is uploaded with a single POST request. Bundling is a technique that is used to reduce protocol overhead by uploading a batch of files [21]. Bundling also reduces performance requirements for the PCs of both the server and the OBU since it reduces the number of HTTP requests to be processed. As shown in Table 6, the proposed API applies the multipart/form-data format that is defined in RFC 7578 [22] to bundle hundreds of image data in a single POST request. A set of metadata attributed to the images to be uploaded, such as capture location data based on GNSS and vehicle ID, is bundled to the same request as well.

At the OBU, from the total stored image data of about 10 GB, around 100 MB of image data, which consists of almost 200 image files, is bundled in a single POST request by the upload client software, and up to two requests are issued concurrently in two worker threads to achieve a sustained data rate of over 1 Gbps. The 100 MB size was selected to balance the trade-off between higher transfer efficiency and loss of performance due to failure of an ongoing upload due to connection loss. The throughput performance of the data upload using the proposed HTTPS-based REST API could reach more than 2.8 Gbps in an indoor environment even with the use of industrial PCs with modest specifications (as shown in Table 7) for the server and the OBU.

3.2.2. Upload Acceleration Using the Reverse Proxy-Based MEC Server. With the proposed REST API and OBU implementation described in the previous subsection, high-speed upload to the MEC server over mmWave communication is achieved. However, the bandwidth and delay of the

Figure 10: Field test environment in Singapore. Cited from [18].

Internet line between the MEC server and the cloud becomes a bottleneck. As illustrated in Figure 9, the MEC server is equipped with a reverse proxy function that terminates HTTPS access from the OBU and buffers the uploaded data from the OBU. As a result, high-capacity transmission between the OBU and the MEC server can be realized by the MEC server which functions as a proxy, returning a high-speed response to the OBU directly without being limited by slower Internet communication speeds between the MEC server and the cloud. The server then transfers the buffered data to the cloud server as a background process even after the vehicle has passed through.

4. Measurement Results

This section shows the measurement results of a field test. The purpose of the field test was to measure the performance of high-capacity data upload during pass-through communication by a single vehicle with 60 km/h speed. The effectiveness of the technologies proposed in Section 3 is discussed based on the measurement results.

4.1. Field Test Environment. Figure 10 shows the field test environment which is a public road in Singapore. One RSU and one MEC server were installed at a bus stop as an experimental setup, and an OBU was installed inside a test vehicle. The test was conducted with the developed data collection platform that implemented the proposed methods described in Section 3, including the countermeasures described in Sections 3.1 and 3.2. The OBU on the moving vehicle performed pass-through communication to upload image data to the bus stop setup. Table 8 shows the experimental configuration, and the PC specifications for the RSU, OBU, and MEC servers are shown in Table 7 in Section 3.2.1.

4.2. Test Results. Figure 11 shows the CDF of the initial link setup delay performance. When employing the proposed method, the shortest delay was 0.25 seconds, which is a 30 times reduction from the conventional method's 7.65 seconds shown in Figure 5. The establishment of the initial link was successfully completed within the communication area for all 46 test runs, and in about 94% of cases (=43 test runs), the measured delay was better than the target delay of 4 seconds. The reduction of delay and suppression of delay fluctuations after association processing failure in pass-through communication were achieved. Still, about 6% of cases, as shown in Figure 11, took 4 seconds or more. This was due to the PHY/MAC wireless environment, as evident from the solid line's behavior in Figure 7. It is suspected that these occurred when no beacons were received for some time after an initial beacon reception at a far distance and will be investigated further in the future.

Table 8: Experimental configuration.

Item	Value
Communication module	Peraso [23] X710
Wireless protocol	IEEE 802.11ad
Carrier frequency	60.48 GHz
Modulation and coding scheme (MCS)	0~12
Beam sweep direction	Vertical
Antenna polarization	Vertical
RSU antenna height	3.0 m
OBU antenna height	1.2 m (inside vehicle)
Number of vehicles	1
Number of OBU, RSU, and MEC servers	1 unit each
Vehicle speed	About 60 km/h
Throughput measurement method	Measured on HTTPS
Number of test runs	46

Figure 12 shows the complementary cumulative distribution function (CCDF) of average throughput performance during pass-through communication for uploading image data. By employing the proposed methods, the median value of the entire 46 test runs was 1.1 Gbps, which is 11 times higher than the conventional 0.1 Gbps. In addition, the

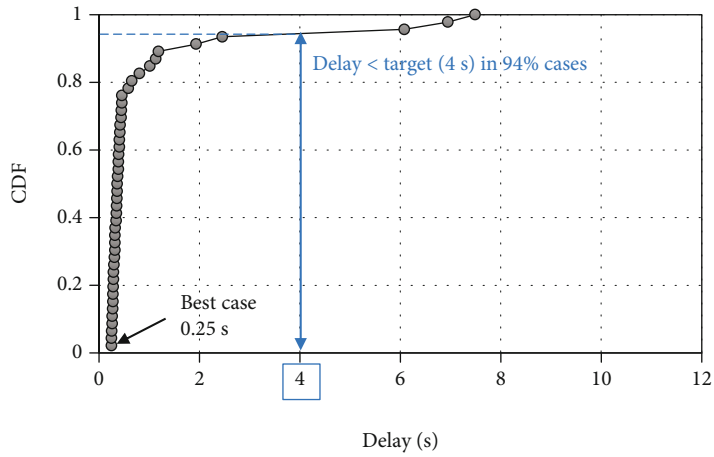

Figure 11: Delay performance with the proposed method. Cited from [18].

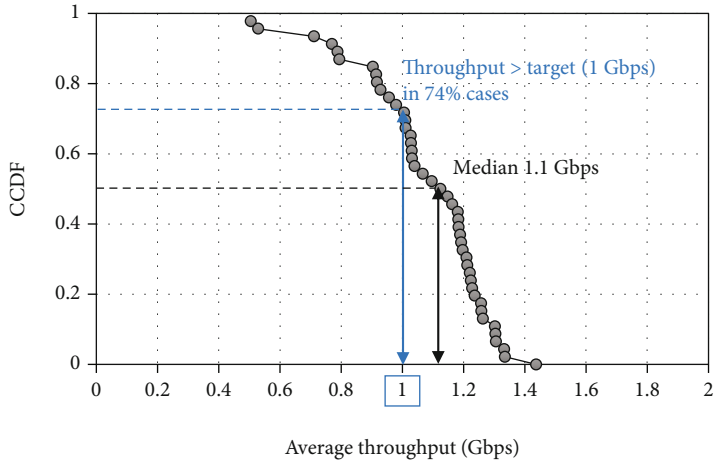

Figure 12: Average throughput performance with the proposed method. Cited from [18].

target of 1 Gbps or more was achieved in about 74% of cases (=34 out of 46 test runs). Although the measured throughput satisfied the target performance, it was still lower than expected. The authors analyzed and improved on the data upload client software in the OBU as described in Section 5.2 after this test.

Tables 9 and 10 show the benchmark comparisons that summarize the above results. In summary, the delay for the initial link setup was shortened by 30 times (7.65 seconds to 0.25 seconds), and about 94% of cases achieved the target of 4 seconds or less. In addition, the average throughput for uploading image data was improved by 11 times (0.1 Gbps to 1.1 Gbps), and the target of 1 Gbps or more was achieved in about 74% of cases. These results show that it is possible to consistently upload a large amount of data from a moving vehicle to the MEC server on the roadside, which was challenging in the past based on the conventional methods.

Table 9: Performance comparison.

	Delay	Throughput
Conventional	7.65 s	0.1 Gbps
Proposed	0.25 s	1.1 Gbps
Improvement rate	30 times	11 times

Table 10: Achievement rate of the target.

	Delay	Throughput
Conventional	$\ll$1%	0%
Proposed	94%	74%

5. Proof of Concept

This section presents a demonstration of the data collection platform incorporating data visualization application software, which was trialed in the city of Marysville, Ohio, USA.

5.1. System Installation. The prototype platform was installed, as shown in Figure 13, in early 2020 with the cooperation of Marysville City Hall, which is leading advanced initiatives for smart cities. RSUs and the MEC server were installed at the intersection of 6th/Main Street, Marysville, and the OBU system including a drive recorder, which consisted of a smartphone with a camera, was installed on a utility vehicle operated by the city. The system on the vehicle

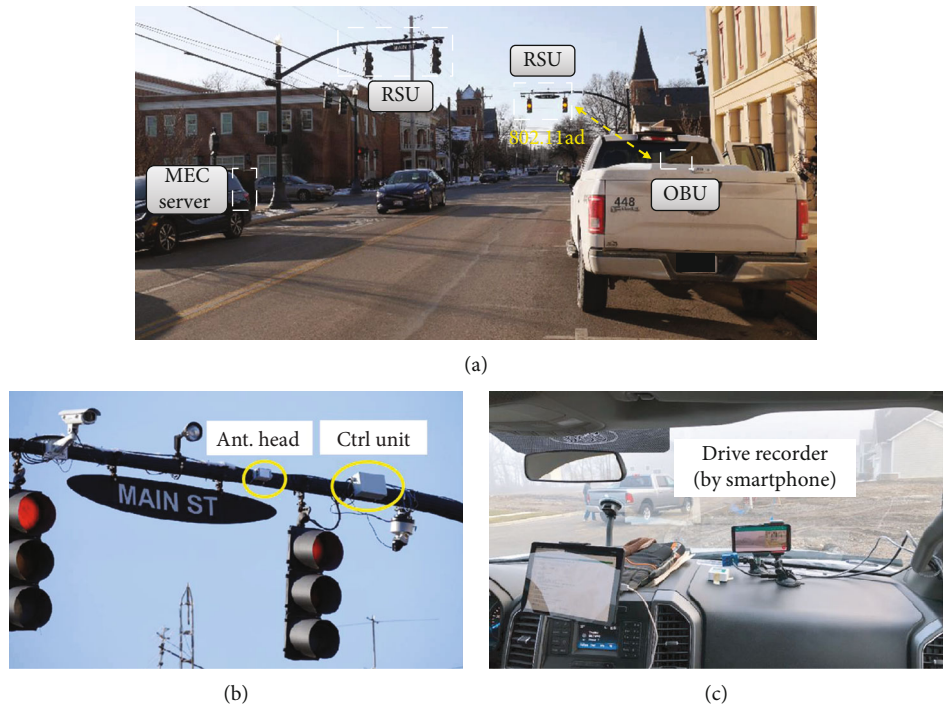

(a)

(b)

(c)

Figure 13: Experimental demonstration environment in (a) 6th/Main Street, Marysville. (b) RSU and (c) OBU installation setup.

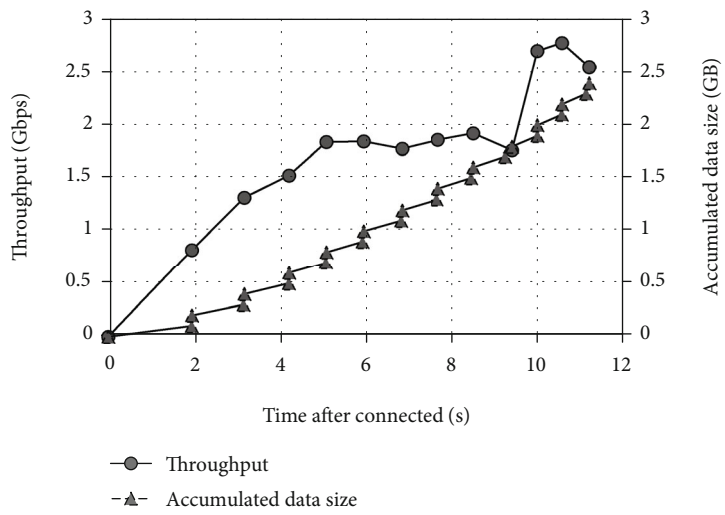

Figure 14: Throughput and accumulated data size performance in the trial.

automatically collected images of the city as the vehicle was used for operations by the city staff. In the prototype system, the vehicle's drive recorder takes a picture every second and continuously transfers the image data to the OBU via Wi-Fi (2.4 GHz/5 GHz) and stores it in the OBU's storage. When the vehicle approaches the intersection, the system automatically uploads the collected image data, which is then processed by the application software for visualizing the city.

5.2. Demonstration. Figure 14 shows an example of the measured performance during pass-through communication for uploading image data. The throughput is indicated by the solid line and the left axis, which shows a gradual increase after connection and a peak throughput of 2.8 Gbps at the application layer. The antennas of the RSU and the OBU were arranged so that the beam is swept vertically as described in Section 2.1, resulting in a high throughput just before the disconnection of V2I pass-through communication. The accumulated data size uploaded in two worker threads is indicated by the dashed line and the right axis, and it shows that a total amount of 2.4 GB of data was uploaded within the 11.2 seconds of pass-through communication at the intersection.

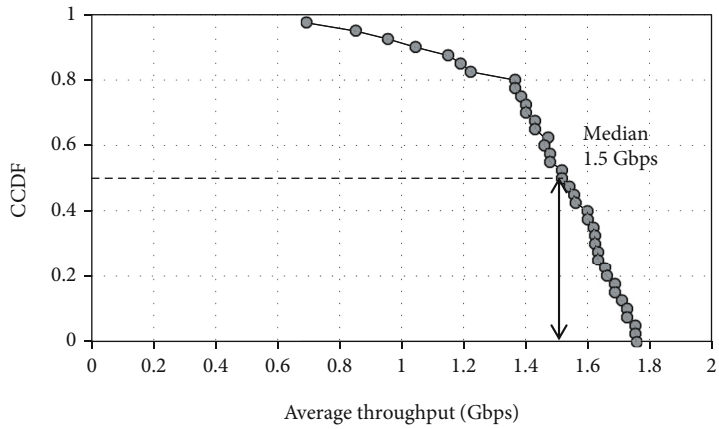

Figure 15: Average throughput performance in the trial.

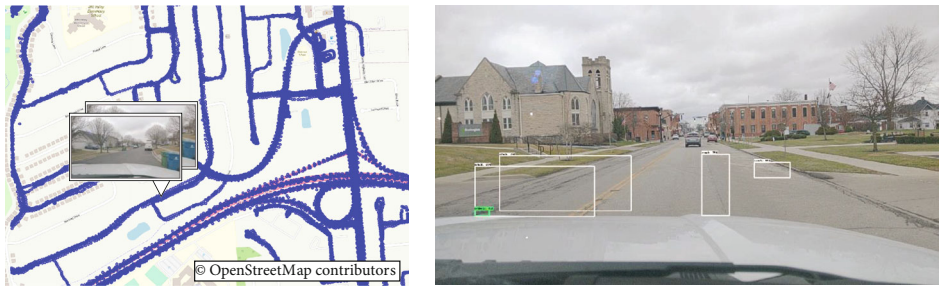

(a) (b)

Figure 16: City visualization using collected data in a demonstration. (a) Dashboard and (b) AI-analyzed image with detected road defects.

Figure 15 shows the CCDF of average throughput performance measured during the trial. The median value of the entire 40 runs was 1.5 Gbps, and higher throughput was observed compared to the field test in Singapore. This improvement may be attributed to optimizations in the data upload client software at the OBU to reduce unnecessary memory copies and simplify file selection for bundled data upload. In addition, due to the regulatory rules for the 60 GHz band in the US allowing higher transmit power than in Singapore, the range of communication for 16 QAM, which realized over 2 Gbps throughput, was increased. Slower vehicle speed during the US test due to the actual traffic condition in the city may have also contributed to the higher average throughput.

During the trial, image data of 10 GB or more per vehicle was collected daily by the cloud, and the data could be searched and browsed. Figure 16(a) shows a dashboard that visualizes the city using the collected data. Blue dots correspond to the image data taken by the camera on the vehicle. As an example, the collected image data were used for detecting road defects. As shown in Figure 16(b), the post-processing analytics using artificial intelligence (AI) successfully detected dents and cracks on the road. By detecting the road defects in their early stage, the city can take proactive action for repair, leading to reduced personnel and maintenance costs. There are tremendous opportunities for using the data to derive insights and take actions for the benefit of the city. This work paves the way for improving the quality of services in smart cities.

6. Conclusions

This paper has presented a data collection platform that realizes high-capacity data upload from vehicles to the cloud using the next-generation gigabit V2X communication using 60 GHz mmWave based on IEEE 802.11ad. The platform features the proposed fast initial V2X link setup and high-capacity data upload using a MEC server, which enables full utilization of the high-throughput performance of mmWave communication. The evaluation results show a 30 times shorter delay and 11 times higher average throughput from the vehicle to the cloud in a typical V2X pass-through scenario. As a proof of concept, the platform was installed in the city of Marysville and successfully demonstrates the potential for solving problems in smart cities through high-capacity data collection, analytics, and city visualization. Further work is planned for evaluating the initial link setup according to the distance between the vehicle/OBU and the RSU based on GNSS position information and also for evaluating the simultaneous connection/communication from multiple vehicles.

Data Availability

The data generated or analyzed during this study are included within the article.

Conflicts of Interest

The authors declare that there is no conflict of interest regarding the publication of this paper.

Acknowledgments

The authors would like to thank Ryo Takahashi, Fumihiko Onoda, and Kyosuke Mishima with Panasonic Automotive Systems Company of America; Mike Andrako, Darick Moore, Mark Dilsaver, and Terry Emery with the city of Marysville, Ohio; and Eric Philips with Union County, Ohio, for their invaluable support for the demonstration experiment in the city of Marysville, Ohio. Funding was provided by in-house R&D expenses.

References

[1] A. D. Angelica, "Google's self-driving car gathers nearly 1 GB/sec," March 2022, http://www.kurzweilai.net/googles-self-driving-car-gathers-nearly-1-gbsec.

[2] "Data is the new oil in the future of automated driving," March 2022, https://newsroom.intel.com/editorials/krzanich-the-future-of-automated-driving/.

[3] K. H. Law and J. P. Lynch, "Smart city: technologies and challenges," *IT Professional*, vol. 21, no. 6, pp. 46–51, 2019.

[4] U. Yutaka, "Start-up of data utilization-type smart cities," *NEC Technical Journal*, vol. 13, no. 1, 2018.

[5] F. Z. Benhamida, A. Bouabdellah, and Y. Challal, "Using delay tolerant network for the Internet of Things: opportunities and challenges," in *2017 8th International Conference on Information and Communication Systems (ICICS)*, pp. 252–257, Irbid, Jordan, April 2017.

[6] "IEEE Standard for Information Technology– local and metropolitan area networks– specific requirements– part 11: wireless LAN medium access control (MAC) and physical layer (PHY) specifications amendment 6: wireless access in vehicular environments," in *IEEE Std 802.11p-2010*, July 2010, https://standards.ieee.org/ieee/802.11p/3953/.

[7] "Study on LTE-based V2X services," in *3GPP TR 36.885, vol. 14.0.0*, July 2016, https://portal.3gpp.org/desktopmodules/Specifications/SpecificationDetails.aspx?specificationId=2934.

[8] K. Sakaguchi, R. Fukatsu, T. Yu et al., "Towards mmWave V2X in 5G and beyond to support automated driving," *IEICE Transactions on Communications*, vol. E104.B, no. 6, pp. 587–603, 2021.

[9] T. Okuyama, S. Suyama, N. Nonaka, Y. Okumura, and T. Asai, "Outdoor experimental trials of millimeter-wave base station cooperation with digital beamforming in high-mobility environments for 5G evolution," in *2020 IEEE 92nd vehicular technology conference (VTC2020-fall)*, pp. 1–5, Victoria, BC, Canada, Nov. 2020.

[10] "IEEE Standard for Information Technology—telecommunications and information exchange between systems local and metropolitan area networks—specific requirements - part 11: wireless LAN medium access control (MAC) and physical layer (PHY) specifications," in *IEEE Std 802.11-2016*, Dec. 2016, https://standards.ieee.org/ieee/802.11/5536/.

[11] K. Sakaguchi, T. Haustein, S. Barbarossa et al., "Where, when, and how mmWave is used in 5G and beyond," *IEICE Transactions on Electronics*, vol. 100, no. 10, pp. 790–808, 2017.

[12] P. Mach and Z. Becvar, "Mobile edge computing: a survey on architecture and computation offloading," *IEEE Communications Surveys & Tutorials*, vol. 19, no. 3, pp. 1628–1656, 2017.

[13] "Amendment 1: fast initial link setup," in *IEEE Std 802.11ai-2016*, 2016, https://standards.ieee.org/ieee/802.11ai/5017/.

[14] H. Kushida, H. Mano, M. Takai, Z. Liu, and S. Ishihara, "On the effectiveness of FILS in IEEE 802.11ad wireless networks," in *2017 23rd Asia-Pacific conference on communications (APCC)*, pp. 1–6, Perth, WA, Australia, Dec. 2017.

[15] "Multi-access edge computing (MEC); general principles, patterns and common aspects of MEC service APIs," in *ETSI GS MEC 009 V3.1.1*, June 2021, https://www.etsi.org/deliver/etsi_gs/MEC/001_099/009/03.01.01_60/gs_MEC009v030101p.pdf.

[16] Z. Zhang, Z. Chen, and B. Xia, "Cache-enabled uplink transmission in wireless small cell networks," in *2018 IEEE International Conference on Communications (ICC)*, pp. 1–6, Kansas City, MO, USA, May 2018.

[17] S. D. A. Shah, M. A. Gregory, S. Li, and R. D. R. Fontes, "SDN enhanced multi-access edge computing (MEC) for E2E mobility and QoS management," *IEEE Access*, vol. 8, pp. 77459–77469, 2020.

[18] K. Nakano, A. Egami, H. Motozuka et al., "Data collection platform for smart city with gigabit V2X communication over 60 GHz band," in *2021 IEEE 93rd vehicular technology conference (VTC2021-spring)*, pp. 1–5, Helsinki, Finland, April 2021.

[19] M. Irie, G. W. Y. Huang, M. S. H. Cheng, and K. Takahashi, "Bulk sensor data sharing using millimeter wave V2X for enhanced safety and comfort in mobility," in *2018 Asia-Pacific microwave conference (APMC)*, pp. 186–188, Kyoto, Japan, Nov. 2018.

[20] "Linux WPA/WPA2/IEEE 802.1X supplicant," March 2022, https://w1.fi/wpa_supplicant/.

[21] M. Akter, A. Gani, M. O. Rahman, M. M. Hassan, A. Almogren, and S. Ahmad, "Performance analysis of personal cloud storage services for mobile multimedia health record management," *IEEE Access*, vol. 6, pp. 52625–52638, 2018.

[22] L. Masinter, "Returning values from forms: multipart/form-data," in *RFC 7578, IETF*, Jul. 2015, https://datatracker.ietf.org/doc/html/rfc7578.

[23] "mmWave 60GHz chipset products," June 2022, https://perasotech.com/60ghz-hardware/.

Hindawi
Wireless Communications and Mobile Computing
Volume 2022, Article ID 8279098, 11 pages
https://doi.org/10.1155/2022/8279098

Research Article

Dynamic Analysis of Multicenter Spatial Structure with Big Data in Smart City

Juan Liu

School of History and Public Administration, Yancheng Teachers University, Yancheng, 224000 Jiangsu, China

Correspondence should be addressed to Juan Liu; liuj01@yctu.edu.cn

Received 11 February 2022; Accepted 27 May 2022; Published 23 June 2022

Academic Editor: Sohail Jabbar

Based on dynamic big data, the multicenter spatial structure of cities is studied, which provides help for scientific planning of urban space and rational use of urban land. Firstly, the research background and significance of this topic is expounded in the Introduction, and then, the related concepts and theories, which lay a theoretical foundation for this research, are summarized. After that, the paper focuses on the design of the scheme of urban multicenter spatial structure and puts forward the method of multicenter identification, method of aggregation feature analysis, and method of spatial structure feature. Finally, the proposed scheme is verified by a case.

1. Introduction

Rapid urbanization and rapid population growth have led to rapid social and economic growth in developing countries and at the same time led to the expansion of urban space scale and the adjustment of urban internal structure. Multicore urban structure has increasingly become a trend, which alleviates various problems caused by the single-center urban structure, such as traffic congestion, excessive population density, environmental deterioration, and other typical "urban diseases." Multicore is an important concept in urban planning. This kind of "multicore" is formed by the rational spatial distribution of several core areas of different sizes in a city. The urban core area is an important component of urban spatial structure, which gathers the core service functions of a city and supports the development of urban economy, society, and culture. Therefore, it is of great significance to accurately identify the urban core region and analyze the multicore urban structure in space for urban planning and sustainable development.

Traditional research on urban spatial structure is mainly based on experience and investigation, which relies too much on subjective judgment. However, the study of the urban spatial structure by remote sensing data has the problems of complicated data processing, time-consuming, and labor-consuming. With the relative development of large-scale information technology and the rapid popularization of Internet applications, big data is rapidly entering people's life and production. Big data can supplement traditional spatial data in many ways and is gradually being used in the construction of smart cities and digital cities [1]. By describing the real geographical entities such as urban residence, commerce, transportation, and public resources, meanwhile crossing with other disciplines, we can study the behavior of microsubjects, which can strengthen the mastery of urban functions and provide angles and idea analysis for the study of urban problems. Big data technology has been widely used in urban research in recent years, providing important data support for the development of smart cities. POI is an important information contained in modern electronic maps, providing people with important spatial reference information, and its emergence has greatly promoted the application of spatial geographic information technology. As an important manifestation of spatial information, POI data can provide information about human activities in urban space. POI is widely used in urban research because of its advantages in urban spatial work orientation.

Therefore, the dynamic big data of the multicenter spatial structure of a smart city is analyzed based mainly on the multicenter theory.

2. Overview of Related Theories

2.1. Definition of Related Concepts

2.1.1. Urban Spatial Structure. Bourne (1952) gave an authoritative definition of urban spatial structure [2] on the basis of defining concepts of urban form and urban interaction. He believes that urban form is the spatial form and arrangement of individual urban elements (such as architecture, land use, social groups, economic activities, and public institutions) in urban areas. Urban interaction is a set of fundamental relationships, which integrate individual land use, types, and behaviors of group activities into a subsystem. The urban spatial structure connects the behavior and interaction between the urban form and subsystems through a set of organizational rules and connects these subsystems into an urban system [3]. This definition not only points out the constituent elements of urban spatial structure but also emphasizes the interaction network among the elements [4]. There are two main definitions of urban spatial structure in China: one is the start from the fact that urban economic activities are the basis of urban existence and development, which is considered that urban spatial structure is the embodiment of urban socioeconomic activities in urban areas. Besides economic activities, other functions of cities are also recognized in that urban spatial structure is the embodiment of various elements and functional organizations of cities in urban areas. Comparatively speaking, the second definition broadens the research object of urban spatial structure, which comprehensively reflects the characteristics of a city as a complex system.

2.1.2. Multiple Center. The meaning of multiple center is broader. By combing the previous studies, it can be seen that morphological polycentricity, functional polycentricity, and administrative polycentricity are all important branches of multicenter research in a broad sense. Urban form is the comprehensive result of the spatial distribution of elements within the city by following the analysis of the concept of "urban spatial structure." The multiple center discussed in this study is the concept of urban form, taking the basic definition of morphological polycentricity, which emphasizes the comprehensive distribution and morphological layout of static socioeconomic attributes within urban space [5].

At the same time, the multicenter spatial structure has dependence on spatial scale and certain fractal characteristics [6]; that is, there is self-similarity between different spatial scales [7]. From the national scale, the metropolitan area, city-region, continuous urban area, and urban agglomeration with relatively concentrated economic activities can be regarded as a single center. From the regional scale, the internal structure of these cities-region, urban sprawl, and urban agglomeration can be further deepened, or it will present a multicenter structure of administrative or functional regional scale with some cities or urban areas as the center. From the perspective of the city scale, the city which is the center in the previous scale will further explore its internal structure or will show the multicenter degree comprehensively reflected by units of small spatial scale [8]. This study focuses on the urban scale, and the object is the multicenter spatial structure within the megacities.

2.1.3. Big Data. Big data has become a popular word in today's society only a few years since its birth and development. Because it is an abstract concept, there is no clear definition of big data up to now. Figure 1 shows the characteristics of big data. At present, the comprehensive definition of big data is the "5V" feature put forward by IBM, which namely means volume, variety, velocity, value, and durability [9]. Volume refers to the large amount of collection, calculation, and storage of data; variety refers to the variety of types and sources of data; velocity refers to the high speed of data generation, collection, processing, and updating; value refers to the low value density of data, which seems to pan for gold in the sand; and veracity refers to the accuracy and authenticity of data, that is, the quality of data [10]. In urban planning, the value of big data is mainly reflected in the large scale and wide coverage of urban basic data. The application of big data is an innovation to the means of preparation in urban planning, and it expands the way for all sectors of society to participate in urban planning which transforms traditional static blueprint-describing planning into planning of optimization in a dynamic process [11].

2.2. Introduction of Related Theories.

Urban spatial structure involves multidisciplinary researches, including economics, geography, urban and rural planning, and others. There are differences in the focus of different disciplines, while the breakthrough and analysis perspective of research on urban spatial structure are also different [12]. "Space" is the basic concept and core element of geography, where the research on "urban spatial structure" in geography focuses on exploring the evolution law and analyzing the characteristics of spatial evolution and development patterns based on land use. The main research object of urban and rural planning emphasizes the research and design of urban space form, which discusses the law of combination and visual art principles among elements of material space. Economics highlights the formation mechanism, development, and evolution mechanism of urban spatial structure and focuses on the mechanism analysis behind the phenomenon. Since the new economic geography first integrated spatial factors into the process of economic construction and quantitative analysis, the role of spatial structure has been appreciated in the economic field [13]. Based on this, the theoretical analysis of the research on the spatial structure of multicenter cities will be made from the following three perspectives, specifically, including the perspective of planning, geography, and economics.

2.2.1. Planning Perspective: The Origin of Multicenter Concept. The concept of multicenter originates from the field of planning and belongs to the research scope of "urban form" which refers to the evolution of urban physical environment under the action of various activities within the city, including the structure of land use and functional layout within the city, as well as the external contour formed by the boundary in urban construction [14]. In the field of

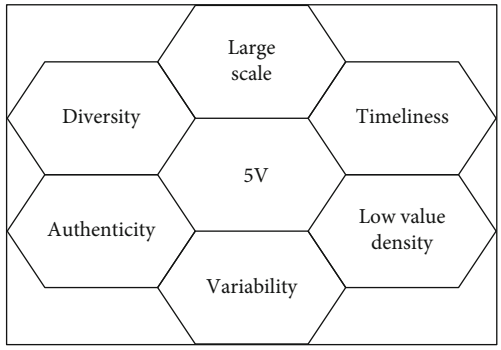

Figure 1: Characteristics of big data.

planning, the spatial structure of multicenter cities focuses on the evolution and development trend of the internal structure of cities, which is the spatial layout of various resources, and is also the result and comprehensive form of interaction of various activities in urban material space [15].

2.2.2. Geographical Perspective: Decentralization and Multiple Center of Element. In the traditional concept of urban geography, the regional shape of urban space is generally formed under the mutual influence of centrifugal force and centripetal force continuously emitted by the dominant "center of traditional city." After the 1920s, the phenomenon that the functions within the traditional city center gradually shift to the periphery of the city began to be recognized, which follows the concentric circle model, belt model, and multicore city model proposed by Burgess, Huo Yite, Harris, and others. Subsequently, the phenomenon of suburbanization of population was also reflected in some cities in the United States, and relevant theories surrounding the development trend of decentralization within the city continued to emerge at this stage. These theories focus on the emergence, evolution of suburban areas, feature induction, and relationship with traditional urban centers [16]. Then, in 1984, after the appearance of suburbanization in some metropolises in Britain and America, Peter Hall summed up a large number of urban phenomena and put forward the model of urban evolution which systematically depicts the evolution of urban internal structure [17]. According to this, the spatial process of the development of urban centers and suburbs can be understood under traditional urban geography theory as the process of agglomeration and dispersion of some urban functional areas that extends outward from the urban centers.

2.2.3. Economic Perspective: The Mechanism of Multicenter Formation and Evolution. The essence of economics is that it is dedicated to exploring the law of rational decision-making made by the subject through comprehensive cost-benefit to maximize utility [18]. Generally speaking, the theory of urban economics mainly focuses on the theory of land rent and agglomeration economy theory to analyze the formation and evolution of urban spatial structure, where the theory of land rent reveals the reasons and mechanisms of urban interior space and land layout from the perspective of individual residents, while the theory of agglomeration economy analyzes the reasons and rules of the comprehensive selection of location and the tendency of agglomerated distribution from the perspective of enterprises' pursuit of benefit maximization. By combining together the two above, they constitute the mechanism of the formation and evolution of urban internal spatial structure.

3. Analytics Scheme of Dynamic Data of Urban Multicenter Spatial Structure

For security reasons such as confidentiality, the original coordinates of the data needed for research belong to the Mars coordinate system, etc. Therefore, the coordinates of data should be corrected first, and then, the POI points, roads, urban boundaries, and other data should be projected to the coordinate system "WGS1984-UTM-Zone-51N" with the help of ArcGIS to establish a complete urban information database in geography for the next analysis.

3.1. Design of Multicenter Identification Scheme. The multicenter spatial structure of a city is a unique and complex spatial structure which gradually evolved under the joint action of natural conditions, historical development, planning guidance, and population migration, where the spatial distribution of city centers with different functions also has certain differences, as well as the distribution of different types of POI [19]. The amount of POI data varies greatly with different types. For example, there are 14,672 POI data for restaurants and only 857 POI data for business offices, while the same type of POI data also has different influences on the formation of urban centers that their influences on the formation of commercial centers are far less than those of shopping centers and shopping malls. To sum up, the specific design of multicenter identification based on POI data is shown in Figure 2.

The steps are as follows:

The first step is to classify urban facilities again according to different functions and carry out average nearest neighbor analysis. The results show that the nearest neighbor ratio (R) of all kinds of facilities is less than 1, which means that all facilities are clustered in space.

The second step is to study the distribution of various facilities by nuclear density analysis and normalize the results, which are divided into 1~10 grades.

The third step is to use the expert scoring method and use YAAHP software to calculate the influence weight of various facilities on different functional city centers.

The fourth step is to superimpose the normalized core density of the facility according to the weight which finally identifies the administrative center, business center, cultural and educational center, and leisure center of the city.

3.1.1. Analysis of Kernel Density Based on Average Nearest Neighbor Analysis. Average nearest neighbor analysis is used to calculate the distance between the POI point and its nearest neighbor POI point; then, the average value of all nearest neighbor distances is calculated. The final result will feed

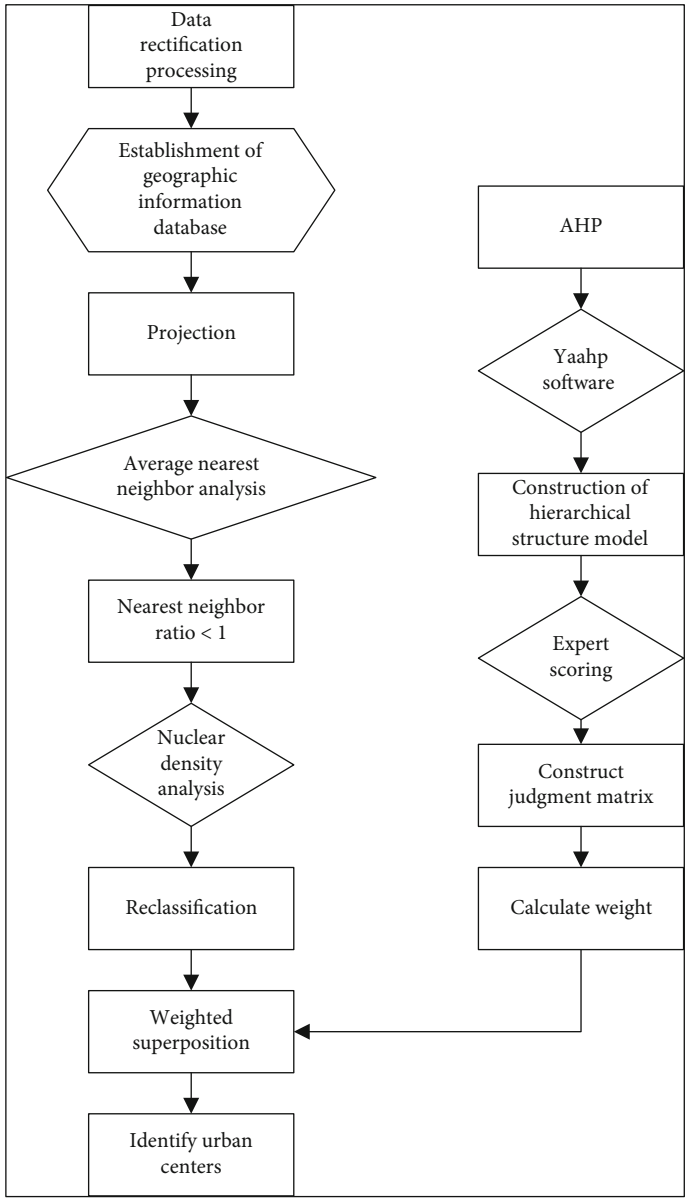

Figure 2: Design of identification in city center.

back five values, namely, average observation distance, expected average distance, nearest neighbor index, score of Z, and value of P. If the r is less than 1, the expression mode of this group is clustering, and the smaller the value, the higher the degree of clustering.

$$\bar{D}O = \frac{\sum_{i=1}^{n} d_i}{n},$$
$$\bar{D}E = \frac{0.5}{\sqrt{n/A}}, \quad (1)$$
$$R = \frac{\bar{D}0}{\bar{D}E}.$$

In the above formula, d_i refers to the distance between a certain point and its nearest neighbor, n is the total number of elements, and A refers to the minimum rectangular area around all elements or the value of the specified area.

Core density analysis means that any point is regarded as the core, and a certain range around it is the range of density calculation. According to the location of facilities, the spatial distribution form of this area is calculated and analyzed [20]. In this paper, nuclear density analysis is used to explore the gathering areas of various facilities in the East Coast City of Qingdao. Among them, the distance from the position of the core point determines the weight given to it, and the value of the final density is obtained from each data after weighted average analysis [21]. If the core density P_i of any point I in the space is defined as the core point with the highest weight, the value of the surrounding data points will decrease with the increase of distance, and when the

distance reaches the critical value r, the density value of the surrounding data points will be zero. The function expression is as follows:

$$P_i = \sum_{i=1}^{n} \frac{1}{\pi r^2} \varphi\left(\frac{d_{is}}{r}\right), \tag{2}$$

where P_i is the estimated value of nuclear density at i, r is the calculation radius of the function of kernel density, n is the total number of samples, d_{is} is the distance between the POI point i and s, and φ is the weight of the distance.

The purpose of the reclassification is to normalize the results of nuclear density with different particle sizes, which makes them in the grade of the same particle size that is convenient for the next calculation. For example, in the place of leisure and entertainment in the East Coast City of Qingdao, the range of nuclear density of picking gardens, resorts, and other facilities is 0~3.84, that of leisure places is 0~30.04, and that of entertainment facilities is 0~85.31. The numerical granularity of nuclear density of three types of facilities is quite different, and the results cannot be simply superimposed. Therefore, the reclassification in ArcGIS is used to reclassify the results into 1~10 grades for weighted calculation.

3.1.2. Weight Calculation Based on AHP. The Analytic Hierarchy Process (AHP) refers to the quantitative analysis method which decomposes the problems with strong subjectivity, many influencing factors, and difficulty in quantification to form a model of stepped hierarchical structure [22]. In the process of identifying the centers of different functions of cities, there are some differences in the influencing weights on the formation and distribution of urban centers, due to the different scales and quantities of facilities. Therefore, urban centers are firstly divided into four categories: administration centers, business office centers, culture and education centers, and leisure centers, and then quantitatively calculate the influence weights of various POI facilities on urban centers with the help of YAAHP [23]. The whole calculation is mainly divided into three steps: In the first step, according to the classification of POI facilities and the principle that the lower elements belong to the upper elements, the multilevel structure of the decision-making layer and middle layer is established. The second step is to build a matrix of pairwise comparison judgment between elements and divide the comparison of pairwise elements into five numerical grades of 9, 7, 5, 3, and 1 (respectively: absolutely important, very important, relatively important, slightly important, and equally important) and four levels between two adjacent levels, with values of 8, 6, 4, and 2. Meanwhile, experts in related fields are invited to judge the model of the hierarchical structure. The third step is to calculate the results and finally obtain the weights of various facilities [24]. Figure 3 shows the model of the multilevel structure of the leisure center.

3.2. Analysis Method of Aggregation Feature

3.2.1. Data Conversion and Analysis Ideas of Heat Map. In order to facilitate data analysis and calculation, different color areas are divided into seven grades of thermal values from 1 to 7 by means of classification and reclassification of a natural break point, among which grade 7 is the highest population density in this area [25]. For the convenience of description, the area with thermodynamic degree of 6~7 is defined as the high-heat area, and the area with thermodynamic degree of 4~5 is collectively referred to as the subheat area. The core idea of the analysis is to calculate the area of different thermal values, in which the larger the area of the high-heat zone and subheat zone, the higher the spatial concentration of people. Figure 4 shows the calculation ideas of the high-heat zone and subheat zone. Based on the conventional understanding of the law of urban activity and the demonstration of existing research, the law of activities is influenced by work factors to a great extent, showing periodic changes on a weekly basis, and there is a certain difference between the law of population distribution of working days from Monday to Friday and rest days on Saturday and Sunday [26]. Therefore, in this paper, the thermodynamic values displayed by Baidu heat maps on working days and rest days are investigated. After the study of the distribution and area of the high-heat zone and subheat zone, the location of the urban population center of gravity in different periods and the law of track of the population center of gravity in urban space are calculated by the "Spatial Statistics Tools-measuring geographical distribution-average center" system.

3.2.2. Analysis of Aggregation Based on Classification Method of Natural Discontinuities. The classification method of natural discontinuities is that the category of "natural discontinuities" is based on the natural grouping in the data. The similar values can be grouped appropriately by identifying the classification interval, while the differences between classes is maximized, as shown in Figure 5. Also, the features will be divided into several categories, and for these categories, the boundaries will be set at the positions where the values are relatively different [27]. Therefore, the classification of all data in this paper adopts this method, so as to ensure that the characteristics of the data can be more clearly and intuitively displayed after classification. The formula is as follows:

$$X = \frac{\sum_i^n \times W_i X_i}{\sum_{i=1}^n W_i},$$
$$Y = \frac{\sum_i^n \times W_i Y_i}{\sum_{i=1}^n W_i}. \tag{3}$$

In the formula above, x and y, respectively, represent the coordinates of latitude and longitude of the center of gravity of population distribution, W_i represents the thermal value of the i-th element, X_i and Y_i represent the coordinates of the i-th element, and n is the total number of elements in the region.

3.3. Analysis Method of Characteristics in Spatial Structure. In order to analyze accurately whether there is a spatial coincidence relationship between each functional center and

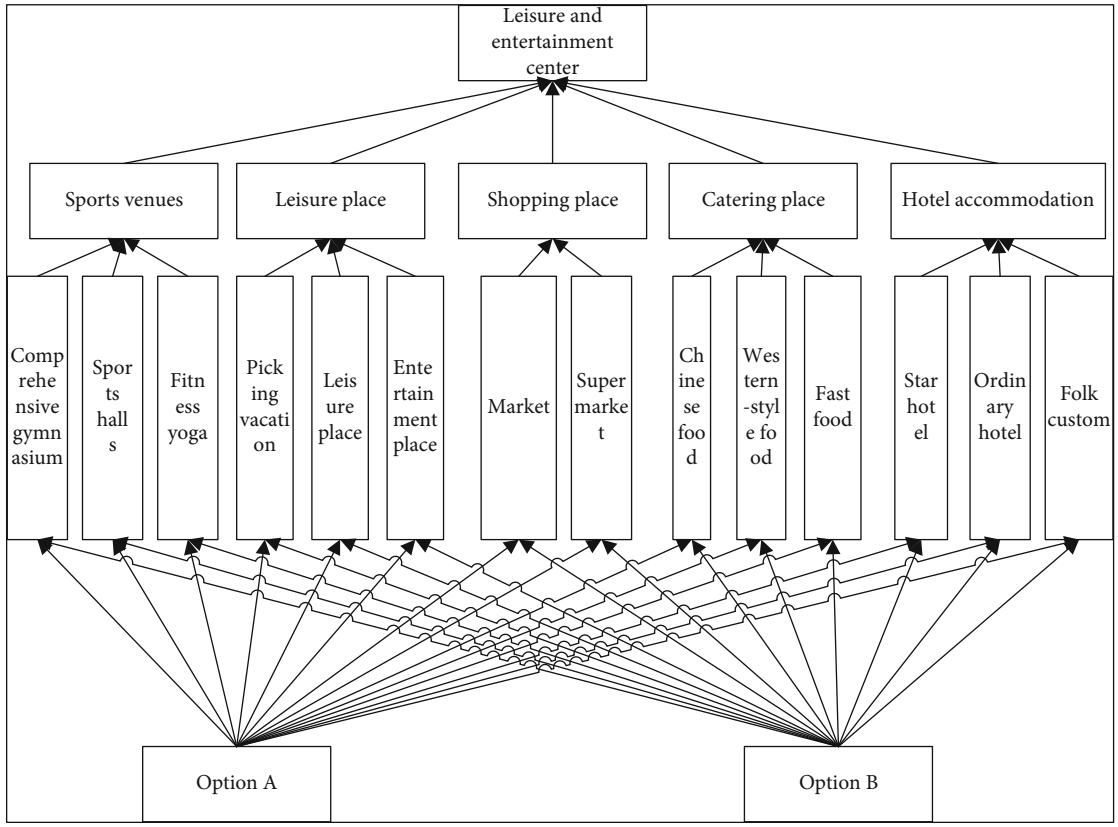

Figure 3: Model of multilevel structure of leisure center.

population gathering area, this paper adopts the visualization method of two-factor superposition mapping. The principle of two-factor superposition mapping is to combine two groups of different data into four different results according to their numerical values, which can form a transition zone between these combinations and combine them into more combinations [28]. However, this paper is only to study whether there is a relationship of spatial coincidence between the functional centers of cities and the gathering areas of population. Therefore, only the 3×3 classification method is adopted, and finally, nine different factors are combined. In order to more intuitively analyze and express the spatial coupling relationship between POI data and thermal value data, POI data was assigned 0, 5, and 9 according to its conditional function, while thermal value data was assigned 3, 1, and 0. Figure 6 shows the process of mapping in two-factor superposition.

As the principle of heat map in Baidu is also a kind of analysis of kernel density based on the user's location in the Baidu map APP which belongs to a kind of raster data, as shown in Figure 7, it is possible to extract the high-density (Grade 9 and Grade 10) and medium-density (Grade 7 and Grade 8) areas in a map of POI kernel density and assign 1, 3, 5, and 9 to the high-heat area and subheat area in the heat map, respectively, while the low-density area (Grades 1–6) and low-heat area are assigned to 0 and combined in pairs to obtain 9 types of combination relationships and color matching (which is shown in Figures 3–6 for details). According to the superposition and spatial distribution of different relationship types, this paper discusses the spatial coupling relationship between POI data and the heat map in Baidu and further analyzes the relationship between its spatial differences and the multicenter spatial structure of Qingdao.

4. Analysis of Case

4.1. Overview of the Research Area. Qingdao is located in the south of Shandong Peninsula, at 119°30′~121°00′ east longitude and 35°35′~37°09′ north latitude. In the master urban plan of Qingdao (2010-2020), the coastal area around Jiaozhou Bay is called the central urban area, including Shinan District, Shibei District, Licang District, and Laoshan District on the east bank of Jiaozhou Bay, Chengyang District and Hongdao Economic Zone on the north bank, and Qingdao Economic and Technological Development Zone on the west bank. The area studied in this paper is the eastern urban area under the urban space expansion strategy of "Linkage of the Three Cities."

The research area selected in this paper is the city in the east coast of Qingdao, which covers an area of 592.95 square kilometers with a permanent residence of 2,678,400 that accounts for 28.83% of the city's permanent residents. Table 1 shows the information on the subdistrict area, population, and economy. The city in the East Coast of Qingdao is the key area of transformation and development of urban space, which is a comprehensive service center with administration, culture, finance, business, and tourism.

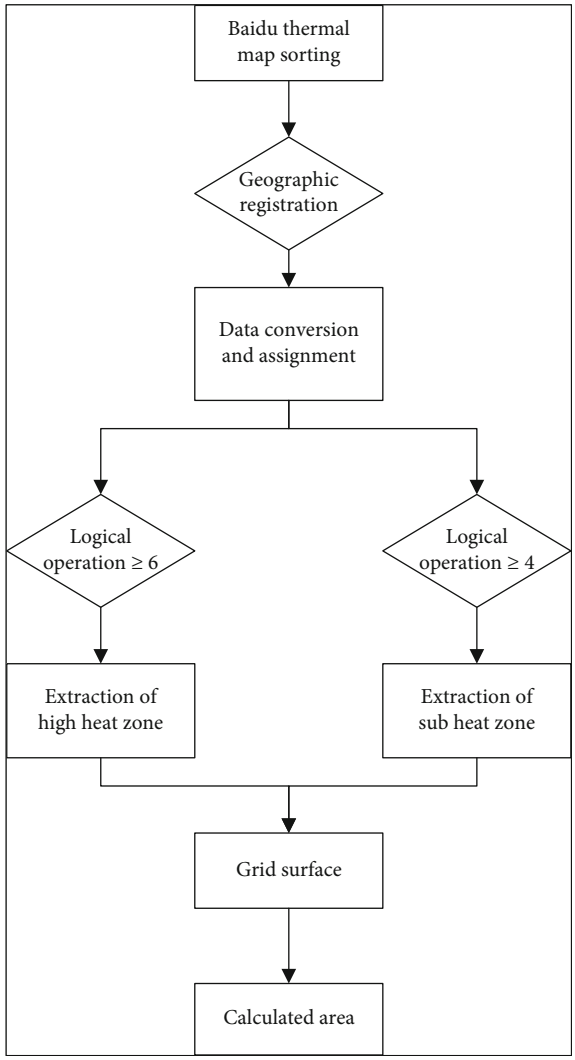

Figure 4: Process of calculating the area of heat diagram.

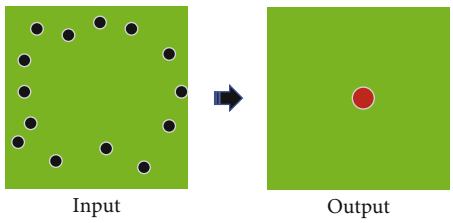

Figure 5: Schematic diagram of average center.

4.2. Results of Multicenter Identification

4.2.1. Administrative Center. POI interest of administrative facilities mainly include administrative units at or above the municipal level, district/county level, and township level and below; departments of public security and inspection; agencies of traffic and vehicle management; industrial and commercial tax authorities; and various social organizations. A total of 3565 pieces of data are obtained after deduplication. On the basis of summarizing the results of existing research, the administrative facilities are reclassified according to the level and function of the facilities.

4.2.2. Business Office Center. The main body of facilities in business office studied in this paper not only includes facilities such as finance, insurance, law, advertising, information, and technical services but also includes management and service departments of various industries. Therefore, the facilities are divided into banks, insurance institutions, securities companies, office buildings, commercial and residential buildings, companies, and hotels, which are a total of 19,714. Among them, the number of companies is the largest, with a total of 14,927, which accounts for about three quarters of the total facilities. Financial facilities, including all kinds of banks and their branches (excluding ATM facilities), insurance companies, investment companies, and securities companies, are 1906 in total. Office buildings include 857 commercial buildings and commercial and residential buildings which are the core element of forming a business office center, as shown in Table 2.

4.2.3. Cultural and Educational Center. In this paper, it is simply divided into a book exhibition category, including libraries, archives, museums, and art galleries, as shown in Table 3, totaling 201 according to the POI, and news media, including newspapers, magazines, advertising media, and other facilities, a total of 217. The number of training facilities is the largest, including primary and secondary schools and other basic educational facilities, colleges, and universities and various training and counseling institutions, which total 7747.

4.2.4. Leisure Center. As shown in Table 4, there are a large number of leisure facilities, up to 25,301, which are mainly divided into sports venues, including comprehensive gymnasiums and gymnasiums; leisure places, including picking gardens, resorts, chess and card rooms, and KTV; shopping places, including large shopping malls, shopping centers, supermarket chains, and convenience stores; catering services, including Chinese restaurants, western restaurants, and fast-food restaurants, which account for the largest proportion among leisure and entertainment facilities; and hotel accommodation facilities, mainly including star-rated hotels, ordinary hotels and homestays, and partying halls.

4.3. Results of Aggregation. Table 5 shows the results of multicenter aggregation.

4.4. Analysis of Spatial Structure Characteristics. The mixed function multicenter is the embodiment of the multicenter structure of urban cluster, which is more appropriate to the connotation of the multicenter space structure inside the city. The eastern urban area is the central urban area showing the characteristic cultural deposits of Qingdao and is the key area of urban space transformation and development. It should focus on improving the living environment, solving urban problems, and taking the road of connotative development. Under the guidance of the intervention of the master plan, urban elements continue to gather in specific areas and produce a city subcenter with comprehensive

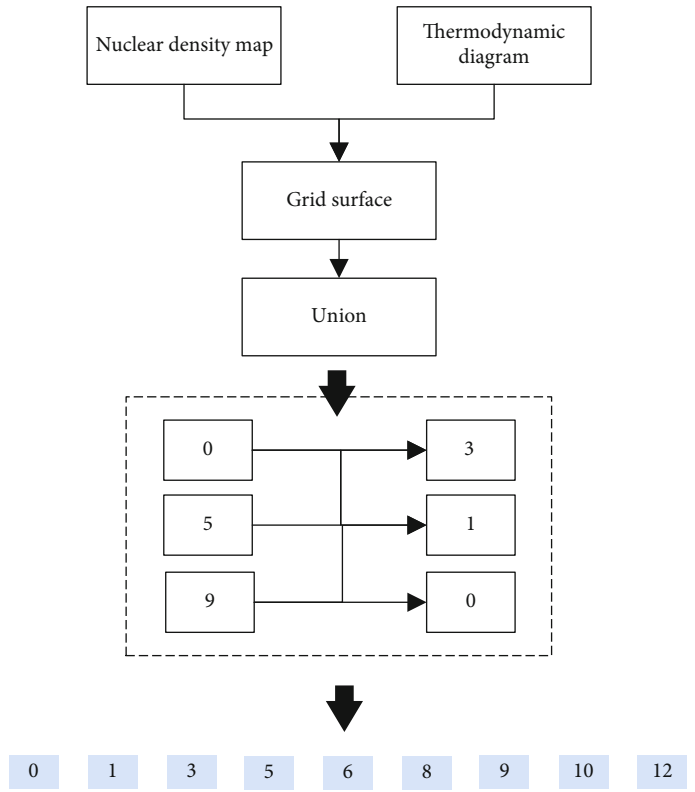

Figure 6: Process of mapping in two-factor superposition.

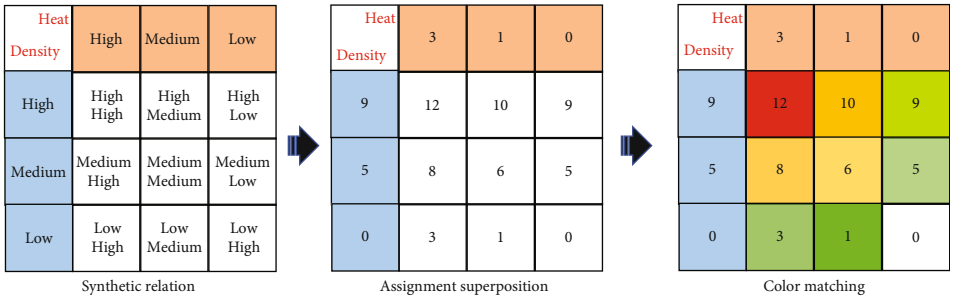

Figure 7: Method of mapping in two-factor superposition.

Table 1: Data and classification of administrative facilities.

General category	Medium class	Subclass	Quantity (PCs)	Proportion (%)	Nearest neighbor ratio (R)	Weight
Administrative center	Administrative units at or below the county and township levels	District and county administrative units	238	6.68%	0.43	0.165
		Township administrative unit	343	9.62%	0.17	0.043
		Below township level	800	22.44%	0.24	0.019
	Government office	Above prefecture-level city	361	10.13%	0.31	0.500
		Public security, procuratorial, and judicial departments	680	19.07%	0.34	0.168
	Social groups	Social groups	1143	32.06%	0.39	0.100
Total			3565	100%		

Table 2: Data and classification of business centers.

General category	Medium class	Subclass	Quantity (PCs)	Proportion (%)	Nearest neighbor ratio (R)	Weight
Business office center	Balance insurance	Bank	773	3.92%	0.31	0.045
		Insurance institutions	1026	5.20%	0.30	0.072
		Securities company	107	0.54%	0.60	0.171
	Office building	Office building	487	2.47%	0.49	0.377
		Apartment building	370	1.88%	0.59	0.126
	Company	Company enterprise	14,927	75.72%	0.29	0.158
		Hotel	216	1.10%	0.48	0.038
		Guesthouse	1808	9.17%	0.37	0.013
Total			19,714			

Table 3: Data and classification of cultural and educational facilities.

General category	Medium class	Subclass	Quantity (PCs)	Proportion (%)	Nearest neighbor ratio (R)	Weight
Culture and education center	Book exhibition	Library and archives	52	0.57%	0.66	0.182
		Art exhibition	109	1.19%	0.53	0.363
		Bookstore book bar	40	0.44%	0.62	0.031
	News media	Newspapers and magazines	78	0.85%	0.85	0.093
		Media organization	139	1.52%	1.52	0.024
	Education and training	Elementary education	1082	11.80%	11.80	0.102
		Colleges and universities	226	2.47%	2.47	0.129
		Training institutions	6439	70.23%	70.23	0.056
	Famous scenery	Famous scenery	824	8.99%	8.99	0.070
	Cultural activities	Cultural activity center	179	1.95%	1.95	0.051
Total			9168	100%		1

Table 4: Date and classification of leisure centers.

General category	Medium class	Subclass	Quantity (PCs)	Proportion (%)	Nearest neighbor ratio (R)	Weight
Leisure and entertainment center	Sports venues	Comprehensive gymnasium	27	0.11%	0.70	0.181
		Sports halls	372	1.47%	0.50	0.060
		Yoga gym	1188	4.69%	0.42	0.027
	Leisure place	Picking resort	73	0.29%	0.74	0.066
		Leisure entertainment	416	1.64%	0.46	0.030
		Entertainment place	1252	4.95%	0.31	0.041
	Shopping place	Market	140	0.55%	0.52	0.068
		Supermarket	878	3.47%	0.45	0.024
	Food and beverages	Chinese food	11,887	46.97%	0.21	0.014
		Western-style food	615	2.43%	0.34	0.039
		Fast food	2170	8.57%	0.29	0.015
	Hotel accommodation	Star hotel	216	0.85%	0.47	0.018
		Ordinary accommodation	1808	7.14%	0.36	0.010
		Homestay	4259	16.83%	0.27	0.047
Total			25,301			

Table 5: Results of multicenter aggregation.

	Nearest neighbor ratio	Aggregation characteristics
Administrative center	The nearest neighbor ratio of administrative POI points is less than 1, which passes the test at the significance level of 0.01.	It shows that the spatial distribution of such facilities has significant agglomeration characteristics, in which the index of township level administrative and public institutions is the lowest ($r = 0.17 < 1$, $z = -29.38$); that is, the aggregation degree of such facilities is the highest, and the nearest neighbor index of district- and county-level administrative units is the highest ($r = 0.43 < 1$, $z = -16.87$), indicating that the aggregation degree is the lowest.
Business office center	The nearest neighbor ratio of business office POI points is less than 1, which passes the test at the significance level of 0.01.	It shows that the distribution of business office facilities in the urban area presents a cluster model. However, the nearest neighbor ratio of securities companies ($r = 0.60 < 1$, $z = -7.83$) and apartment buildings ($r = 0.59 < 1$, $z = -15.10$) is the highest, indicating that the aggregation degree of the two types of facilities is relatively low. The number of corporate facilities is not only large, but also, the nearest neighbor ratio is the lowest ($r = 0.29 < 1$, $z = -166.67$), indicating that the aggregation degree of corporate office facilities is the highest.
Culture and education center	The nearest neighbor ratios of cultural and educational POI points are less than 1, which pass the test at the significance level of 0.01.	The distribution of cultural and educational facilities in the urban area presents a cluster model. Among them, the nearest neighbor ratio of training institutions ($r = 0.25 < 1$, $z = -114.41$) is the lowest, which means that the aggregation degree of such facilities is higher than that of other cultural and educational facilities. Book exhibition hall ($r = 0.66 < 1$, $z = -4.75$), art exhibition ($r = 0.53 < 1$, $z = -11.04$), newspapers and magazines ($r = 0.62 < 1$, $z = -6.48$), and media institutions ($r = 0.60 < 1$, $z = -8.94$) have a high nearest neighbor ratio, indicating that the spatial aggregation degree of these facilities in the urban area is relatively low [29].
Leisure and entertainment center	The nearest neighbor ratio of leisure and entertainment POI points is less than 1, which passes the test at the significance level of 0.01.	It shows that the distribution of such facilities in the urban area presents a cluster model. Among them, the comprehensive gymnasium ($r = 0.7 < 1$, $z = -3.01$) and picking resort garden ($r = 0.74 < 1$, $z = -4.20$) have the lowest degree of aggregation due to their large scale and small number. Chinese restaurant ($r = 0.27 < 1$, $z = -164.53$), homestay ($r = 0.27 < 1$, $z = -91.56$), and other catering and accommodation facilities have the largest number, and the nearest neighbor ratio is relatively low, indicating that their aggregation characteristics in the urban area are significant compared with those in the urban area.

functions. If an area has two or more functions at the same time, it is called an urban center.

At present, the Qingdao east bank urban area has formed a total of 6 urban centers; the aggregation of various facilities in the east coast of Qingdao presents a spatial structure of "one main center, two subcenters, and three groups" and shows a strong main center, weak subcenter, and multilevel multicenter spatial pattern. The main center is the central district of Hong Kong Middle Road, which is the largest multifunctional urban center with the city government as the core and a radius of 2 km, where the main administrative, commercial, commercial, entertainment, and other functions of Qingdao are gathered. The two subcenters are the Zhongshan Road Historic Block and Taitung Dengzhou Road Block. The former is the origin of Qingdao's urban development and used to be the city center. The latter is a traditional commercial center rising rapidly with the relocation of industrial facilities, located between the old and new city centers. The three groups are Fuxin Road street, Li Cun street, and Jinjialing street along the Haier Road; in addition to the Fuxin Road street, the other two groups are far from the main center of the city. As a whole, the distribution of urban centers in the eastern urban area of Qingdao is not balanced. Most of the urban centers are located in the southern coastal areas. In the inland area, only a multicenter cluster is formed in Licun, while other inland areas are not multicenters with comprehensive functions.

5. Conclusion

To sum up, the multicenter theory, based on the POI of Gaode map and data of heat map in Baidu, is combined in this paper, and the scheme of a dynamic data based on the urban multicenter spatial structure is designed, in which the analysis method of the average nearest neighbor is used to classify urban multiple centers, and the analytic hierarchy process is used to calculate the weights. Classification intervals are identified by means of classification

and reclassification of the natural break point, so as to ensure that the data can present its characteristics more clearly and intuitively. Finally, the city in the east coast of Qingdao is taken as a case, which refers to the above scheme. The case shows that the center of the city in the east coast of Qingdao is divided into an administrative center, business office center, cultural and educational center, and leisure center. At present, the Qingdao east bank urban area has formed a total of 6 urban centers, which are "one main center, two subcenters, and three groups," and shows a strong main center, weak subcenter, and multilevel multicenter spatial pattern.

Data Availability

The dataset can be accessed upon request.

Conflicts of Interest

The authors declare that there are no conflicts of interest.

References

[1] Y.-Y. Jeong Moon et al., "Analysis of Seoul urban spatial structure using pedestrian flow data-comparative study with '2030 Seoul Plan'," *Journal of The Korean Regional Development Association*, vol. 26, no. 3, pp. 139–158, 2014.

[2] T. Wen, *The optimization measures of Dalian city spatial structure from the perspective of global urbanization*, Shanxi Architecture, 2015.

[3] G. Cao, Q. Shi, and L. Tao, "An integrated model of urban spatial structure: insights from the distribution of floor area ratio in a Chinese city," *Applied Geography*, vol. 75, pp. 116–126, 2016.

[4] X. Zhang, L. I. Pengfei, and G. U. Qiong, "Research on urban spatial structure based on cell phone signaling data: job-housing analysis and evaluation in Shenyang city," *Journal of Urban and Regional Planning*, vol. 14, 2018.

[5] N. Q. Liu and M. Deng, *Urban spatial structure and optimization of population distribution in Yangtze River Delta region*, Review of Industrial Economics, 2018.

[6] A. Getis, "Second-order analysis of point patterns: the case of Chicago as a multi-center urban region," *Professional Geographer*, vol. 35, no. 1, pp. 73–80, 1983.

[7] L. Hu, T. Sun, and L. Wang, "Evolving urban spatial structure and commuting patterns: a case study of Beijing, China," *Transportation Research Part D Transport and Environment*, vol. 59, pp. 11–22, 2018.

[8] Y.-X. Song and H.-b. Zheng, "Study on the optimum pattern of Daqing urban spatial structure," *Chinese Geographical Sciences*, vol. 12, no. 3, pp. 206–211, 2002.

[9] X. Y. Liu, S. L. Li, and M. Qin, "Urban spatial structure and regional economic efficiency-on the mode choice of China's urbanization development," *Management World*, vol. 1, pp. 51–64, 2017.

[10] I. Aquilué, E. Roca, and J. Ruiz, "Topological analysis of contemporary morphologies under conflict: The urban transformation of Dobrinja in Sarajevo and the Central District of Beirut," in *24th ISUF International Conference. Book of Papers. Editorial Universitat Politècnica de València*, pp. 1005–1013, Valencia, Spain, 2018.

[11] Y. Zhang, T. Wang, A. Supriyadi, K. Zhang, and Z. Tang, "Evolution and optimization of urban network spatial structure: a case study of financial enterprise network in Yangtze River Delta, China," *ISPRS International Journal of Geo-Information*, vol. 9, no. 10, p. 611, 2020.

[12] G. Ma and Z. Zhang, "The change of urban population spatial structure of Nanjing, 1982–2007: Based on ESDA, density function and GIS," in *2010 18th International Conference on Geoinformatics*, pp. 1–4, Beijing, China, 2010.

[13] W. C. Wheaton, "A comparative static analysis of urban spatial structure," *Journal of Economic Theory*, vol. 9, no. 2, pp. 223–237, 1974.

[14] A. Krehl and S. Siedentop, "Towards a typology of urban centers and subcenters - evidence from German city regions," *Urban Geography*, vol. 40, no. 1, pp. 58–82, 2019.

[15] G. J. Tian, "Urban spatial-temporal dynamic pattern in Xiamen multi-center metropolitan area," *Tropical Geography*, vol. 43, 2008.

[16] Z. Wu, Y. Ji, and G. Cheng, *Optimizing Logic of Dingbian Urban Spatial Structure, Shaanxi Province*, Planners, 2019.

[17] C. Li, L. Meng, T. Zhang, and T. Zhang, "Study on the influence of multi railway stations on urban spatial structure," vol. 33, Tech. Rep. 6, Urban Planning International, 2018.

[18] D. H. Liu, "A study on influence of urban spatial structure on residents' commute travel: the cases of Chengdu and Lanzhou," *World Regional Studies*, vol. 24, no. 4, pp. 78–84, 2015.

[19] Y. X. Pei, "Development of the information intensive services and their impacts on the urban spatial structure of Guangzhou, China," *Scientia Geographica Sinica*, vol. 19, no. 5, pp. 405–410, 1999.

[20] H. Zhou and H. Gao, "The impact of urban morphology on urban transportation mode: A case study of Tokyo," *Case Studies on Transport Policy*, vol. 8, no. 1, pp. 197–205, 2020.

[21] D. Cui and S. Qi, *Experience and suggestions on urban transit and urban spatial development*, Modern Urban Transit, 2019.

[22] T. W. Geng and L. I. Jiu-Quan, "Analysis on development zone and urban spatial structure evolution–taking Xi'an city as an example," *Resource Development & Market*, vol. 36, 2018.

[23] L. Hao, X. Wang, W. Qiao, and L. Zhang, "The characteristics of urban spatial expansion in Nanjing since 1936," *Geographical Research*, vol. 38, no. 4, pp. 911–925, 2019.

[24] W. U. Qianbo and Q. Chen, *Population spatial change and urban spatial restructuring in Hangzhou from 2000 to 2010*, City Planning Review, 2015.

[25] Y. Wang, L. I. Guangbin, and W. Shi, *Urban space production of Suzhou: characteristics and mechanisms–discussion on evolution of urban spatial structure of Suzhou*, Modern Urban Research, 2015.

[26] Y. E. Zu-Pan, *The practice of "multi-center, group" city spatial structure in Chongqing city zone*, Shanxi Architecture, 2013.

[27] H. G. Xiong, G. H. Zou, and J. Y. Cui, "Evolution of urban land spatial structure in Urumqi based on GIS," *Entia Geographica Sinica*, vol. 30, no. 1, pp. 86–91, 2010.

[28] W. U. Yuan-Bo, "Study on urban spatial structure optimization in the process of Shanghai's suburbanization," *Journal of Tongji University (Social Science Section)*, vol. 38, 2010.

[29] L. E. Xiaohui, J. Chen, and J. Yang, "Impact of rail transit on urban spatial structure in Shenzhen: analysis based on land parcel price and FAR gradients," *Geographical Research*, vol. 11, pp. 2091–2104, 2016.

Hindawi
Wireless Communications and Mobile Computing
Volume 2022, Article ID 6783777, 12 pages
https://doi.org/10.1155/2022/6783777

Research Article

An Ant-Hocnet Routing Protocol Based on Optimized Fuzzy Logic for Swarm of UAVs in FANET

Saifullah Khan,[1] **Muhammad Zahid Khan**,[2] **Pervez Khan**,[2] **Gulzar Mehmood**,[3] **Ajab Khan**,[4] **and Muhammad Fayaz**[5]

[1]*Computer Science Virtual University, Pakistan*
[2]*Network Systems & Security Research Group (NSSRG), Department of Computer Science and IT, University of Malakand, 18800 Chakdara, KP, Pakistan*
[3]*Department of Computer Science, IQRA National University, Swat Campus 19220, Pakistan*
[4]*Abbottabad University of Science & Technology, 22500, Havelian, Abbottabad, Pakistan*
[5]*Department of Computer Science, University of Central Asia, Naryn, Kyrgyzstan*

Correspondence should be addressed to Muhammad Fayaz; muhammad.fayaz@ucentralasia.org

Received 12 March 2022; Revised 11 May 2022; Accepted 31 May 2022; Published 23 June 2022

Academic Editor: Zahid Khan

Drones or unmanned aircraft are commonly known as unmanned aerial vehicles (UAVs), and the ad hoc network formed by these UAVs is commonly known as Flying Ad Hoc Network (FANET). UAVs and FANET were initially associated with military surveillance and intelligence gathering; moreover, they are now excessively used in civilian roles including search and rescue, traffic monitoring, firefighting, videography, and smart agriculture. However, due to the distinctive architecture, they pose considerable design and deployment challenges, prominently related to routing protocols, as the traditional routing protocols cannot be used directly in FANET. For instance, due to high mobility and sparse topology, frequent link breakage and route maintenance incur high overhead and latency. In this paper, we employ the bio-inspired Ant Colony Optimization (ACO) algorithm called "Ant-Hocnet" based on optimized fuzzy logic to improve routing in FANET. Fuzzy logic is used to analyze the information about the status of the wireless links, such as available bandwidth, node mobility, and link quality, and calculate the best wireless links without a mathematical model. To evaluate and compare our design, we implemented it in the MATLAB simulator. The results show that our approach offers improvements in throughput and end-to-end delays, hence enhancing the reliability and efficiency of the FANET.

1. Introduction

An unmanned aircraft is stated to as a drone. Drones are also known as unmanned aerial vehicles (UAVs) or unmanned aircraft systems. A drone is a flying robot that can be controlled remotely or flow independently using software-driven flight plans in embedded systems that work in tandem with sensing devices and a global positioning system (GPS). Recently, with the rapid advancement and development in sensors, computation, and networking technologies, many researchers consider the usage of several small-unmanned aerial vehicles or UAVs for a variety of military and civilian applications [1]. UAVs are a collection of independent flying wireless nodes, which communicate with each other and a ground base through wireless links [2]. Mobile Ad hoc Network (MANET) is a self-organizing, infrastructure-less, and on-demand network, which can be adapted in dynamic conditions, but suffers from several limitations in terms of communication range and availability [3]. MANET has a few application territories such as emergency handling, patient monitoring, fault-tolerant mobile sensor grids, environment control, and intelligent transportation systems. However, MANETs do not provide the required level of performance for disaster and war field applications such as flood handling, battlefield, earthquake, search, and rescue operations where MANETs cannot be deployed. For such cases, Flying Ad Hoc network (FANET) is a distinct subgroup of MANET and Vehicular Ad Hoc

Network (VANET) [4], which works in scenarios where communication service is out of reach or simply not accessible. The nodes in FANET play role of communication relay, rapidly deployable and self-managed ad hoc network. FANET is developed as a capable technique in both civilian and military applications, such as border surveillance, search and destroy, search and rescue, road traffic management, airborne photography, disaster management, urban security, remote sensing, and wind estimation, as shown in Figure 1 [5].

FANET can be seen as multi-UAV and single UAV systems. Multi-UAV systems have several advantages over single UAV systems such as scalability, stability, accuracy and precision, and effectiveness [6]. However, multi-UAV systems have several challenges because of their unique characteristics such as high mobility and infrequent deployment. One of the major issues is routing among the UAVs and base stations [7]. Furthermore, there is also the issue of range limitation between UAVs and ground-based station. On the off chance that a UAV is outside the inclusion of the ground base station, it ends up disconnected [8]. In this respect, it is important to build a wireless ad hoc network, in particular, a decentralized network with powerfully evolving topology and high node mobility.

In [9], fuzzy-logic-assisted AODV (FL-AODV) routing algorithm is proposed for MANET. In [10], the authors propose the use of Q-learning-based fuzzy logic for the FANET routing protocol. The authors in [11] use fuzzy logic for a QoS and QoE aware routing protocol for FANET networks. Link Defined OLSR (OLSR-LD) is proposed for MANET in [12]. Link Stability Estimation-based Preemptive Routing (LEPR) protocol for FANET is proposed in [13]. A common issue in the existing ad hoc routing protocols is that they did not consider the important factors (i.e., bandwidth, mobility, and link quality) all together for choosing the best routing path for more effective and robust routing.

In terms of implementation and architecture, FANET presents significant obstacles. Bandwidth, link quality, and determining the optimum routing path for data exchange are all significant problems in routing among the swarm of UAVs. The rationale for this is that these parameters have a significant impact on the network's overall performance. According to research, existing systems in FANETs do not take into account aspects such as bandwidth, mobility, or link quality when picking a routing option ([2] and Mukherjee et al.). Finding a new path in a highly mobile UAV network is inconvenient in typical protocols, resulting in a greater delay. Ant-Hocnet, on the other hand, is less effective in locating a high-quality routing link and so is unsuitable for higher packet loads. In this paper, we focus on how to improve the existing routing protocol for highly mobile UAV networks and how to calculate the best routing path for sending lager packets in FANET. We do further research for routing algorithm and proposed an algorithm based on Ant-Hocnet and fuzzy logic to increase throughput and packet delivery ratio and decrease end-to-end delay and improve overall network communication ability.

The rest of the paper includes the related work being summarized in Section 2. In Section 3, we present the overview of Ant-Hocnet, and Section 4 presents a fuzzy logic system. The detailed explanation of the calculation of bandwidth, mobility, and link quality is presented in Section 5. Section 5.4 presents the simulation results and comparison FAnt-Hocnet (FAHR) and existing Ant-Hocnet algorithm. Finally, the conclusion and future direction are given in Section 6.

2. Related Works

In this section, we review state-of-the-art existing routing protocols for MANETs, FANETs, and VANETs and analyze their strengths and weaknesses. The reason for reviewing related work to MANET and VANET is that they provide the basic foundation to from FANETs. Furthermore, most of the early work on FANET trace back to the use of MANET and VANET protocol usage for FANET.

Zheng et al. [14] proposed a novel hybrid protocol for routing based on location prediction directional MAC protocol (PPMAC) and a self-learning and reinforcement learning routing protocol called RLSRP. PPMAC merges the location prediction and directional antennas in the MAC layer to solve the directional deafness issue. The RLSRP empowers updating the local routing strategies with the location information of drones and an advantage task defined based on the global network efficacy; however, this protocol cannot support multichannel structure. Zheng et al. [15] proposed Stable Ant-based Routing Protocol (SARP). In SARP, a HELLO message is broadcasted occasionally to get the neighbor information. However, SARP route selection considers only the shortest path, which is not enough for routing in FANET with high mobility nodes and hence result in possibly weak links. In [16], Fatemidokht and Kuchaki Rafsanjani propose an optimize routing scheme called F-Ant for VANET; this scheme comprises of ACO algorithm and fuzzy logic. The scheme design is based on bandwidth, received signal strength metric (RSSM), and congestion metric (CM) for computing link's validity. In [17], the authors present a Fuzzy control Q-learning Ad Hoc On Demand Distance Vector (FQLAODV) approach for VANET. Fuzzy logic estimates a wireless link whether it is good or bad by determining metrics of signal limitation, bandwidth, and mobility, whereas Q-learning selects a route which can offer multihop consistency and effectiveness. The biggest downside of this method is its computational overhead. In [18], the authors proposed Ant-Hocnet based on the ACO routing algorithm for MANET. It uses both reactive and proactive approaches; proactive approach maintains and improves path before reactive path setup phase. Ant-Hocnet is enlivened by the stigmergy-driven which emerges from the behavior of ant colonies and the ACO system. The authors compared Ant-Hocnet with Ad Hoc On Demand Distance Vector (AODV), and the results show that Ant-Hocnet outperforms AODV. However, Ant-Hocnet is not efficient in terms of routing overhead.

The utmost challenge of FANET is to make sure the ubiquitous communication in a needy situation, where real-time transmission of data is prerequisite. Routing in FANET is much difficult than MANET and VANET due

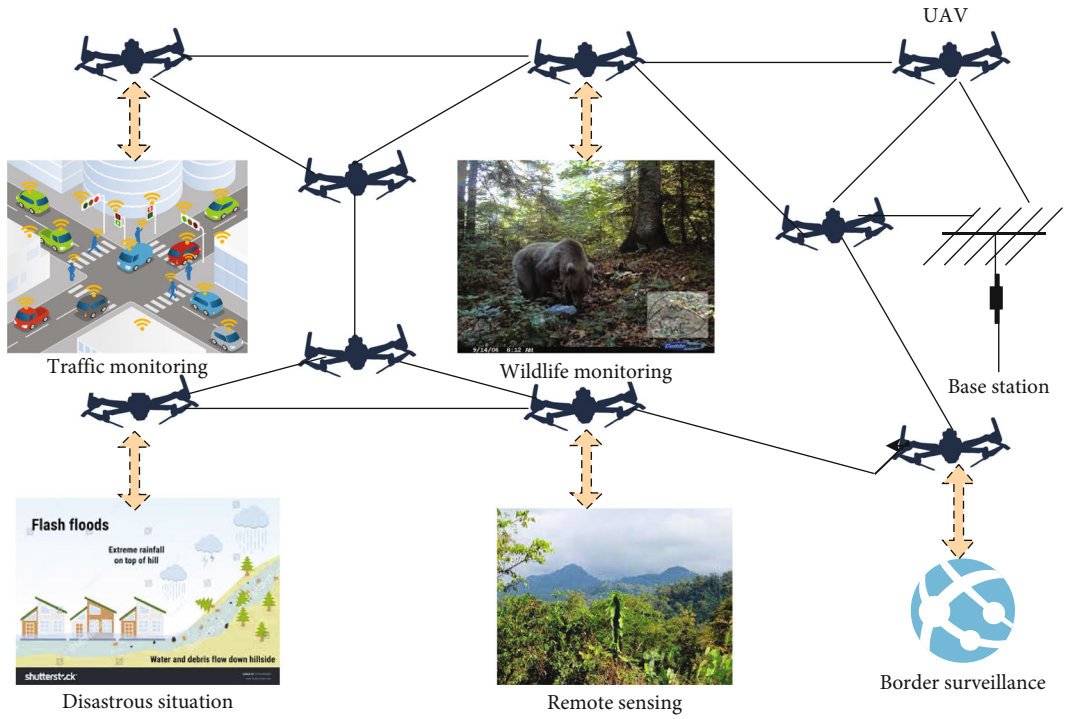

Figure 1: Multiple scenarios of Flying Ad Hoc Networks.

to its complex characteristics. A routing link may be weak, or a link may be broken in the network due to the high mobility and rapidly changing topology, sending a segmented packet produces high overhead resulting in higher latency and congestion, and these issues occur with most of the existing routing protocols. A vital problem arising in FANET is to choose the finest route among the UAV nodes. From literature review, it is concluded that a common issue in the existing ad hoc routing protocols is that they did not consider the important factors (i.e., bandwidth, mobility, and link quality) all together for choosing the best routing path for more effective and robust routing and requires a suitable technique to solve the issue.

In summary, the following are the limitations of the existing related work:

(i) The proposed scheme is not effective in decreasing the link failure as well as ensuring successful packet retransmission [12]

(ii) E-Ant-DSR leads to more delay as topology changes occur more frequently in FANET [19]

(iii) The RLSRP empowers updating the local routing strategies with the location information of drones and an advantage task defined based on the global network efficacy; however, this protocol cannot support multichannel structure [14]

(iv) SARP route selection considers only the shortest path, which is not enough for routing in FANET with high mobility nodes and hence result in possibly weak links [15]

(v) LEPR has not shown considerable results in both the finding frequency of route and the routing overhead [13]

There are various approaches to solve routing issues in FANET, the bio-inspired ACO-based algorithm is broadly used for routing issues in ad hoc networks. We use ACO-based Ant-Hocnet algorithm along with fuzzy logic to improve routing in FANET. Fuzzy logic is used to analyze the wireless link status info (i.e., available bandwidth, node mobility, and link quality) and calculate the best wireless links without a mathematical model.

3. The Proposed Scheme

In this research work, we exploit the bio-inspired Ant Colony Optimization (ACO) algorithm called "Ant-Hocnet" along with fuzzy logic to improve routing in FANET. Fuzzy logic considers the communication wireless link status info (i.e., available bandwidth, node mobility, and link quality) and calculates the best wireless links without a mathematical model in the swarm of UAVs. Fuzzy logic-based Ant-Hocnet selects the best routing path for sending larger packet loads more reliably with less delay.

3.1. System Design. Our proposed scheme is constructed on the ACO family algorithm for Ant-Hocnet routing. We consider Ant-Hocnet routing as it is a widely recognized routing protocol. The proposed scheme objective is to discover the best multihop routing path from the source node to the destination node. The effectiveness of a multihop routing path relies on the direct wireless links (one-hop links) that

establish the routing path. Every node broadcasts a hello packet periodically. Every hello packet contains the accessible bandwidth and all neighbors' addresses of the sender node. Through using a hello packet, every node preserves its two-hop neighbor information. The mobility factor (MoF) in our proposed scheme is estimated by using location information or one-hop and two-hop neighbor data. Therefore, our proposed scheme can still work even if the information on the position is not available. The reception ratio of the hello packet is estimated by every node to assume the quality of a wireless link to a neighbor. On the hello packet reception, every node computes the link status value of the wireless link to the hello message of a source node. The bandwidth, UAV mobility, and link quality estimate the link status value. Fuzzy logic is used to measure these three metrics jointly while choosing the best routing path shown in Figure 2.

To address the issue of improving routing protocol for reliable communication in FANET with the best available route among the UAV swarm as mentioned above, we consider the existing bio-inspired approaches used in ad hoc networks, which help us to classify the issues and challenges in FANETs. In FANET for the analysis of routing issues, the bio-inspired algorithms have been effectively implemented. Moreover, bio-inspired algorithms enable us to improve the intelligence in wireless ad hoc networks. Thus, in proposed method, the same algorithm has been adopted to achieve our intended results.

The models of fuzzy set theory are the description of inaccurate and incomplete sensory information as imagine by human brain. Consequently, it characterizes and mathematically works with such linguistic data in a natural method via the membership functions and the set of fuzzy rules. We tend to use fuzzy logic to resolve this issue without obtaining the mathematical model and to assess a link-based method to choose a route that might offer a multihop reliability and efficiency and examine available bandwidth, node mobility, and link quality in the selection of route. Fuzzy rules are efficiently stated to obtain the last fuzzy value. The fuzzy membership functions and the accompany fuzzy rules can be adapted to assure a specific situation. Moreover, by defuzzification, the resultant fuzzy values are changed to a numerical value.

3.2. Ant Colony Optimization (ACO). We exploit the bio-inspired Ant Colony Optimization (ACO) algorithm called "Ant-Hocnet" along with fuzzy logic to improve routing in FANET. Fuzzy logic considers the communication wireless links status info (i.e., available bandwidth, node mobility, and link quality) and calculates the best wireless links without a mathematical model in the swarm of UAVs. Fuzzy logic-based Ant-Hocnet selects the best routing path for sending larger packet loads more reliably with less delay.

For the proposed scheme, we exploit the Ant-Hocnet routing protocol which is constructed on Ant Colony Optimization (ACO) family algorithm. We consider Ant-Hocnet routing since it is a widely recognized routing protocol. ACO is a bio-inspired algorithm like Bee Colony Optimization (BCO), birds flock, etc.; mainly, it represents

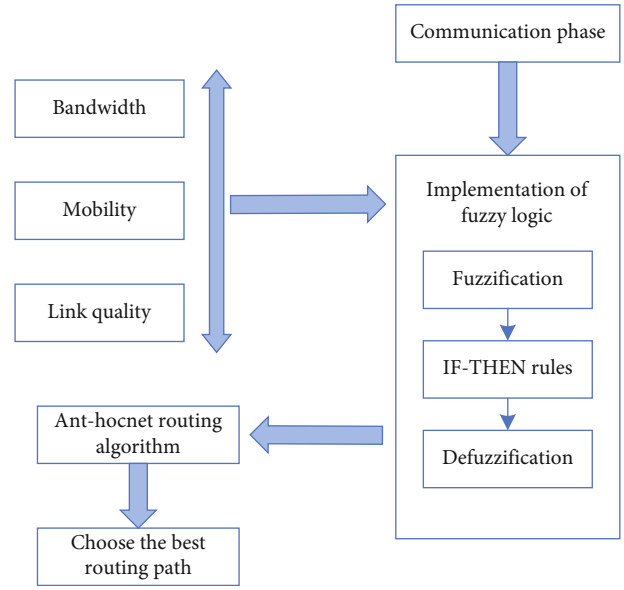

Figure 2: Block diagram of fuzzy logic-based Ant-Hocnet.

and uses the actions of ants and their liveliness. Ant-Hocnet has lots of similarity with reactive protocols such as AODV and Dynamic Source Routing (DSR) and as well as proactive protocol behavior similarities such as Destination-Sequenced Distance Vector (DSDV) and Optimized Link State Routing (OLSR). The proposed scheme objective is to discover the best multihop routing path to the destination node from the source node. The effectiveness of a multihop routing path relies on entirely the direct wireless links (one-hop links) that establish the routing path. Every node broadcasts a hello packet periodically. Every hello packet contains the accessible bandwidth and all neighbors' addresses of the sender node. By using the hello packet, every node preserves its two-hop neighbor info. The mobility factor (MoF) in our proposed scheme is estimated by using location info or one-hop and two-hop neighbor data. Therefore, our proposed scheme can still work even if the information of the position is not available. The reception ratio of the hello packet is estimated by every node to assume the quality of a wireless link to a neighbor. On the hello packet reception, every node computes the wireless link status to the hello packet of a source node. The bandwidth, UAV mobility, and link quality estimate the link status value. Fuzzy logic is used to measure these three metrics jointly as shown in Figure 2. The estimation of the considered factors are as follows.

3.2.1. Estimation of Each Link. Due to high mobility in FANET, wireless link quality changes more frequently. A good routing link in FANET is dependent on the bandwidth, mobility, and link quality of the network. Hence, in the estimation of a routing link, these matrices are considered together as shown in Figure 2. Mathematical model for choosing the routing path is complicated to derive, and a solution created on it would not be flexible. Meanwhile, a fuzzy logic system can manage uncertain and vague information. The use of fuzzy logic system is to resolve this issue

by not using the mathematical model. The range of the fuzzy logic numerical values is characterized by the fuzzy membership functions. The following is the process for estimating a direct wireless link.

3.2.2. Estimation of Bandwidth Factor (BwF). It is dependent on the channel idle time ratio (CITR), so first we derived CITR as follows:

$$\omega = \frac{\tau_i}{\tau_o}. \tag{1}$$

In equation (1), CITR is represented by ω, τ_i denotes the idle time interval, and τ_o is the observation time interval, where the observation time can be adjusted relative to the execution complication and essential accuracy (by default 50 ms). It is never a good idea to reach 100% bandwidth utilization. A typical rule is that average utilization should not exceed 70 percent, because beyond this limit, the collision rate allegedly becomes excessive. The average to avoid this may be as low as 30%, although 50% would be more common.

The idle time calculation as shown by [17] (same for all equations) is given as follows:

$$\text{idle time} = \begin{cases} T_{\text{ob}} - \sum_{k=1}^{n} \frac{S_k}{\text{Rate}_{\text{avg}}}, \sum_{k=1}^{n} \frac{S_k}{\text{Rate}_{\text{avg}}} < T_{\text{ob}}, \\ 0, \text{otherwise.} \end{cases} \tag{2}$$

In equation (2), n denotes the number of packets managed in the observation period T_{ob}, and S_k describes the kth packet size. The Rate_{avg} denotes the average channel data rate which is deliberate by the variation scheme. The channel usage specifies by the application programming interface (API), some of the wireless cards can offer the API. In that situation, the CITR is estimated in our proposed scheme with the help of MAC layer data. CITR is updated from every observation time with the help of a moving weighted exponential average as follows:

$$\omega \longleftarrow (1 - \psi) \times \omega_{j-1} + \psi \times \omega_j, \tag{3}$$

where ω_j represents the current CITR value and ω_{j-1} represents the previous CITR value. The constant ψ is set default to 0.7, which is the finest value in our simulation results for various cases. Each node affixes its personal CITR to hello packets and reactive forward ant (ReFANT) packets. Every node senses the channel and estimates a BwF as follows:

$$\text{BwF} = \min\left(\omega(s), \omega(d)\right), \tag{4}$$

where $\omega(s)$ represents the CITR at the source node s and $\omega(d)$ represents the CITR at destination node d. For estimation of mobility factor (MoF), in our proposed scheme, the GPS accessibility is not adopted, and the MoF is estimated from the neighbor data. Additional coverage of the node d is used to signify the set of nodes that are one hope neighbors of the node d; nonetheless, one hop neighbors are not of the recent node s. Explicitly, $\lambda(s, d)$ is described as follows:

$$\lambda(s, d) = \bar{N(s)} \cap N(d). \tag{5}$$

In equation (5), $N(d)$ represents the one hop neighbor of node d, and $N(s)$ denotes the one hop neighbor of the s node. Here, we observe that node d is associated to $N(s)$. On the hello packet reception, a node estimates a MoF for the hello source node. The MoF at time j for a node d is calculated as follows:

$$\text{MoF}_j(s, d) = \begin{cases} \sqrt{\frac{\left|\lambda_j(s, d) \cap \lambda_{j-1}(s, d)\right|}{\left|\lambda_j(s, d) \cup \lambda_{j-1}(s, d)\right|}}, \left|\lambda_j(s, d) \cup \lambda_{j-1}(s, d)\right| \neq \psi, \\ 0, \text{otherwise.} \end{cases} \tag{6}$$

In equation (6), $\lambda_{j-1}(s, d)$ denotes the previous value, and $\lambda_j(s, d)$ denotes the current value, respectively. For removing some errors, we use a moveable exponential average to compute the MoF as follows:

$$\text{MoF}(s, d) \longleftarrow (1 - \psi)\text{MoF}_{j-1}(d) + \psi\text{MoF}_j(d), \tag{7}$$

where ψ is a constant value set to 0.7 and MoF is adjusted to 0. In equation (6), the alteration in the additional coverage is used to calculate the neighbor node comparative mobility. With the movement of a neighbor UAV at the similar speed as the current UAV, the distinction of the additional coverage is minimum because of the comparatively static neighbor set. As earlier discussed, the proposed scheme can compute the MoF from neighbor data. Consequently, the proposed scheme performs when location data is not available. Nevertheless, when the location is easy to obtain, the protocol estimated the MoF by using data of the location. The MoF is estimated as follows:

$$\text{MoF}_j(s, d) = \begin{cases} 1 - \sqrt{\frac{\left|x_j(s, d) - x_{j-1}(s, d)\right|}{R}}, \left|x_j(s, d) - x_{j-1}(s, d)\right| < R, \\ 0. \end{cases} \tag{8}$$

In equation (8), $x_j(s, d)$ is the distances among the current node s and node d at the time j, and R is the average transmission range. Distances $x_j(s, d)$ and $x_{j-1}(s, d)$ can be calculated by every sender node attaching its location information to the hello messages. For estimating link quality factor (LqF), we consider link quality metric for reliable forwarding and minimize packet retransmissions and delay. The LqF is estimated from neighbor's data. A source node keeps a counter of every neighbor within a sliding window size to estimate the number of received

hello packet. Meanwhile, the hello packets are sent with a defined time interval, the hello packet reception ratio can be computed by each node, and also, there is a probability of collision of hello packets. To address this issue, the hello reception ratio (φ) is updated for each hello interval depends on the amount of hello packet reception within the last 10 s as follows:

$$\varphi_j(s,d) = \begin{cases} \dfrac{\eta_r(s,d)}{\eta_s(d)}, & \eta_s(d) \geq 10, \\ \dfrac{\eta_r(s,d)}{\eta_s(d)}, \left(1 - \left(\dfrac{1}{2}\right)^{\eta_s(d)}\right). \end{cases} \tag{9}$$

In equation (9), $\varphi_j(s,d)$ denotes the hello reception ratio, $\eta_r(s,d)$ is the amount of received hello packets at s from d, and $\eta_s(d)$ is the amount of hello packets transmitted from d. In the above equation, we define that the nodes that are only neighbors are discounted for less than 10 s (when $\eta_s(d) < 10$). The LqF was estimated as follows:

$$\mathrm{LqF}(s,d) \longleftarrow (1-\psi)\mathrm{LqF}_{j-1}(s,d) + \psi \times \varphi_j(s,d). \tag{10}$$

When $\mathrm{LqF}_{j-1}(d)$ is adjusted to 0, estimation of the LqF, $\mathrm{LqF}_{j-1}(s,d)$ is given as follows:

$$\mathrm{LqF}_{j-1}(s,d) = \begin{cases} 0, & \eta_s(d) < 10, \\ \mathrm{LqF}(s,d). \end{cases} \tag{11}$$

4. Fuzzy Logic

Models of fuzzy set theory [20, 21] are used to investigate imprecision and fractional data. Fuzzy set theory models, in particular, behave in a similar fashion to the human brain, in that they have a goal and make decisions in an uncertain environment. Nevertheless, for communication in FANETs, a specific model is not existing, because of high mobility, unreliable links, and limited resources. Hence, the control decision system has been executed by fuzzy logic theory whichever to manage the issue. The inputs to the fuzzy logic to be considered for routing are (1) bandwidth, (2) mobility, and (3) link quality. These metrics make the pheromone to reproduce the network rank and the node's capability to reliably send packets over the network.

4.1. Fuzzification of Inputs/Outputs. In the inference system, fuzzification is the process of converting multiple types of input data into a single output. The bandwidth factor (BwF), mobility factor (MoF), and link quality factor (LqF), all three-input metrics, need to be fuzzified. We have provided three kinds of labels for different factor in this work, but for more accurate results, the different factors can be labeled with more possible labels. We intend to add more possible labels for our future works. On the base of current information of FANET, the labels "small," "medium," and "large" are used to define the bandwidth factor, and to define the mobility factor, the labels "slow," "medium," and "fast" are used, and "good," "medium," and "bad" are labels for the representation of link quality factor. The membership functions are demonstrated in Figure 3.

4.2. Inference Engine and Knowledge Base System. The fuzzy inference system is a set of instructions developed with the help of experts. Fuzzy set theory models are the description of incorrect and incomplete information, as imagined by human mind. Furthermore, it illustrates linguistic information in ordinary simple method via membership functions and fuzzy rules. The fuzzy rules are well defined for getting the final fuzzy value. The IF-THEN pattern of the fuzzy set rules is used to infer output fuzzy values. The IF component is used to create conditions using predicates and logical linkages, whereas the THEN element is used to determine the degree of membership. Fuzzy membership functions and fuzzy rules are applied effectively to ensure an explicit situation. Furthermore, by defuzzification process, the final fuzzy value is changed to a numerical value.

Figure 3 shows the fuzzy inference system rules for the bandwidth factor, mobility, and link quality factors respectfully in a fuzzy logic system, while Figure 4 shows the graphical interface of these factors. The linguistic variables describe the ranks, i.e., "Perfect, Good, Acceptable, Unpreferable, Bad, Very Bad" are shown in Figure 5. The fuzzy rules are generated by using MATLAB app in the fuzzy logic toolbox, based on the proposed FAnt-Hocnet composes of 27 rules, as shown in Table 1.

4.3. Defuzzification. The procedure of translation of fuzzy output into a single value is called the defuzzification, and the defuzzification technique used in our proposed approach is the center of gravity (CoG). The fuzzy sets are used as an input for the defuzzification procedure. The fuzzy inference system includes the set of output values, which must be defuzzified in directive to determine a single yield value from the fuzzy inference system as presented in Figure 6.

5. Implementation and Analysis

This section gives a detailed interpretation of the simulation environment and the output results that are obtained using the proposed scheme, i.e., FAnt-Hocnet and the existing Ant-Hocnet algorithm. The simulation scenario is shown in Figure 7. We show the results for three different scenarios in which we consider different packet sizes. The performance of throughput, end-to-end delay, and packet delivery ratio is evaluated with the existing method.

To evaluate and implement the proposed solution, simulation is widely used for this purpose. There are various simulation tools available for the evaluation. However, we use MATLAB for our evaluation because of it suitability [22]. The proposed method is compared with one of the most important protocol called Ant-Hocnet protocol. We assume that 100 nodes are randomly located in an area of 500×500 m, and the nodes move as per the mobility model.

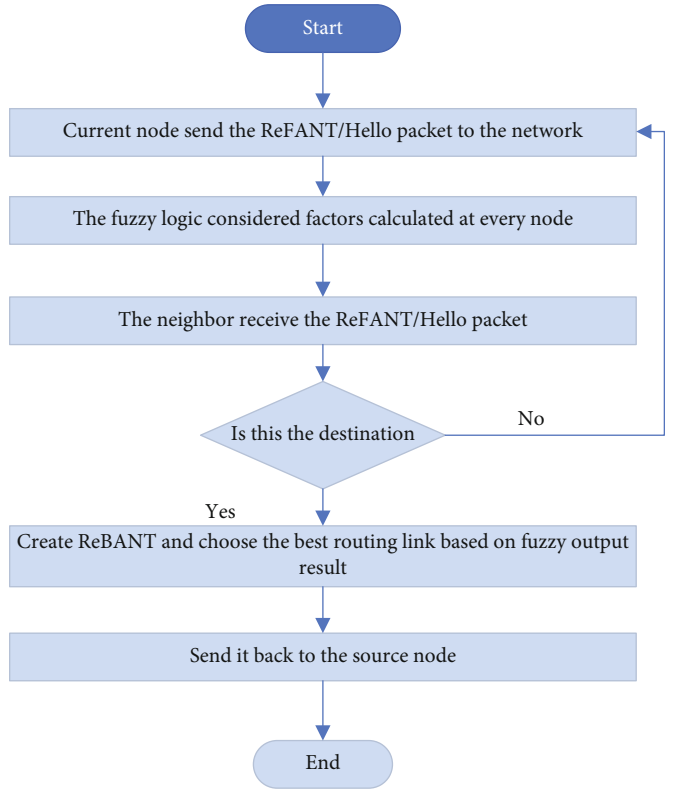

Figure 3: Flow chart of fuzzy logic-based Ant-Hocnet.

We have kept the simulation area 500×500 meters square to allow the swarm of UAVs to communicate with each other using the IEEE 802.11 (WLAN) standard, which has a maximum range of 100 meters in the 2.4 GHz ISM band. If the flying area is increased, the number of UAVs needs to be increased; consequently, the number of hop-count to the sink node will increase, and hence, delay will increase. We use the Gauss–Markov (GM) mobility model. The maximum speed is 100 m/s. Each node randomly chooses a destination point for communicating. Data traffic is generated by 10 constant bit rate (CBR) stream, and the packet size is 512 bytes as shown in Table 2. The results are generated for different data rates, i.e., 4, 6, 8, 10, 12, and 14 packets/s. At the MAC layer, the popular 802.11 protocol has been used as it is commonly used in ad hoc routing. Hence, we assume the MAC layer of IEEE 802.11 so the transmission range is that of IEEE 802.11 MAC. Moreover, we consider an Ideal FreeSpace propagation model with clear line of sight between transmitter and receiver.

In our simulation, we consider three different experiments for varying packet sizes (i.e., 64 bytes, 512 bytes, and 1024 bytes).

(i) First case: in this case, the packet size is 64 bytes

(ii) Second case: in this case, the packet size is 512 bytes

(iii) Third case: in this case, a larger packet size is assumed, i.e., 1024 bytes

Assumptions: designed and development for the FAnt-Hocnet and its working procedure, the following various assumption are established:

(i) We assume a swarm of UAVs moving freely in area of $500 * 500\,m^2$

(ii) We assume a collision free atmosphere

(iii) The range among the UAVs is 15 meters

(iv) We assume that no UAV node die due to power drainage

(v) We assume Ant-Hocnet reactive behavior

(vi) In our proposed scheme, we consider no queueing delay

Performance metrics: to validate the efficiency of the FAnt-Hocnet routing, we simulate the FANET scenario of Ant-Hocnet and FAnt-Hocnet. There are numerous measurable parameters which are exploited to estimate and examine the results, to estimate different scenarios of the network and routing performance. The following are the measurable parameters which are analyzed in this work.

5.1. Throughput. The throughput is defined as the average total amount of data that can be profitably transferred by a sender over a communication medium in a unit

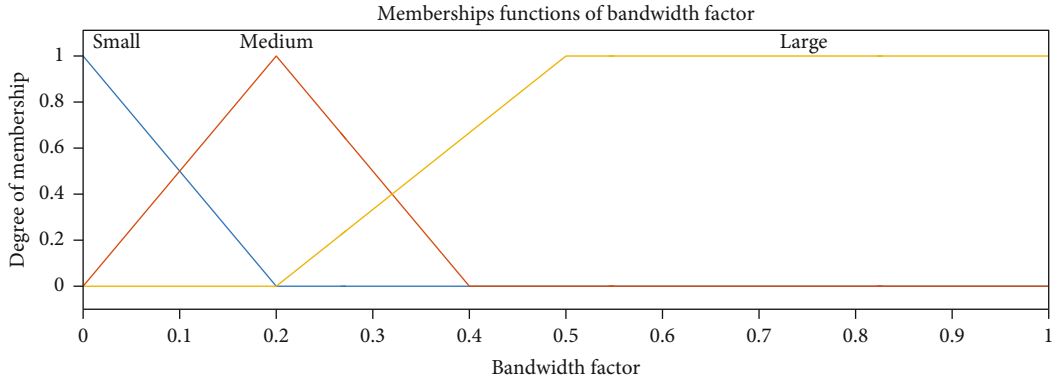

(a) Membership function of bandwidth factor

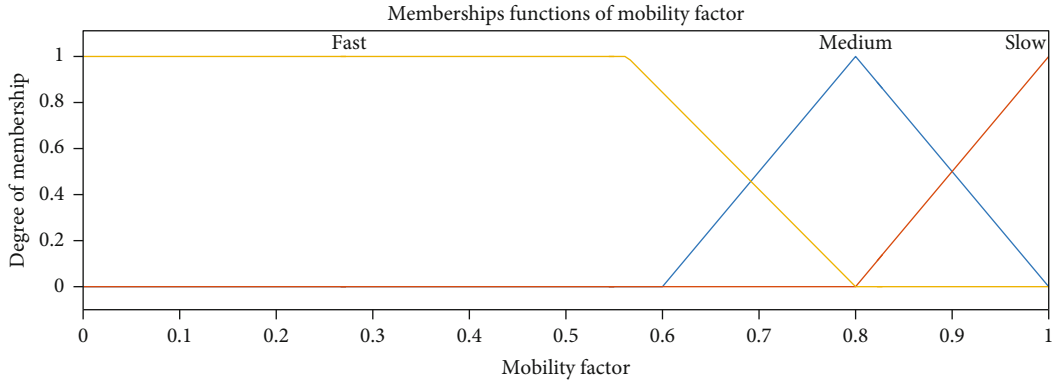

(b) Membership function of mobility factor

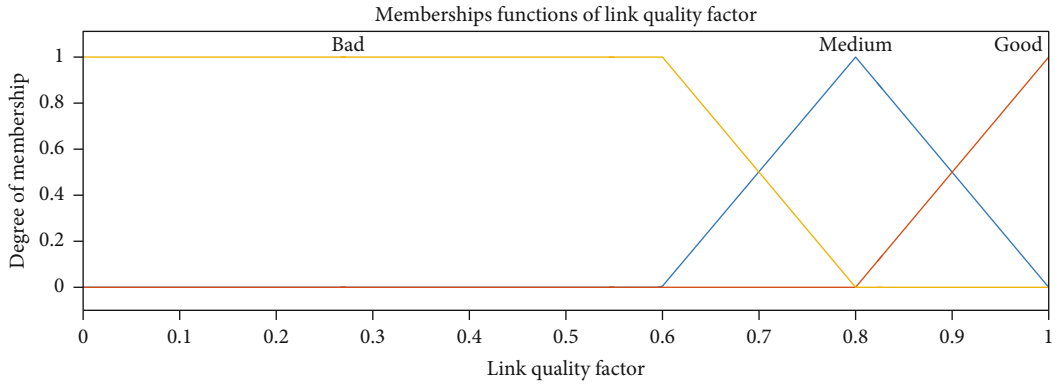

(c) Membership function of link quality factor

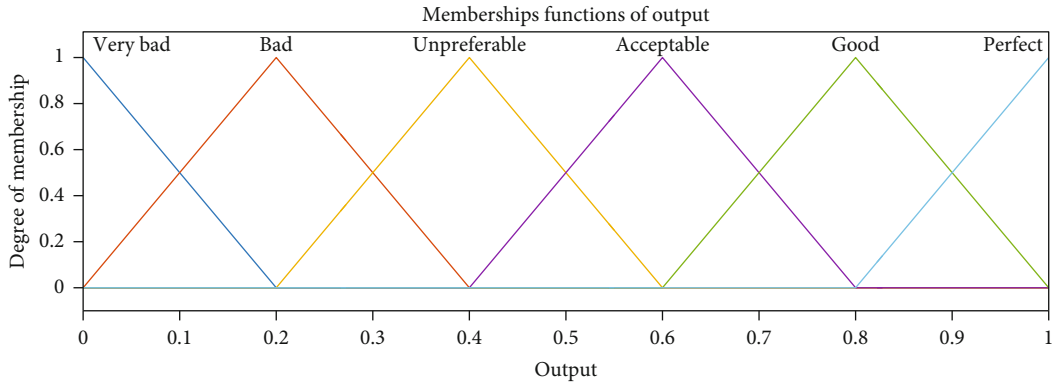

(d) Membership function of output

Figure 4: Membership functions.

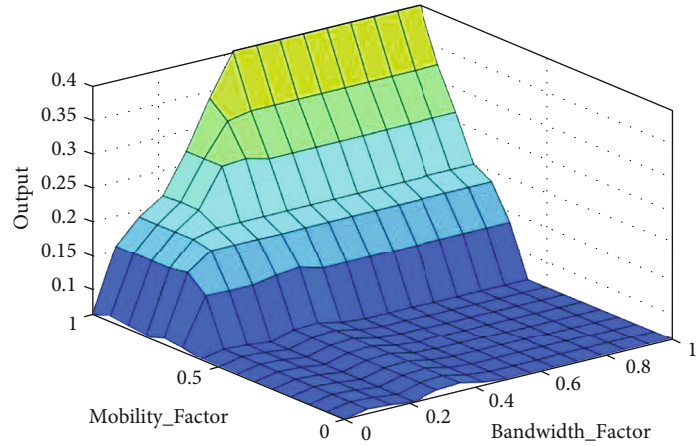

Figure 5: Surface view of membership function.

Table 1: Fuzzy logic rules.

	Bandwidth	Mobility	Link quality	Rank
Rule 1	Large	Slow	Good	Perfect
Rule 2	Large	Slow	Medium	Good
Rule 3	Large	Slow	Bad	Unpreferable
Rule 4	Large	Medium	Good	Good
Rule 5	Large	Medium	Medium	Acceptable
Rule 6	Large	Medium	Bad	Bad
Rule 7	Large	Fast	Good	Unpreferable
Rule 8	Large	Fast	Medium	Bad
Rule 9	Large	Fast	Bad	Very bad
Rule 10	Medium	Slow	Good	Good
Rule 11	Medium	Slow	Medium	Acceptable
Rule 12	Medium	Slow	Bad	Bad
Rule 13	Medium	Medium	Good	Acceptable
Rule 14	Medium	Medium	Medium	Unpreferable
Rule 15	Medium	Medium	Bad	Bad
Rule 16	Medium	Fast	Good	Bad
Rule 17	Medium	Fast	Medium	Bad
Rule 18	Medium	Fast	Bad	Very bad
Rule 19	Small	Slow	Good	Unpreferable
Rule 20	Small	Slow	Medium	Bad
Rule 21	Small	Slow	Bad	Very bad
Rule 22	Small	Medium	Good	Bad
Rule 23	Small	Medium	Medium	Bad
Rule 24	Small	Medium	Bad	Very bad
Rule 25	Small	Fast	Good	Bad
Rule 26	Small	Fast	Medium	Very bad
Rule 27	Small	Fast	Bad	Very bad

time. In fact, it is an associated metric to packet delivery ratio. However, the throughput is measured in bits not in the number of data packets. Characteristically, it is calculated in kbps, Mbps, and Gbps. The throughput can be calculated as by [23] as follows:

$$P_t = \left(\frac{\sum_{i=1}^{n} R_{ij}}{\sum_{i=1}^{n} S_{ij}}\right) * 100, \tag{12}$$

where P_t denotes the throughput (in packets), R_{ij} denotes the packets collected by node j sent from node i, and S_{ij} denotes the packets sent by the node i to node j.

5.2. End-to-End Delay. End-to-end delay denotes the time taken by a data packet transmitted by a source node to reach the destination. End-to-end delay is the sum of all probable delays created by buffering through route-finding latency, queuing at the interface queue, retransmission delays in MAC layer, propagation, and transmission times. In this work, we do not consider the queuing delay. In the situation, no link breaking prediction algorithm and multipath routing protocol are existing; then, this delay will be high since the time consumed in discovering a route is involved in the end-to-end delay. Mathematically, average end-to-end delay can be defined as follows:

$$\text{End-To-End Delay} = \frac{1}{n}\sum_{i=1}^{n=1}(p_i(T_r) - p_i(T_s)), \tag{13}$$

where p_i represents the ith packet, $p_i(T_r)$ represents the receiving packet time, $p_i(T_s)$represents the sending packet time, and n is the total number of successfully delivered packets.

5.3. Packet Delivery Ratio. This parameter is computed among the amount of data packets successfully sent from the sources and the number of data packets received by the destinations. In this work, we consider the average packet delivery ratio, which is the average value of the packet delivery ratios of the whole traffic inside network. The fewer data loss at the receiver side of all the destinations shows that the

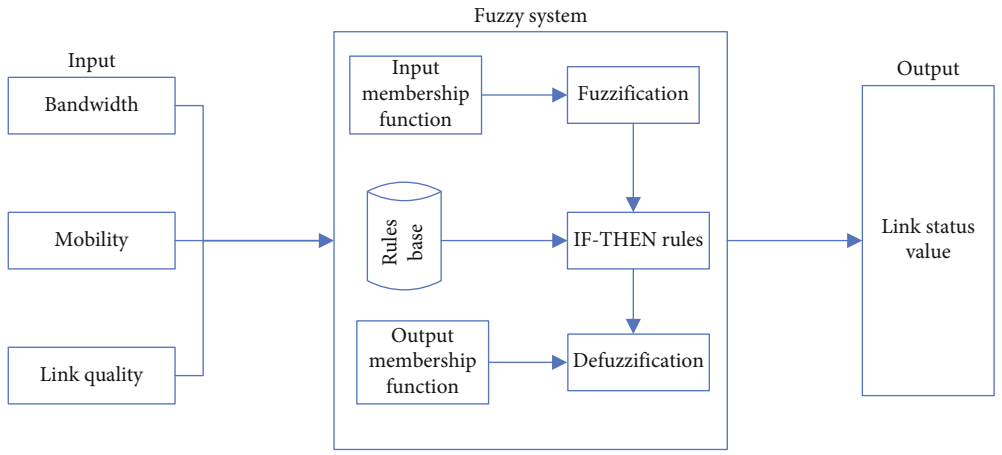

Figure 6: Fuzzy inference system.

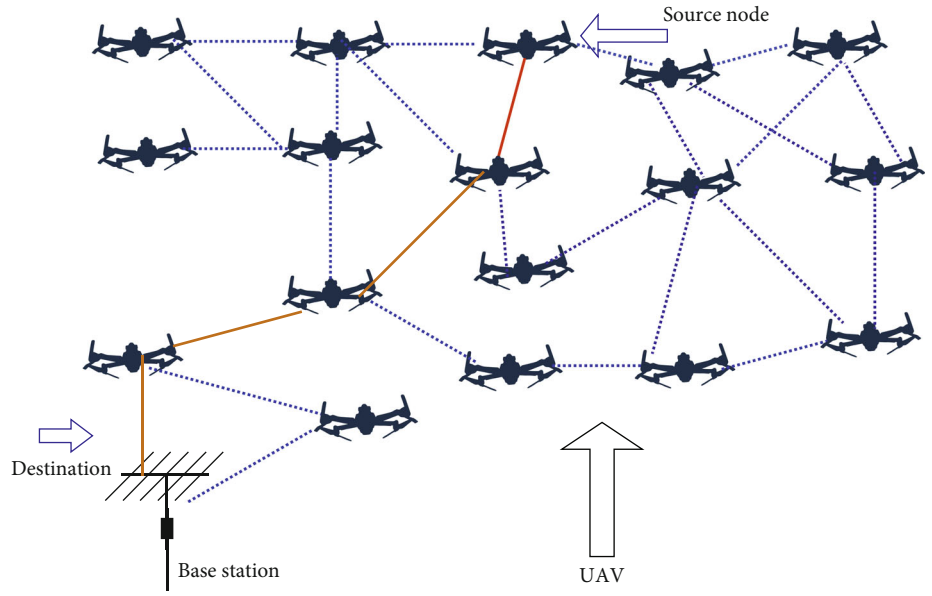

Figure 7: Simulation scenario.

Table 2: Simulation parameters.

Parameter	Values
Simulation tool	MATLAB 2013b
Simulation area	500 m ∗ 500
Number of UAVs	100
UAV speed	100 m/s
Data rate	4, 6, 8, 10, 12, and 14 packets/s
Traffic type	CBR
CBR packets per second	10
Packet size	512 bytes
MAC layer	802.11
Protocol	Ant-Hocnet
Mobility model	Gauss-Markov

packet delivery ratio is significantly higher and the improved network performance. The formula is given as follows:

$$\text{PDR} = \frac{\sum \text{RP}_d}{\sum \text{SP}_s} \times 100, \tag{14}$$

where RP_d is the receiving packets at destination and SP_s is the sending packets from source.

5.4. Comparison of Results and Discussion. We show the result for throughput in Figure 8. Here, FAnt-Hocnet exceptionally outperforms the Ant-Hocnet routing protocol. Ant-Hocnet shows lower throughput than FAnt-Hocnet; this is due to the fact that Ant-Hocnet does not consider UAV's bandwidth, mobility, and link quality in the routing path selection and, therefore, result in the throughput degradation. For larger packets, the FAnt-Hocnet algorithm shows higher throughput than Ant-Hocnet from the start because

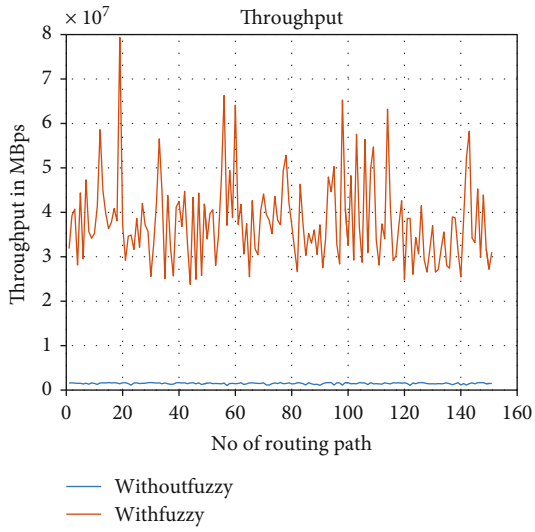

Figure 8: Throughput vs. number of routing path.

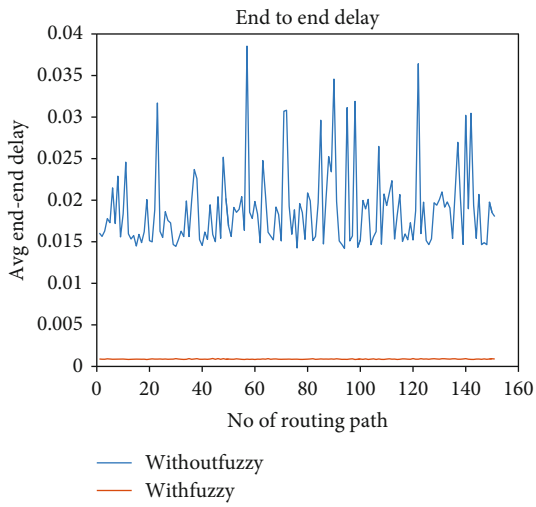

Figure 9: Avg. end-to-end delay vs. number of routing path.

FAnt-Hocnet chooses the best routing path for routing by using the fuzzy logic [24], while retransmission of larger packets due to poor-quality channel selection in the case of Ant-Hocnet degrades its throughput.

Figure 9 shows the end-to-end delay for both the schemes; the FAnt-Hocnet considers the bandwidth, mobility, and link quality which decreases the number of weak links and hence result in less end-to-end delay than Ant-Hocnet. The frequent changes in topology, route discoveries, and retransmission of larger packet result in higher end-to-end delay for Ant-Hocnet. FAnt-Hocnet decrease the end-to-end delay by choosing the fuzzy logic-based best routing path for reliable communication.

Figure 10 shows the PDR of the proposed scheme vs. the Ant-Hocnet algorithm. The FAnt-Hocnet algorithm shows higher PDR as compared to the Ant-Hocnet algorithm. For larger packet, the FAnt-Hocnet algorithm shows higher

Figure 10: PDR in % vs. number of routing path.

PDR than Ant-Hocnet from the start, because FAnt-Hocnet choose the best routing path for routing by using the fuzzy logic.

6. Conclusions

In this paper, we employ the bio-inspired Ant Colony Optimization (ACO) algorithm called "Ant-Hocnet" and propose FAnt-Hocnet routing protocol based on optimized fuzzy logic to improve routing in FANET. Fuzzy logic is used to analyze the information about the status of the wireless links, such as available bandwidth, node mobility, and link quality, and calculate the best wireless links without a mathematical model. FAnt-Hocnet being a multipath routing protocol achieves the highest throughput and low end-to-end delay especially in high network loads and high mobility as it chooses the best routing path for packet transmission. The results show that by applying the intelligence of fuzzy logic systems provides the best routing path from source to destination in a network. Thus, it provides effective and robust communication channel for packets.

In future, we intend to expand the proposed work and to measure the packet drop probability and priority-based packet reliable communication. Moreover, the security consideration will also be address in the future to prevent the malicious nodes. To reduce the congestion in FANETs, a novel smart solution will be proposed.

Data Availability

Data is available in the paper.

Conflicts of Interest

The authors declare that they have no conflicts of interest.

References

[1] A. AlKhatieb, E. Felemban, and A. Naseer, "Performance evaluation of ad-hoc routing protocols in (FANETs)," in *2020 IEEE Wireless Communications and Networking Conference Workshops (WCNCW)*, pp. 1–6, Seoul, Korea (South), 2020.

[2] M. Y. Arafat and S. Moh, "Routing protocols for unmanned aerial vehicle networks: a survey," *IEEE Access*, vol. 7, pp. 99694–99720, 2019.

[3] V. K. Gunjan, J. M. Zurada, B. Raman, and G. Gangadharan, *Modern Approaches in Machine Learning and Cognitive Science: A Walkthrough*, Springer, 2020.

[4] R. Hussain, J. Lee, and S. Zeadally, "Trust in VANET: a survey of current solutions and future research opportunities," *IEEE Transactions on Intelligent Transportation Systems*, vol. 22, no. 5, pp. 2553–2571, 2020.

[5] M. I. B. Azevedo, C. Coutinho, E. M. Toda, T. C. Carvalho, and J. Jailton, "Wireless communications challenges to flying ad hoc networks (FANET)," *Mobile Computing*, vol. 3, 2020.

[6] F. Noor, M. A. Khan, A. Al-Zahrani, I. Ullah, and K. A. Al-Dhlan, "A review on communications perspective of flying AD-HOC networks: key enabling wireless technologies, applications, challenges and open research topics," *Drones*, vol. 4, no. 4, p. 65, 2020.

[7] J. Jiang and G. Han, "Routing protocols for unmanned aerial vehicles," *IEEE Communications Magazine*, vol. 56, no. 1, pp. 58–63, 2018.

[8] A. Nadeem, T. Alghamdi, A. Yawar, A. Mehmood, and M. Siddiqui, "A review and classification of flying ad-hoc network (FANET) routing strategies," *Journal of Basic and Applied Scientific Research*, vol. 8, no. 3, pp. 1–8, 2018.

[9] J. Li, M. Wang, P. Zhu, D. Wang, and X. You, "Highly reliable fuzzy-logic-assisted AODV routing algorithm for mobile ad hoc networks," *Sensors*, vol. 21, no. 17, p. 5965, 2021.

[10] Q. Yang, S.-J. Jang, and S. J. Yoo, "Q-learning-based fuzzy logic for multi-objective routing algorithm in flying ad hoc networks," *Wireless Personal Communications*, vol. 113, no. 1, pp. 115–138, 2020.

[11] J. Souza, J. Jailton, T. Carvalho, J. Araújo, and R. A. Francês, "A proposal for routing protocol for FANET: a fuzzy system approach with QoE/QoS guarantee," *Wireless Communications and Mobile Computing*, vol. 2019, Article ID 8709249, 10 pages, 2019.

[12] R. Jain and I. Kashyap, "An QoS aware link defined OLSR (LD-OLSR) routing protocol for MANETs," *Wireless Personal Communications*, vol. 108, no. 3, pp. 1745–1758, 2019.

[13] X. Li and J. Yan, "LEPR: link stability estimation-based preemptive routing protocol for flying ad hoc networks," in *2017 IEEE symposium on computers and communications (ISCC)*, pp. 1079–1084, Heraklion, 2017.

[14] Z. Zheng, A. K. Sangaiah, and T. Wang, "Adaptive communication protocols in flying ad hoc network," *IEEE Communications Magazine*, vol. 56, no. 1, pp. 136–142, 2018.

[15] X. Zheng, Q. Qi, Q. Wang, and Y. Li, "A stable ant-based routing protocol for flying ad hoc networks," in *2017 4th International Conference on Machinery, Materials and Computer (MACMC 2017)*, pp. 410–416, Atlantis Press, 2018.

[16] H. Fatemidokht and M. Kuchaki Rafsanjani, "F-Ant: an effective routing protocol for ant colony optimization based on fuzzy logic in vehicular ad hoc networks," *Neural Computing and Applications*, vol. 29, no. 11, pp. 1127–1137, 2018.

[17] C. Wu, S. Ohzahata, and T. Kato, "Routing in VANETs: a fuzzy constraint Q-learning approach," in *2012 IEEE global communications conference (GLOBECOM)*, pp. 195–200, Anaheim, CA, USA, 2012.

[18] G. Di Caro, F. Ducatelle, and L. M. Gambardella, "AntHocNet: an adaptive nature-inspired algorithm for routing in mobile ad hoc networks," *European Transactions on Telecommunications*, vol. 16, no. 5, pp. 443–455, 2005.

[19] S. Chatterjee and S. Das, "Ant colony optimization based enhanced dynamic source routing algorithm for mobile ad-hoc network," *Information Sciences*, vol. 295, pp. 67–90, 2015.

[20] L. A. Zadeh, *Fuzzy Sets, Fuzzy Logic, and Fuzzy Systems. Chapter Fuzzy Sets and Information Granularity*, World Scientific Publishing Co., Inc., River Edge, NJ, USA, 1996.

[21] G. Mehmood, M. Z. Khan, A. Waheed, M. Zareei, and E. M. Mohamed, "A trust-based energy-efficient and reliable communication scheme (trust-based ERCS) for remote patient monitoring in wireless body area networks," *IEEE Access*, vol. 8, pp. 131397–131413, 2020.

[22] G. Mehmood, M. Z. Khan, M. Fayaz, M. Faisal, H. U. Rahman, and J. Gwak, "An energy-efficient mobile agent-based data aggregation scheme for wireless body area networks," *Computers, Materials & Continua*, vol. 70, no. 3, pp. 5929–5948, 2022.

[23] A. Husen, M. H. Chaudary, F. Ahmad, M. I. Alam, A. Sohail, and M. J. P. C. S. Asif, "Improving scheduling performance in congested networks," *PeerJ Computer Science*, vol. 7, article e754, 2021.

[24] C. Wu, S. Ohzahata, and T. Kato, "Flexible, portable, and practicable solution for routing in VANETs: a fuzzy constraint Q-learning approach," *IEEE Transactions on Vehicular Technology*, vol. 62, no. 9, pp. 4251–4263, 2013.

Hindawi
Wireless Communications and Mobile Computing
Volume 2022, Article ID 7979766, 21 pages
https://doi.org/10.1155/2022/7979766

Research Article

Towards a Low-Cost Teacher Orchestration Using Ubiquitous Computing Devices for Detecting Student's Engagement

Ibrar Ahmad,[1] Shah Khusro,[1] Iftikhar Alam,[2] Inayat Khan,[3] and Badam Niazi[4]

[1]*Department of Computer Science, University of Peshawar, Peshawar 25000, Pakistan*
[2]*Department of Computer Science, City University of Science and Information Technology, Peshawar 25010, Pakistan*
[3]*Department of Computer Science, University of Buner, Buner 19290, Pakistan*
[4]*Department of Computer Science, University of Nangarhar, 2600, Afghanistan*

Correspondence should be addressed to Badam Niazi; niazi5.48@gmail.com

Received 7 April 2022; Accepted 13 May 2022; Published 18 June 2022

Academic Editor: Zahid Khan

The ubiquitous devices and technologies to support teachers and students in a learning environment include the Internet of things (IoT), learning analytics (LA), augmented or virtual reality (AR/VR), ubiquitous learning environment (ULE), and wearables. However, most of these solutions are obtrusive, with substantial infrastructure costs and pseudo-real-time results. Real-time detection of students' activeness, participation, and activity monitoring is important, especially during a pandemic. This research study provides a low-cost teacher orchestration solution with real-time results using off-the-shelf devices. The proposed solution determines a teacher's activeness using multimodal data (MMD) from both teacher and student's devices. The MMD extracts different features from data, decodes them, and displays them to the instructor in real time. It allows the instructor to update their teaching methodology in real time to get more students on board and provide a more engaging learning experience. Our experimental results show that real-time feedback about the classroom's current status helped improve learning outcomes by about 45%. Also, we investigated a 50% increase in classroom engaging experience.

1. Introduction

This pervasive development in technology has made computers more robust and smaller. The computers successfully made their way from giant PCs to small portable mobile devices, which created a new era of ubiquitous computing that made accessible computers anywhere with more excellent perception and understanding of the surrounding environment through sensors [1]. Mark Weiser coined the term "ubiquitous" in the 90s [1], resulting in several smart devices including smartphones, smartwatches, and smart TV [2] being used in various scenarios. For example, wearable devices (smartwatches, bands, etc.) are advantageous in health-related applications and others. Users' gestures are required as they are constantly connected to the skin and fixed on the human body [3]. Like other fields, including business, health, and entertainment, these devices have more potential to be efficiently and effectively exploited to improve education quality. One such prominent example is smart wearable devices for teacher orchestration [4]. These technologies are utilized for teaching, learning, and orchestration in a learning environment.

Teacher orchestration refers to managing different classroom activities encompassing individual, small group, and whole class in a face-to-face classroom by a teacher [5]. The word orchestration came from *orchestra*, which means carefully organizing a complicated event [6]. In the context of a smart classroom, teacher orchestration is the careful arrangement of a technologically more prosperous classroom environment and activities to achieve the required learning outcomes [6]. The main focus is facilitating a teacher in monitoring and healthier students' performance in a ubiquitous learning environment (ULE) [7]. In ULE, small and handheld devices perform various monitoring and data visualization tasks to support teachers' and students' learning pedagogies. A typical classroom contains multiple kinds of activities. A teacher must manually manage several paper-based activities, such as taking attendance

by calling students' names and marking them present or absent. It can be technology-assisted by using different sensors and other devices [8]. Traditional orchestration is more ubiquitous in most institutes because it is easy to use and requires less training.

Still, time consumption and resource wastage are among the expected downsides of this approach. Technological devices were employed to assist teachers and students in the learning process to overcome these issues, which created the smart classroom concept. Smart classrooms are technologically rich learning spaces where computers and other devices are exploited to help teachers and students [9]. Although this approach helped overcome these issues, there are other complications regarding user acceptance and development costs due to giant infrastructures. Several custom-built hardware with multiple sensors are used [10], increasing the setup cost and affecting user experience and social acceptance. Therefore, smartphones were deployed instead of using custom-built hardware and equipped with different sensors [11–13]. Using handheld devices, a new era of ULEs evolved, transforming the educational context into complex social and technological ecologies by expanding the scope of education beyond the classroom [7].

Several studies proposed numerous approaches to perform the orchestration process using multimodal data from multiple sources. These studies leverage different technologies, including the Internet of things (IoT) [10, 14, 15], intelligent tutoring systems (ITSs), learning dashboards [16], augmented and virtual reality (AR/VR) [17, 18], smart wearables [19], different sensors, and ubiquitous computing devices [7]. However, most of the proposed solutions are either not real time or expensive and less user-friendly because they need technical assistance to be used.

Most studies focused on custom-made hardware, which provided good results in some circumstances, such as lab environments [20]. Still, the setup cost and acceptability in the real-world classroom are a matter of concern. It requires technical assistance from paid experts or specially hired employees to deploy and use these clumsy infrastructures in a learning space. Using ubiquitous computing devices reduces setup costs, but they are not real time and provide results after the classroom session. This delay is becoming the main reason for time wastage for teachers and learners as they cannot adjust their behaviors in that specific session. To mitigate these issues, it is required to provide a real-time teacher orchestration solution using off-the-shelf and low-end devices, which is the paper's main aim. The proposed solution is low-cost, easy-to-use, with a real-time feedback facility about the class's current status. The main goal of this research work is to leverage the potential of off-the-shelf smart devices, including smartphones and smartwatches, in teacher orchestration to reduce the use of custom-made and specialized hardware, which increases the setup cost and requires technical assistance for deployment and usage.

This study attempts to avoid using any external server for data acquisition, processing, or result generation. Thus, it significantly reduces the cost and effort required for setting up and using the system in real-world classroom scenarios. The proposed solution needs a smartwatch, i.e., a wearable device worn by the teacher in their dominant hand and connected to a smartphone placed in front of the teacher. The connected smartwatch sends its sensor's data to the connected smartphone, processing and analyzing for final result generation on the smartphone. The application collects data from both teachers and students. The facial orientation of the teacher is used to measure her activeness or tiredness level. A server application is developed and deployed on the teacher's smartphone to collect and process the multimodal data from the teacher's and students' devices. The processed data is displayed on the teacher's smartphone showing statistics about the current state of the class, e.g., how many students are active and inactive and what is his voice quality during the lecture. Results show a significant increase in learning outcomes, i.e., a 45% increase. Also, we investigated a 50% increase in classroom engagement. The gathered data shows that this solution is less intrusive and has no serious issues for students and teachers. Also, the system can be applied in other lecture-demonstration methods.

The rest of the paper is divided into six sections. Section 2 is a comprehensive yet concrete literature review. Section 3 is the proposed methodology that elaborates the technical aspects. Section 4 is the implementation of the system. Section 5 is the experimental setup section. Section 6 shows results and analysis that further discusses the obtained results. The *last section* is the conclusion section. The references are numbered in the last section.

2. Literature Review

Mobile and computer technology have been introduced into educational contexts over the past two decades [21]. Access to computers and large-scale one-to-one computing programs have been implemented in several countries globally [22–24], such that elementary and middle school student(s) and teacher(s) have their electronics and mobile devices. In terms of encouraging and promoting innovation and modernization in education through mobile and information technology (IT), it also supports traditional lecture-style teaching, convenient information gathering, and information sharing and promotes innovative teaching methods such as cooperative learning [25, 26], exploratory learning outside the classroom, and game-based learning [27]. On the flip side, the marvelous expansion of sensor technology in smartphone(s), along with their sensing capabilities for accurate capturing, monitoring, and analysis of information, helps us know about traffic conditions [28–30], road conditions [31–33], environmental impacts of noise level [34], air quality and pollution level [35–39], humidity and temperature [40], understand patterns of objects movements [41–43], alerting and monitoring disaster [44, 45], weather information [46], etc.

The IT and mobile technologies can facilitate and enable innovative educational methods. Simultaneously, these patterns in educational practices will likely help subject content learning and facilitate the development of communication, problem-solving, creativity, and other high-level skills among students [20]. Also, it will support teachers in orchestrating different classroom activities and increase the

learning outcomes. The technological use for teacher orchestration has evolved from computers [47] and IoT devices to handled smartphones. Table 1 shows a variety of sensor technologies and their inevitable usages in teacher orchestration.

2.1. Assessments during Class. Student monitoring and engagement are positively linked with the required learning outcome. For instance, good grades in curricular and extracurricular activities are directly linked to critical thinking and the efficiency of the subject(s) [61].

Being a teacher is one of the most important factors for student(s) engagement and attention [62]. Teachers' coordination and proper communication facilitated by a verbal, gestural, and written connection with their student(s) can benefit the student(s) mesmerization and attention. Classroom monitoring can be considered a powerful tool to determine the quantity and quality of active learning in the classrooms [63]. Monitoring activities lead to many engagement improvements, e.g., to improve learning [64], engagement to improve throughput rates and retention [65, 66], engagement for equality/social justice [67], and curricular relevance [68]. Submissive to the important monitoring and engagement, different tools [69], technologies [54], algorithm(s) [70], and strategies have been used to measure and estimate the attention level of both student(s) and teacher(s).

According to [71], only 46% to 67% of the students pay positive attention to the class during lecture delivery. It means half of the students could never be productive. With this information in hand, both the teachers and researchers have examined potential problems that arise during their classes, and efforts have been made to eradicate and correct them, which may have a long-term benefit on the learning efficiency of the learner and students. The study also showed that students' engagement and focus are positively linked with good grades and critical thinking [61]. It is only possible with full attention and focus, which depends on numerous elements and factors, including the teacher [62]. According to [72], a classroom's size influences student attention and engagement. In large classes, the teacher needs to use more time to draw students' attention, which is sometimes emotionally exhausting.

Face detection, face recognition, facial features, pose estimation, etc. techniques have been used for student monitoring, for instance, student attendance monitoring system based on deep learning [73, 74], tracking through eye tracking [75], monitoring meeting through head orientation, and gaze direction [76], assessing and monitoring classroom attention [77], and estimation of activeness, transcribing, unavailing, distracted and transition, automatic recognition of engagement from students' facial expressions [78].

2.2. State-of-the-Art Orchestration Solutions. According to Chan, "orchestration" is derived from orchestra in teacher orchestration [79]. Each student interacts with a digital device in a smart classroom to support them in the learning process. A smart classroom is an intelligent learning space equipped with different devices, sensors, and custom software agents [19]. Leeuwen and Rummel [80] reviewed various orchestration tools for teachers to help them understand students' collaboration in their groups. Smart wearables were also analyzed in a pedagogical context, like [81, 82], to explore wearable technologies in the educational aspect and discuss different approaches to using smart wearable and smartphones for m-learning [10] and teacher orchestration. Suárez et al. [82] discussed using smartphones in education using inquiry-based learning by examining multiple approaches and their strengths and limitations.

The IoT was extensively used in the classroom to support both teachers and students [17]. Subbarao et al. [83] analyzed different IoT-based approaches providing solutions for several learning pedagogies using devices and sensors. Also, different augmented and virtual reality (AR/VR) solutions for supporting learning activities are discussed in [10, 84]. These approaches are categorized based on their technology stack and used infrastructure in the following subsections.

2.2.1. Internet of Things (IoT). The connection of different devices (things) with the Internet is known as the Internet of things [83, 85]. A smart classroom contains multiple intelligent devices, which eventually need to communicate to enrich the learning experience. IoT is one of the widely used approaches in different solutions; unlike other fields of life, it also evolved in teaching and learning pedagogies. Most of the solutions found in the literature, which use sensors for getting data from learning space, are based on the IoT paradigm. Rico et al. in [86] and Subbarao et al. in [9] review different IoT-based approaches providing multiplicity solutions for several learning pedagogies using a combination of devices and sensors.

Gligoriü et al. [87] determine lecture quality using different sensors like PIR and sound sensors and a video camera. Similarly, another study [84] finds the student's satisfaction from a classroom session using physical environment parameters. The student uses their smartphones to input their feedback as satisfied or not satisfied [88]. In another study, Gligorić et al. [8] designed an LED lamp to show students' interest or satisfaction levels using Raspberry Pi (https://www.raspberrypi.org). They record 30 lectures using cameras and microphones and annotate students' data using their smartphones. Students click exciting or not interesting when they find something satisfactory or unsatisfactory. A 30-second window was labelled when more than 90% of votes were received.

Mahmood et al. [14, 84] used a camera connected with Raspberry Pi to calculate students' interest levels from their facial expressions and notify the teacher about their current status. Besides getting data about the lecture, IoT is also used for classroom attendance; in [89], Atabekov designed a smart chair for getting classroom attendance and time spent by a student in the classroom.

2.2.2. Near-Field Communication. The Near-Field Communication (NFC) technology is also used for automatic student attendance, indoor classroom location, and real-time feedback [90]. In [91], an RFID-based campus security system is proposed by Mirza and Brohi, which monitors and

Table 1: Mobile senor technologies and their usages in teacher orchestration and smart classroom.

S. no.	Mobile sensor	Application
a	Camera sensors	Mostly used to capture images of both user(s) and its surrounding with numerous applications—such as user recognition, recognizing user(s) inclination and its surrounding context [48] Can be exploited in teacher orchestration, for example, student head-movement detection, body pose, and facial expression estimation for better performance [15, 49–51]
b	Microphone sensor	Used to capture voice(s) generated in the surrounding, either by the user itself or other objects with numerous applications—such as voice identification system, accident detection, and spying system A microphone sensor has been used in the classroom to detect voice level created by student and teacher and for discourse analysis among student(s) or between teacher(s) and student(s). In education and teacher orchestration, microphone sensor has also been used in affective student modeling [52], teaching and learning [47], teacher-student dialogue recognition [53], etc.
c	Ambient light sensor	Used to measure the light intensity of the surrounding atmosphere, with numerous applications—such as environmental pollution monitoring systems, weather forecasting systems, and picture capturing systems In teacher orchestration, ambient light sensors can be exploited to measure the light level of the classroom for the healthy projection of light [54, 55] and students-to-board focus
d	Accelerometer sensor + gyroscope sensor	Used to measure movements, acceleration information of users, angles, and inclination with numerous applications—such as old people healthcare systems, automatic traffic accident detection systems, and games [56, 57] In teacher orchestration, an accelerometer sensor has been used in measuring student-teacher communication [58], assessment of voice quality among college students [59], etc.
e	Proximity sensor	Used to detect objects with numerous applications—such as blind people guidance systems for navigating them through the pattern of their steps
f	GPS sensor	GPS sensor is used in several capacities ranging from general navigation, tourist assistive system, helping soldier in the battlefield, etc. GPS sensor has been used in orchestration too; for instance, Sun et al. [60] showed how GPS can be used to increase self-efficacy, self-regulation, and student achievement. Also, GPS can be used for indoor location or seat mapping
g	Compass sensor	Usually used to measure phones or user's location and their direction

tracks different resources, including students' records, exam papers, and student certificates, using cloud computing. Another similar approach [92] used PIR and RFID sensors with Arduino to monitor classrooms and parking lots and determine which occupied or empty classroom or parking space. Furthermore, they used a video camera with a cloud platform to offer a virtual classroom for e-learning. Said et al. in [91] introduced an IoT-based e-learning system called "free learning" or F-learning, consisting of smart classrooms and virtual labs that autonomously communicate with each other using cloud infrastructure. And finally, Haung et al. [93] and John et al. [94] used multiple sensors to control smart classrooms by getting different data and decreasing energy conservation.

2.2.3. Augmented and Virtual Reality. Augmented and virtual reality (AR/VR) allows users to be physically involved in different blended scenarios and create a hybrid learning environment by combining physical and digital objects [18]. As students learn 50% of what they hear and read while 90% of what they do [95], AR/VR for learning purposes might significantly provide positive results and help students grasp more helpful information. Herpich et al. [96] discussed different mobile-based augmented reality solutions for supporting learners.

Elkoubaiti et al. [97] explore AR/VR in education and smart classrooms. They describe the technical requirements including latency, field of view, resolution, frame rate, network requirements, and measurements for the privacy and security of AR and VR applications. Similarly, Munoz et al. [98] represent a case study using an AR-based tool named GLUEPS-AR and a VR game (Game of Blazons). The study conducted different VR/AR-based activities for students and showed that these VR/AR tools help teachers create different learning situations. Also, Kosmas et al. [93] evaluate the effect of the motion-based game on student performance during language learning classes.

Khan et al. [99] developed an augmented reality mobile application to examine their learning motivation. They used the ARCS (attention, relevance, confidence, and satisfaction) model to find the significance of AR technology on students' learning performance. Although the available literature has extensive studies focused on AR/VR, according to Murat and Gokçe [16], many students cannot arrange AR/VR headsets. Also, it distracts students' attention, and undoubtedly, it is expensive as well.

2.2.4. Learning Dashboards. A learning dashboard is a visualization tool supporting teachers and learners in different learning scenarios for better decision-making [100]. It is a

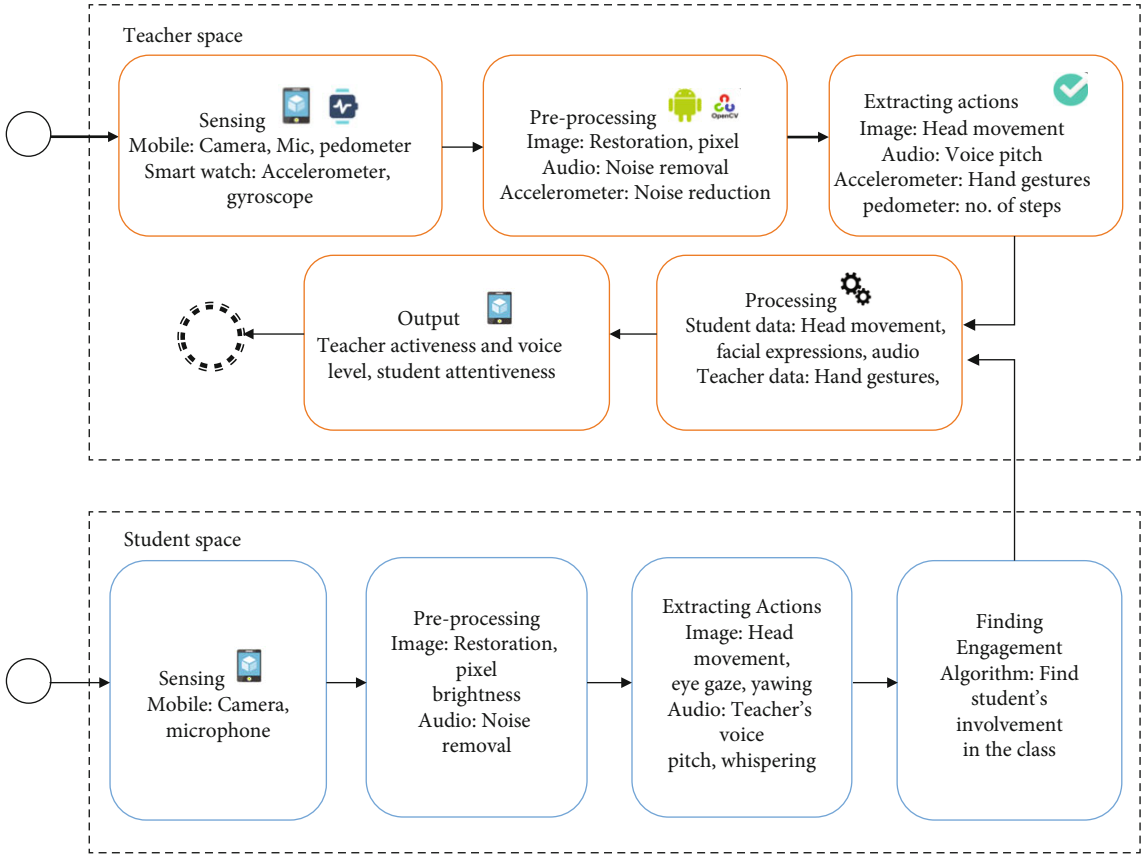

Figure 1: Activity diagram of the proposed solution.

Input: camera image ***img*** in Bitmap//Google Vision APIs only accept bitmap images
Output: facial features (head rotation/title)
1. Detect faces in img using Google APIs FaceDetector and store them in list<FirebaseVisionFace> object faces
2. For $i = 0 - >$length of faces list
    i. Set face to faces [i]
    ii. Set headRotation to angle Y of face
    iii. Set headTilt to angle Z of face
        //Now using this data for decision-making
    iv. If headRotation > 20 and headRotation < −20//means the student is not looking straight
        a. If warnTeacher is false//if last time he was looking straight, then wait for the next iteration before marking him inactive
            I. Set warnTeacher to true
        b. Else//it means he was also looking somewhere else last time
            I. Mark this student inactive
        c. Else//means the student is looking straight
        d. Set warnTeacher to false//clear previous state
3. End

Algorithm 1: Detect facial feature and head direction.

specific intervention of learning analytics used to identify meaningful data for various stakeholders (like teachers, students, and administrators) and how data representation can be helpful in sense-making [16]. Korozi et al. [5] developed LECTOR—a web-based tool for students' reengaging systems in smart classrooms using multimodal data from different sources, including an eye tracker, depth camera, microphone, and other embedded sensors.

Similarly, another approach used LECTOR [100] and a smartwatch app called NotifEye [101], which shows a teacher's smartwatch notification with different information regarding students' current learning status, activeness, and other positive interventions. Holstein et al. [102] developed a real-time dashboard for the intelligent tutoring system (ITS), which assists students during their programming course for learning http://ASP.net (https://dotnet.microsoft

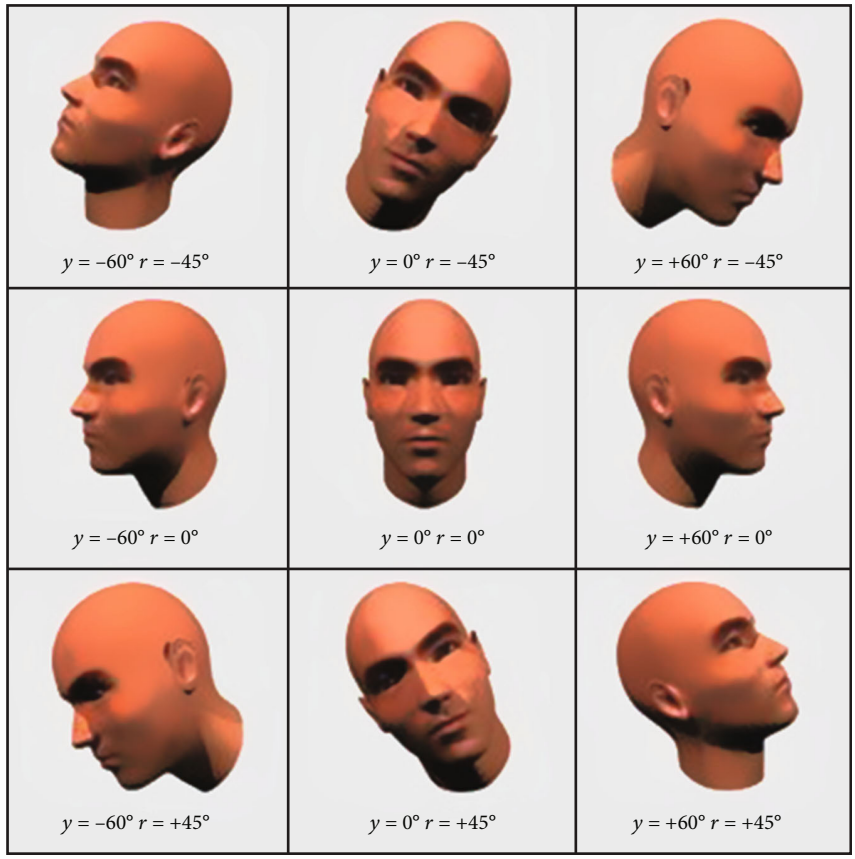

Figure 2: Head pose example where y represents left-right rotation and r represents tilt angle (https://developers.google.com/vision/face-detection-concepts).

Input: application context to create MediaRecorder object
Output: class activity ("lecturing, Q&A")
1. Create MediaRecorder object mRecorder using application context
2. Set voiceLevelFromStudentA to amplitude received from student A
3. If voiceLevelFromStudentA > 40
    1. If voiceLevelOfTeacher from mRecorder > 40//it means teacher is lecturing but student is talking with someone else
        i. Set student A as inactive
        ii. Set currentActivity as "lecturing"
    2. Else//means teacher is not talking only student A is speaking
        i. Set student A as active (only if he is looking straight)
        ii. Set currentActivity as "question answering"
4.Else
    1. Voice is not clear for student A, notify teacher

Algorithm 2: Infer class activity from audio data.

.com/apps/aspnet). VanLehn et al. developed a FACT multimedia system [7]—a web-based AI tool that records students' collaborative activities of arranging paper cards on the math class poster. Wetzel et al. [103] analyze the same FACT system with a traditional paper-pen-based approach to evaluate the time wastage factor of both conventional and electronic systems in learning pedagogies. Although learning dashboards better visualize students' data, most systems require extra hardware and sensors.

2.2.5. Ubiquitous Computing and Other Sensors. The educational contexts have evolved into complex technological and social ecologies using different ubiquitous devices to transform the traditional learning space in ubiquitous learning environments (ULEs) [104]. Iqbal [46] represented a mobile application for teachers to mark quiz and exam papers and input feedback about students' performance. Viswanathan and VanLehn in [105] and Tissenbaum et al. in [106] used students' interaction logs with web app and tablet apps,

Input: application context to create SensorsManager object
Output: raw values from sensors
1. Start
a. Create SensorsManagers object sensorManager using application context
b. Get sensorsList from SensorsManagers
c. For eachSensor in sensorsList:
i. Set sensor X to value of x-axis of eachSensor
ii. Set sensor Y to value of y-axis of each sensor
iii. Set sensor Z to value of z-axis of eachSensor
iv. Wait for 300 milliseconds
v. If application is not closed
1. Go back to step c//to continuously capture sensor data
d. Release sensorManager//to avoid resource leakage
2. End

Algorithm 3: Get sensor data from smartwatch.

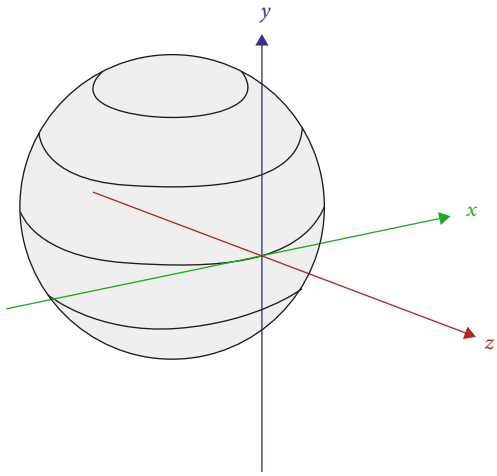

Figure 3: Accelerometer axes (http://developer.android.com/reference/android/hardware/SensorEvent.html).

respectively, to identify their collaboration in a classroom session. In [107], Yu-Gang et al. proposed a mobile-based learning model, enhancing smartphones' traditional learning. Smartphones are also used for automating the attendance process in ULE to facilitate teachers. Budi et al. [108] used image processing to take students' attendance by using a mobile camera and a trained machine learning model running on the server for face recognition to identify different individuals in the uploaded image. Yang et al. [20] used voice print to mark students' attendance and detect their indoor location in the classroom. In [109], Gligoric et al. measure the level of interest of a lecture by detecting student movements using a video camera, classroom sound (with microphone), and teacher's movement from his smartphone accelerometer.

Prieto et al. [110] used the teacher's smartphone's accelerometer with other devices like a camera, microphone, and electroencephalogram (EEG) sensor (for capturing brain activities) to identify different classroom activities like an explanation, questioning, and monitoring. They identify teachers' actions in a classroom session from multimodal data and build an "orchestration graph." And while the orchestration graph defines who does what and when [111], it is a time-series graph plotting different activities with a given time and duration. Similarly, other approaches [112–114] reduce the infrastructure and use low-end devices; they used microphones to capture audio data and segment the lecture into different subactivities like question-answering. But these approaches require training the system for each teacher individually because of the change in voice tone and different speaking styles.

Recommendation techniques recommend tailored items to a user [115–118]. Liu et al. [119] proposed a smart learning recommendation system, which captures data from different sources to determine students' current learning state and then suggests or reinforces different learning strategies (like quiz). In another approach, Bdiwi et al. [109] investigated the impact of teachers' positions on students' performance in higher education. Wang et al. [19] used an eye tracker to determine how much the teacher's gaze guidance affects the students learning performance in video lectures. Similarly, Viilo et al. [120] perform teacher orchestration video data recorded in the classroom.

2.2.6. Wearables. The advantage of wearables over mobile devices is that they can be available most of the time, unlike mobile technology, mainly in pockets or bags [121]. In a study, Garcia [122] proposed a smartwatch app named "ScienceStories," where students can record their science concepts. They find that the gamification mode has the highest use among the students. Quintana et al. [123] evaluate the acceptability of wearables in education by using the smartwatch to remind different tasks to the teacher during the classroom session.Also, Lu et al. [124] used a smartwatch for learning analytics to predict various activities using the hand gestures of a particular student. Another study designed, developed, and evaluated a wearable application for students with intellectual and developmental disabilities (IDDs) to assist them in the educational environment [19]. Wearables like smartwatches and smart bands are another common type of wearables named optical head-mounted

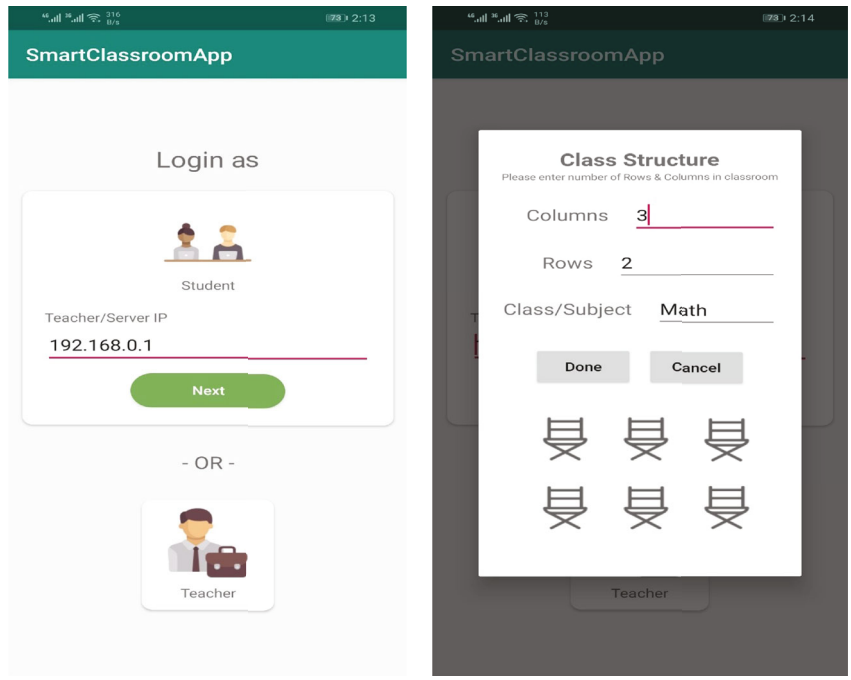

(a) (b)

FIGURE 4: (a) Choose to start the application in either teacher or student mode. (b) Ask the teacher to enter the number of rows and seats in each row for classroom structure.

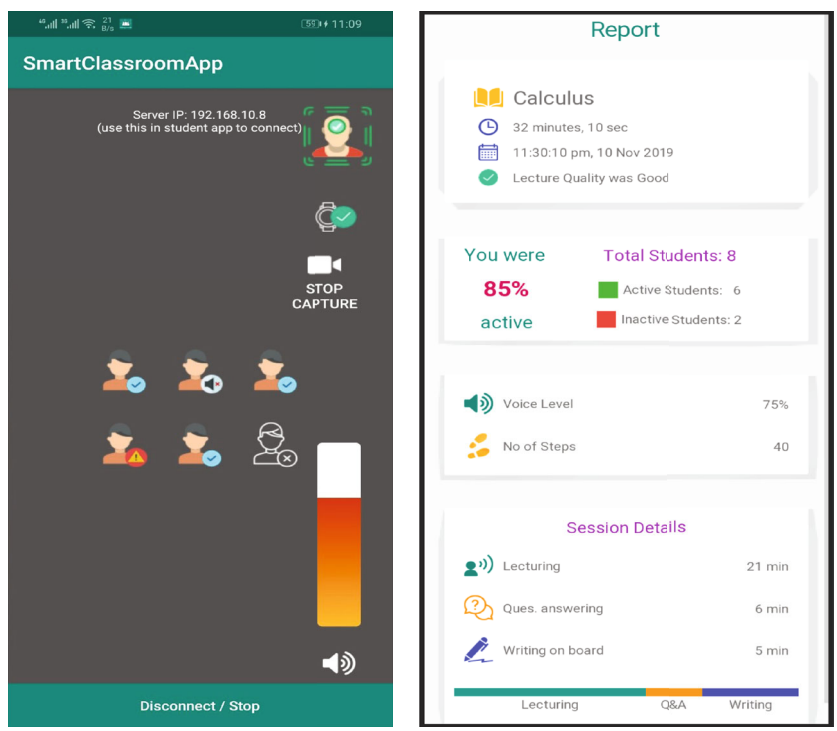

(a) (b)

FIGURE 5: (a) Teacher application showing class status and activeness level in real time. (b) The final report was presented at the end of a class.

displays (OHMDs) or simply head-mounted displays (HMDs). They are usually worn over the eyes, which can either be utterly immersive like VR headset (Oculus (https://www.oculus.com)) or nonimmersive such as smart glasses (Google Glass [124] or Microsoft HoloLens (https://www.microsoft.com/en-us/hololens/)) [110]. In [112], the

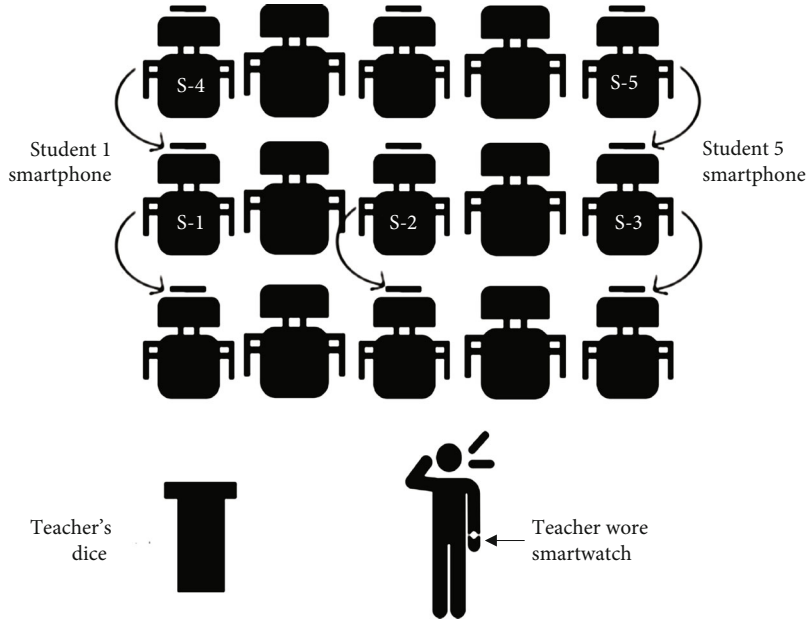

Figure 6: Classroom structure with student and teacher's positions during the experiment.

Figure 7: (a) Smartphone jacket installed at the chair's back to keep the smartphone in front of a student. (b) Teacher wearing a neck holder to monitor classroom status on his smartphone and wearing a smartwatch.

teacher wore Google Glass to view the emotional status of each student in the classroom.

Patrick [114] used audio data from the microphone for different segment activities in a learning session. The author used a machine learning approach to train a classifier and then predict various activities from the given audio data, like answering, supervising students, and lecturing. Similarly, Donnelly et al. [86] also used audio data from the microphone to detect teacher questions from a live classroom session. Finally, Bdiwi et al. [108] used RFIDs to find the impact of the teacher's position on students' performance using an IoT-based approach.

Gligorić et al. [87] also used IoT devices, including PIR and sound sensors, to detect the lecture quality. Finding the lecture quality in real time is a positive approach, but using extra hardware raises costs and acceptability-related issues. In another study, Gligoric et al. [84] used a video camera, mic, and Android smartphone to detect the level of interest a lecture created. The author also proposes another IoT-based solution to show students' satisfaction levels [84]. Finally, Mahmood and Salman [125] used a video camera and Raspberry Pi to find students' attentiveness levels using their facial expressions and assist teachers in improving their teaching methodology.

The materials and methods should contain sufficient detail so that all procedures can be repeated. It may be divided into headed subsections if several methods are described.

3. Proposed Methodology

The proposed solution needs a smartwatch worn by the teacher in their dominant hand and connected to a smartphone placed in front of the teacher. First, it helps collect the teacher's hand and foot movement to identify if the teacher is moving during the lecture or remains static. Then, the smartwatch sends its sensor data to the connected

Figure 8: Scan QR code for the indoor location.

smartphone, processing and analyzing for final result generation on the smartphone.

The application collects data from teachers and students, as shown in Figure 1. The system gets the teacher's hand and foot movements and her audio- and face-related information using a smartphone and smartwatch from the teacher's side. The foot movements help identify whether the teacher is static or moves and interacts with students. Hand movement is used to capture hand gestures and remember different actions. The audio data is used to measure the teacher's sound level and helps differentiate who is currently speaking. If it is only the teacher's voice, it is classified as a lecturing event. If there is a combination of students' and teachers' voices, it is counted as a question-answer session or discussion. The facial orientation of the teacher is used to measure her activeness or tiredness level. A server application is developed and deployed on the teacher's smartphone to collect and process the multimodal (different sources) data from the teacher's and students' devices. The processed data is displayed on the teacher's smartphone showing statistics about the current state of the class, e.g., how many students are active and inactive and what is his voice quality during the lecture.

The application shows the current status of the classroom after collecting multimodal data in real time. It also provides a short glimpse of different activities at the end of a classroom session, for example, how much time the teacher spent lecturing, question answering (discussion), and writing on board. The application can mark students as active and inactive by processing the head and voice-related data discussed later in sections. The teacher's activeness (Equation (3)) is calculated from two factors, i.e., classroom current status and voice level of individual students. The classroom's current status can be found using

$$\mathrm{CS} = \frac{\text{no.of active students}}{n}, \tag{1}$$

where n is the total number of connected students, i.e., both active and inactive in that specific learning session, at the same time, and CS stands for classroom status, which will be a decimal value between 0 and 1. Similarly, the voice level can be calculated using

$$\mathrm{VL} = \frac{\sum_{i=1}^{n} V_i}{n * \text{max-voice-level}}. \tag{2}$$

Here, V_i represents voice level for an individual student, max-voice-level is the maximum threshold set for voice level, i.e., 90 decibels (dB) for our experiment, and n is the total number of connected students. The resulted value of voice level (VL) will be a decimal number between 0 and 1. And finally, Equation (3) uses these CS values, and VL can compute the teacher's activeness level, which will be again a decimal number from 0 to 1.

$$\text{Teacher}'\text{s activeness} = \frac{\mathrm{CS} + \mathrm{VL}}{2}. \tag{3}$$

Finding the value of the teacher's activeness fulfils our first object of this research work. Now to meet the second objective, i.e., finding the contribution of each modality, we analyze the kind of data captured from these modalities and then find the use of that captured data.

4. Implementation

The system works in a local area network to get data from different stakeholders. The teacher's application acts as a

Table 2: Demographics of participants.

S. no.	Type	Min age	Max age	Male	Female	Total
1	Teacher	34	51	12	6	18
2	Student	24	28	17	5	23

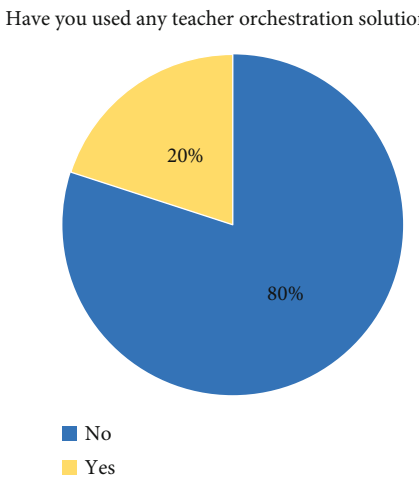

Figure 9: Participants used teacher orchestration tools before.

server to collect data from connected students. The student's application running on different students' smartphones is responsible for collecting and processing the data and then sending that processed data to the teacher's smartphone for final representation and results in a generation. This section discusses how the application captures and processes this multimodal data in real time.

4.1. Data Acquisition and Processing. The following data is collected from both teachers and students, analyzed and used to find the classroom status and voice level as stated in Equations (1) and (2).

4.1.1. Facial Data. According to Mahmood et al. [84], the understanding of student interest level is allied with the quality of the lecture. Therefore, the application captures face-related data from teachers and students to get their level of interest and activeness in the current classroom session. This study focuses on head movement to analyze how much head direction helps identify the current attention level of the student. For this purpose, Google Vision APIs (https://cloud.google.com/vision/) detect users' faces from images captured using a smartphone's camera. These APIs provide a framework for detecting and tracking objects in images and videos. It supports face detection, barcode reading, and text recognition. For example, the head left to right movement represents head rotation, with a value between −60 and +60 and represented with y. Similarly, it also gives clockwise rotation, representing head tilt angle from −45 to +45 annotated as r. The application takes a picture every 5 seconds and passes the captured bitmap image to Algorithm 1 to detect different face-related features.

The APIs offer different face-related data, including the number of faces detected, head rotation, head tilt (in degrees), smiling probability, eye-opening probability, and facial landmarks. Shown in Figure 2 is how these APIs consider head rotation tilt angle. Since the APIs provide head rotation and tilt, the rotation exceeds 20 degrees, i.e., +20 degrees on the right side, while −20 for looking at the left side (Step vii). Then, the application checks whether he exceeded this limit last time; if this is the first time he was noted, the application will wait for the next cycle/iteration; otherwise, it marks him as inactive. So, for example, if a student is not looking straight in the first cycle, the system will set a flag value warnTeacher to true, but in the next process, if the student is found looking straight, the application will mark him active and set warnTeacher back to false.

4.1.2. Voice Data. The application also collects voice data to infer classroom activities like lecturing or question-answer session. The microphone is used from existing smartphone devices in front of the teacher and students. The application collects audio data and performs preprocessing for noise removal on the student side. This cleaned data is used to measure the voice level of teachers and students in the classroom environment. If it detects only the teacher's voice, it is marked as a lecture. But if there is a combination of both teacher and student's voices within a defined threshold, then the system considers it a discussion or question-answering session. It uses standard Android APIs to collect and extract features from audio data for audio processing. As the application measures the voice level, we used the MediaRecorder class from Android APIs to get the maximum amplitude of audio data. The student application sends this amplitude value to the teacher's smartphone, and the teacher application compares these values captured from different students. As given in Algorithm 2, if the voice difference between the two nearest students is noticeable, i.e., a value from student A is 35 dB, while the next student (student B) sends a value of 60 dB, then the application checks whether voice amplitude is captured on the teacher's smartphone if the teacher's voice is around 50 to 60 dB. Thus, the application infers that the teacher is lecturing while student B talks with someone. But suppose the teacher's voice amplitude is less than 30 dB. In that case, the application considers that the student is asking a question and therefore marks that session as "discussion" or "question answering," as shown in Algorithm 2.

4.1.3. Hand and Foot Movement Data. To find the teacher's mobility and interaction in the classroom, the system captures her hand and feet to infer whether the teacher is standing still or moving. The system includes an off-the-shelf Android Wear-OS (https://wearos.google.com/) available smartwatch worn by the teacher on the dominant hand. In addition, it captures data from IMU (Inertial Measurement Units) sensors, including accelerometer, gyroscope, and pedometer mainly. The application uses Android APIs to interact with sensors and captures data at the rate of 40 samples per second to correctly recognize gestures from raw data [126]. Further details of these sensors are given below. Algorithm 3 shows steps getting sensory data from smartwatches.

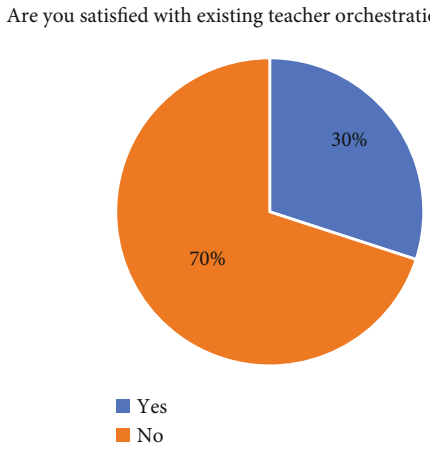

Figure 10: Satisfaction level after using existing teacher orchestration solutions.

Table 3: Question asked after a test run.

S. no	Questions
1	Is the application easy to use?
2	Did the application improve teacher performance?
3	Did the application produce disturbance during the classroom session?
4	Did smartphone-based orchestration provide a more engaging experience in the classroom?
5	Are you satisfied with smartphone-based teacher orchestration?
6	Should this application be used in other classrooms as well?
7	Any comments or suggestions.

(1) Accelerometer. An accelerometer is used to measure the acceleration (change of velocity) in three axes (x, y, and z) [127]; see Figure 3. It reads these acceleration values from the smartwatch accelerometer to find hand gestures.

(2) Gyroscope. A gyroscope is used to measure the angular velocity (orientation/tilt) of a device's three dimensions (x, y, and z) [8]. Therefore, it correctly identifies hand gestures by combining them with the accelerometer data.

(3) Pedometer. A pedometer is an electromechanical sensor used to detect and count each person's step [127]. The application uses several steps to identify whether the teacher is standing still or moving toward the students in the classroom.

4.1.4. Data Representation. To better user experience and reduce cognitive overload, the application shows a seating map on the screen to mimic the real classroom structure. Therefore, when the teacher starts the application to monitor, he is prompted to input the number of rows and seats in each row in the classroom (Figure 4(a)). Then, starting the application in server mode, the teacher presents a grid of icons representing student setting in the classroom (Figure 4(b)). This icon changes according to the current student status; for example, when a student is not connected, the white icon, but when a new student gets connected, the application captures his seat number from the connection request packet and updates their status from the white icon to a colored icon. To decide which icon will be updated in the grid of the application, use the seat number.

After collecting multimodal data from several connected devices, all the data is combined on the teacher's smartphone for final calculation and result generation. The system contains different features regarding face and voice data from the student's side. The application continuously updates the seat-map grid to show the latest data on the screen. For example, if the voice level is less than 40 dB (see Algorithm 2, Step 3). Similarly, suppose the user's face is not detected or their head direction exceeded by 20 degrees (see Algorithm 1), in that case, the application provides real-time feedback to the teacher.

On the teacher side, after getting this multimodal data from all students, the application first calculates the class status CS using the number of active students (marked using Algorithm 1) and total students using Equation (1). Similarly, the overall classroom voice level VL is also calculated using Equation (2). And finally, by substituting the values of CS and VL in Equation (3), the teacher's current activeness level can be calculated. The application continuously calculates the activeness value and updates a progress bar on the teacher's smartphone to provide real-time feedback, as shown in Figure 5(a).

The system also included a smartwatch (Asus Zenwatch 2) worn by the teacher to capture his hand and foot movement. The application captures sensor data of a five-second window and processes that data on the teacher's smartphone to get the number of steps taken and process hand gesture data. If the number of steps in three consecutive time windows is less than 1 or greater than 3, the system's foot movement is less efficient for better lecture quality. In addition, it counts the number of steps during a particular classroom session, shown in the final report presented at the end of the class and a detailed summary of a learning session (Figure 5(b)).

5. Experimental Setup

This section describes the environment setup used for our experiments during actual classroom sessions.

5.1. Classroom/Environment Setup. Figure 6 depicts the layout and management of teacher and students' positions in the classroom during the experiment. The smartphone was placed in front of a student using the specialized smartphone jacket installed on the back of the student's chair in front of them. Figure 7 shows a chair with a smartphone jacket installed at the back to get students' faces and audio data. Five positions were selected to sit a student with a smartphone, whereas a teacher is equipped with a smartphone and smartwatch (Figure 6). The teacher is standing and moving during the classroom session. Therefore, his smartphone is placed in a neck holder to make it easier to move

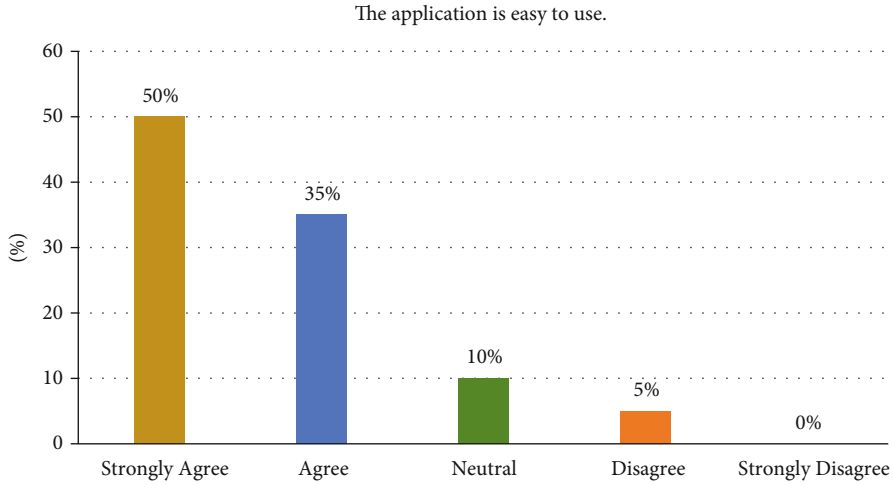

Figure 11: Students' response regarding the easiness of the proposed solution.

Table 4: Performance improvement after using the proposed solution.

	Frequency	Percent	Valid percent	Cumulative percent
Strongly agree	18	45	45	45
Agree	14	35	35	80
Neutral	6	15	15	95
Disagree	2	5	5	100
Strongly disagree	0	0	0	100
Total	40	100	100	

and provide real-time statistics on his smartphone screen. In addition, the teacher wears a smartwatch on his dominant hand to capture their hand movements and count their steps during the classroom using the built-in pedometer of the smartwatch.

5.2. Display Seating Map. Real-world classroom size is not fixed, and the system must show a student's exact position in the classroom. Therefore, to offer the exact indoor location, the application uses QR codes to recognize a student's accurate seat map, unlike some existing solutions that use RFID [8] for indoor location, which is costly and requires technical assistance. The QR code is placed in front of each seat to get the seat number and position in the classroom, as shown in Figure 8.

5.3. Evaluation. For the evaluation of the proposed system, we conduct questionnaire-based surveys. We first take a pretask study from participating teachers during the experiment to know how many teachers had used an orchestration solution before. After that, we conduct experiments in several classroom sessions to try our Android application in real classroom scenarios. Finally, we take a posttask questionnaire to get participants' responses after using the Android application. The statistical data from both questionnaires are gathered and coded in SPSS version 21 for further analysis and significance testing.

6. Results and Discussion

After implementing the proposed system, we conducted several experiments in different classroom sessions for one month to better understand and impact our developed Android application. This section discusses the results and findings obtained from pre- and posttask questionnaires.

6.1. The Demographics of Participants. For the experiments, we asked several teachers and students to voluntarily participate and use the Android application on their smartphones during classroom sessions. First, we explain how the system works to all participants and provide a more engaging user experience using low-cost off-the-shelf devices. By requesting approximately 30 teachers, 18 teachers (12 males and 6 females) agreed to use this application and contribute their feedback voluntarily. Similarly, by asking 40 students, 22 agreed to participate, where 17 were male, and 5 were female students between 24 and 28 years (see Table 2).

6.2. The Pretask Findings. We asked the participants whether they had used any teacher orchestration solution before and their experience with those solutions/tools in the pretask questionnaire. As shown in Figure 9, around 80% of participants did not use any orchestration tool before, and they were not familiar with teacher orchestration. The other 20% were mostly teachers, who were also unfamiliar with teacher orchestration, but they used MOOCs to assist their students in the learning process.

We further asked those teachers whether they were satisfied after using those applications for managing their classroom activities. As a result, only 30% said they were satisfied, while 70% said the results were unsatisfactory (Figure 10).

6.3. The Posttask Findings. After the experimental classroom sessions, we conducted a posttask questionnaire-based survey. The participants were asked about their experience

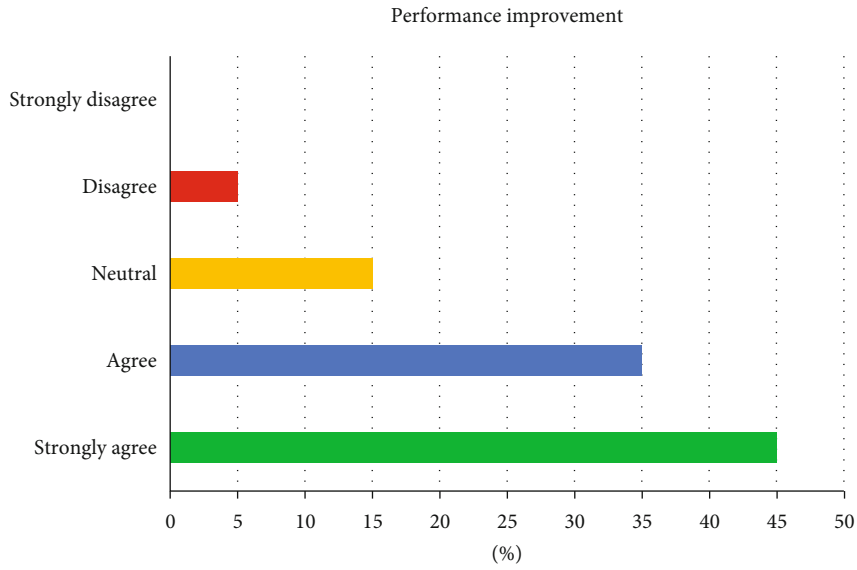

Figure 12: Performance improvement after using the proposed solution.

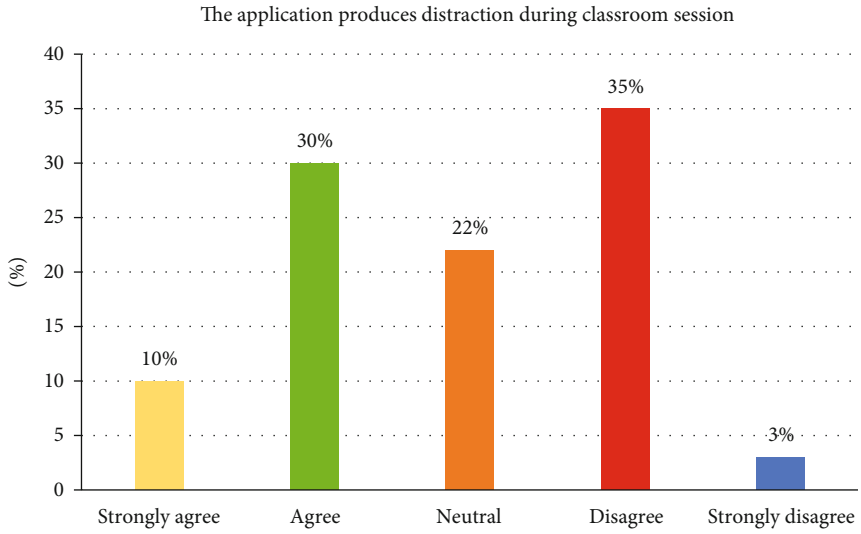

Figure 13: Participants' response to the disturbance they feel using the proposed solution.

and observations after using the Android application. In addition, they were asked whether they feel any improvement and how much the smartphone-based orchestration solution will help create a more engaging learning experience. These questions are given in Table 3.

After collecting their responses, we coded all the recorded data in SPSS version 21 and performed a paired sample t-test for these different questions and variables. The first question in our survey was about knowing how the user felt in terms of easiness regarding the proposed solution. As shown in Figure 11, around 50% of the participants strongly agreed that the application was easy to use because the user could join and start with only 2 to 3 clicks. In contrast, the rest of the 10% and 5% mark the easiness as neutral and disagree.

The proposed solution's primary purpose is to improve teacher performance and increase learning outcomes. Table 4 shows the statistical data gathered from participating students presenting the improvements made after using the proposed solution. About 45% of the students strongly agreed, and 35% agreed that the application improved performance by presenting valuable data to the teacher, which supported him in understanding the entire classroom's current status. The same data is also represented in Figure 12 using a bar graph.

Along with improving teacher performance, we were also fascinated by the proposed system's negative factor or downside. Therefore, we asked the participants whether the application produced any disturbance or distracted them during the classroom session. Only 35% of the participants marked a slight annoyance (Figure 13) because the teacher was wearing a neck holder stand to hold his smartphone, and the majority of participants in this 30% were teachers. In contrast, most students, around 35%, disagree with the

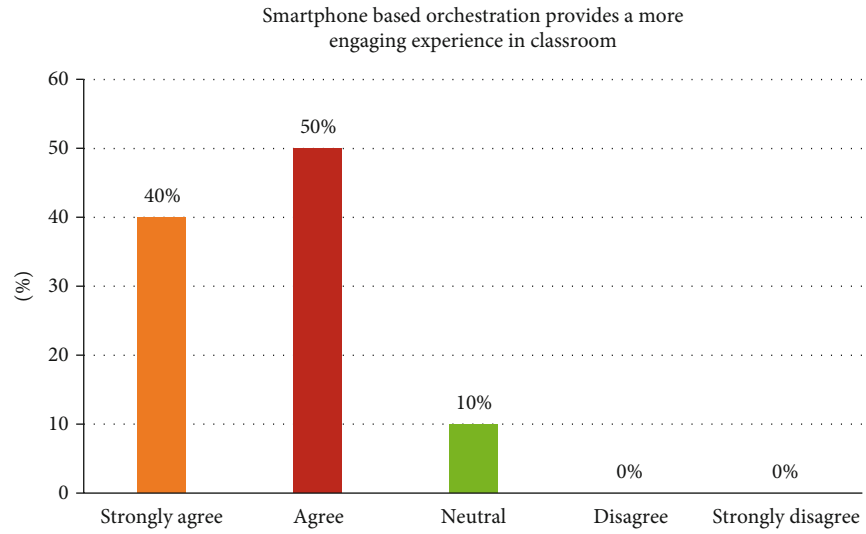

Figure 14: Smartphone-based orchestration provides a more engaging experience in the classroom.

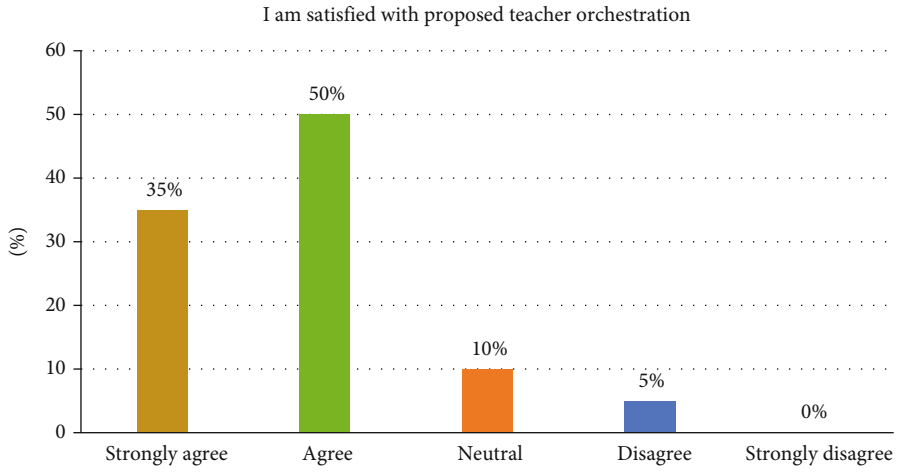

Figure 15: Participants' satisfaction level after using smartphones for teacher orchestration.

Table 5: Paired sample *t*-test of the proposed solution with existing teacher orchestration solutions.

Paired sample test									
		Paired differences					*t*	df	Sig. (2-tailed)
		Mean	Std. deviation	Std. error mean	95% confidence interval of the difference				
					Lower	Upper			
Pair 1	You are satisfied with existing T.O. solutions–you are satisfied with smartphone-based T.O. solution	-33.80000	14.56709	6.51460	-51.88743	-15.71257	-5.188	4	0.007

disturbance, and only 20% mark it as neutral. Of course, a neck holder in the classroom might create a slightly negative impact, which was only used to allow the teacher to view data easily on his smartphone. But it can be replaced with a monitor screen installed behind the students, which provides the teacher with a freer environment to move. Still, on the other hand, it will add some extra cost to the proposed solution because the primary purpose was to use the existing devices to create a low-cost solution.

We also investigate how much the proposed smartphone-based orchestration solution helped create an engaging experience in the classroom. The majority of the

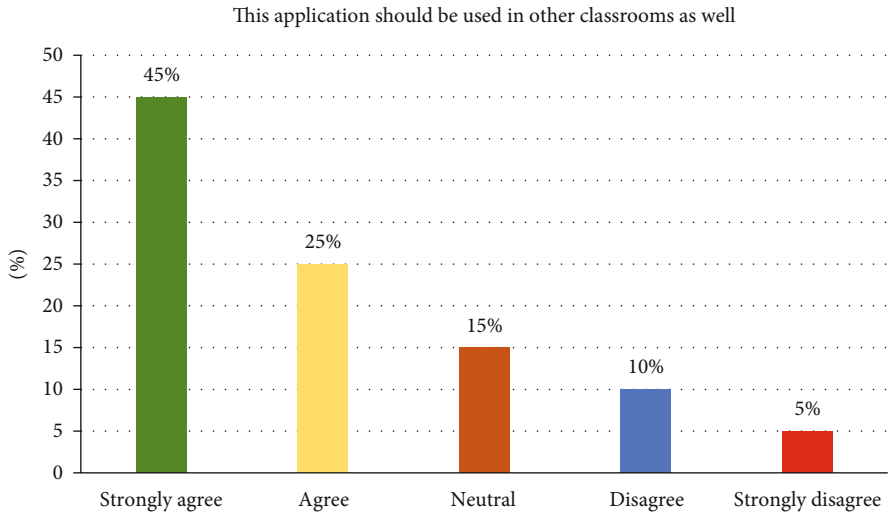

Figure 16: This application should be used in other classrooms as well.

participants, i.e., 90%, accepted that the proposed solution successfully made an engaging experience in their learning environments, while only 10% answered this question as neutral but none of the participants disagreed with the engaging impact created by our proposed solution (Figure 14).

Similarly, to know the impact of using low-cost smartphone devices rather than huge and expensive infrastructures, we asked the participants how satisfied they were with using smartphones for teacher orchestration; 35% strongly agreed and 50% agreed that they were satisfied with using off-the-shelf smartphone devices (Figure 15). While 10% responded neutral, only 5% disagreed that using their smartphones is a good idea because of the privacy concerns.

Now, we compare this satisfaction result with the post-task results. We asked the participants about their satisfaction level after using the existing teacher orchestration solutions. Therefore, we perform a paired sample t-test and use this hypothesis and alternate hypothesis:

H0: the satisfaction level of participants is not significant.

H1: the difference between these satisfaction levels is significant.

A confidence interval value of 95% shows the generated results in Table 5, where the p value is calculated as 0.007. This is less than 0.05. Therefore, we can drop the null hypothesis and accept the alternative hypothesis as valid. The participants are more satisfied with the proposed smartphone-based teacher orchestration solution than the available solutions.

Lastly, we asked whether this application should be used in their other classrooms. After getting the satisfaction level, the response to this question was also very encouraging. Around 70% of the students recommend using this application in other classrooms for teacher orchestration; see Figure 16. And 15% mark this question as neutral, while only 10% disagree with utilizing this application.

7. Conclusion

This study presented state of the art in teacher orchestration and provided a more engaging student experience in a smart classroom. It evaluated several learning pedagogies and their effect on different stakeholders, including students, teachers, and administrators. This study proposed a solution that used off-the-shelf devices for teacher orchestration in a smart learning environment. The solution captures data from teacher and students and processes it, where each device processes its data and sends the results to the teacher's smartphone to provide real-time results. We also evaluate the significance of the proposed solution by using the application in real classrooms and get participants' feedback using a brief questionnaire survey. The results were significantly positive and also encouraged smartphone-based orchestration solutions. Pose recognition significantly impacts studying body language [128]; therefore, processing a teacher's pose in a learning session can open numerous opportunities in a teacher's orchestration.

Data Availability

The data that support the findings of this study are available upon request from the first author.

Conflicts of Interest

The authors claim no conflict of interests.

References

[1] J. Chong, S. See, L. L.-H. Seah, S. L. Koh, Y.-L. Theng, and H. B. Duh, "Ubiquitous computing history, development, and scenarios," in *Ubiquitous Computing: Design, Implementation and Usability*, pp. 1–8, IGI Global, 2008.

[2] I. Alam, S. Khusro, and M. Naeem, "A review of smart TV: past, present, and future," in *2017 International Conference*

on Open Source Systems & Technologies (ICOSST), pp. 35–41, 2017.

[3] R. Rawassizadeh, E. Momeni, C. Dobbins, P. Mirza-Babaei, and R. Rahnamoun, "Lesson learned from collecting quantified self information via mobile and wearable devices," *Journal of Sensor and Actuator Networks*, vol. 4, no. 4, pp. 315–335, 2015.

[4] B. K. Engen, T. H. Giæver, and L. Mifsud, "Teaching and learning with wearable technologies," in *E-Learn: World Conference on E-Learning in Corporate, Government, Healthcare, and Higher Education*, pp. 1057–1067, Vancouver, British Columbia, Canada, 2017.

[5] J. Wetzel, H. Burkhardt, S. Cheema et al., "A preliminary evaluation of the usability of an AI-infused orchestration system," in *International Conference on Artificial Intelligence in Education*, pp. 379–383, 2018.

[6] T.-W. Chan, "Sharing sentiment and wearing a pair of 'field spectacles' to view classroom orchestration," *Computers Education*, vol. 69, pp. 514–516, 2013.

[7] J. A. Muñoz-Cristóbal, I. M. Jorrín-Abellán, J. I. Asensio-Perez, A. Martinez-Mones, L. P. Prieto, and Y. Dimitriadis, "Supporting teacher orchestration in ubiquitous learning environments: a study in primary education," *IEEE Transactions on Learning Technologies*, vol. 8, no. 1, pp. 83–97, 2015.

[8] A. Atabekov, "Internet of things-based smart classroom environment: student research abstract," in *Proceedings of the 31st annual ACM symposium on applied computing*, pp. 746-747, 2016.

[9] A. Uzelac, N. Gligorić, and S. Krčo, "System for recognizing lecture quality based on analysis of physical parameters," *Telematics and Informatics*, vol. 35, no. 3, pp. 579–594, 2018.

[10] D. Rico-Bautista, Y. Medina-Cárdenas, and C. D. Guerrero, "Smart university: a review from the educational and technological view of Internet of things," in *International Conference on Information Technology & Systems*, pp. 427–440, 2019.

[11] S. Khusro, M. Naeem, M. A. Khan, and I. Alam, "There is no such thing as free lunch: an investigation of bloatware effects on smart devices," *Journal of Information Communication Technologies and Robotic Applications*, vol. 8, pp. 20–30, 2018.

[12] M. Khan, S. Khusro, I. Alam, S. Ali, and I. Khan, "Perspectives on the design, challenges, and evaluation of smart TV user interfaces," *Scientific Programming*, vol. 2022, 14 pages, 2022.

[13] I. Khan, S. Khusro, N. Ullah, and S. Ali, "AutoLog: toward the design of a vehicular lifelogging framework for capturing, storing, and visualizing LifeBits," *IEEE Access*, vol. 8, pp. 136546–136559, 2020.

[14] C.-W. Shen, Y.-C. J. Wu, and T.-C. Lee, "Developing a NFC-equipped smart classroom: effects on attitudes toward computer science," *Computers in Human Behavior*, vol. 30, pp. 731–738, 2014.

[15] K. Anwar, T. Rahman, A. Zeb et al., "Improving the convergence period of adaptive data rate in a long range wide area network for the Internet of things devices," *Energies*, vol. 14, no. 18, p. 5614, 2021.

[16] B. A. Schwendimann, M. J. Rodriguez-Triana, A. Vozniuk et al., "Perceiving learning at a glance: a systematic literature review of learning dashboard research," *IEEE Transactions on Learning Technologies*, vol. 10, no. 1, pp. 30–41, 2017.

[17] J. Bacca, S. Baldiris, R. Fabregat, and S. Graf, "Augmented reality trends in education: a systematic review of research and applications," *Journal of Educational Technology and Society*, vol. 17, no. 4, pp. 133–149, 2014.

[18] F. Herpich, F. B. Nunes, G. Petri, and L. M. R. Tarouco, "How mobile augmented reality is applied in education? A systematic literature review," *Creative Education*, vol. 10, no. 7, pp. 1589–1627, 2019.

[19] A. Ezenwoke and O. Ezenwoke, *Wearable Technology: Opportunities and Challenges for Teaching and Learning in Higher Education in Developing Countries*, Iated Digital Library, 2016.

[20] L. P. Prieto, K. Sharma, P. Dillenbourg, and M. Jesús, "Teaching analytics: towards automatic extraction of orchestration graphs using wearable sensors," in *Proceedings of the Sixth International Conference on Learning Analytics & Knowledge*, pp. 148–157, 2016.

[21] Y.-T. Sung, K.-E. Chang, and T.-C. Liu, "The effects of integrating mobile devices with teaching and learning on students' learning performance: a meta-analysis and research synthesis," *Computers & Education*, vol. 94, pp. 252–275, 2016.

[22] D. Bebell and L. O'Dwyer, "Educational outcomes and research from 1: 1 computing settings," *The journal of technology, learning and assessment*, vol. 9, no. 1, 2010.

[23] H. Fleischer, "What is our current understanding of one-to-one computer projects: a systematic narrative research review," *Educational Research Review*, vol. 7, no. 2, pp. 107–122, 2012.

[24] A. A. Zucker and D. Light, "Laptop programs for students," *Science*, vol. 323, no. 5910, pp. 82–85, 2009.

[25] T.-C. Liu, Y.-C. Lin, M.-J. Tsai, and F. Paas, "Split-attention and redundancy effects on mobile learning in physical environments," *Computers & Education*, vol. 58, no. 1, pp. 172–180, 2012.

[26] J. Roschelle, K. Rafanan, R. Bhanot et al., "Scaffolding group explanation and feedback with handheld technology: impact on students' mathematics learning," *Educational Technology Research and Development*, vol. 58, no. 4, pp. 399–419, 2010.

[27] E. Klopfer, J. Sheldon, J. Perry, and V. H. Chen, "Ubiquitous games for learning (UbiqGames): weatherlings, a worked example," *Journal of Computer Assisted Learning*, vol. 28, no. 5, pp. 465–476, 2012.

[28] R. Tatum, M. Bays, J. Hyland, and B. Hartman, "Traffic monitoring using an adaptive sensor power scheduling algorithm," *SN Applied Sciences*, vol. 1, no. 12, p. 1552, 2019.

[29] Z. Wang, F. Wang, T. Brown, J. Xue, and J. Zhang, "Traffic aware wireless visual sensor network deployment for 3D indoor monitoring," in *ICC 2019-2019 IEEE International Conference on Communications (ICC)*, pp. 1–6, 2019.

[30] M. Sarrab, S. Pulparambil, N. Kraiem, and M. Al-Badawi, "Real-time traffic monitoring systems based on magnetic sensor integration," in *International Conference on Smart City and Informatization*, pp. 447–460, 2019.

[31] C. Ruan, Y. Wang, X. Ma, and H. Kang, "Road meteorological condition sensor based on multi-wavelength light detection," in *Third International Conference on Photonics and Optical Engineering*, p. 110521F, 2019.

[32] W. Li, M. Burrow, and Z. Li, "Automatic road condition assessment by using point laser sensor," in *2018 IEEE SENSORS*, pp. 1–4, 2018.

[33] T. Sekizawa, M. Mori, and R. Kanbayashi, *Tire-Mounted Sensor and Road Surface Condition Estimation Apparatus including the Same*, Google Patents, 2019.

[34] Z. Yang, X. Shi, and J. Chen, "Optimal coordination of mobile sensors for target tracking under additive and multiplicative noises," *IEEE Transactions on Industrial Electronics*, vol. 61, no. 7, pp. 3459–3468, 2013.

[35] F. Mao, K. Khamis, S. Krause, J. Clark, and D. M. Hannah, "Low-cost environmental sensor networks: recent advances and future directions," *Frontiers in Earth Science*, vol. 7, p. 221, 2019.

[36] M. Haghi, R. Stoll, and K. Thurow, "Pervasive and personalized ambient parameters monitoring: a wearable, modular, and configurable watch," *IEEE Access*, vol. 7, pp. 20126–20143, 2019.

[37] M. J. González-Campo, J. E. Serrano-Casteneda, and J. C. Martınez-Santos, *A Proposal for an Air Quality Monitoring System for Cartagena de Indias*, Latin American and Caribbean Consortium of Engineering Institutions (LACCEI), 2019.

[38] S.-B. Kwon, Y.-M. Cho, D.-S. Park, E.-Y. Park, S.-Y. Kim, and M.-Y. Jung, "Temperature and humidity monitoring using ubiquitous senor network in railway cabin," in *Proceedings of the KSR Conference*, pp. 948–951, 2008.

[39] H. Wang, D. Li, C. Wu, and X. Yu, "Depth perception of moving objects viaing structured light sensor with unstructured grid," *Results in Physics*, vol. 13, p. 102163, 2019.

[40] A. J. Golparvar and M. K. Yapici, "Graphene smart textile-based wearable eye movement sensor for electro-ocular control and interaction with objects," *Journal of the Electrochemical Society*, vol. 166, no. 9, pp. B3184–B3193, 2019.

[41] M. A. Wohl and J. J. O'hagan, "Method, apparatus, and computer program product for combined tag and sensor based performance modeling using real-time data for proximity and movement of objects," Google Patents, 2015.

[42] S. M. Kumar and L. Lakshmanan, "A situation emergency building navigation disaster system using wireless sensor networks," in *2018 International Conference on Communication and Signal Processing (ICCSP)*, pp. 0378–0382, 2018.

[43] H.-B. Choi, K.-W. Lim, and Y.-B. Ko, "Sensor localization system for AR-assisted disaster relief applications," in *Proceedings of the 17th Annual International Conference on Mobile Systems, Applications, and Services*, pp. 526-527, 2019.

[44] C. T. Ulmer, *Weather Sensor including Vertically Stacked Multi-Power Modules*, Google Patents, 2019.

[45] M. Warschauer, "A teacher's place in the digital divide," *Yearbook of the National Society for the Study of Education*, vol. 106, no. 2, pp. 147–166, 2007.

[46] M. Tissenbaum, C. Matuk, M. Berland et al., *Real-Time Visualization of Student Activities to Support Classroom Orchestration*, International Society of the Learning Sciences, Singapore, 2016.

[47] H. Matsuno, H. Ogasawara, A. Noguchi, K. Hasegawa, and R. Wajima, "Effective lecturer-student microphone use in a lecture room: a useful approach for teaching and learning pharmaceutical science English," *Journal ofAcademic Society for Quality of Life*, vol. 1, no. 1, pp. 21–25, 2015.

[48] I. Khan, S. Khusro, S. Ali, and A. Din, "Low dose aspirin like analgesic and anti-inflammatory activities of mono- hydroxybenzoic acids in stressed rodents," *Proceedings of the Pakistan Academy of Sciences*, vol. 148, no. 1, pp. 53–62, 2016.

[49] B. Ngoc Anh, N. Tung Son, P. Truong Lam et al., "A computer-vision based application for student behavior monitoring in classroom," *Applied Sciences*, vol. 9, no. 22, p. 4729, 2019.

[50] R. Kulkarni, "Real time automated invigilator in classroom monitoring using computer vision," in *2nd International Conference on Advances in Science & Technology (ICAST)*, p. 3367715, 2019.

[51] D. Canedo, A. Trifan, and A. J. Neves, "Monitoring students' attention in a classroom through computer vision," in *International Conference on Practical Applications of Agents and Multi-Agent Systems*, pp. 371–378, 2018.

[52] E. Alepis, M. Virvou, and K. Kabassi, "Affective student modeling based on microphone and keyboard user actions," in *Sixth IEEE International Conference on Advanced Learning Technologies (ICALT'06)*, pp. 139–141, 2006.

[53] M. C. Brady, S. D'Mello, N. Blanchard, A. Olney, and M. Nystrand, "Evaluating microphones and microphone placement for signal processing and automatic speech recognition of teacher-student dialog," *The Journal of the Acoustical Society of America*, vol. 136, no. 4, pp. 2215–2215, 2014.

[54] Y.-M. Huang, C.-C. Hsu, Y.-N. Su, and C.-J. Liu, "Empowering classroom observation with an e-book reading behavior monitoring system using sensing technologies," *Interacting with Computers*, vol. 26, no. 4, pp. 372–387, 2014.

[55] W. Jintao, J. Cheng, L. Kai, N. Yiming, R. Yinglu, and W. Jing, "Study on energy efficiency of new intelligent classroom lighting control system," *China Computer & Communication*, vol. 13, no. 8, p. 21, 2017.

[56] I. Khan, S. Khusro, S. Ali, and J. Ahmad, "Sensors are power hungry: an investigation of smartphone sensors impact on battery power from lifelogging perspective," *Bahria University Journal of Information & Communication Technologies (BUJICT)*, vol. 9, no. 2, 2016.

[57] I. Khan, S. Ali, and S. Khusro, "Smartphone-based lifelogging: an investigation of data volume generation strength of smartphone sensors," in *International conference on simulation tools and techniques*, pp. 63–73, 2019.

[58] N. Harada, M. Kimura, T. Yamamoto, and Y. Miyake, "System for measuring teacher–student communication in the classroom using smartphone accelerometer sensors," in *International Conference on Human-Computer Interaction*, pp. 309–318, 2017.

[59] M. J. Schloneger and E. J. Hunter, "Assessments of voice use and voice quality among college/university singing students ages 18-24 through ambulatory monitoring with a full accelerometer signal," *Journal of Voice*, vol. 31, no. 1, pp. 124.e21–124.e30, 2017.

[60] J. C.-Y. Sun, K.-Y. Chang, and Y.-H. Chen, "GPS sensor-based mobile learning for English: an exploratory study on self-efficacy, self-regulation and student achievement," *Research and Practice in Technology Enhanced Learning*, vol. 10, no. 1, p. 23, 2015.

[61] R. M. Carini, G. D. Kuh, and S. P. Klein, "Student engagement and student learning: testing the linkages∗," *Research in Higher Education*, vol. 47, no. 1, pp. 1–32, 2006.

[62] G. Hagenauer, T. Hascher, and S. E. Volet, "Teacher emotions in the classroom: associations with students' engagement, classroom discipline and the interpersonal teacher-student relationship," *European Journal of Psychology of Education*, vol. 30, no. 4, pp. 385–403, 2015.

[63] M. P. Wenderoth, *Monitoring the Level of Active Learning in your Classroom and Its Impact on Your Students*, The Western Conference on Science Education, Western University, Canada, 2019.

[64] H. Coates, "The value of student engagement for higher education quality assurance," *Quality in Higher Education*, vol. 11, no. 1, pp. 25–36, 2005.

[65] G. D. Kuh, *Excerpt from High-Impact Educational Practices: What They Are, Who Has Access to Them, and Why They Matter*, Association of American Colleges and Universities, 2008.

[66] G. D. Kuh, "Promoting student success: what campus leaders can do. Occasional paper no. 1," *National Survey of Student Engagement*, vol. 2005, 2005.

[67] G. D. Kuh, "What student affairs professionals need to know about student engagement," *Journal of College Student Development*, vol. 50, no. 6, pp. 683–706, 2009.

[68] G. D. Kuh, "What we're learning about student engagement from NSSE: benchmarks for effective educational practices," *Change: The Magazine of Higher Learning*, vol. 35, no. 2, pp. 24–32, 2003.

[69] M. May, S. George, and P. Prévôt, "TrAVis to enhance students' self-monitoring in online learning supported by computer-mediated communication tools," *Computer Information Systems and Industrial Management Applications*, vol. 3, pp. 623–634, 2011.

[70] C.-C. Hsu, H.-C. Chen, Y.-N. Su, K.-K. Huang, and Y.-M. Huang, "Developing a reading concentration monitoring system by applying an artificial bee colony algorithm to e-books in an intelligent classroom," *Sensors*, vol. 12, no. 10, pp. 14158–14178, 2012.

[71] M. Raca, L. Kidzinski, and P. Dillenbourg, "Translating head motion into attention-towards processing of student's body-language," in *Proceedings of the 8th international conference on educational data mining*, 2015.

[72] P. Blatchford, P. Bassett, and P. Brown, "Examining the effect of class size on classroom engagement and teacher-pupil interaction: differences in relation to pupil prior attainment and primary vs. secondary schools," *Learning and Instruction*, vol. 21, no. 6, pp. 715–730, 2011.

[73] R. Fu, D. Wang, D. Li, and Z. Luo, "University classroom attendance based on deep learning," in *2017 10th International Conference on Intelligent Computation Technology and Automation (ICICTA)*, pp. 128–131, 2017.

[74] A. Haq, S. Khusro, and I. Alam, "Towards better recognition of age, gender, and number of viewers in a smart TV environment," in *2021 Mohammad Ali Jinnah University International Conference on Computing (MAJICC)*, pp. 1–6, 2021.

[75] K. Krafka, A. Khosla, P. Kellnhofer et al., "Eye tracking for everyone," in *Proceedings of the IEEE conference on computer vision and pattern recognition*, pp. 2176–2184, 2016.

[76] R. Stiefelhagen and J. Zhu, "Head orientation and gaze direction in meetings," *CHI'02 Extended Abstracts on Human Factors in Computing Systems*, pp. 858-859, ACM Digital Library, 2002.

[77] M. Raca and P. Dillenbourg, "System for assessing classroom attention," in *Proceedings of 3rd International Learning Analytics & Knowledge Conference*, 2013.

[78] D. Dinesh and K. Bijlani, "Student analytics for productive teaching/learning," in *2016 International Conference on Information Science (ICIS)*, pp. 97–102, 2016.

[79] A. van Leeuwen and N. Rummel, "Orchestration tools to support the teacher during student collaboration: a review," *Unterrichtswissenschaft*, vol. 47, no. 2, pp. 143–158, 2019.

[80] D. Sapargaliyev, "Wearables in education: expectations and disappointments," in *International Conference on Technology in Education*, pp. 73–78, 2015.

[81] A. Althunibat, "Determining the factors influencing students' intention to use m-learning in Jordan higher education," *Computers in Human Behavior*, vol. 52, pp. 65–71, 2015.

[82] Á. Suárez, M. Specht, F. Prinsen, M. Kalz, and S. Ternier, "A review of the types of mobile activities in mobile inquiry-based learning," *Computers Education*, vol. 118, pp. 38–55, 2018.

[83] V. Subbarao, K. Srinivas, and R. Pavithr, "A survey on internet of things based SMART, digital green and intelligent campus," in *2019 4th International Conference on Internet of Things: Smart Innovation and Usages (IoT-SIU)*, pp. 1–6, 2019.

[84] S. Mahmood, S. Palaniappan, R. Hasan, K. U. Sarker, A. Abass, and P. M. Rajegowda, "Raspberry PI and role of IoT in education," in *2019 4th MEC International Conference on Big Data And Smart City (ICBDSC)*, pp. 1–6, 2019.

[85] K. Anwar, T. Rahman, A. Zeb, I. Khan, M. Zareei, and C. Vargas-Rosales, "RM-ADR: resource management adaptive data rate for mobile application in LoRaWAN," *Sensors*, vol. 21, no. 23, p. 7980, 2021.

[86] N. Gligorić, A. Uzelac, and S. Krco, "Smart classroom: real-time feedback on lecture quality," in *2012 IEEE International Conference on Pervasive Computing and Communications Workshops*, pp. 391–394, 2012.

[87] N. Gligorić, T. Dimčić, S. Krčo, V. Dimčić, J. Vasković, and I. Vojinović, *Internet of Things Enabled LED Lamp Controlled by Satisfaction of Students in a Classroom*, A publication of IPSI Bgd Internet Research Society New York, 2014.

[88] S. Khusro, B. Shah, I. Khan, and S. Rahman, "Haptic feedback to assist blind people in indoor environment using vibration patterns," *Sensors*, vol. 22, no. 1, p. 361, 2022.

[89] Z. Mirza and M. N. Brohi, "An in-depth analysis on integrating campus radio frequency identification system on clouds for enhancing security," *Journal of Computer Science*, vol. 9, no. 12, pp. 1710–1714, 2013.

[90] M. W. Sari, P. W. Ciptadi, and R. H. Hardyanto, "Study of smart campus development using Internet of things technology," in *IOP Conference Series: Materials Science and Engineering*, p. 012032, 2017.

[91] O. Said and Y. Albagory, "Internet of things-based free learning system: performance evaluation and communication perspective," *IETE Journal of Research*, vol. 63, no. 1, pp. 31–44, 2017.

[92] L.-S. Huang, J.-Y. Su, and T.-L. Pao, "A context aware smart classroom architecture for smart campuses," *Applied Sciences*, vol. 9, no. 9, p. 1837, 2019.

[93] M. Akçayır and G. Akçayır, "Advantages and challenges associated with augmented reality for education: a systematic review of the literature," *Educational Research Review*, vol. 20, pp. 1–11, 2017.

[94] M. Hayat, R. Hasan, S. I. Ali, and M. Kaleem, "Active learning and student engagement using activity based learning," in *2017 International Conference on Infocom Technologies and Unmanned Systems (Trends and Future Directions)(ICTUS)*, pp. 201–204, 2017.

[95] H. Elkoubaiti and R. Mrabet, "How are augmented and virtual reality used in smart classrooms?," in *Proceedings of the 2nd International Conference on Smart Digital Environment*, pp. 189–196, 2018.

[96] J. A. Munoz-Cristóbal, V. Gallego-Lema, H. F. Arribas-Cubero, J. I. Asensio-Pérez, and A. Martínez-Monés, "Game of blazons: helping teachers conduct learning situations that integrate web tools and multiple types of augmented reality," *IEEE Transactions on Learning Technologies*, vol. 11, no. 4, pp. 506–519, 2018.

[97] P. Kosmas and P. Zaphiris, "Embodied interaction in language learning: enhancing students' collaboration and emotional engagement," in *IFIP Conference on Human-Computer Interaction*, pp. 179–196, 2019.

[98] T. Khan, K. Johnston, and J. Ophoff, "The impact of an augmented reality application on learning motivation of students," *Advances in Human-Computer Interaction*, vol. 2019, Article ID 7208494, 14 pages, 2019.

[99] I. Jivet, M. Scheffel, M. Specht, and H. Drachsler, "License to evaluate: preparing learning analytics dashboards for educational practice," in *in Proceedings of the 8th International Conference on Learning Analytics and Knowledge*, pp. 31–40, 2018.

[100] M. Korozi, A. Leonidis, M. Antona, and C. Stephanidis, "LECTOR: towards reengaging students in the educational process inside smart classrooms," in *International Conference on Intelligent Human Computer Interaction*, pp. 137–149, 2017.

[101] E. Stefanidi, M. Korozi, A. Leonidis, M. Doulgeraki, and M. Antona, "Educator-oriented tools for managing the attention-aware intelligent classroom," in *the Tenth International Conference on Mobile, Hybrid, and on-Line Learning*, 2018.

[102] K. Holstein, B. M. McLaren, and V. Aleven, "Intelligent tutors as teachers' aides: exploring teacher needs for real-time analytics in blended classrooms," in *Proceedings of the Seventh International Learning Analytics & Knowledge Conference*, pp. 257–266, 2017.

[103] M. Z. Iqbal, "Enhancing classroom engagement through smart phone based paper marking solution," in *Proceedings of the 6th International Conference on the Internet of Things*, pp. 161-162, 2016.

[104] S. A. Viswanathan and K. VanLehn, "Using the tablet gestures and speech of pairs of students to classify their collaboration," *IEEE Transactions on Learning Technologies*, vol. 11, no. 2, pp. 230–242, 2018.

[105] S. Yu-Gang, W. Jia-Bao, and H. Feng, *Research on Mobile Learning Model Based on Internet of Things*, DEStech Transactions on Social Science, Education and Human Science, no. eshd, 2016.

[106] S. Budi, O. Karnalim, E. D. Handoyo, S. Santoso, H. Toba, H. Nguyen et al.et al., "IBAtS-image based attendance system: a low cost solution to record student attendance in a classroom," in *2018 IEEE International Symposium on Multimedia (ISM)*, pp. 259–266, 2018.

[107] S. Yang, Y. Song, H. Ren, and X. Huang, "An automated student attendance tracking system based on voiceprint and location," in *2016 11th International Conference on Computer Science & Education (ICCSE)*, pp. 214–219, 2016.

[108] N. Gligoric, A. Uzelac, S. Krco, I. Kovacevic, and A. Nikodijevic, "Smart classroom system for detecting level of interest a lecture creates in a classroom," *Journal of Ambient Intelligence and Smart Environments*, vol. 7, no. 2, pp. 271–284, 2015.

[109] M. Viilo, P. Seitamaa-Hakkarainen, and K. Hakkarainen, "Long-term teacher orchestration of technology-mediated collaborative inquiry," *Scandinavian Journal of Educational Research*, vol. 62, no. 3, pp. 407–432, 2018.

[110] P. J. Donnelly, N. Blanchard, B. Samei et al., "Multi-sensor modeling of teacher instructional segments in live classrooms," in *Proceedings of the 18th ACM International Conference on Multimodal Interaction*, pp. 177–184, Tokyo, Japan, 2016.

[111] P. J. Donnelly, N. Blanchard, B. Samei et al., "Automatic teacher modeling from live classroom audio," in *Proceedings of the 2016 conference on user modeling adaptation and personalization*, pp. 45–53, 2016.

[112] P. J. Donnelly, N. Blanchard, A. M. Olney, S. Kelly, M. Nystrand, and S. K. D'Mello, "Words matter: automatic detection of teacher questions in live classroom discourse using linguistics, acoustics, and context," in *Proceedings of the Seventh International Learning Analytics & Knowledge Conference*, pp. 218–227, 2017.

[113] S. Liu, Y. Chen, H. Huang, L. Xiao, and X. Hei, "Towards smart educational recommendations with reinforcement learning in classroom," in *2018 IEEE International Conference on Teaching, Assessment, and Learning for Engineering (TALE)*, pp. 1079–1084, 2018.

[114] R. Bdiwi, C. de Runz, S. Faiz, and A. A. Cherif, "Smart learning environment: teacher's role in assessing classroom attention," *Research in Learning Technology*, vol. 27, 2019.

[115] I. Alam, S. Khusro, and M. Khan, "Personalized content recommendations on smart TV: challenges, opportunities, and future research directions," *Entertainment Computing*, vol. 38, p. 100418, 2021.

[116] I. Alam and S. Khusro, "Tailoring recommendations to groups of viewers on smart TV: a real-time profile generation approach," *IEEE Access*, vol. 8, pp. 50814–50827, 2020.

[117] M. Jan, S. Khusro, I. Alam, I. Khan, and B. Niazi, "Interest-based content clustering for enhancing searching and recommendations on smart TV," *Wireless Communications and Mobile Computing*, vol. 2022, Article ID 3896840, 14 pages, 2022.

[118] I. Alam, S. Khusro, and M. Khan, "Factors affecting the performance of recommender systems in a smart TV environment," *Technologies*, vol. 7, no. 2, p. 41, 2019.

[119] H. Wang, Z. Pi, and W. Hu, "The instructor's gaze guidance in video lectures improves learning," *Journal of Computer Assisted Learning*, vol. 35, no. 1, pp. 42–50, 2019.

[120] B. Garcia, S. L. Chu, B. Nam, and C. Banigan, "Wearables for learning: examining the smartwatch as a tool for situated science reflection," in *Proceedings of the 2018 CHI conference on human factors in computing systems*, p. 256, Montreal QC, Canada, 2018.

[121] R. Quintana, C. Quintana, C. Madeira, and J. D. Slotta, "Keeping watch: exploring wearable technology designs for K-12 teachers," in *Proceedings of the 2016 CHI Conference Extended Abstracts on Human Factors in Computing Systems*, pp. 2272–2278, San Jose, California, USA, 2016.

[122] Y. Lu, S. Zhang, Z. Zhang, W. Xiao, and S. Yu, "A framework for learning analytics using commodity wearable devices," *Sensors*, vol. 17, no. 6, p. 1382, 2017.

[123] H. Zheng and V. G. Motti, "WeLi: a smartwatch application to assist students with intellectual and developmental disabilities," in *Proceedings of the 19th International ACM SIGACCESS Conference on Computers and Accessibility*, pp. 355-356, 2017.

[124] J. Hernandez and R. W. Picard, "SenseGlass: using Google Glass to sense daily emotions," in *Proceedings of the Adjunct Publication of the 27th Annual ACM Symposium on User Interface Software and Technology*pp. 77-78, Honolulu, Hawaii, USA, 2014.

[125] W. Wu, S. Dasgupta, E. E. Ramirez, C. Peterson, and G. J. Norman, "Classification accuracies of physical activities using smartphone motion sensors," *Journal of Medical Internet Research*, vol. 14, no. 5, p. e130, 2012.

[126] A. Al-Haiqi, M. Ismail, and R. Nordin, "A new sensors-based covert channel on Android," *The Scientific World Journal*, vol. 2014, Article ID 969628, 14 pages, 2014.

[127] M. B. Nair, S. R. Kumar, N. Mohan, and J. Anudev, "Instantaneous feedback pedometer with emergency GPS tracker," in *2018 2nd International Conference on I-SMAC (IoT in Social, Mobile, Analytics and Cloud)(I-SMAC) I-SMAC (IoT in Social, Mobile, Analytics and Cloud)(I-SMAC), 2018 2nd International Conference on*, pp. 122–126, 2018.

[128] K. Schindler, L. Van Gool, and B. de Gelder, "Recognizing emotions expressed by body pose: a biologically inspired neural model," *Neural Networks*, vol. 21, no. 9, pp. 1238–1246, 2008.

Hindawi
Wireless Communications and Mobile Computing
Volume 2022, Article ID 8684138, 12 pages
https://doi.org/10.1155/2022/8684138

Research Article

A Deep Learning-Based Semantic Segmentation Architecture for Autonomous Driving Applications

Sharjeel Masood[1], **Fawad Ahmed**[2], **Suliman A. Alsuhibany**[3], **Yazeed Yasin Ghadi**[4], **M. Y. Siyal**[5], **Harish Kumar**[6], **Khyber Khan**[7] and **Jawad Ahmad**[8]

[1]*Healthhub, Seoul, Republic of Korea*
[2]*Department of Cyber Security, Pakistan Navy Engineering College, NUST, Pakistan*
[3]*Department of Computer Science, College of Computer, Qassim University, Buraydah 51452, Saudi Arabia*
[4]*Department of Computer Science and Software Engineering, Al Ain University, Abu Dhabi 122612, UAE*
[5]*School of Electrical and Electronic Engineering, Nanyang Technological University, Singapore*
[6]*Department of Computer Science, College of Computer Science, King Khalid University, Abha 61413, Saudi Arabia*
[7]*Department of Computer Science, Khurasan University, Jalalabad, Afghanistan*
[8]*School of Computing, Edinburgh Napier University EH10 5DT, UK*

Correspondence should be addressed to Khyber Khan; khyber.khan.khurasan@gmail.com

Received 30 March 2022; Revised 21 May 2022; Accepted 2 June 2022; Published 18 June 2022

Academic Editor: Farhan Ullah

In recent years, the development of smart transportation has accelerated research on semantic segmentation as it is one of the most important problems in this area. A large receptive field has always been the center of focus when designing convolutional neural networks for semantic segmentation. A majority of recent techniques have used maxpooling to increase the receptive field of a network at an expense of decreasing its spatial resolution. Although this idea has shown improved results in object detection applications, however, when it comes to semantic segmentation, a high spatial resolution also needs to be considered. To address this issue, a new deep learning model, the M-Net is proposed in this paper which satisfies both high spatial resolution and a large enough receptive field while keeping the size of the model to a minimum. The proposed network is based on an encoder-decoder architecture. The encoder uses atrous convolution to encode the features at full resolution, and instead of using heavy transposed convolution, the decoder consists of a multipath feature extraction module that can extract multiscale context information from the encoded features. The experimental results reported in the paper demonstrate the viability of the proposed scheme.

1. Introduction

Computer vision stands as the backbone of various modern autonomous driving systems [1] with semantic segmentation being one of its fundamental tasks. The goal of semantic segmentation is to assign a label to every pixel of an image. Deep convolutional neural networks have opened up a wide area of extremely effective solutions to problems like object detection [2], lane detection [3], object tracking [4], and semantic segmentation.

Improvements in the performance of deep neural networks have largely been achieved by increasing the number of learnable parameters along with careful network designing, making them computationally expensive. Reducing computational cost and extracting the maximum possible performance from the minimum number of learnable parameters is undoubtedly an extremely important requirement when dealing with embedded systems in autonomous driving. To detect large objects in an image, it is necessary to have a receptive field large enough to gather enough context information, and the use of pooling layers in many recent networks to increase the receptive field means that this information is found on a courser scale at higher layers. Finer details like edges of an object or small/thin objects

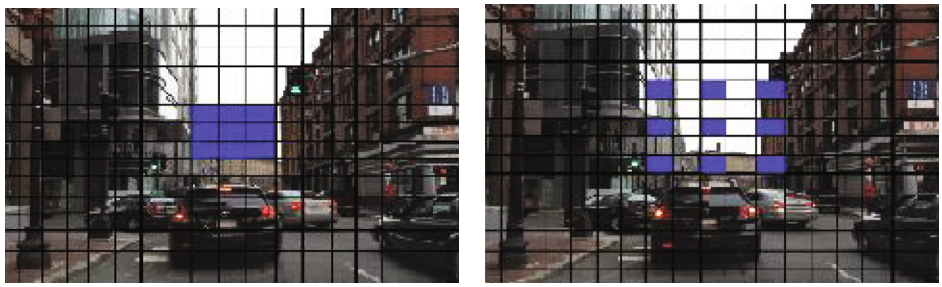

(a) Dilation = 1 (b) Dilation = 2

FIGURE 1: The pixels in the blue contribute in the calculation of the center pixel in the output feature map. (a) shows a 3×3 convolution with dilation rate of 1. (b) shows a 3×3 convolution with dilation rate of 2.

need high spatial resolution to perform accurate segmentation.

To increase the receptive field of the network, the encoder in encoder-decoder methods normally downsamples the image using strided convolution or pooling layers or both, at an expense of reducing the spatial resolution. The decoder then uses transposed convolution to upsample these encoded features to obtain a high-resolution final feature map; this makes segmenting small objects difficult. Encoder-decoder structures like FCN [5] and U-Net [6] use skip connections to connect the lower layers in an encoder to higher layers of the decoder; this partially solves the problem by allowing both high layer course information and low layer fine information to contribute to the prediction of the final feature map. This technique is effective to some extent but can lead to deeper models with a large number of learnable parameters.

An alternative way can be to maintain the spatial resolution of the features in the encoder while using atrous convolution to increase the receptive field. DeepLab [7] modifies FCN [5] by replacing the last 2 downsampling operations with atrous convolutions to maintain the receptive field. In the architecture proposed by [8], atrous convolutions are used extensively to effectively increase the receptive field while maintaining the spatial resolution throughout the network to segment smaller objects. Figure 1 shows how atrous convolution expands the receptive field by adding holes into a normal convolutional layer. A convolution layer with a 3×3 kernel and a dilation rate of 2 has the same field of view as a layer with a 5×5 kernel, while only using 9 parameters. Dilated convolution is an effective way to maintain spatial resolution, but going deeper with high-resolution feature maps can also introduce latency in the system. Processing features in full resolution can be computationaly expensive, to reduce the latency in our system we used maxpooling half way down our network to reduce the spacial resolution by half, this reduces the run time of our network and at the same time increases the receptive field for larger objects. Capturing useful image context information at multiple scales has proven to enhance segmentation accuracy. Pyramid pooling modules like the one introduced in [9] uses pyramid pooling operation for multiple scale context aggregation. The authors in [10] divided the initial input into four subregions and obtained the pooled features from each of those four subregions, respectively. DeepLab [7] on the other hand use atrous spatial pyramid pooling(ASPP) that exploits atrous convolution to divide the features into different scales instead of pooling layers. A deeper version of the ASPP module was introduced in [11] by adding a standard 3×3 convolution after 3×3 atrous convolutions. We have taken a similar approach by using a multipath feature extraction module as a decoder to fuse together the key information from three different scales, leading to better segmentation ability.

2. Related Work

Semantic segmentation is of great importance in self-driving cars and various driving aids. Deep convolutional neural networks when used in encoder-decoder network architectures have shown remarkable segmentation performance. Encoder-decoder network architectures were first introduced by Bayesian SegNet [12] and SegNet [13]; they used the encoder to downsample the features, and then, the decoder was responsible for recovering the spacial dimensions of the features. FCN [5] used a similar approach by using a classification model like VGG [14] as an encoder to extract features and those extracted features were then upsampled to perform pixelwise prediction in full resolution.

Recent works have brought various changes to the encoder-decoder structure. Instead of using transposed convolution in the decoder, the architecture in [15] introduced a JPU unit to decode the features encoded by FCN [5], the joint pyramid upsampling (JPU) unit upsamples the last 3 feature maps from FCN and then uses 4 dilated convolution layers to extract the features at multiple scales; this decreases the size of the network and also speeding up the network. Encoder-decoders like the ones in [16, 17] use an encoder to extract multilevel features and then used a decoder to combine them into a high-resolution final prediction, avoiding the extensive use of transposed convolution.

DeepLabs [7, 18] introduced atrous spatial pyramid pooling (ASPP) to extract context information at different scales for better segmentation. PSPNet [9] used global average pooling to capture context information. A similar multipath module has been used by [19] to generate a feature

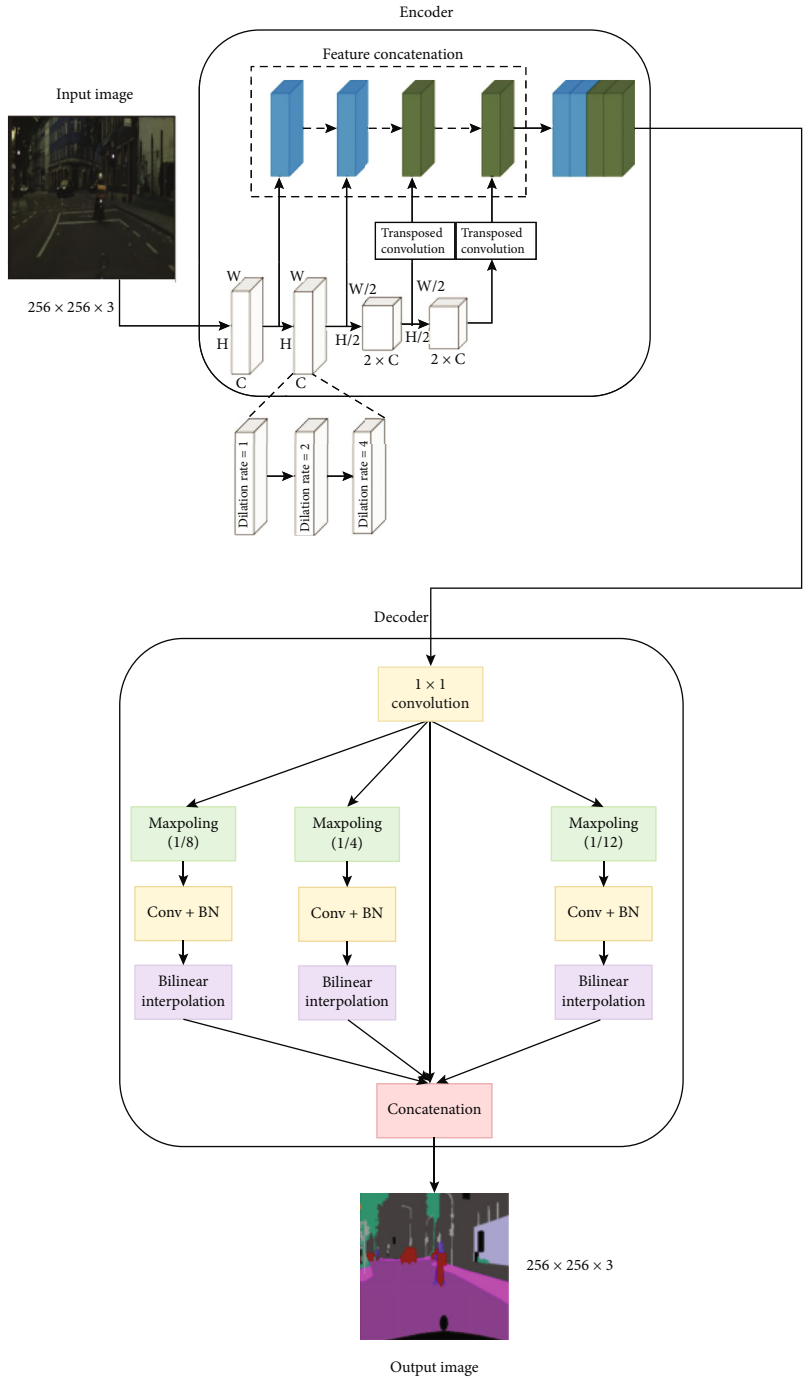

Figure 2: Structure of architecture 1: M-Net encoder+PSP decoder.

pyramid in a generative adversarial network for road segmentation. The authors in [20] use multiple paths in the decoder to capture different variations in the face with the same expression label. In [21], the input is taken at three different scales and an attention map for each scale is then learned. Yap [22] proposed an architecture to segment damages on the road; the architecture contained detail branch and segmentation branch using VGG net [14] and MobileNetV2 [23], respectively, as backbone architectures.

All these developments lead to a huge improvement in prediction accuracy but some of them are hard on computations. There have been developments to reduce the computational complexity required to achieve certain segmentation accuracy. ENet [24] used early downsampling to reduce the cost of processing large frames and used PReLU as activation. The use of PReLU tends to increase the computational cost, but the reduction in computations caused by reducing the spatial dimensions of the features early in the network was large enough to make the overall network faster than its counterparts. SINet [25] introduced an extremely lightweight multipath structure containing spacial squeeze modules. These spacial squeeze modules

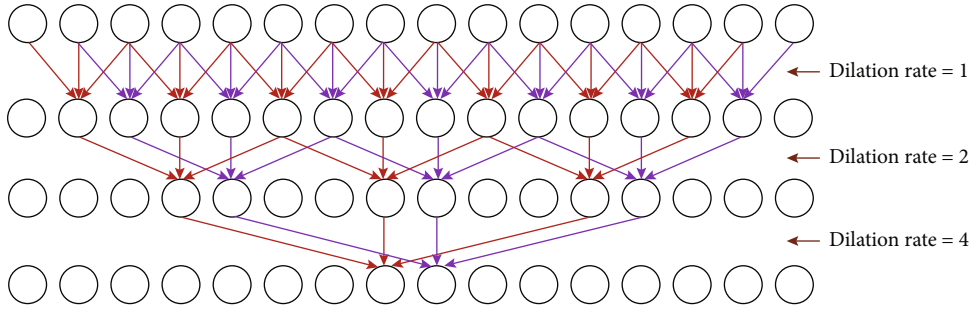

Figure 3: Connections between 3 convolutional layers of dilation factors 1, 2, and 4.

Table 1: Detailed architecture of the encoder.

	Layers	Input	Output	
	Conv2d	$32 \times 56 \times 256$	$32 \times 256 \times 256$	$k = 3, p = 1, d = 1$
Conv-block 1	Conv2d	$32 \times 256 \times 256$	$32 \times 256 \times 256$	$k = 3, p = 2, d = 2$
	Conv2d	$32 \times 256 \times 256$	$32 \times 256 \times 256$	$k = 3, p = 4, d = 4$
	Conv2d	$32 \times 256 \times 256$	$32 \times 256 \times 256$	$k = 3, p = 1, d = 1$
Conv-block 2	Conv2d	$32 \times 256 \times 256$	$32 \times 256 \times 256$	$k = 3, p = 2, d = 2$
	Conv2d	$32 \times 256 \times 256$	$32 \times 256 \times 256$	$k = 3, p = 4, d = 4$
	MaxPooling	$32 \times 256 \times 256$	$32 \times 128 \times 128$	$k = 3, s = 2, p = 1$
	Conv2d	$32 \times 128 \times 128$	$64 \times 128 \times 128$	$k = 3, p = 1, d = 1$
Conv-block 3	Conv2d	$64 \times 128 \times 128$	$64 \times 128 \times 128$	$k = 3, p = 2, d = 2$
	Conv2d	$64 \times 128 \times 128$	$64 \times 128 \times 128$	$k = 3, p = 4, d = 4$
	Conv2d	$64 \times 128 \times 128$	$64 \times 128 \times 128$	$k = 3, p = 1, d = 1$
Conv-block 4	Conv2d	$64 \times 128 \times 128$	$64 \times 128 \times 128$	$k = 3, p = 2, d = 2$
	Conv2d	$64 \times 128 \times 128$	$64 \times 128 \times 128$	$k = 3, p = 4, d = 4$

k denotes the kernel size, p denotes the padding used, d denotes the dilation rate, and s denotes the strides.

reduce the number of feature maps by half by using pointwise convolution, to further reduce the computations they used average pooling to squeeze the resolution of the feature maps, beating ENet [24] in the total number of parameters.

3. Proposed Method

This section will discuss our proposed methodology in detail. Our encoder is designed to effectively encode the features in full resolution without allowing too much latency into the system. Since our encoded features will be in full resolution it would eliminate the need to use extensive transposed convolutions in our decoder. The decoder in our case is a multipath feature extraction module; this would extract features at different scales, making better use of high-resolution encoded features. We have proposed two architectures both with the same encoder but one with PSP module as the decoder and the second one with ASPP module as the decoder.

3.1. Architecture 1: M-Net Encoder+PSP Decoder. The encoder is aimed at encoding the features at full resolution making much finer predictions possible, while also having a large enough receptive field to effectively segment large objects.

Our encoder is four conv-blocks deep as shown in Figure 2. Each conv-block has one standard convolutional layer and two atrous convolutional layers with dilation rates of 2 and 4, respectively, and each of them with a 3×3 kernel. Stacking up convolutional layers in this particular order connects each output pixel with 15×15 input pixels. To explain this concept, we have used 1D convolutions to make things look a bit less complicated. Figure 3 shows a set of 1D convolutions each with a kernel size of 3 and a dilation factor of 1, 2, and 4 is used for convolutional layers going from the top, middle, to bottom layers, respectively. Each conv-block effectively increases the receptive field by 15 pixels while maintaining constant spatial dimensions; this order of dilation rate also avoids the problem where the information from the adjacent pixels do not overlap if only even dilation rates are used as pointed out by [8]. Since going deep with high spatial resolution can be computationally expensive, the first 2 conv-blocks are followed by a MaxPooling layer which reduces the spatial dimensions of the features by half, after which 2 more conv-blocks are added. This also helps to increase the receptive field of the network and enables it to segment larger objects in the image. Table 1 shows the input and output dimensions of every layer. We selected a kernel size of 3 for each layer throughout the

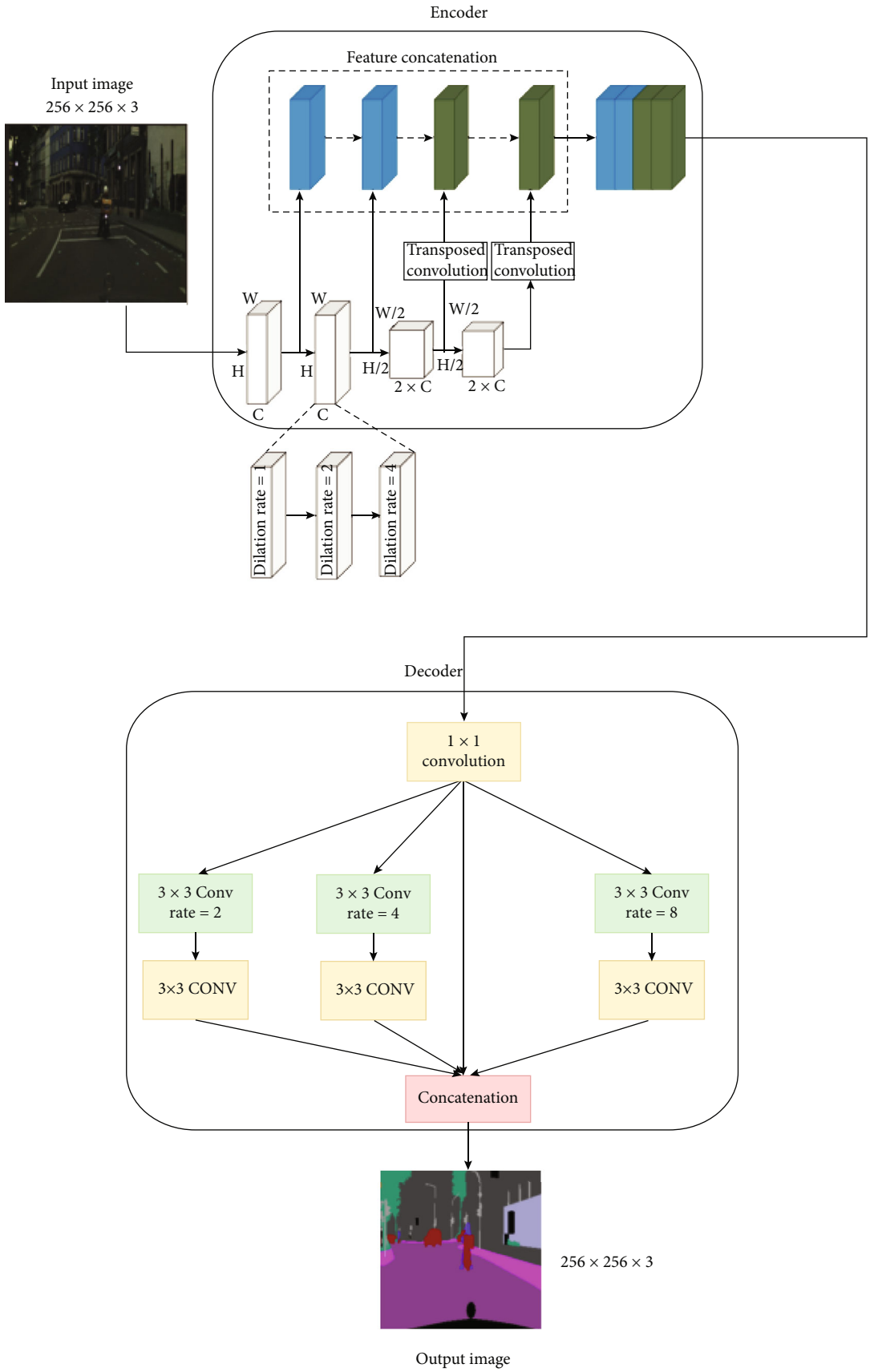

Figure 4: Structure of architecture 2: M-Net encoder+ASPP decoder.

Table 2: The architectural difference between PSP and ASPP modules.

	PSP		ASPP	
Branch	Layers	Parameters	Layers	Parameters
Branch 1	MaxPooling	$k = 9, s = 8, p = 1$	Conv2d	$k = 3, p = 8, d = 8$
	Conv2d	$k = 3, s = 1, p = 1$	Conv2d	$k = 3, p = 1, d = 1$
Branch 2	MaxPooling	$k = 5, s = 4, p = 1$	Conv2d	$k = 3, p = 4, d = 4$
	Conv2d	$k = 3, s = 1, p = 1$	Conv2d	$k = 3, p = 1, d = 1$
Branch 3	MaxPooling	$k = 3, s = 4, p = 1$	Conv2d	$k = 3, p = 2, d = 2$
	Conv2d	$k = 3, s = 1, p = 1$	Conv2d	$k = 3, p = 1, d = 1$

Table 3: Experimental results of segmentation models on Cityscapes.

Model	Number of parameters	Size	mIoU
ENet	688 K	3 Mb	53
M-Net+ASPP	375 K	1.5 Mb	58
M-Net+PSP	348 K	1.38 Mb	56
SINet	43 K	0.3 Mb	43

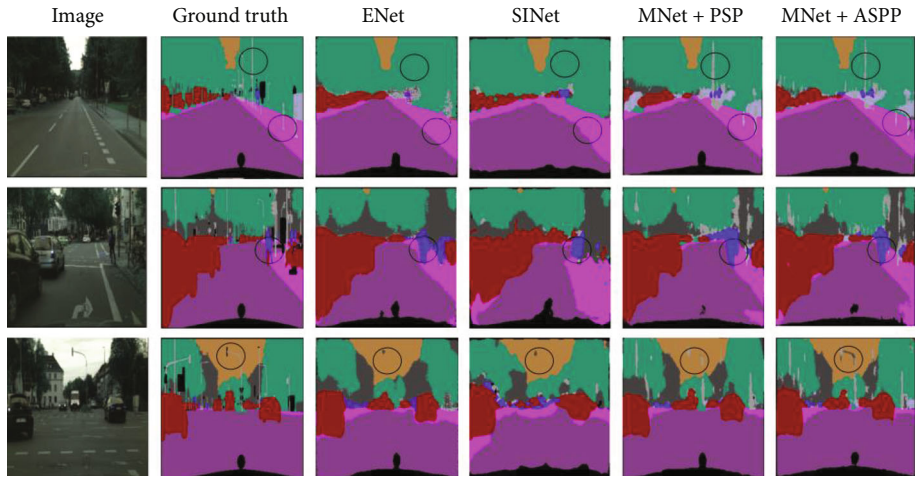

Figure 5: Visual comparison of segmentation masks with different models on Cityscapes dataset.

network; we have avoided using larger kernel sizes to reduce computations. Specific padding is used for each dilation rate to maintain the spacial resolution. The outputs from the last two conv-blocks are upscaled using transposed convolution to recover the spatial dimensions of the features from the last 2 conv-blocks. All four feature maps are then concatenated together resulting in a feature map of shape $128 \times 256 \times 256$ which is then passed on to the decoder which in this first case is a PSP module.

The emphasis behind using a PSP module as the decoder is to extract features from different scales further increasing the receptive field and to fuse the information received from different scales. This increases the range of context information obtained.

This idea was inspired by the PSP module proposed by [9] which uses spacial pyramid pooling to capture the global context information from the high-resolution features.

Multipath structures like the ones used in google's inception nets and the ones used in this PSP module can be hard on computations. To counter the high computational requirements, we have used a 1×1 convolution layer to reduce the number of channels. The feature maps are then pooled into their respective subregions each followed by a 3×3 convolution layer and batch normalization as shown in Figure 2. The features from each scale are then upsampled using bilinear interpolation and are then concatenated together.

3.2. Architecture 2: M-Net Encoder+ASPP Decoder. Another way to extract multiple-scale information is by using atrous spatial pyramid pooling (ASPP). The ASPP module replaces pooling layers with atrous convolution at different dilation rates to extract features at multiple scales. The reason why we have not completely gone with pooling layers in the PSP module to extract multiscale features is that despite

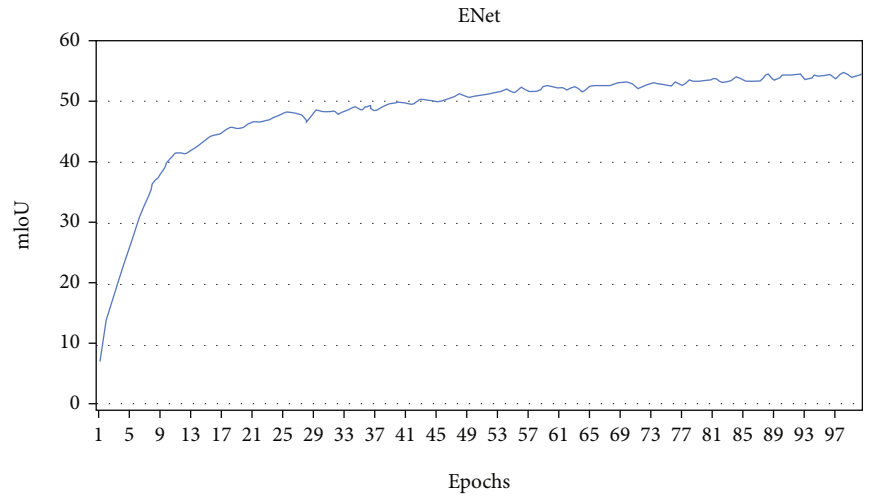

(a)

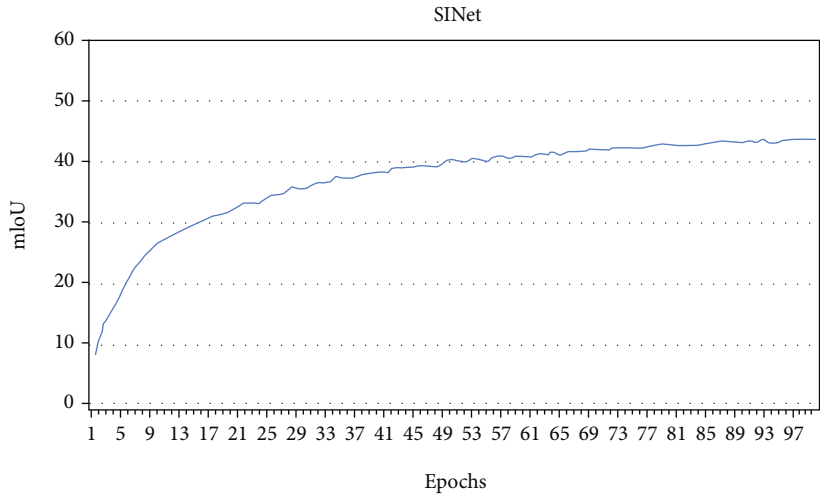

(b)

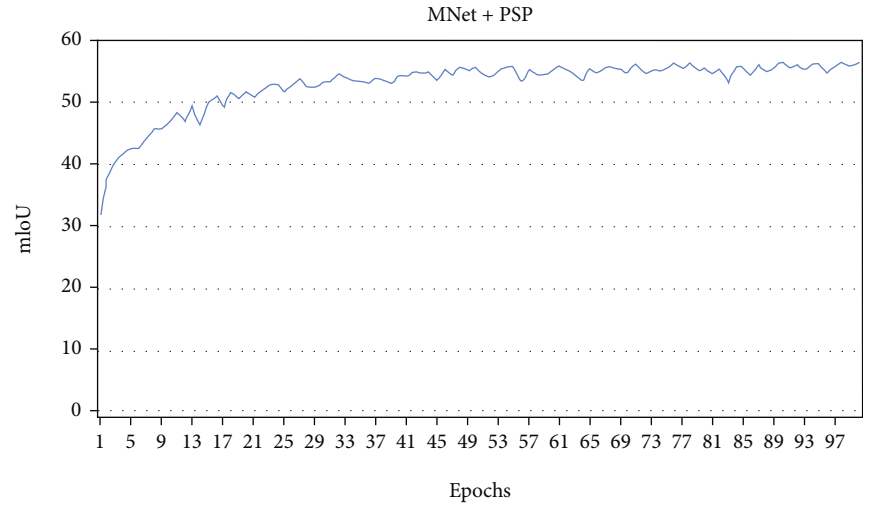

(c)

Figure 6: Continued.

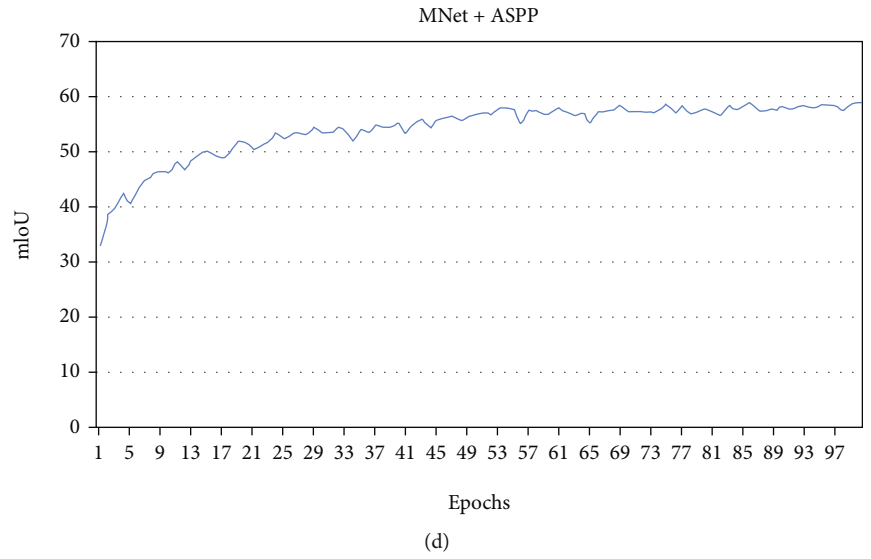

(d)

Figure 6: Graphical comparison of validation mIoU against epoch on the Cityscapes dataset. (a) The graph of ENet. (b) The graph of SINet. (c) The graph of M-Net with a PSP decoder. (d) The graph of M-Net with ASPP decoder.

Table 4: Experimental results of segmentation models on Mapillary Vistas.

Model	Number of parameters	Size	mIoU
ENet	688 K	3 Mb	56
M-Net+ASPP	375 K	1.5 Mb	61
M-Net+PSP	348 K	1.38 Mb	59
SINet	43 K	0.3 Mb	50

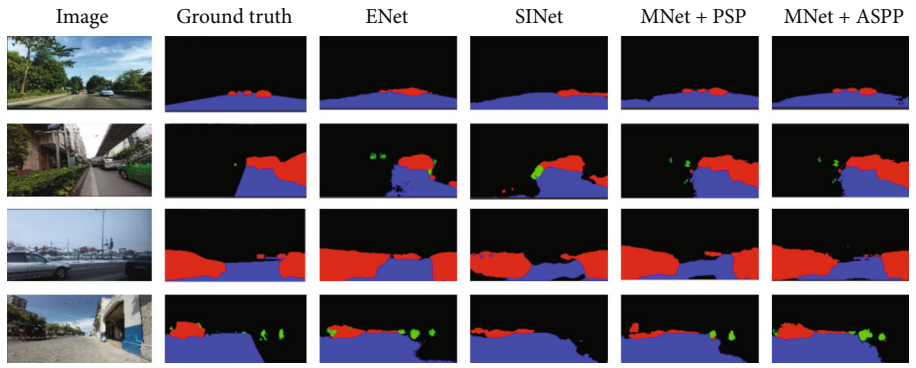

Figure 7: Visual comparison of segmentation masks with different models on Mapillary Vistas dataset.

being robust at increasing the receptive field of the network maxpooling layers have shown to lose some of the information; this effect is shown by the authors in [26], and we have also observed finer results with ASPP module. We have used three atrous convolution layers with the dilation rates of 2, 4, and 8, respectively. Each atrous convolution is followed by a standard convolution layer with a 3×3 kernel as shown in Figure 4. We decided not to go deep with the convolution layers in PSP and ASPP modules as a large number of computations on multiple paths can make the system slower. Table 2 shows the architectural difference between our PSP and ASPP decoders.

4. Experiments and Results

We have used Pytorch as our deep learning framework to train and test our model. Adam Optimizer [27] with a learning rate of $4e-6$, weight decay of $2e-4$, and batch size of 10

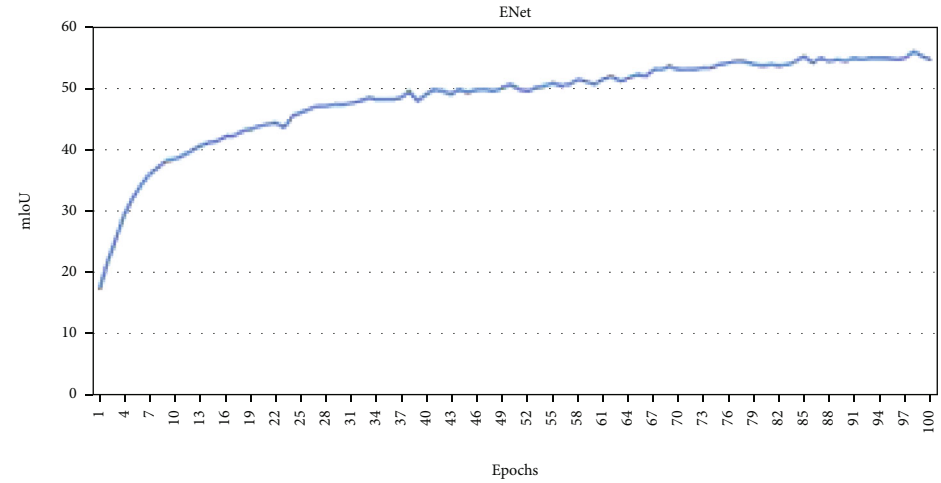

(a)

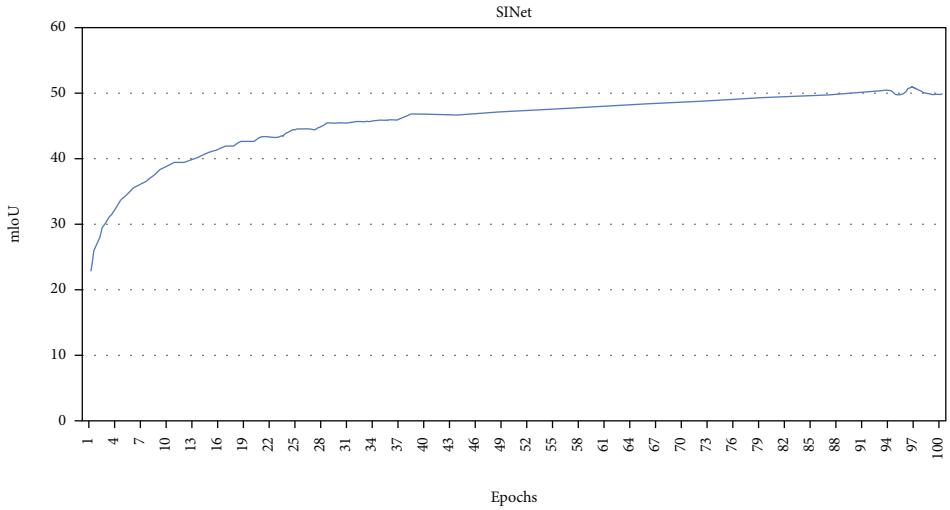

(b)

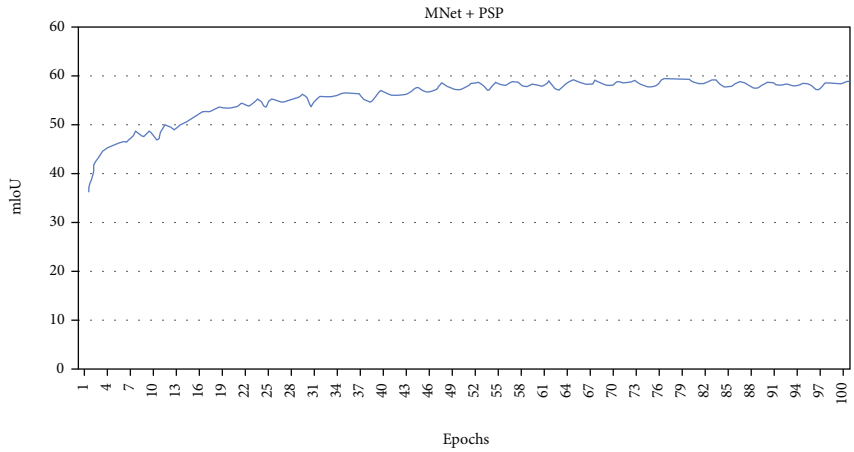

(c)

Figure 8: Continued.

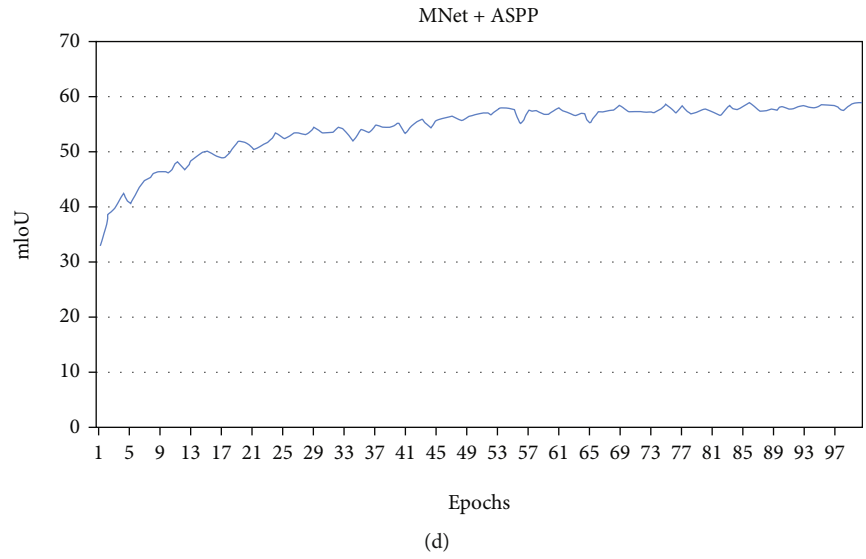

(d)

Figure 8: Graphical comparison validation mIoU against epoch on the Mapillary dataset. (a) The graph of ENet. (b) The graph of SINet. (c) The graph of M-Net with a PSP decoder. (d) The graph of M-Net with ASPP decoder.

was used to train our networks on Cityscapes [28] and Mapillary vistas [29]. We have compared our results with ENet and SINet since they both are known for working with a low number of parameters.

We have used mean intersection over union as our evaluation metric; mIoU is the mean of IoU scores for each class Equation (1), where TP, FP, and FN represent true positives, false positives, and false negatives, respectively.

$$\text{mIoU} = \frac{1}{C}\sum_{x=1}^{C}\frac{\text{TP}(x)}{\text{TP}(x) + \text{FP}(x) + \text{FN}(x)}. \quad (1)$$

4.1. Cityscapes. Cityscapes is a large dataset with video sequences recorded from the streets of 50 different cities. The dataset has 2975 training samples, 500 validation samples, and 1525 test images. We trained our networks at an image resolution of 256×256 and with 10 classes. To test the performance of both multipath feature extraction methods, we have trained our network first with a PSP module as our decoder and then with an ASPP module. Table 3 shows the comparison between ENet, SINet, and our proposed networks on the CityScapes dataset, the number of parameters of SINet are still much less than our proposed architecture but the jump in mIoU is significant while still using half trainable parameters; the graphical comparison between the models is shown in Figure 5 shows that both of our models tend to converge a bit sooner. Despite having slightly more parameters than the PSP module, the ASPP module is still faster than the PSP module while still producing better results.

The results in Figure 6 show that high-resolution feature encoding in our model makes it better at segmenting thin and small objects and also at predicting fine-edged feature masks. The pole in the first example is segmented by both of our networks with reasonable accuracy while ENet and SINet completely ignored it. The person in the second image is segmented as a blob by SINet and ENet, whereas our proposed architectures have managed to produce better edges and a more human-like shape.

4.2. Mapillary Vistas. Mapillary Vistas has 25,000 high-resolution images which are 5 times larger than Cityscapes; it contains 66 object categories with labels for 37 classes. It contains images from all devices from all around the world in various weather conditions and seasons. We have augmented our dataset by flipping the images along the y-axis, doubling the dataset. We divided our dataset so that we had 40,000 training samples, 5,000 validation, and 5,000 test samples. Table 4 shows how each network performed on the Mapillary dataset. Figure 7 shows that our architectures maintain a pattern similar to the one presented by Figure 5 on a much larger Mapillary vistas dataset.

All 4 networks are trained on 3 classes naming vehicle, pedestrian, and road. Figure 8 shows the visual comparison between the results of all 4 networks on Mapillary Vistas.

Both of our networks have shown similar improvements on both datasets. Careful encoding of features in high resolution combined with multipath feature extraction has shown to segment finer edges without any increase in the number of learnable parameters. The first example in Figure 8 shows how both of our M-Net architectures were able to segment 3 different cars separately instead of segmenting all three cars as one. In the second example both M-Nets are able to produce much finer results showing how it is able to segment both large and small objects. The graphs below from (a) to (d) show the change in mIoU with every epoch on a validation set.

5. Discussion

This paper improves on the traditional encoder-decoder technique for segmentation and proposes a technique to encode the features in full resolution and uses a multipath

feature extraction feature extraction module to predict much finer segmentation masks as compared to its traditional encoder-decoder counterparts.

U-Net [6] has been one of the most widely used encoder-decoder architecture for semantic segmentation; its effectiveness and simplicity is the main reason behind its popularity. It is safe to say that aggressive down sampling in segmentation models can cause the loss of important spacial information. It can be argued that the skip connections in U-Net [6] and SegNet [13] can overcome the loss of information due to downsampling, but looking at it from a different angle, it is clear that the convolutional layer immediately after the pooling layer will not receive the needed spacial information. Small models like ENet [24] and SINet [25] downsample the features in the beginning of the network and then go deep with much smaller feature maps to reduce the size and computational requirements of the model. In this paper, we show why that is not a good idea when network is to be used for road scene segmentation. Encoding the features in full resolution and using a multipath feature extraction module has shown to result in much finer and accurate segmentation masks while still maintaining low computational requirements. The future work of this study may include upscaling the network to compare its performance with larger segmentation models. The main limitation of this technique is that going too deep with full scale features can be expensive this is one of the reasons why we had to use max-pooling to be better than the networks under consideration (ENet and SINet) in both size and speed. Future work might also be able to study the effect of going deeper with full scale features for applications where computation resource is not an issue.

6. Conclusion

Unlike detection and classification applications, spacial resolution of features is extremely important when it comes to segmentation. This is also true for road scenes when segmenting small objects like a person and traffic sign, etc. This paper proposes a new deep learning-based model for semantic segmentation using an encoder-decoder architecture.

Instead of following the conventional approach of doing extensive downsampling of features in the encoder, we have introduced the idea of high-resolution feature encoding, thus enabling the decoder to extract valuable multiscale features from the high-resolution encoded features. To address the issue of latency due to high-resolution features, the spatial resolution is reduced by half after every two convolution blocks. The downsampled features are then upsampled before being concatenated with the rest of the features. This way the output of the encoder is in full resolution. The decoder consists of a multipath feature extraction module to decode the necessary information from three different scales. The proposed scheme is also compared with some classical encoder-decoder architectures for semantic segmentation. The experimental results reported in the paper show that encoding in full resolution has resulted in the prediction of much finer segmentation masks for both large and small objects. This research shows the overall effectiveness of the proposed architecture in terms of improved segmentation performance.

Data Availability

Two datasets were used in this set of experimentation namingly Cityscapes and Mapillary vistas; they both are open access datasets and are available on the following links: https://www.kaggle.com/datasets/zhangyunsheng/cityscapes-data and https://www.mapillary.com/dataset/vistas.

Conflicts of Interest

There are no potential conflicts of interest. The work has been undertaken to accept standards of ethics and of professional standards.

Acknowledgments

One of the authors (Harish Kumar) extends his gratitude to the Deanship of Scientific Research at King Khalid University for funding this work through research groups program under grant number R. G. P. 2/198/43.

References

[1] M. Bojarski, D. Del Testa, D. Dworakowski et al., "End to end learning for self-driving cars," 2016, http://arxiv.org/abs/1604.07316.

[2] J. Redmon and A. Farhadi, "YOLOv3: an incremental improvement," 2018, http://arxiv.org/abs/1804.02767.

[3] Q. Zou, H. Jiang, Q. Dai, Y. Yue, L. Chen, and Q. Wang, "Robust lane detection from continuous driving scenes using deep neural networks," *IEEE Transactions on Vehicular Technology*, vol. 69, no. 1, pp. 41–54, 2020.

[4] Z. Li, G.-A. Bilodeau, and W. Bouachir, "Multiple convolutional features in Siamese networks for object tracking," *Machine Vision and Applications*, vol. 32, no. 3, pp. 1–11, 2021.

[5] T. Darrell, J. Long, and E. Shelhamer, "Fully fonvolutional networks for semantic segmentation," 2015, http://arxiv.org/abs/1411.4038.

[6] O. Ronneberger, P. Fischer, and T. Brox, "U-Net: convolutional networks for biomedical image segmentation," 2015, http://arxiv.org/abs/1505.04597.

[7] L.-C. Chen, G. Papandreou, I. Kokkinos, K. Murphy, and A. L. Yuille, "DeepLab: semantic image segmentation with deep convolutional nets, atrous convolution, and fully connected CRFs," *IEEE Transactions on Pattern Analysis and Machine Intelligence*, vol. 40, no. 4, pp. 834–848, 2018.

[8] R. Hamaguchi, A. Fujita, K. Nemoto, T. Imaizumi, and S. Hikosaka, "Effective use of dilated convolutions for segmenting small object instances in remote sensing imagery," in *2018 IEEE Winter Conference on Applications of Computer Vision (WACV)*, pp. 1442–1450, 2018.

[9] H. Zhao, J. Shi, X. Qi, X. Wang, and J. Jia, "Pyramid scene parsing network," in *2017 IEEE Conference on Computer Vision and Pattern Recognition (CVPR)*, pp. 6230–6239, 2017.

[10] Z. Shao, Z. Zhou, X. Huang, and Y. Zhang, "MRENet: simultaneous extraction of road surface and road centerline in complex urban scenes from very high-resolution images," *Remote Sensing*, vol. 13, no. 2, p. 239, 2021.

[11] T. Emara, H. E. Abd, E. Munim, and H. M. Abbas, "LiteSeg: a novel lightweight ConvNet for semantic segmentation," in

2019 Digital Image Computing: Techniques and Applications (DICTA), 2019.

[12] V. B. A. Kendall and R. Cipolla, "Bayesian SegNet: model uncertainty in deep convolutional encoder-decoder architectures for scene understanding," in *Proceedings of the British Machine Vision Conference (BMVC)*BMVA press.

[13] V. Badrinarayanan, A. Kendall, and R. Cipolla, "SegNet: a deep convolutional encoder-decoder architecture for image segmentation," *IEEE Transactions on Pattern Analysis and Machine Intelligence*, vol. 39, no. 12, pp. 2481–2495, 2017.

[14] K. Simonyan and A. Zisserman, "Very deep convolutional networks for large-scale image," 2015, http://arxiv.org/abs/1409.1556.

[15] H. Wu, J. Zhang, K. Huang, K. Liang, and Y. Yu, "FastFCN: rethinking dilated convolution in the backbone for semantic segmentation," 2019, http://arxiv.org/abs/1903.11816.

[16] G. Lin, A. Milan, C. Shen, and I. Reid, "RefineNet: multi-path refinement networks for high-resolution semantic segmentation," 2016, http://arxiv.org/abs/1611.06612.

[17] C. Yu, J. Wang, C. Peng, C. Gao, G. Yu, and N. Sang, "Learning a discriminative feature network for semantic segmentation," 2018, http://arxiv.org/abs/1804.09337.

[18] L.-C. Chen, G. Papandreou, F. Schroff, and H. Adam, "Rethinking atrous convolution for semantic image segmentation," 2017, http://arxiv.org/abs/1706.05587.

[19] P. Shamsolmoali, M. Zareapoor, H. Zhou, R. Wang, and J. Yang, "Road segmentation for remote sensing images using adversarial spatial pyramid networks," *IEEE Transactions on Geoscience and Remote Sensing*, vol. 59, no. 6, pp. 4673–4688, 2021.

[20] S. Xie, H. Hu, and Y. Wu, "Deep multi-path convolutional neural network joint with salient region attention for facial expression recognition," *Pattern Recognition*, vol. 92, pp. 177–191, 2019.

[21] A. Tao, K. Sapra, and B. Catanzaro, "Hierarchical multi-scale attention for semantic segmentation," 2020, http://arxiv.org/abs/2005.10821.

[22] M. Yap, *Road damage segmentation for mobile hardware, [M.S. thesis]*, KTH Royal Institute of Technology, Stockholm, Sweden, 2021.

[23] M. Sandler, A. Howard, M. Zhu, A. Zhmoginov, and L. C. Chen, "MobileNetV2: inverted residuals and linear bottlenecks," in *Proceedings of the IEEE conference on computer vision and pattern recognition*, pp. 4510–4520, 2018.

[24] A. Paszke, A. Chaurasia, S. Kim, and E. Culurciello, "ENet: a deep neural network architecture for real-time semantic segmentation," 2016, http://arxiv.org/abs/1606.02147.

[25] H. Park, L. L. Sjösund, Y. Yoo, N. Monet, J. Bang, and N. Kwak, "SINet: extreme lightweight portrait segmentation networks with spatial squeeze modules and Information Blocking Decoder," 2020, http://arxiv.org/abs/1911.09099.

[26] Y. Li, X. Zhang, and D. Chen, "CSRNet: dilated convolutional neural networks for understanding the highly congested scenes," in *Proceedings of the IEEE conference on computer vision and pattern recognition*, pp. 1091–1100, 2018.

[27] D. P. Kingma and J. Ba, "Adam: a method for stochastic optimization," 2017, http://arxiv.org/abs/1412.6980.

[28] M. Cordts, M. Omran, S. Ramos et al., "The Cityscapes dataset for semantic urban scene understanding," in *Proceedings of the IEEE conference on computer vision and pattern recognition*, pp. 3213–3223, 2016.

[29] G. Neuhold, T. Ollmann, S. Rota Bulo, and P. Kontschieder, "The Mapillary Vistas dataset for semantic understanding of street scenes," in *2017 IEEE International Conference on Computer Vision (ICCV)*, pp. 5000–5009, 2017.

Hindawi
Wireless Communications and Mobile Computing
Volume 2022, Article ID 8219377, 11 pages
https://doi.org/10.1155/2022/8219377

Research Article

Smart Transportation in Developing Countries: An Internet-of-Things-Based Conceptual Framework for Traffic Control

Haleem Farman,[1] **Zahid Khan**,[2] **Bilal Jan**,[3] **Wadii Boulila**,[2] **Shabana Habib**,[4] **and Anis Koubaa**[2]

[1]*Department of Computer Science, Islamia College Peshawar, Peshawar 25120, Pakistan*
[2]*College of Computer and Information Sciences, Prince Sultan University, Riyadh 11586, Saudi Arabia*
[3]*Department of Computer Science, FATA University Kohat, 26100, Pakistan*
[4]*Department of Information Technology, College of Computer, Qassim University, Buraydah 52571, Saudi Arabia*

Correspondence should be addressed to Zahid Khan; zskhan@psu.edu.sa

Received 20 January 2022; Accepted 18 May 2022; Published 14 June 2022

Academic Editor: SK Hafizul Islam

In recent years, an exponential increase has been witnessed in the population of the urban area worldwide, causing a significant increase in the use of transportation services. The traditional transportation system in metropolitan cities is overwhelmed, leading to many challenges. The Internet-of-Things- (IoT-) based technology has the potential to optimize transportation services in several ways. This paper highlights the challenges and consequences of an existing transportation system in Peshawar, Pakistan, in response to the rapid growth in population. Apart from the common issues, some areas in Peshawar are highly vulnerable to massive traffic jams. For this purpose, we have proposed an IoT-based framework for busy traffic junctions. The proposed framework considers the route selection problem as a game of two players, where Nash Equilibrium (NE) sets traffic for each route so that no individual can improve its performance by changing its strategy. NE calculates the traffic density from a roadside unit (RSU) collected data, which later detects and avoids traffic congestion by an alternate route selection. The framework in this paper provides a platform for the academia and transport department to convert the existing transportation system to IoT-based intelligent transportation in Peshawar, Pakistan.

1. Introduction

The rapid growth in the world population is causing a gradual decrease in the quality of services within urban areas. According to the United Nations, around 55% of people live in urban areas and are expected to reach 68% by 2050 [1]. The exponential increase in the metropolitan area is due to the migration of people for jobs, education, business, health, and other essential facilities of modern life. This increasing number puts a great burden on the city administration to manage resources more efficiently. The city administration needs to have sustainable solutions to deal with an increasing number of citizens. A smart city is the integration of information with communication technologies to enhance the services and operations of the city to facilitate citizens. Intelligent transport is a vital factor of a smart city where vehicles are connected to a centralized controller or cloud [2]. Public transport is one of the leading services that need to be streamlined to assist citizens. Peshawar city (the capital of Khyber Pakhtunkhwa) in Pakistan is one of the busiest and most congested area linking Afghanistan at North West borders. The population of Peshawar city in 2020 was 2.3 million [3], with an increase of 3.8% from 2019. This number is increasing day by day as people move towards the city for better resources and opportunities. The city administration finds it difficult to provide support to this rapid growth, especially in public transportation. The current status of public transport in the city is highly deplorable. The primary sources of public transport are buses, wagons, and rickshaws, as shown in Figure 1. Peshawar has mainly one trunk road from the central city to the Karkhano market and few diversions to Saddar Bazar and Hayatabad town. The

(a) (b) (c)

Figure 1: Public transport in Peshawar city: (a) buses [4]; (b) wagon [5]; (c) rickshaw [6].

geographic location and existing traffic infrastructure of Peshawar city make it an excellent use-case for this research.

Public safety and a clean environment are essential public transportation factors in developing countries. Road accidents are widespread. It reveals the inadequacy of safety measures in traffic management systems. Some areas are highly vulnerable and often subject to massive traffic jams in Peshawar, Pakistan. Traffic jam in Hasthnagri and Firdaus areas is a routine matter that causes severe problems for students, employees, and patients to reach their destinations on time. This work not only elaborates on the challenges in the current traffic status but also proposes a framework for efficient management of massive traffic zone like Firdaus chowk to minimize the occurrence of severe traffic jams. The proposed traffic jam avoidance framework is an application of Internet-of-Vehicles (IoV) technology [7]. According to the suggested framework, all the participant vehicles must be equipped with GPS, an onboard unit (OBU), and IEEE 802.11p. The route selection problem at the massive congested intersection point is considered as a game of players, i.e., drivers, where Nash Equilibrium (NE) sets traffic for each route so that no individual can improve its performance by changing its strategy [8]. NE calculates the traffic density from a roadside unit (RSU) collected data, which later detects and avoids traffic congestion by an alternate route selection. Our game represents vehicles, available routes, travel time as a player, strategies, and payoff, respectively. In the proposed framework, the intelligent cars act as players to compete with other opponents in an appropriate route selection to receive an optimum payoff in a short traveling time. It estimates the traffic density based on the frequent beacon messages. Additionally, concerning the relevant density of vehicles, it recommends a particular speed based on the space head-ways aiming to avoid the intercollision of ongoing cars. Additionally, it also provides an alternate route to minimize the congestion level.

The rest of the paper is divided into six sections, where Section 2 focuses on the related work. Sections 3 and 4 deal with the potential challenges and consequences of smart transportation on the public, respectively. Section 5 explains the proposed framework, and Section 6 represents the evaluation of the proposed traffic game framework. Finally, Section 7 concludes the paper with recommendations for the future.

2. Relevant Literature

The rapid deployment of IoT-based applications provides a tremendous change in human lives. Some of the IoT applications are intelligent transportation, smart hospital, smart home, smart grid, etc. [9–12]. Different sensors (visual and scalar) are used in smart transportation, and roadside units (RSU) are deployed along the traffic routes [13–16]. Transportation has always been necessary for any country, whether through trains, cars, ships, buses, or airplanes. Public transport facilities like buses are widespread and frequently used in everyday life. On the global scale, around 1.2 million people die due to road accidents every year, and nearly 50 million people get injured [17]. Nowadays, driver fatigue and drowsiness are among the leading causes of road accidents throughout the world. Various sensors are used for this purpose in vehicles to detect drowsiness. Furthermore, different sensors are installed on the roadside connected to the driver's phone or car to detect road surface anomalies to minimize road accidents by alerting the driver. Apart from this, many researchers in the literature have contributed to smart transportation by proposing different techniques [18–20]; a few of them are discussed here.

In smart transportation, route optimization or navigation system is one of the most crucial areas. User mobile data [15] or roadside units on specific locations [21] try to approximate traffic congestion. The congestion of traffic is the primary concern of cities, and the ratio of congestion is increasing day by day due to the increased number of vehicles. Route optimization or navigation is a technique to provide the best path from source to destination in such a way to reduce traffic congestion that will decrease vehicle emissions and traveling time [21].

Smart street light (SSL) is another essential service in smart cities. It ensures a reduction in energy consumption, which detects the condition of traffic to operate accordingly, rather than simply following a predefined schedule. An energy-efficient approach presented in [22] proposed a Raspberry Pi-based automatic light on and off system by using a light sensor to detect the intensity of light and IR sensors to detect bypassing pedestrians or vehicles. A smart lighting system is presented in [23], where different kinds

of environmental sensors were used to automatically switch on/off or dim depending on the environment to preserve energy.

Another application of intelligent transportation is smart parking, where various intelligent devices, such as sensors, are used for vehicle detection. For example, the authors in [24, 25] used a scalar sensor (IR sensors or magnetic field) for vehicle detection in a parking area and information sent to a centralized system to increase parking slots and decrease the searching time. Furthermore, a vehicle-to-vehicle (V2V) communication based on an IoT framework using M2M communication is proposed in [26], where vehicles share their GPS position, movements, and speed with the nearest cars and simultaneously upload to a server.

In light of the above literature, this paper highlights the potential challenges of the existing transport in developing countries (i.e., Pakistan). Traffic congestion is at the top of all transport issues. In this paper, we proposed a framework based on the game theory to reduce the intensity of traffic congestion.

3. Challenges: Smart Transportation

The concept of a smart city is adopted in numerous developed countries. Some cities are already declared smart cities, such as Singapore, Seoul, London, and Barcelona. However, the transformation from traditional cities to smart cities is still a big challenge in these countries. One of the challenging and vital aspects of the smart city is smart transportation to contribute positively to the regional economy. Smart transportation in developing countries aims to improve the region's public transport and minimize traffic jams. Some of the challenges in developing countries are highlighted in this section. Peshawar city is considered as a case study.

3.1. Technology Infrastructure. In developing countries, the public transport system in even the major cities is often void of technological advancements. One of the main challenges for adapting smart transportation is the lack of robust supporting infrastructure. Consequently, there is no such public transport system in Peshawar city where drivers can get real-time information about road conditions or accidents. Traffic jams at certain junctions are very often badly affects the citizens' activities. In intelligent transportation, the drivers can be updated on traffic conditions, route suggestions, accidents, and infotainment using various applications.

Three modes of communication can achieve smart transportation, i.e., vehicle-to-vehicle (V2V) communication, vehicle-to-infrastructure (V2I), and connectivity with regional transport authority (RTA). The vehicles with intelligent devices share information with other cars in the neighborhood, while V2I communicates vehicles with the roadside unit (RSU) [27]. All of the RSUs are connected and installed at different points in the city along different routes. Moreover, a pedestrian can also communicate with RSU to get updated information. The collected data is passed to RTA for monitoring purposes and can further plan to avoid traffic jams. For intelligent and sustainable infrastructure, RTA needs to implement these technologies to improve citizens' quality of life to breathe in a clean and safe environment.

3.2. Governance. Governance plays a significant role when it comes to new technology adaptation. Policymakers at the city level need to contribute positively to uplift the region's transport infrastructure and contribute towards the betterment of the overall traffic conditions of a city. In developing countries, unregistered vehicles such as cabs and rickshaws also burden the traffic that needs to be controlled. The government needs to get them to register and streamline public transport to minimize traffic's adverse effects. The government's role is very crucial to uplift the transportation of any region. In developing countries, bus transit and metros need to be started to minimize vehicles on the routes, especially within the city. Due to the rapid growth in the population, the number of cars on the road also increases. RTA needs to think seriously by allocating funds to improve the road and public transport conditions. As a case study, the Peshawar local government has started a bus rapid transit (BRT) project to improve the city's traffic condition and transport facility [28]. Intelligent and sustainable transportation is the need of the day to give improved services to the citizen keeping in view the current resources and future predictions.

3.3. Education. In most developing countries, low-income people use public transport, especially the labor class, as they cannot afford a personal car. In this part of the world, the poverty rate is 31% [29], due to which people are unable to continue their education and start earning to look after their families. It is one of the main reason of unregistered cabs and rickshaw that puts an extra burden on the roads. It is a big challenge for Peshawar to adapt smart transportation as many citizens are not educated. Citizens cannot use the mobile application for updates regarding traffic conditions, infotainment, bus or wagon schedules, online map, etc. The interactive screens are often deployed at bus stops to facilitate citizens. Various parameters are recorded and displayed inside the bus to keep citizens updated. It is also a big challenge for those who are not educated enough to benefit from intelligent transportation.

3.4. Cost. The current condition of public transport is not good because the drivers/owners are not upgrading their vehicles despite the pathetic conditions. Moreover, almost all public transport that moves in Peshawar city is privately owned. The local administration has no funds for the transport chain to facilitate both citizens and drivers. To deploy the government-funded public transport across the city requires a handsome budget to buy well-equipped buses and wagons that run on the main roads while the rest of the vehicles will use other specified tracks. The overall management and control rooms need to be established at different city locations to monitor the traffic condition and avoid traffic jams, especially at peak hours. Technology-assisted buses need to be hired with proper infrastructure deployed that can be connected to each vehicle. A complete setup is required to implement the features offered by intelligent transportation.

4. Consequences of Smart Transportation on General Public

In developed countries, citizens benefit from different transport facilities in the form of public transport, either through full-fledged smart transportation or a rapid transit bus. In this section, the impact of intelligent transportation in developing countries is explored; Peshawar city is considered a case study. Below are the crucial factors that directly impact the general public, whether they use public transport or not.

4.1. Social

4.1.1. Problem. In Peshawar city, the citizens are not satisfied with public transport in its current form, and most of them are reluctant to use it. Most students and low-income people travel on the local buses, and others opt for private transport or cab services. The amount of traffic on the road, comfortability of the buses, the behavior of the drivers, travel time, and making stops at their determination can lead to frustration and tension. It can be on the higher side during summers, severely affecting an individual, whether a student or an ordinary person. Increased traffic means more time on-road, and it becomes even worse at peak times. It is highly recommended that user behavior be adequately analyzed depending on the city to better plan its available resources and forecasts future services [30].

4.1.2. Opportunity. Citizen's satisfaction is essential, and it can be achieved if the government adopts intelligent technologies to facilitate them. Smart transportation can significantly contribute to citizen satisfaction by giving maximum system accessibility, minimizing trip time and affordable fare, and reducing traffic accidents. In an intelligent environment, citizens can track the bus, vacant seat, bus schedule, optimum routes, notification of traffic jams on specific roads, and an accident alert. Moreover, comfortable buses and dedicated routes will minimize the stress and frustration of citizens and spend less time. The less you travel on the local bus, the more you feel good. The government needs to upgrade the public transport of the citizen to give a better and safe life.

4.2. Environmental

4.2.1. Problem. An increase in the number of vehicles on the road increases the emission that severely affects the environment. In Peshawar, public transport, private cars, and cabs are not well maintained, which causes pollution [31]. It is dangerous for health, causing various diseases such as cancer, heart attack, and respiratory problems. If a vehicle spends more time on the road, it will cause more pollution, and according to the World Health Organization (WHO), every year, around 5.5 million people die due to air pollution. Therefore, local administration needs to divert attention towards a clean and healthy environment. Less time on the road means less consumption of fuel resulting in money savings and time.

4.2.2. Opportunity. Adapting an intelligent transportation system can reduce emissions and minimize overall pollution, thus contributing to a clean and healthy environment. In smart transportation, standard buses with routine maintenance can result in less fuel consumption and less emission. Intelligent devices such as environmental sensors are installed at certain places where the number of pollutants in the environment is monitored. Local administration can be reported for taking any precautionary measure or future planning. Suppose people are provided with excellent public transport facilities, in that case, they will minimize their private transport usage, reducing the number of vehicles on the road. Thus, as a result, it will reduce traffic congestion, emission, and even traffic accidents.

4.3. Economic

4.3.1. Problem. Poor public transport compels people to opt for their private conveyance or use a cab service. In Peshawar, if you travel from Hayatabad town to Saddar bazaar in your car, it will take around 20-25 minutes, depends on the traffic condition, and the fuel consumed will be about 200 PKR. However, if you opt for public transport, it takes around 45-55 minutes, costing 15-20 PKR, although it is economical at the cost of time wastage. If you choose cab (taxi) services, it will charge around 300–350 PKR. Public transport seems to be very economical, but it wastes time and adds fatigue and stress. You can opt for rickshaws to the nearby destination in Peshawar city, but it is rarely used on the main trunk's lanes. Due to poor services offered, public transport is decreasing daily, which results in lower drivers' earnings and can contribute to poverty and unemployment. Moreover, people mostly prefer a shared cab to reach the destination on time by giving a bit more fare than public transport [32]. In addition to the above economic factor, it is reported in [16] that air pollution directly impacts our health and wallets. The medical cost is in trillion dollars due to the increase of various diseases caused by pollutant air.

4.3.2. Opportunity. The government needs to focus on the improvement of public transport. Reliable transportation can surely minimize the use of private conveyance and cab services. Using the above example, the passenger can reach the destination in less time. It is good to pay 20-30 PKR instead of paying 300-350 PKR. People will be encouraged to use public transport rather than private transport, resulting in less fuel consumption and saving money and time (dedicated routes). The drivers can be trained and educated regarding traffic rules and regulations. Moreover, they can be compensated in these buses to contribute towards poverty reduction and to society. A clean and healthy environment can undoubtedly minimize the diseases caused by these pollutants as citizens will breathe in a clean environment and reduce medical expenses.

4.4. Public Health Improvement

4.4.1. Problem. The number of vehicles on the road directly impacts the environment due to emissions. The more cars

(a) [18]

(b) [19]

Figure 2: Traffic condition in Peshawar city at day time; the more vehicle emits pollutants, the more it badly affects the environment; thus, having negative impact on human health can cause health diseases.

on the road, the more environment will be polluted, as shown in Figure 2. According to a report published in [17], particulate matter (PM2.5) has surpassed in Peshawar the threshold defined by the National Environmental quality standard (NEQS). The NESQS recommends 15 micrograms/cubic meters. According to [17], Peshawar has a minimum of 40 and a maximum of up to 90 PM2.5 levels, alarming that it causes an increase in age-specific deaths and can severely affect the heart and lungs. There are many other reasons for this cause: dust, waste burning, etc. But vehicular emission is a significant factor. In Peshawar, the condition of vehicles used for public transport and even cabs is not maintained. The number of motorcycles is increasing day by day for easy transport. Furthermore, nitrogen dioxide (NO_2) is also on the higher side that weakens the respiratory system causing various problems to respiration. Mostly traffic police wardens and people doing roadside businesses are highly exposed daily for the whole day.

4.4.2. Opportunity. Smart transportation can control the increasing number of vehicles on the road by providing excellent and affordable public transit. Most of the problems, such as traffic congestion, vehicle emission, and accidents, can be minimized to a greater extent. In Peshawar, the current transport system is fragile. The worst condition of the buses and wagon is possible to convert to a well-maintained transport. Minimizing the number of vehicles, especially motorcycles and cabs, will undoubtedly reduce the PM2.5 and NO2 levels to improve public health. Moreover, environmental sensors can be deployed at congested points to check different pollutants and help local administration accordingly.

4.5. Quality of Life

4.5.1. Problem. The quality of life index is crucial for every citizen around the globe. It is considered very seriously in developed countries, whereas in developing countries, it is pretty ignored or the statistics are not satisfactory as per standards. Quality of life index is the aggregate of various parameters such as safety index, health care, cost of living, traffic commute time, pollution, and few others. High pollution adds to poor public health. The traffic police, shopkeepers, and those having their small setup at the roadside

Figure 3: Traffic intersection point (Firdous Intersection) for the proposed traffic framework.

are highly exposed. Due to the high traffic and bad condition of public transport, those who cannot afford private transportation or cab are even reluctant to travel. Social gatherings, visiting parks, and tourist spots play a vital role in individual health. Peshawar city is named a city of flowers [33], but it is a polluted city due to increasing pollution and the local administration's poor management.

4.5.2. Opportunity. To improve the quality of life from the perspective of transport, citizens can easily travel to different tourist spots of the city and parks by providing good public transport facilities. They even can visit their relatives at affordable prices. If you need to go to any garden or social point in Peshawar, you might think several times also if you are using your transport. It is of utmost importance for the government to conduct a survey and identify the significance of various cities in terms of quality of life. The government needs to reduce problems as much as possible in every service offered in the town but mainly transportation services. Their roads and transport facilities can easily judge the quality of life in a particular city.

5. Proposed Traffic Jam Avoidance Framework

The existing transportation system in Pakistan has many issues, as discussed in the above sections. The proposed framework is a step towards intelligent transportation, which is based on IoT [34]. It is assumed that all the vehicles are equipped with onboard units (OBUs), a global positioning system (GPS), and IEEE 802.11p [35]. Additionally, a roadside unit (RSU) is embedded inside the traffic signal near the highly vulnerable zone for congestion, i.e., Firdous Intersection Peshawar. The intersection that we considered in the proposed framework for traffic control is shown in Figure 3 (taken from http://www.openstreet.org).

To assess the traffic congestion at the intersection point, every vehicle frequently exchanges beacon messages with other vehicles and RSU. The RSU on intersection point

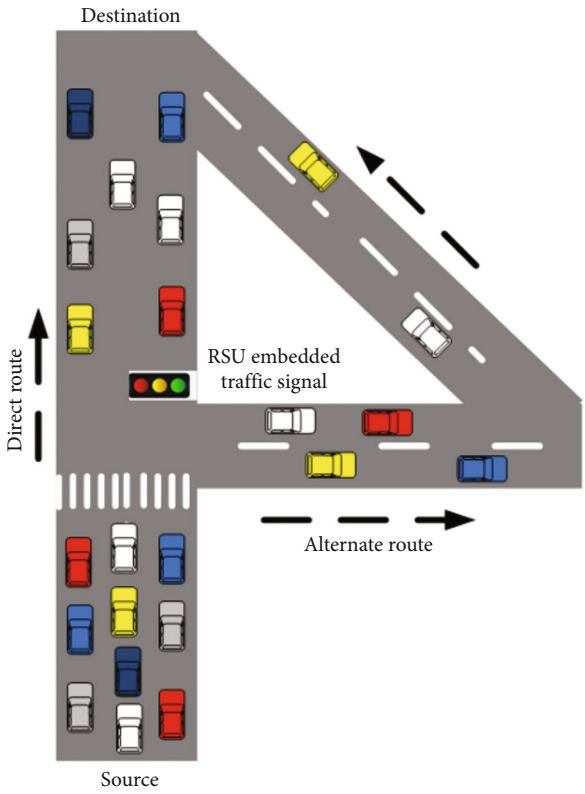

Figure 4: Proposed traffic monitoring and control framework.

estimates the vehicle density, which later uses for traffic jam detection and an alternate route selection. In the frequent beacon messages, every vehicle exchanges necessary information, including vehicle identifier, speed, direction, acceleration, location, lane number, road type, and time with other vehicles and RSU [36]. After receiving the beacon messages, an RSU turns the vehicular network into a directed graph $G(N, E)$, where N and E denote the number of cars and roads linking the junction sites, respectively. RSU creates an adjacency matrix A for a particular road map based on the received beacon messages. The following formula is used to calculate the graphical representation of a vehicular topology:

$$G = \begin{cases} JT & \text{if } (J_i, J_j) \in E, \\ \infty & \text{otherwise,} \end{cases} \quad (1)$$

where JT refers to the journey time between intersection J_i and J_j. The congestion detection in the proposed framework is considered a noncooperative game, where Nash Equilibrium (NE) [8] sets traffic for each route so that no individual can improve its performance by changing its strategy. From the system model, as shown in Figure 4, it is noticed that we have two strategies, i.e., direct and indirect. If all the vehicles use the same strategy, massive congestion will be transferred to one side of the road. Let us consider the proposed intersection point, i.e., Firdous Chowk, where a driver has two routes to reach the destination, as shown in Figure 4. The driver can go directly or indirectly. It is supposed that each route to destination (represented by I_{len}) has a fixed length and speed limit, i.e., 1 km and 40 km/h, respectively. The maximum number of vehicles NV in a high congestion scenario on each route will be:

$$NV = \left(\frac{I_{\text{len}}}{\text{Avg}_{V\text{len}}} \right) l, \quad (2)$$

where l, $\text{Avg}_{V\text{len}}$, and I_{len} represent the number of lanes, the average length of vehicle (length + minimum gap), and the length of the intersection. In the given scenario, the number of vehicles in severe congestion will be 285 by considering $K = 2$ and $\text{Avg}_{V\text{len}} = 7$ m.

5.1. Traffic Control without Equilibrium. Suppose that 250 cars want to move from source to destination. In the absence of proper route planning, it is possible that all cars take the direct route; then, the total travel time for every car is 370 seconds (6 minutes approx.) calculated

Table 1: Strategy profile of the proposed intersection point.

Player 1/player 2		Player 2	
		D	I
Player 1	D	TT_{1D}, TT_{2D}	TT_{1D}, TT_{2I}
	I	TT_{1I}, TT_{2D}	TT_{1I}, TT_{2I}

Table 2: List of parameters and its description.

Parameter	Description
Road type	Intersection point
No. of lanes	2
Arrival and departure of vehicles	Poisson distribution
Arrival rate	(0-5) veh/min
Departure rate	(0-8) veh/min
Vehicle's length	5 m
Vehicle's speed	60–80 km/h
Vehicle's acceleration	(2, 3) m/s/s
Car transmission range	500 m
RSU's transmission range	1000 m
Simulation time	500 s
No. of RSUs on intersection	1
No. of traffic signals	1
Traffic signal mode	Auto
Proposed game	Nash Equilibrium
Players	Cars passing from south to north
Strategies	Direct and indirect
Performance metrics	Average total waiting time, average travel time, average speed
Propagation model	Two ray-ground

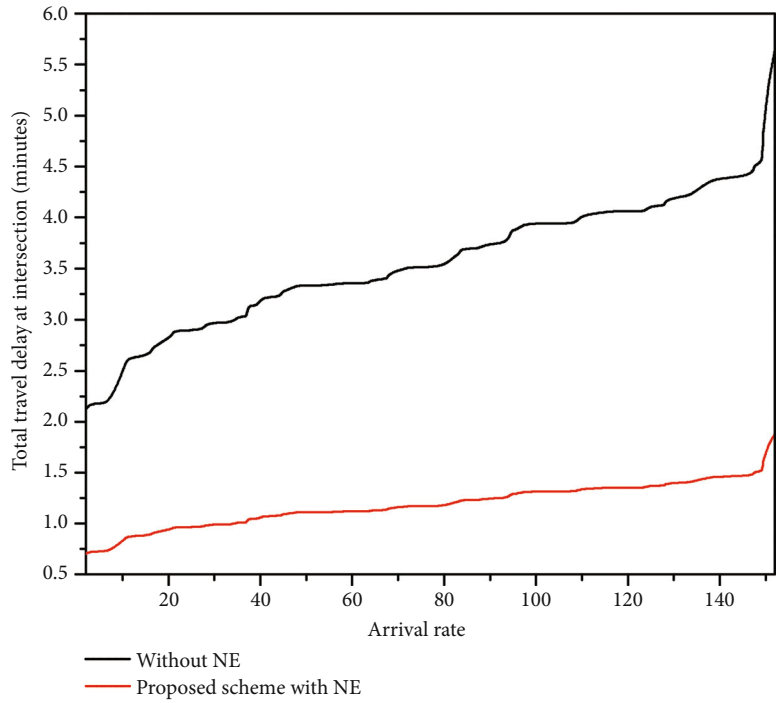

Figure 5: Expected waiting time on road intersection under different arrival rate.

by Equations (3) and (4). The same is true for the indirect route as well.

$$v_i = \left(1 - \frac{d_i}{d_j}\right) v_l, \tag{3}$$

$$TT = \frac{I_{\text{len}}}{v_i}, \tag{4}$$

where v_i, d_i, and v_l represent the current speed, current density, and speed limit, respectively. TT in Equation (4) refers to travel time. Contrarily, if the traffic evenly divides among the two routes, so that each carry 125 cars, then the total travel time on each route is $1000/12.48 = 80$ seconds.

5.2. Traffic Control with Theoretic Game Approach. The traffic control in the above scenario is a game where the opponents/players correspond to the drivers, and their route selection to the destination refers to strategies. In this paper, Nash Equilibrium is used among the opponents to improve traffic flow over the selected strategies, i.e., direct and indirect. In NE, no player/opponent will benefit by changing its current route to the other route. In the above scenario, the payoff to each player in the equilibrium case is optimal, and it degrades in the case of switching the strategy. The game in this paper is limited to two strategies. However, there are no constraints on the number of players. As mentioned earlier, any strategy in which the number of vehicles is not equal to 125 cannot be NE. On the other hand, if both strategies have similar vehicles, i.e., 125, then the given situation will be NE. We used a mixed strategy NE in the proposed framework. The traffic congestion avoidance game is shown in Table 1, where two players, i.e., player 1 and player 2, are fighting to get a good payoff.

The D and I in Table 1 refer to direct and indirect routes, respectively. Let player 1 plays D with probability p and I with probability $(1 - p)$. In addition, player 2 plays D with probability q and I with probability $(1 - q)$. The order pair (TT_{1D}, TT_{2I}) represents the probability that player 1 will select strategy D given that player 2 will select strategy I. From the mixed strategy NE game, the expected payoff of player/agent 1 is a function of player 2 individual strategies' probabilities, i.e., $u_1(D) = f(q, 1 - q)$. If player 1 best responds with a mixed strategy, player 2 must make him indifferent between D and I.

$$\begin{aligned} u_1(D, (q, 1 - q) &= u_1(I, (q, 1 - q), \\ TT_{1D}q + TT_{1D}(1 - q) &= TT_{1I}q + TT_{1I}(1 - q). \end{aligned} \tag{5}$$

The same procedure can be carried out for player 2 payoff calculation considering player 1 strategy probabilities, i.e., $(p, 1 - p)$. Likewise, player 1 must randomize to indifferent player 2.

$$\begin{aligned} u_2(D,(p, 1 - p) &= u_2(I,(p, 1 - p), \\ TT_{1D}p + TT_{1D}(1 - p) &= TT_{1I}p + TT_{1I}(1 - p). \end{aligned} \tag{6}$$

Thus, the given game will be mixed strategy NE, if only player 1 plays direct and indirect strategies with probability p and $1 - p$, respectively. Additionally, player 2 plays with q and $1 - q$ probabilities for direct and indirect strategies, respectively.

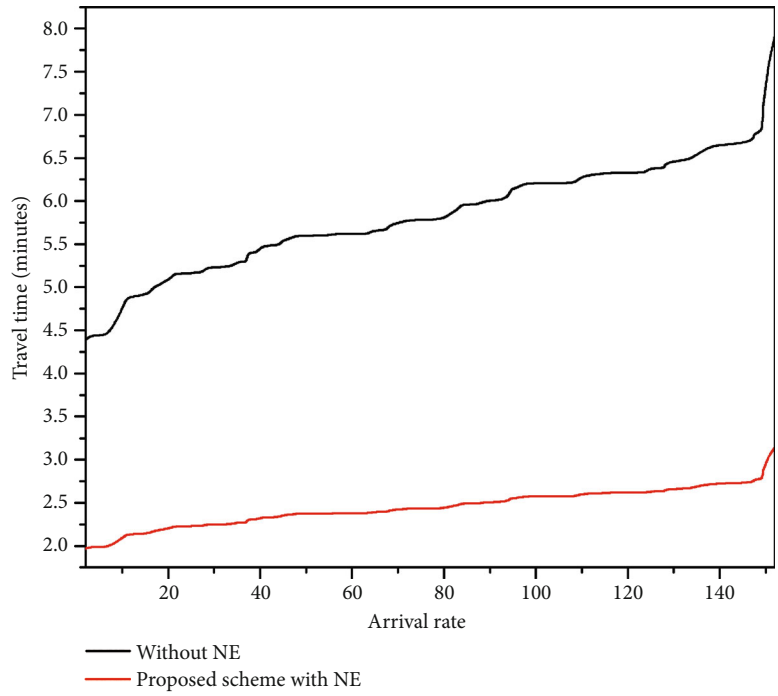

Figure 6: Average travel time from source entrance to destination under different arrival rate.

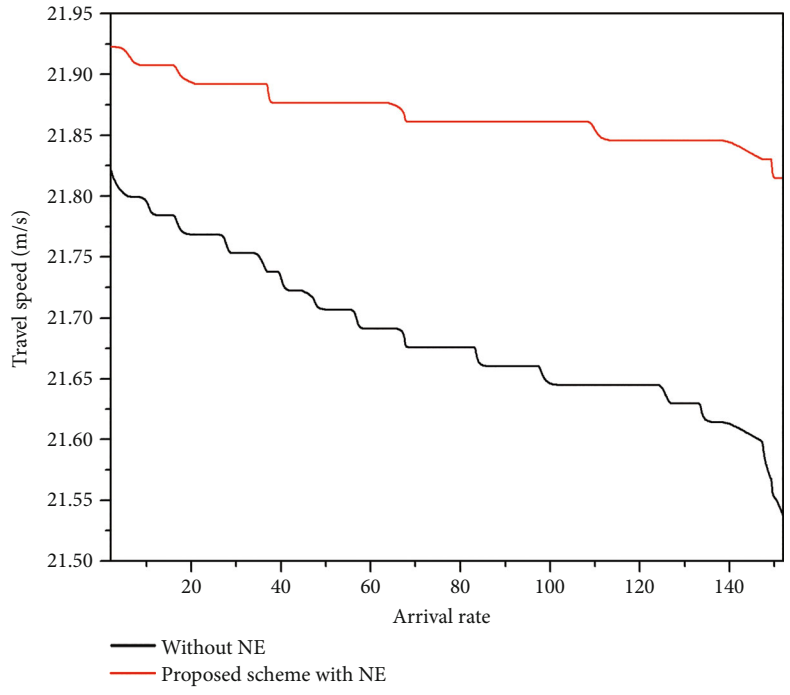

Figure 7: Average travelling speed from source entrance to destination under densities of different arrival rate.

6. Assessment of the Proposed Framework

We conducted various experiments to measure the efficacy of our proposed framework. The performance of the suggested framework is compared with a simple queuing model that ignores the equilibrium of vehicle flow in each direction.

6.1. Environment Setup. The proposed framework is checked and evaluated at a congested intersection where alternate paths exist to a specific destination. For this purpose, we used http://OpenStreetMap.org [37] to extract real road traces of a junction point in Peshawar city, Pakistan, as illustrated in Figure 3. The OpenStreetMap gives a complete overview of the road structures. We set the specified junction

in the OpenStreetMap address bar and extracted it for traffic assessment. Later, for traffic generation and route planning, a well-known traffic simulator SUMO (Simulator for Urban Mobility), version 0.24.0, is employed [38]. The SUMO traffic traces were used as a data set for our suggested system, which was later imported to MATLAB (R2019b) for further assessment. The parameters and performance metrics that we used in our experiments are given in Table 2.

From Table 2, we have three performance metrics that are measured under various densities due to nonpredictive arrival rates. The definitions of all these metrics are taken from the queuing theory, as discussed in the reference in the context of telecommunication [39].

6.2. Results and Discussion. This section evaluates the proposed traffic model with different densities of vehicles under varying arrival rates at the intersection. Three performance metrics, namely, average total waiting time (the average waiting time of a vehicle at intersection), average travel time (the time taken during travelling), and average speed (average speed of an individual vehicle during travelling), are evaluated with different vehicle arrival rates. The relationship between arrival rate and waiting time at the intersection is depicted in Figure 5.

The line graph illustrates that the arrival rate is precisely related to the delay on the junction. In other words, the higher the arrival rate, the longer the delay at the selected junction point. However, the performance of our suggested traffic model in terms of waiting time is not adversely affected by frequent vehicle arrivals. The efficient use of NE, in which players select an optimal path based on the activities of other players, is the cause for the resilience against the high arrival rate. The effectiveness of NE can also be verified by looking at the results of a typical traffic model (without NE), where frequent arrivals have a substantial impact on the waiting time at intersections (see Figure 5). Now look at the performance in terms of travel time, we can see in Figure 6 that our proposed method outperforms the traditional scheme.

The proposed traffic controller takes 2-2.5 minutes to reach the destination after leaving the intersection at a given speed. Because the proposed framework correctly handles traffic on all possible routes, the number of vehicles on any given road segment is insignificant. As a result, travel time is not affected like other conventional schemes. Again, the traditional method performs worse than the suggested traffic control scheme, with a maximum arrival rate of 7 minutes. Finally, the travel speed is evaluated in relation to various arrival rates at the intersection point. Figure 7 depicts the speed of travel from the source entrance to the destination. It can be shown that the arrival rate is inversely related to speed. As a result, increasing the arrival rate reduces the speed of cars, as shown in Figure 7.

7. Conclusions

Smart transportation is an advancement in the conventional transport system which improves quality of public life by providing optimized services and enhances the sustainability of urban cities. The realization of smart transportation has enormous challenges and consequences. The metropolitan city Peshawar is the capital of Khyber Pakhtunkhwa province in Pakistan, one of the most populated city of the region. The current status of public transport in Peshawar is deplorable.

The transport department faces many challenges to support this rapid growth, especially in public transit. Some routes in Peshawar are highly vulnerable to massive traffic jams, which leads to various issues for students, employees, and patients striving to reach their destination without delays. IoT-based smart transportation is the need of the day to cope with massive traffic jams. It optimally assesses the traffic density, detects congestion, recommends appropriate speed to the drivers under various circumstances, and resolves the congestion by discovering an alternate route to the destination. The proposed framework in this paper not only reduces the travel time to the destination but also reduces fuel consumption and environmental pollution. The proposed framework uses two players' games. In the future, we will consider multiple player games aiming to reflect the highly congested traffic scenario effectively.

Data Availability

The data used to support the findings of this study are available from the corresponding author upon request.

Conflicts of Interest

The authors declare that there is no conflict of interest regarding the publication of this paper.

Acknowledgments

The authors would like to acknowledge the support of Prince Sultan University for providing all the resources in the completion of this manuscript. This paper is supported by the research initiative center (RIC) of Prince Sultan University, Riyadh, Saudi Arabia (Grant No. 786).

References

[1] H. Ritchie and M. Roser, "Urbanization," *Our World in Data*, vol. 1, 2018https://ourworldindata.org/urbanization.

[2] H. A. Khattak, H. Farman, B. Jan, and I. U. Din, "Toward integrating vehicular clouds with IoT for smart city services," *IEEE Network*, vol. 33, no. 2, pp. 65–71, 2019.

[3] "Peshawar main city population," 2020, https://www.macrotrends.net/cities/22051/peshawar/population.

[4] "Peshawar buses," 2020, https://www.tnn.com.pk/kp-government-to-compensate-public-transporters-drivers-being-affected-by-brt/.

[5] "Peshawar wagons," 2020, https://www.pakwheels.com/forums/t/ford-janey-tay-road-janey/171016/20/.

[6] "Peshawar riksha," https://www.adb.org/Documents/RRPs/?id=48289-002-3/.

[7] B. Ji, X. Zhang, S. Mumtaz et al., "Survey on the Internet of vehicles: network architectures and applications," *IEEE*

Communications Standards Magazine, vol. 4, no. 1, pp. 34–41, 2020.

[8] P. Zhang, Y. Yuan, H. Liu, and Z. Gao, "Nash equilibrium seeking for graphic games with dynamic event-triggered mechanism," *IEEE Transactions on Cybernetics*, pp. 1–8, 2021.

[9] S. R. Arshad, A. Saeed, V. Akre et al., "Leveraging traffic condition using IoT for improving smart city street lights," in *2020 IEEE International Conference on Communication, Networks and Satellite (Comnetsat)*, pp. 92–96, Batam, Indonesia, 2020.

[10] Z. Khan, A. Koubaa, and H. Farman, "Smart route: Internet-of-vehicles (IoV)-based congestion detection and avoidance (IoV-based CDA) using rerouting planning," *Applied Sciences*, vol. 10, no. 13, p. 4541, 2020.

[11] S. Talari, M. Shafie-Khah, P. Siano, V. Loia, A. Tommasetti, and J. P. Catalão, "A review of smart cities based on the Internet of Things concept," *Energies*, vol. 10, no. 4, p. 421, 2017.

[12] H. Farman, B. Jan, Z. Khan, and A. Koubaa, "A smart energy-based source location privacy preservation model for Internet of Things-based vehicular ad hoc networks," *Transactions on Emerging Telecommunications Technologies*, vol. 33, no. 2, 2022.

[13] M. Munoz-Organero, R. Ruiz-Blaquez, and L. Sánchez-Fernández, "Automatic detection of traffic lights, street crossings and urban roundabouts combining outlier detection and deep learning classification techniques based on GPS traces while driving," *Computers, Environment and Urban Systems*, vol. 68, pp. 1–8, 2018.

[14] G. Jia, G. Han, A. Li, and J. Du, "SSL: smart street lamp based on fog computing for smarter cities," *IEEE Transactions on Industrial Informatics*, vol. 14, no. 11, pp. 4995–5004, 2018.

[15] J. Yang, Y. Han, Y. Wang, B. Jiang, Z. Lv, and H. Song, "Optimization of real-time traffic network assignment based on IoT data using DBN and clustering model in smart city," *Future Generation Computer Systems*, vol. 108, pp. 976–986, 2020.

[16] M. Kokilavani and A. Malathi, "Smart street lighting system using IoT," *International Journal of Advanced Research in Applied Science and Technology*, vol. 3, no. 11, pp. 08–11, 2017.

[17] L. M. Bates, O. Hankivsky, and K. W. Springer, "Gender and health inequities: a comment on the final report of the WHO commission on the social determinants of health," *Social Science & Medicine*, vol. 69, no. 7, pp. 1002–1004, 2009.

[18] S. M. Asad, A. Tahir, R. N. Bin Rais et al., "Edge intelligence in private mobile networks for next-generation railway systems," *Frontiers in Communications and Networks*, vol. 2, 2021.

[19] A. Tahir, W. Taylor, A. Taha et al., "IoT based fall detection system for elderly healthcare," in *Internet of Things for Human-Centered Design*, pp. 209–232, Springer, 2022.

[20] A. Jaleel, T. Mahmood, A. Tahir, S. Aslam, and U. U. Fayyaz, "Autonomic interoperability manager: a service-oriented architecture for full- stack interoperability in the Internet-of-Things," *ICT Express*, 2021.

[21] A. Al-Dweik, R. Muresan, M. Mayhew, and M. Lieberman, "IoT-based multifunctional scalable real-time enhanced road side unit for intelligent transportation systems," in *2017 IEEE 30th Canadian Conference on Electrical and Computer Engineering (CCECE)*, pp. 1–6, Windsor, ON, Canada, 2017.

[22] R. Shastry, B. V. R. Murthy, C. K. K. Reddy, and P. R. Anisha, "Automated lighting smart parking using Internet of Things," in *International Conference on Intelligent Computing, Information and Control Systems*, pp. 645–652, Secunderabad, India, 2020.

[23] A. K. Tripathy, A. K. Mishra, and T. K. Das, "Smart lighting: intelligent and weather adaptive lighting in street lights using IoT," in *2017 International Conference on Intelligent Computing, Instrumentation and Control Technologies (ICICICT)*, pp. 1236–1239, Kerala, India, 2017.

[24] A. Daubaras and M. Zilys, "Vehicle detection based on magneto-resistive magnetic field sensor," *Elek- tronika ir Elektrotechnika*, vol. 118, no. 2, pp. 27–32, 2012.

[25] X. Wu, W. Li, D. Hong, J. Tian, and R. Tao, "Vehicle detection of multi-source remote sensing data using active fine-tuning network," *ISPRS Journal of Photogrammetry and Remote Sensing*, vol. 167, pp. 39–53, 2020.

[26] A. H. El Fawal, A. Mansour, and M. Najem, "V2V influence on M2M and H2H traffics during emergency scenarios: adaptive eNode-B for V2V communications," in *Global Advancements in Connected and Intelligent Mobility: Emerging Research and Opportunities*, pp. 93–134, IGI Global, 2020.

[27] F. Abbas, P. Fan, and Z. Khan, "A novel low-latency V2V resource allocation scheme based on cellular V2X communications," *IEEE Transactions on Intelligent Transportation Systems*, vol. 20, no. 6, pp. 2185–2197, 2019.

[28] S. A. Shah, M. Shahzad, N. Ahmad et al., "Performance evaluation of bus rapid transit system: a comparative analysis of alternative approaches for energy efficient eco-friendly public transport system," *Energies*, vol. 13, no. 6, p. 1377, 2020.

[29] "Peshawar poverity," 2020, https://tribune.com.pk/story/1144351/deprived-capital-peshawar-classif\\ied-one-poorest-provincial-capitalst/.

[30] A. M. Ngoc, K. V. Hung, and V. A. Tuan, "Towards the development of quality standards for public transport service in developing countries: analysis of public transport users' behavior," *Transportation Research Procedia*, vol. 25, pp. 4560–4579, 2017.

[31] "Air pollution," 2020, https://scroll.in/latest/915440/air-pollution-gurugram-worst-in-the-world-\\in-2018-six-other-indian-cities-in-top-10-shows-study/.

[32] "Transport types and expenses," 2020, https://www.tripoto.com/peshawar/trips/peshawar-more-than-the-city-of-flowers-5a59d3aa013bb/.

[33] "Peshawar: city of flowers," 2020, https://www.tripoto.com/peshawar/trips/peshawar-more-than-the-city-of-flowers-5a59d3aa013bb.

[34] J. Sherly and D. Somasundareswari, "Internet of Things based smart transportation systems," *International Research Journal of Engineering and Technology*, vol. 2, no. 7, pp. 1207–1210, 2015.

[35] D. Abada, A. Massaq, A. Boulouz, and M. B. Salah, "An adaptive vehicular relay and gateway selection scheme for connecting VANETs to Internet via 4G LTE cellular network," in *Emerging Technologies for Connected Internet of Vehicles and Intelligent Transportation System Networks*, pp. 149–163, Springer, 2020.

[36] M. Naderi, F. Zargari, and M. Ghanbari, "Adaptive beacon broadcast in opportunistic routing for VANETs," *Ad Hoc Networks*, vol. 86, pp. 119–130, 2019.

[37] P. Mooney and M. Minghini, *A review of OpenStreetMap data*, 2017.

[38] A. F. Acosta, J. E. Espinosa, and J. Espinosa, "Application of the scrum software methodology for extending simulation of urban mobility (SUMO) tools," in *Simulating Urban Traffic Scenarios*, pp. 3–15, Springer, 2019.

[39] S. A. Afolalu, O. M. Ikumapayi, A. Abdulkareem, M. E. Emetere, and O. Adejumo, "A short review on queuing theory as a deterministic tool in sustainable telecommunication system," *Materials Today: Proceedings*, vol. 44, pp. 2884–2888, 2021.

Hindawi
Wireless Communications and Mobile Computing
Volume 2022, Article ID 6539532, 13 pages
https://doi.org/10.1155/2022/6539532

Research Article

Dynamic Naming Scheme and Lookup Method Based on Trie for Vehicular Named Data Network

M. Wasim Abbas Ashraf,[1] **Chuanhe Huang**,[1] **Shehzad Khalid**,[2] **Amir Saeed Rana**,[3] **Mudassar Ahmad**,[4] **and Umar Raza**[5]

[1]*School of Computer Science, Wuhan University, Wuhan 430 072, China*
[2]*Department of Computer Engineering, Bahria University, Islamabad, Pakistan*
[3]*Department of EFS, University of Agriculture, Faisalabad, Pakistan*
[4]*Department of Computer Science, National Textile University, Faisalabad, Pakistan*
[5]*Department of Engineering, Manchester Metropolitan University, Manchester, UK*

Correspondence should be addressed to Chuanhe Huang; huangch@whu.edu.cn

Received 25 January 2022; Accepted 4 May 2022; Published 19 May 2022

Academic Editor: Farhan Ullah

Content naming and lookup are decisive functions of the future architecture named data network (NDN). The core concept of NDN is the content distribution between consumers and content providers. The NDN supports advance vehicular networks that is famous with vehicular-named data network (VNDN) with different naming schemes such as hybrid, flat, attribute-based, and hierarchical names. These schemes are used in a static way for vehicular network, in summary, the hybrid, flat, and attribute-based makes a complex structure, and on the other hand, hierarchical names long in length and name lookup performance are a bottleneck in NDN, which can directly affect the network performance. Therefore, we introduce a dynamic naming scheme and lookup method (DNSL) for VNDN to mitigate these issues. We argue that the dynamic naming scheme is a better approach to VNDN, while the static name is a cost-effective, hefty, integrated fashion, and improper for the vehicular network. This study focuses on (1) a dynamic naming scheme using dynamic-tag and (2) a lookup method based on node partition of trie; the trie approach is very famed in data structure and extensively used for the lookup content, insertion, and deletion processes. Our experimental evaluation shows that the DNSL scheme is highly efficient, scalable, and provably correct for VNDN.

1. Introduction

Coincidentally, NDN is a role model of the information-centric network (ICN) that allows users to request data without knowing the host node. The core focus of NDN is data, identified by names instead of nodes or devices in the networks. In the NDN architecture, all devices keep up information with the NDN table's structure, which commonly uses the content table, pending information, and forward information tables. Typically, VNDN covers these mechanisms like NDN vehicle-to-infrastructure, vehicle-to-vehicle, vehicle-to-everything, and infrastructure-to-vehicle [1].

Inspired by content, the named data networking (NDN) [2] is a new data communication approach that will replace the current IP infrastructure, which can help achieve performance compared to IP-based vehicular networks. Now, much-emerging applications and content distribution networks rely on named-based services for content forwarding and fetching by names. Therefore, a name lookup, insertion, and updates are the core function of the name-based vehicular networks. The vehicular network (VN) is the extended version of mobile ad hoc networks to provide moving vehicles' communication services. Moreover, in [3], VN is very efficient for the large-scale distribution system and many road safety systems. The current trend of VN's communication is entirely based on IP addresses, which may have some issues due to IP limitation. The VN environment requires a vital communication link without session breakage. Hence,

in this regard, VNDN provides a reliable and efficient communication architecture for sharing any information between moving vehicles in the traffic scenario.

The namespace is a crucial component of NDN. The NDN adopts a hierarchical naming structure that is human readable. It seems like a uniform resource locator URL with separate "/." The benefits of the hierarchical structure are the compatibility with the system and minimize the routing aggregation, which helps to improve the search for the routing table. However, the drawback of this scheme has a long length. The hierarchical scheme is not suitable for that network, which already has a long component, and it becomes tough to remember and consumes more memory. On the other hand, a flat naming scheme is introduced and uses in future architecture of information-centric networks (ICN) like MobilityFirst, NetInf, and DONA. The flat naming scheme generates by different encryption-based [4] methods. The flat scheme is globally unique but reduces the aggregation process. Using a flat scheme increases the size of the routing table and may be challenging to read, which requires an additional cost to read it. The suitable naming scheme is still a critical issue for all NDN-based networks and unique in VN.

The vehicular named data network (VNDN) has newly received significant attention in the research community. A name-based lookup method is essential. However, several crucial issues and challenges related to name-based lookup are yet to be addressed to successfully realize a content-oriented network model for the VNDN and the future's internet. The name prefix is considered longer than the IP prefix [5]. The lookup time for the name's unbounded length may take more time and increase the forwarding table's size compared to the IP prefix in a vehicular network. A name-based lookup scheme faces significant problems. As per the NDN rule, the packet's reputation depends on the application naming method for every request identified by a unique name.

Lookup is a core function of NDN to scan hundreds and millions of characters to find the long prefix matching (LPM) in the forwarded information base (FIB). The name length is correlated to the lookup time, which has still a big challenge to achieve the lookup speed [6]. Many naming schemes (flat, hierarchical, and hybrid) are presented to improve the lookup time, but FIB forwarding tables could not give desired results, and the static naming scheme not suitable for VNDN. Therefore, the existing baseline lookup and naming methods based on trie are less efficient as per the above discussion in achieving unique prefix naming and lookup method for the dynamic scenario in VNDN. Furthermore, the trie can play a crucial role in forwarding tables [7] to get the desired content. This data structure supports both the longest prefix match (LPM) and the exact match (EM). Trie is also beneficial to update and removal function, which is the reverse of the insertion [8]. The challenges of existing studies and the benefits of trie motivated us to design a unique naming and fast lookup method to improve the performance of the whole network in VNDN.

In this paper, we address the content naming scheme and name lookup issues for VNDN. We propose a dynamic naming scheme and lookup method, efficient for the VNDN environment, and offers a content lookup guarantee. The dynamic naming scheme uses shared features of hierarchical and hashed naming methods. At the same time, the lookup method is based on node partition of Patricia trie (PT). Moreover, our proposed method does not require any additional computational expenses to manage the trie structure. Our proposed work is specially designed to meet the following objectives:

(i) We design the novel trie based on node partition using compact trie

(ii) The dynamic tag is introduced in this study used for VNDN, which is unique to identify the producer node and the content itself

(iii) We improved the content lookup process and memory usage performance via node partitions that merge the same prefix bytes on a single node. Moreover, which helps to improve the overall network performance

(iv) We also provide a quantitative comparison of our DNSL scheme with the existing approaches

The existing naming approaches and lookup methods based on the trie for vehicular are discussed in Section 2. Section 3 presents the system model and interest process for VNDN. Section 4 introduces the proposed scheme and the evaluation of proposed work with other states of the art. Finally, we conclude our work in Section 5.

2. Related Work

2.1. Naming Schemes. We first address the proposed naming schemes presented in [9], a proposed naming system for vehicular network traffic details, as this paper, focuses on the naming scheme and lookup process. The following is the naming scheme: "/traffic/geolocation/timestamp/datatype/nonce." The author uses the traffic variable as the identifier of the application, current location as road-ID and segment value, timestamp as the time date, data type as the type of data, and nonce as the nonce to prevent interest duplication. To simplify NDN names, the author invented the hash encoding scheme [10] for vehicular networks. The procedure is divided into two parts: (a) compress the name and (b) lookup procedure used the Wu-Manber method, which is expensive due to its complexity.

Communication in ICN uses content information instead of the geolocation and address of the interest source [11]. Inspired by the content's characteristics, the smart house is introduced in [12], which gives an idea about a smart house idea using a hierarchical naming structure based on the NDN architecture. As per a naming scheme structure, a component has specified the activity action and sensing. The subcomponent identifies which exact action will be executed to turn off the light, get its temperature, and get the mac address of the terminal devices inside the indicates by location components. The names in this system are just too long.

The NINQ (name-integrated query) systems introduced a hybrid scheme [13] for the NDN architecture. This scheme is divided into three parts: (1) hierarchical namespace, (2) flat portion based on hashing, and (3) query, which used command and interest as a satisfaction rate and typical latency, use of energy, and volume of data in a network; this scheme seems promising; the namespace and request procedure may be too much longer.

A similar scheme is suggested in [14] in which hierarchical names for reliable models are used to ensure autonomous vehicles' validity in producing data. The scheme follow the format as/applicationprefix/typeof data/datalocation/namemarker/vehiclename/timestamp. The prefix of application is a component that specifies the application name, which generates a data type element that signifies the produced data type and the current position of the component that indicates the content's location. For keeping the historical detail of the vehicle movement, the label is used to identify the starting and ending points. In this strategy, the location may have numerous name components that make redundancy and trouble in access.

The global name scheme is proposed using services-based architecture (SEVen) [15]. The global name is the keystone of this architecture [16]. This naming scheme consists of uppermost groups that indicate three main classes: (1) services for safety, (2) transfer information, and (3) infotainment. Prioritization of content is based on the class level. Applications have identified the type and group of the service into class levels. In conclusion, the name identifier and metadata restrict discrepancies that result in demanding data from the various neighboring producers.

To enhance the names lookup, the author designed the adaptive prefix Bloom filter (NLAPB) [17] and uses a Bloom filter to match the first part of a naming scheme, and a simple trie processes the other part of the scheme.

The similar work presented with a hybrid scheme [18] for vehicular networks (VN's) in ICN takes advantage of flat attributes based on hash method and hierarchical naming structure. The naming format is distributed with three chunks: (1) firstly, the name is used as an identifier of VN; (2) the next part, which has the detail of consumers based on hierarchy scheme, this portion supports simplifying the routing information and name aggregation; and (3) the third or last portion is a flat portion based on the Base64 format to contain owner signature or item information using the hash method. The flat portion promises content integrity. This scheme is theoretical and needs a detailed feasibility analysis. Furthermore, the proposed scheme has some drawbacks, containing long variables and the absence of a name length restriction, resulting in a bulky prefix table and a consumer takes much time to search the contents. Meanwhile, in [19], we improve this study using a managing scheme based on compact trie (CT) for VN. Moreover, the authors examined VN imitation outcomes and determined that the proposed scheme improves space consumption and lookup. The hybrid naming scheme has many benefits rather than hierarchical or flat. However, a critical combination may make a more complex scheme and increases lookup time because of rehashing. Thus, a lithe and suitable naming scheme is required yet for vehicular networks based on NDN.

2.2. Name Lookup Method. In PlusBitmap Caching (PBC) [20], the first lookup request/com/yahoolindexll, since the cache is already empty, the corresponding prefix is admitted to the cache after the main table examine. If no false positives occur when checking the bitmap, the second lookup request/com/yahoolnews returns a cache hit. PBC accepts the third lookup request/com/alibabalindex with a leaf flag since it misses the cache but fits a leaf prefix in the main table. If there are no false positives when checking the bitmap, the fourth lookup request/com/yahoolindexll also hits the cached entry (/come/yahool∗, Rl). As per our knowledge, PCB achieves the cache performance and increases the trie height due to bitmap structure.

The NCIS [21] method adopts dual DHT rings to classify the contents elements. The first portion of this method is based on names, while the other ring is based on contents. Moreover, a pair of keys and values are used for a table. The key represents a content's name, and a value is considered a pointer to the contents. The pointer acts like the lookup service to the entry point, takes NDN-based names as input, and then pushes it back to the contents. It might be possible that if the NDN name fails to be routed, then the pointer will carry the prefix information for routing. A name-based node serves the push-it-back contents and handles the keys/value pair. The ring, based on contents, provides the functions in a similar way to conventional DHTs. The distinction is that the name/other names pair is often pushed back to the name-based ring by the content-based one. This technique joins names with the content of hashes. NCIS is still in its infancy phase and needs to implement on the NDN structure for content lookup and sharing.

The authors suggested BF-PDT [22] name search strategy, which integrates the Bloom filter, popularity graph, and the tire properties. The flowering filter in BF-PDT will help to find out the variables in the application. Meanwhile, the popularity graph is dependent on the content-centric network characteristics and trie properties to improve the trie structure. They also conducted tests for BF-PDT, demonstrating that BF-PDT improves the searching speed at reduced memory cost.

To provide NDN-based location data retrieval, the author suggested a hierarchical name data structure in [23]. The safety info is broadcast in vehicular networks via the publisher and subscriber; the author effort in [24] uses NDN and the hierarchical naming scheme.

To improve efficiency, the authors created a list of localized hops. Subsequently, a piece of information is likely to share with a prefix with earlier data, and the skip list (SL) checks start nearly the node of that prefix that was earlier node. This proposed method eliminates the significant node redundancy for lookup time [25]. As a result, it significantly decreases the searching time. The assessment results indicate that this design achieves a performance compared to the initial design, but the proposed design is complex to implement in reality.

The lookup speed can be achieved by port information in the trie. The study introduced P-Trie [26] based on is based on the trie. Each node has three portions: (i) acceptance (store last bit information of prefix), (ii) advanced node (the node that holds the prefixes of its leaf node that have a similar outgoing port but no one can further be

divided like a child node, and (iii) the intermediary node (holding others nodes). When an identical node arrives at the advanced node, the port's component is given back instantly. Meanwhile, if an identical node occurs on the intermediary node or acceptance node, the process will continue, and the succeeding bits will be compared. On the other hand, if a mismatching happens anywhere, the port push it back to all elements, and the lookup process starts. The proposed trie increase computational cost and not good for VN.

Another trie-based method is proposed to resolve the longest prefix matching (LPM) issues in NDN [27]. The leaf node is merged with their rooted node to achieve memory and processing time performance. The author impresses by the following reasons: (i) binary trie (it can be easy to compress), (ii) use bit string (can be processed quickly in any naming system), and (iii) namespace (name is used for direct lookup and forward it without parsing). The author has used the longest prefix classification (LPC) based on dual binary trie instead of longest prefix matching (LPM). It works like LPM but stores only first-level components rather than whole components' names. A secured method is introduced to extract the hybrid feature in [28], and the deep learning model is designed for different application storages in IoT devices [29].

The complex name strategy takes more processing time in the FIB table [30, 31] than IP-based networks because of the unbounded length of names. Name processing is a core issue in the forwarding engine and needs to reduce the NDN structure's table size. The global services demand a faster lookup method in the forwarding table of NDN.

3. Proposed DNSL For VNDN

This section discusses the system model and presents the proposed naming scheme and name lookup method using dynamic tag. We aim to improve the overall performance of the lookup process, insertion, and deletion entries in the FIB table and reduce the memory using the DNSL scheme.

3.1. System Model. We consider a vehicular network by a graph $G = \{N, C\}$ set of vehicle nodes N, and C is the connections between the two $(n_a, n_b) \in N$ vehicles, where (n_a, n_b) indicates the number of vehicles the moving in a different location. Each node exchanges the packets (interest and data), and each packet carries the content information. A desired content can get from the producer node D_n or content server C_s.

3.1.1. Packet Process. When a request arrives at N, it first checks the local cache; if matched then forward to the requested node. If the content is not matched in local cache, then it will check in PIT; if content is found then add the interface information and discard it. Otherwise, the content can be taken from C_s via FIB.

3.2. Proposed Naming Scheme. Dynamic naming offers a flexible approach for VNDN to maintain communication and record of moving vehicles based on ICN. Our proposed DNSL scheme reduces the memory cost and achieves the desired lookup performance in the routing table that is shown in Figure 1. Firstly, we introduce the basic naming format for a vehicular network and then presented the proposed DNSL scheme's structure and names lookup method for VNDN.

3.2.1. Naming Scheme Format. The naming scheme is an essential part, which helps to implementation in the NDN. This section gives an overview of the NDN naming scheme based on a hierarchical structure. Each application has its proprietary namespaces, and then, the publisher generates the desired data using a namespace giving to prearranged policies. A general naming format of NDN is shown in Figure 2, which is divided into three parts: (a) the first consist of the vehicle information; (b) the second part keeps the content information, which is stored in the content table to serve the consumer request; and (c) used for authentication purpose.

Both the consumer and publisher first register their namespaces to join the NDN network. Each publisher is declaring a list of contents, which they can provide to consumers after registration. The consumers are generating request with their namespace, such as "V117/Wasi/video/aa.mp4/(L1, RSU1)/...," where V117 indicates the vehicle identity, "Wasi" represents the user information, video belongs to a type of content, and aa.mp4 shows the subtype of content, and (L1, RSU1) signifies the current status with location and roadside unit identity of the consumer and publisher. The novelty of the DNSL scheme provides many advantages for VNDN based on ICN.

(1) Static part: in VNDN, the static prefix remains constant once the consumer generates it. The static part must be unique in the VNDN networks. Content naming is played the role of uniqueness in VNDN

(2) Dynamic tag: we proposed a dynamic tag, which is change by the movement of vehicles and gives the current status of vehicles

(3) Dynamic tag helps aggregation, reduces the routing table entries, and improves lookup speed compared to CT scheme [19] and others (seen in Section 4). This portion of our proposed scheme also allows the facility to keep track of vehicle movements with the NDN architecture. Figure 1 shows the structure of the FIB table using a dynamic naming scheme

Figure 1 first stores unique static prefix using the NDN storage structure and a second portion consist of dynamic tag and captures the current position of moving vehicle, and the roadside unit (RSU) acts as a next hop, when a new request arrives, by default is stored in the stack. Then, it performs more queries operations; the most top record is returned by default from the stack of FIB. When RSU collects the payback data, the removal process begins after getting the data from the consumer. Our proposed works reduce the routing table size in the same interest routing; the record lookup and storage based on PT are discussed in Section 3. Our proposed DNSL scheme uses a hierarchical namespace and converts it into twofold chunks of the static and dynamic parts shown in Figure 1.

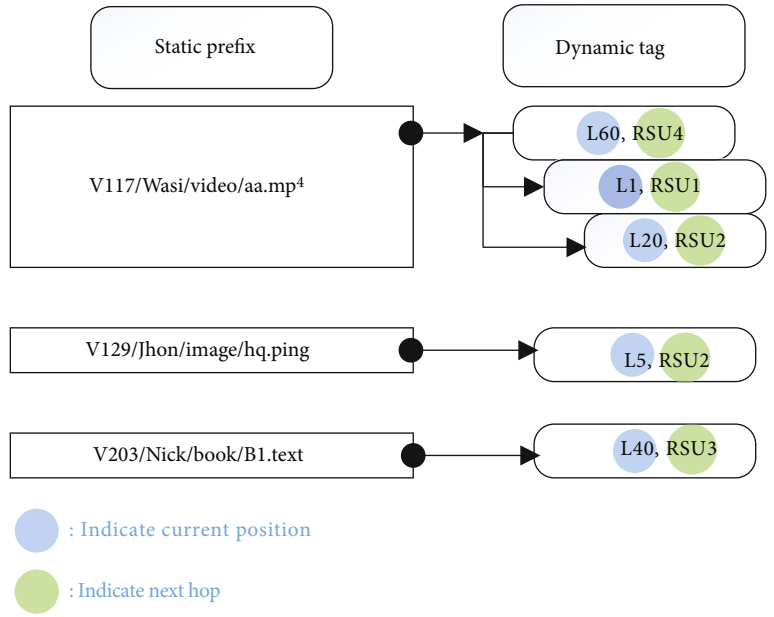

Figure 1: Dynamic naming process in FIB.

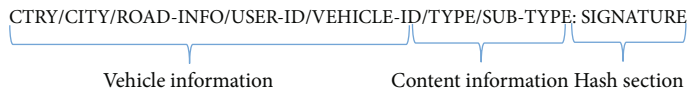

Figure 2: NDN naming format.

Figure 3 shows the comparison of the static naming scheme and dynamic naming scheme in which our proposed dynamic tag is associated with the dynamic scheme. Moreover, 1, 2, and 3 indicate that a single dynamic name can be used for multiple dynamic tag, improving lookup efficiency and reducing memory usage rather than a static naming scheme. Furthermore, Figure 3(b) shows the dynamic and static naming schemes using the same contents in the FIB table, and we found redundancy in the static scheme, whereas the dynamic restricts the redundancy using dynamic tag. Moreover, in Figure 3(a), our proposed scenario illustrates with dynamic naming for VNDN, in which each vehicle first registered and generated its routing information to its nearby RSU. Figure 3(b) shows the process of both dynamic and static naming schemes using the same contents in the FIB table, and we found redundancy in the static scheme, whereas dynamic restricts the redundancy using dynamic-tag. Moreover, the performance is discussed in Section 4.

3.3. Name Lookup for VNDN. The name searching process is the primary function of the forwarding engine in NDN. The proposed scheme keeps elements with familiar characters or symbols in the content set Z and can be signified by a recursive function.

$$\mathrm{DNSL}(W) = \left\langle r, \mathrm{DNSL}\left(\xi_{[p1]}W\right), \mathrm{DNSL}\left(\xi_{[p2]}W\right), .., \mathrm{DNSL}\left(\xi_{\left[a_{p_j}\right]}W\right)\right\rangle, \tag{1}$$

where r represents the root trie, ξ_{p_i} confines the prefix starting set with p_i number of prefix characters at the internal leaf node, and j represents the number of leaf nodes in $DS(W)$ and $j \leq \max_{1\leq i\leq |W|} W[i]$. However, the existing approaches simple trie has overhead in height and width, NLAPB requires many pointers, consumes processing time and more memory to fetch the desired result, and CT has overhead in width that affects lookup time and takes more memory. Therefore, we proposed DNSL, in which the lookup method is based on node partition using PT; which keeps all records in one node with the same characteristics, symbol, and figures. The prefix matching for the given string or name t with the length of y; in our proposed scheme, DNSL $P\mathrm{match}_{\mathrm{DNSL3pt}}(ty)$ required a small number of pointers to fetch the node and branching the nodes, such as

$$P\mathrm{match}_{\mathrm{DNSL3pt}}(ty) = \sum_{m=1}^{y} \begin{cases} \mathrm{match}(t[m]), \\ \delta. \end{cases} \tag{2}$$

Suppose the symbols and characters from the ASCII code are represented with C, where $t[m] \in C$. Besides, $\leq$ use as a pointer to fetch the node's record. As per Equation (2), the lookup processing time is reduced rather than simple trie, NLAPB, and CT. Moreover, CT required rehashing to mitigate the collision concerning lookup and insertion.

We design the trie based on node partition. The partition policy has two characteristics: first, we keep the record of the

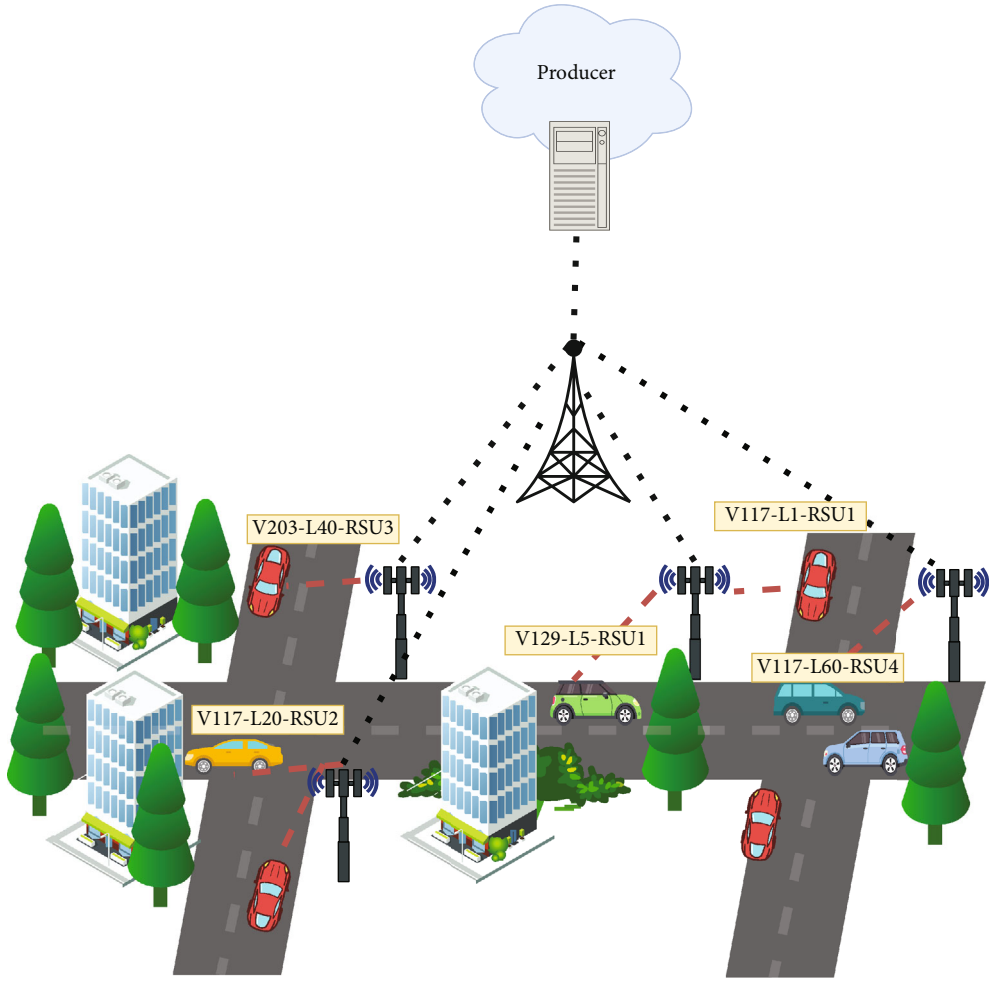

(a) VNDN scenario

Static Naming Scheme

Content	Next-Hop
V117/Wasi/video/aa.mp4/L60/	RSU4
V129/Jhon/image/hq.png/L5/	RSU5
V117/Wasi/video/aa.mp4/L1/	RSU1
V203/Nick/book/b1.txt/L40/	RSU3
V117/Wasi/video/aa.mp4/L20/	RSU2

Dynamic Naming Scheme

Content		Dynamic-Tag
V117/Wasi/video/aa.mp4/	1	L60,RSU4
	2	L1,RSU1
	3	L20,RSU2
V129/Jhon/image/hq.png/		L5,RSU1
V203/Nick/book/b1.txt/		L40,RSU3

(b) Naming scheme

Figure 3: VNDN scenario using dynamic tag.

previous node; second, a new node is created instead of the previous. A new node is further split into classes: (a) remaining bytes of the previous node and (b) the rest of the input name. Furthermore, we discussed a node partition model in Section 3.4, and Figure 4(a) shows the node partition when we insert two prefixes, "/V117/wasim/Movie/Mission1" and "/V117/wasim/Movie/Mission2."

3.4. Node Partition Model

Definition 1. (node partition model): gven table T and split node position N_p, each requested interest is divided into two portions at position N_p, namely, P_n and C_n $(P_n + C_n)$. The name lookup function for desired interest is determined by

$$\text{Interest} = \text{LPM}(X_1 \cup X_2) = \begin{cases} \text{LPM}(X_1), \\ y \cup \text{LPM}(X_2), \end{cases} \tag{3}$$

where $P_n \in X_1$, $C_n \in X_2$, and y = remaining bytes.

$$X_2 = \{y | \in T \text{ and } y \geq C_n\} \tag{4}$$

As per giving Definition 1, the node partition is based on content bytes. If the contents partially match the given

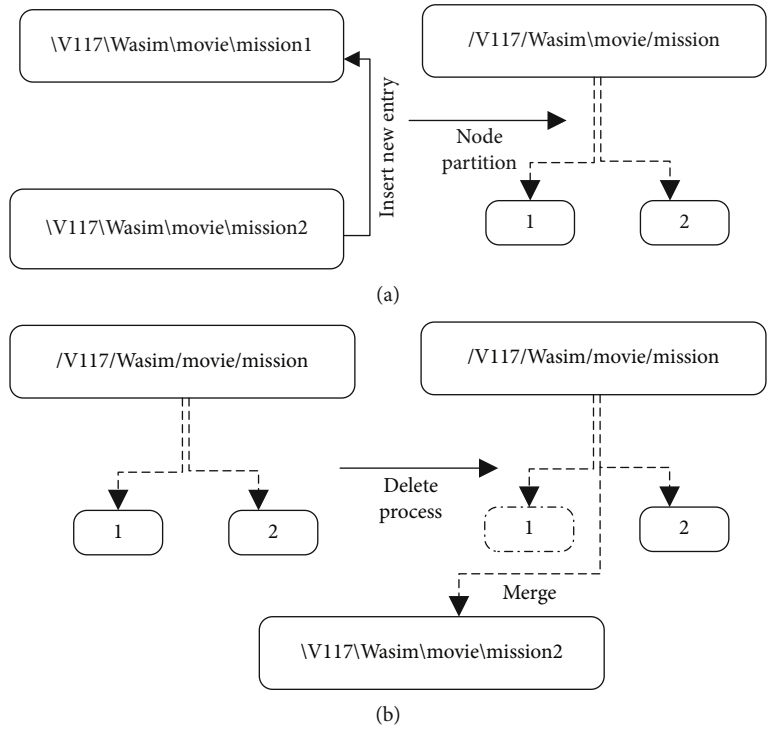

Figure 4: Insertion and deletion process with node partition.

Input: Interest [Vehicle_information, Content_information]
Output: Get desired data
1 Node=R_n;
2.**if** $C_n[b_{id}]$!= "/" **then**
3. Return 0; //contents must start with "/"
4.**while**($b_{id} < C_{len}$)**do**
5. **if** !(C_n)= H_t**then**
6. return 0; //not matched with hash table
7. Node = N_{node}; //insert new record
8. **if** Exact match **then**
9. V_n [V_{id}] = node;
10. V_{id} + +;
11 **while**($N - B_{id}$!$Node_{len}$&&B_{id}!C_{len})**do**
12 **if** (node[N_{id}]= $C_n[B_{id}]$**then**
13 B_{id} + +;
14 N-B_{id} + +;
15 continue;
16 **if**(!$N - B_{id}$)**then**
17 return 0; //first byte not matched
18 break;
19 **if** ($b_{id} = C_{len}$) **then**
20 **if**(($N - B_{id} = Node_{len}$)**then**
21 return node; //content found
22 **else**
23 return 0; //lookup failed due to partially match
24 **if**($N - B_{id} = Node_{len}$)**then**
25 $N - B_{id}$=0; continue;
26 **else**
27 return 0; //invoke Algorithm-2(partition)

Algorithm 1: Lookup and interest contents.

Input: Enter prefix
Output: Set the node with parent and child relationship
1 Initialize hash table;
2 **if**P_n matched & C_n not matched then
3 Keep record P_n; //at position N_p
4 Create N_{node} // with remaining bytes;
5 ontinue: until node is not set;
6 else
7 Node partition failed;

Algorithm 2: Node partition.

interest, then the splitter node such as C_n will keep a record of its corresponding node P_n and then creates a new node.

The deletion process is the inverse of insertion. When the content is matched, we delete the leaf entry node, and the content will merge when the root entity is left with a single node or child content. We consider the invalid removal function if the content mismatching. The invalid has occurred because the lookup function fails to match the contents inside the trie. Figure 4(b) illustrates the reverse of insertion with remove â€œ/V117/wasim/Movie/Mission2."

3.5. Algorithm for Interest and Data Processing. Assume all contents starting with slash "/." When a request arrives for content by the consumer, it invokes the following algorithms. Algorithms 1 and 2 are a core function of our DNSL scheme for VNDN. When a request arrives in the consumer's form of interest, it invokes Algorithm 1. Algorithm 1 first matched the consumer's request using lookup function.). If the content is a partial match for insertion, it invokes the partitioning Algorithm 2, in which it keeps the P_n previous information and merge the prefix with bytes and creates the new node for mismatched bytes. The process will continue until set the prefix bytes, and the process is shown in Figure 4. Moreover, if the requested content is not matched, and it looks in the leaf node, and for insertion entry, and then nothing changes in content tables if an exact match occurred. This paper designed an Algorithm 1 for lookup and insertion contents requested by the consumer to get the desired information. Lookup algorithm can be implemented in NDN routing architecture without changing the core design of the NDN for the vehicular networks. Our proposed algorithms are suitable as compared to existing approaches regarding fast lookup, quick insert contents, and less time to remove contents from the content table. Algorithm 3 is designed for content deletion process, which is the reverse of the insertion Algorithm 1 and the detail process shown in Figure 4(b). Table 1 describes some important notations, which used in this work.

4. Performance Evaluation

This section has conducted an immense analysis to evaluate the proposed dynamic naming scheme's performance and the lookup method in the FIB table.

Input: Desired interest for delete
Output: Delete interest from content table
1 **if**!$(C_n) = H_t$ then
2 return 0; // not matched with hash table
3 Nothing change;
4 **if** Exact match **then**
5 $V_n[v_{id}]$ = Node;
6 V_{id}− −Node Merge;
7 **else**
8 return 0; failed to remove contents

Algorithm 3: Remove content.

Table 1: Table of notations.

Notation	Description
C_{n}	Content name
R_{n}	Root node
V_{n}	Visited node
V_{id}	Visited node index
B_{id}	Name of index
$N - B_{\text{id}}$	Current node index
C_{len}	Content length
Node_{len}	Working node length
P_{n}	Parent node
C_{n}	Child node
V_{n}	Visited node

4.1. Simulation Parameters and Metrics. Our proposed work is aimed at achieving the performance of prefix lookup, insertion, and deletion times in milliseconds (ms) and reduce memory consumption. Besides, we choose NLAPBT [17], simple tire [18], and CT [19] as comparison. The proposed trie is designed using C++ language, proposed naming scheme is implemented on Figure 3(a) using NDN simulator (NDNsim-2.7) [32], and performance measure in a virtual machine on PC, and with Linux Ubuntu 20.04.1 (64-bit) dual processor of inter-core i7-4600U CPU 2.7 GHZ and RAM 8 GB. Moreover, the empirical distribution function shows the distribution process time in milliseconds (ms) of

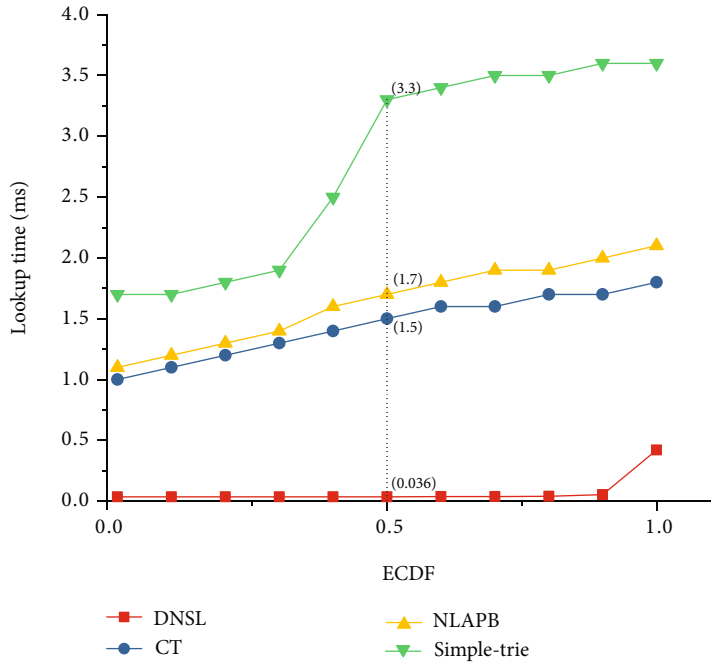

Figure 5: Lookup time per content from content table.

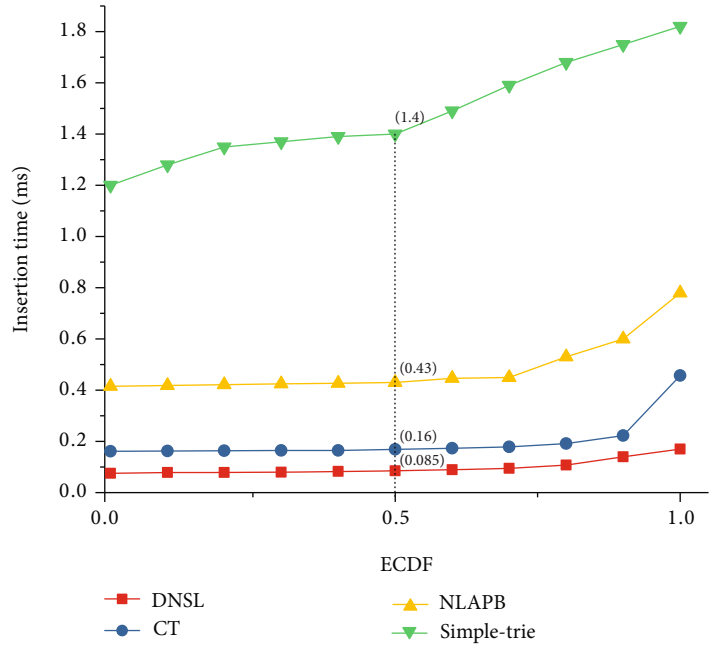

Figure 6: Insertion-Time to add contents in content table.

each prefix lookup, insert, and delete operation. The URL dataset is collected from Shallalist [33], Alexa [34], DGA [35], and DMOZ [36]. The range of prefix names are 10^10 = 10,000 to 50,000,000 with 16 characters to 250 characters. The program has run 1000 times to compute the result with the 95% confidence interval.

4.2. Content Lookup Time. The lookup function is the primary step of insert content in the table and removes the content from the table. We randomly choose 100 contents for the lookup operation that has shown in Figure 5. The size of the content table is 1 M to analyze the lookup performance. Average lookup processing time 0.036(ms), which is less than CT, NLAPB, and simple trie that is 1.5 (ms), 1.7 (ms), and 3.3 (ms), respectively. The DNSL scheme achieves the lookup performance 97.6% CT, 97.8% NLAPB, and 98.90% from simple trie.

4.3. Content Add Time. In Figure 6, we show the contents insertion time for 100 contents inserted in the content table

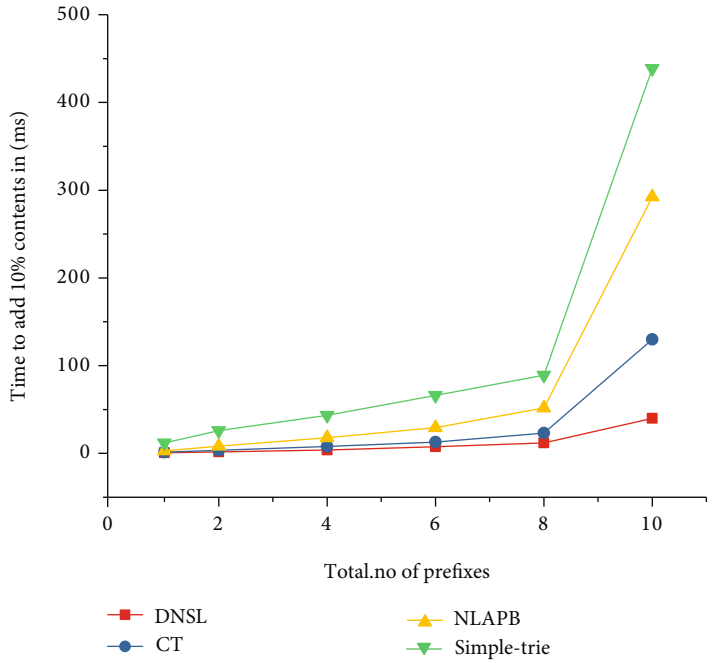

Figure 7: Processing time to add 10% of total contents.

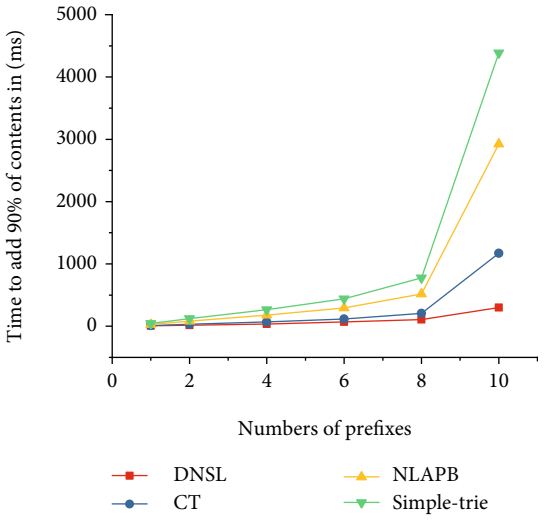

Figure 8: Processing time to add 90% of total contents.

for a total of 1 million. We noted that our proposed DNSL scheme takes less time with 0.085 ms as with CT takes 0.16 ms, and NLAPB takes 0.43 ms, and the simple trie takes 1.4 ms. Figure 6 indicates that the proposed scheme DNSL achieves insertion performance 47% from CT, and 80% from NLAPB, and 94% from simple trie.

4.4. Processing Time to Add 10% and 90% Contents. The overall processing time is shown in Figure 7 for the total prefixes 10^n where n = {2, 4, 6, 8, 10} and 2 million contents for Figure 8 in the tables. The 10% contents are insert of the total contents. Similarly, Figure 8 shows the whole time to insert 90% contents of the total contents. The results show that CT, NLAPB, and simple trie are linearly high when the numbers of contents increase compared to the DNSL scheme. The reason is behind that existing approaches have complex methods to add the content in the content table.

4.5. Content Delete Time. Figure 9 shows the average deletion time of 100 contents from the content table. The result clarifies that the DNSL scheme is efficient for deletion function. As per graph figures, CT consumes 1.8 ms, NLAPB 2.3 ms, and simple trie takes 3.3, respectively, while DNSL takes 0.73 ms. DNSL achieve performance 54.4%, 76.8%, and 77.8% than CT, NLAPB, and simple, respectively.

4.6. Memory Performance. The DNSL scheme has a unique structure and efficient lookup method for VNDN. According to our proposed scheme, the routing information with the same prefix or common contents store in a FIB stack only once time and a dynamic tag is used for further routing rather than storing complete content information. This naming scheme helps to reduce the FIB table size and restrict the redundant information. Let suppose, static name occupies the memory using the prefix static length *Sl*, dynamic tag *Dl*, and *Hl* is the next-hop length. Thus the length of each record using a static scheme in the table for M_s:

$$M_s = \sum_{i=1}^{n} S\ell_i + \sum_{j=1}^{j} D\ell_j + \sum_{k=1}^{k} H\ell_k, \tag{5}$$

and the length of each record in DNSL occupies the memory with M_d is

$$M_d = \sum_{i=1}^{1} S\ell_i + \sum_{j=1}^{j} D\ell_j + \sum_{k=1}^{k} H\ell_k. \tag{6}$$

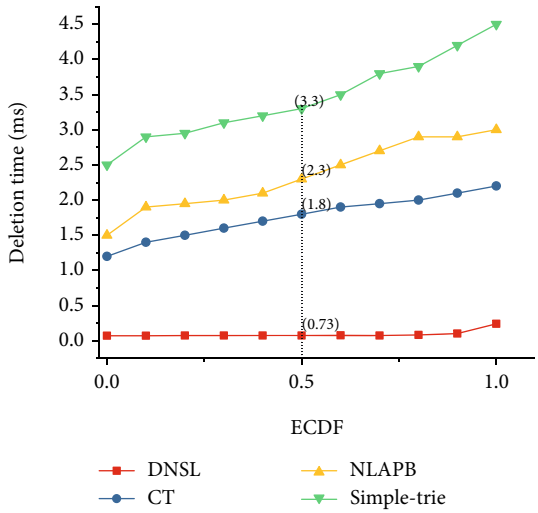

Figure 9: Deletion time to delete contents from content table.

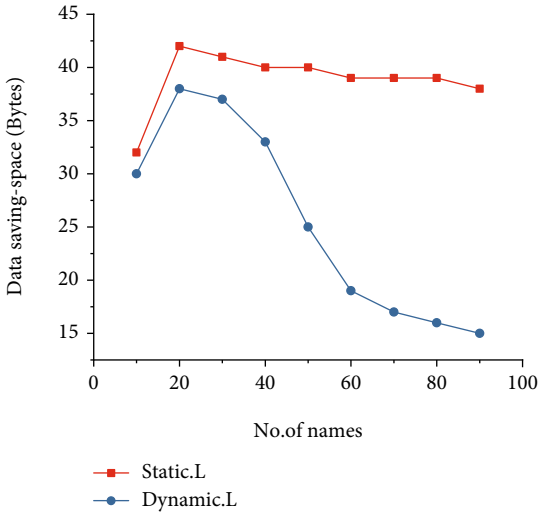

Figure 10: Memory performance between the static and dynamic naming schemes.

The calculation of the compression ratio C_r to save the total space in the FIB table T_s between the static and dynamic naming schemes is

$$C_r = \frac{M_s}{M_d}, \quad C_r = 1 - \frac{M_s}{M_d}. \tag{7}$$

Figure 10 compares both the dynamic and static naming schemes. We achieve 33% memory performance. Our proposed scheme DNSL is better than static naming for VNDN. Moreover, it illustrates that when a vehicle joined the structure of DNSL, and it takes a little bit more memory but also less than a static approach. After registration, the dynamic tag is enough to store the vehicle's information, reduce the content length stores in the FIB table, consume less memory, and provide a dynamic environment for VNDN.

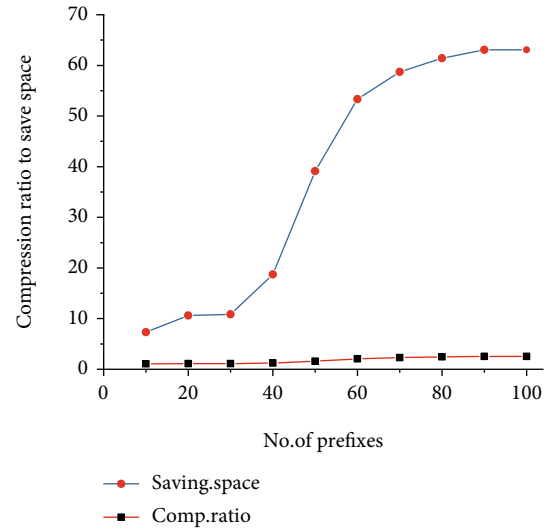

Figure 11: Compression ratio to save memory.

We can see in Figure 11 that the compression rate of static content and achieve the space performance from 5% to 60% and averagely 33% using the above mathematical model.

5. Conclusion

The choice of the naming scheme for lookup in vehicular named data networks can significantly affect the network performance. The static and dynamic naming approaches have not yet been studied well. This article makes three key contributions: (1) our proposed dynamic naming scheme to solve the lengthy namespace problem and restrict the redundancy contents in the naming scheme. Moreover, our proposed work reduces the FIB table size and achieves memory performance. (2) Our proposed work is unique to identify the consumer and producer requests using the common characteristic of the vehicle and the dynamic-tag, which improves the vehicular network's overall performance. (3) Lookup plays a decisive role in improving network performance. Therefore, we designed a lookup method based on node partition based to improve the lookup, insertion, and deletion time. However, the results show (see Section 4) that our proposed DNSL scheme is best for VNDN and achieves the merit of structure in terms of fast lookup, unique approach, and less memory usage. In conclusion, our proposed work was found great when the short namespace, fast lookup, and low memory requirements are the genuine concern.

Data Availability

The simulation data used to support the findings of this study are available from the corresponding author upon request.

Conflicts of Interest

The authors declare that they have no conflicts of interest.

Acknowledgments

This research study is funded by the National Natural Science Foundation of China under Grant 61772385. The authors acknowledge this financial support.

References

[1] X. Wang, Z. Wang, and S. Cai, "Data delivery in vehicular named data networking," *IEEE Networking Letters*, vol. 2, no. 3, pp. 120–123, 2020.

[2] H. Khelifi, S. Luo, B. Nour et al., "Named data networking in vehicular ad hoc networks: state-of-the-art and challenges," *IEEE Communications Surveys & Tutorials*, vol. 22, no. 1, pp. 320–351, 2020.

[3] L. B. Rondon, J. B. da Costa, G. P. Rocha Filho, D. Rosário, and L. A. Villas, "Degree centrality-based caching discovery protocol for vehicular named-data networks," in *2020 IEEE 91st vehicular technology conference (VTC2020-spring)*, pp. 1–5, Antwerp, Belgium, May 2020.

[4] B. Li, D. Huang, Z. Wang, and Y. Zhu, "Attribute-based access control for ICN naming scheme," *IEEE Transactions on Dependable and Secure Computing*, vol. 15, no. 2, pp. 194–206, 2018.

[5] X. Guo, Y. Chen, L. Cao, D. Zhang, J. Jiang, and L. Villas, "A smart forwarding scheme for the interest packet in VNDN," in *2019 2nd International Conference on Hot Information-Centric Networking (HotICN)*, vol. 2019, pp. 7–12, Chongqing, China, December 2019.

[6] W. Xu, X. Ji, C. Zhang, B. Liu, and J. Jiang, "NIHR: name/ID hybrid routing in information-centric VANET," in *2020 IEEE Wireless Communications and Networking Conference (WCNC)*, pp. 1–7, Seoul, Korea (South), May 2020.

[7] B. Indira, K. Valarmathi, D. Deverag, and D. Zhang, "A trie based IP lookup approach for high performance router/switch," in *2019 IEEE International Conference on Intelligent Techniques in Control, Optimization and Signal Processing (INCOS)*, pp. 1–6, Tamilnadu, India, April 2019.

[8] D. Saxena and V. Raychoudhury, "Scalable, memory-efficient pending interest table of named data networking," in *2020 IEEE 17th International Conference on Mobile Ad Hoc and Sensor Systems (MASS)*, pp. 533–540, Delhi, India, December 2020.

[9] B. Sun and V. Raychoudhury, "An improved PLC-trie based routing table design for variable length IP address lookup," in *2019 In Proceedings of the 14th International Conference on Future Internet Technologies*, pp. 1–8, New York, USA, August 2019.

[10] L. Wang, R. Wakikawa, R. Kuntz, R. Vuyyuru, and L. Zhang, "Data naming in vehicle-to-vehicle communications," in *2012 in IEEE Conference on Computer Communications Workshops (INFOCOM WKSHPS)*, pp. 328–333, Orlando, FL, USA, March 2012.

[11] H. Khelifi, S. Lou, B. Nour, and H. Moungla, "A name-to-hash encoding scheme for vehicular named data networks," in *2019 International Wireless Communications & Mobile Computing Conference (IWCMC)*, pp. 603–608, Tangier, Morocco, June 2019.

[12] I. Din, B. S. Kim, S. Hassan, M. Guizani, M. Atiquzzaman, and J. J. Rodrigues, "Information-centric network-based vehicular communications: overview and research opportunities," *Sensors*, vol. 18, no. 11, article 3957, 2018.

[13] M. Rehman, R. Ullah, and B. S. Kim, "NINQ: name-integrated query framework for named-data networking of things," *Sensors*, vol. 19, no. 13, article 2906, 2019.

[14] M. Chowdhury, A. Gawande, and L. Wang, "Secure information sharing among autonomous vehicles in NDN," in *2017 IEEE International Conference on Internet-of-Things Design and Implementation (IoTDI)*, pp. 15–26, Pittsburgh, PA, USA, April 2017.

[15] F. M. Modesto and A. Boukerche, "SEVeN: a novel service-based architecture for information-centric vehicular network," *Computer Communications*, vol. 117, pp. 133–146, 2018.

[16] W. Quan, C. Xu, J. Guan, H. Zhang, and L. A. Grieco, "Social cooperation for information-centric multimedia streaming in highway VANETs," in *Proceeding of IEEE International Symposium on a World of Wireless, Mobile and Multimedia Networks 2014*, pp. 1–6, Sydney, Australia, June 2014.

[17] W. Quan, C. Xu, J. Guan, H. Zhang, and L. A. Grieco, "Scalable name lookup with adaptive prefix Bloom filter for named data networking," *IEE Communications Letters*, vol. 18, pp. 102–105, 2014.

[18] S. H. Bouk, S. H. Ahmed, and D. Kim, "Hierarchical and hash-based naming scheme for vehicular information centric networks," in *2014 IEEE International Conference on Connected Vehicles and Expo (ICCVE)*, pp. 765-766, Vienna, Austria, November 2014.

[19] S. H. Bouk, S. H. Ahmed, and D. Kim, "Hierarchical and hash based naming with compact trie name management scheme for vehicular content centric networks," *Computer Communications*, vol. 71, pp. 73–83, 2015.

[20] C. Zhang, Y. Feng, H. Song et al., "PBC: effective prefix caching for fast name lookups," in *2020 IFIP Networking Conference (Networking)*, pp. 1–9, Paris, France, June 2020.

[21] S. H. Park, Y. Y. Shin, and N. Ko, "A scalable name lookup service for NDN," in *2020 International Conference on Information and Communication Technology Convergence (ICTC)*, pp. 1025–1027, Jeju, Korea (South), October 2020.

[22] H. Hao, C. Xu, S. Yang, J. Guan, Y. Lu, and L. Zhong, "BF-PDT: a new name lookup mechanism in content-centric networking," in *2017 Networking and Network Applications (NaNA)*, pp. 69–74, Kathmandu City, Nepal, October 2017.

[23] Y. Kurihara, Y. Koizumi, and T. Hasegawa, "Compact data structures for location-based forwarding in NDN networks," in *2018 IEEE International Conference on Communications Workshops (ICC Workshops)*, pp. 1–6, Kansas City, MO, USA, May 2018.

[24] J. Chen, M. Jahanian, and K. Ramakrishnan, "Black ice! Using information centric networks for timely vehicular safety information dissemination," in *2017 IEEE International Symposium on Local and Metropolitan Area Networks (LANMAN)*, pp. 1–6, Osaka, Japan, June 2017.

[25] T. Pan, T. Huang, J. Liu et al., "Fast content store lookup using locality-aware skip list in content-centric networks," in *2016 IEEE Conference on Computer Communications Workshops (INFOCOM WKSHPS)*, pp. 187–192, San Francisco, CA, USA, April 2016.

[26] D. Li, J. Li, Z. Du, and J. Zhang, "An improved trie-based name lookup scheme for named data networking," *2016 IEEE*

Symposium on Computers and Communication (ISCC), pp. 1294–1296, Messina, Italy, April 2016.

[27] G. Ghasemi, H. Yousefi, K. G. Shin, and B. J. Zhang, "On the granularity of trie-based data structures for name lookups and updates," *IEEE/ACM Transactions on Networking*, vol. 27, no. 2, pp. 777–789, 2019.

[28] H. Naeem, B. Guo, and M. R. Naeem, "A light-weight malware static visual analysis for IoT infrastructure," in *2018 International Conference on Artificial Intelligence and Big Data (ICAIBD)*, pp. 240–244, Chengdu, China, May 2018.

[29] F. Ullah, M. R. Naeem, A. S. Bajahzar, and F. Al-Turjman, "IoT-based cloud service for secured android markets using PDG-based deep learning classification," *ACM Transactions on Internet Technology (TOIT)*, vol. 22, no. 2, pp. 1–17, 2021.

[30] S. Arshad, B. Shahzaad, M. A. Azam, J. Loo, S. H. Ahmed, and S. Aslam, "Hierarchical and flat-based hybrid naming scheme in content-centric networks of things," *IEEE Internet of Things Journal*, vol. 5, no. 2, pp. 1070–1080, 2018.

[31] J. Huang, P. Wang, Z. Wang, and Y. Zhu, "TCAM-based IP address lookup using longest suffix split," *IEEE/ACM Transactions on Networking*, vol. 26, no. 2, pp. 976–989, 2018.

[32] NDNSim, 2019, https://ndnsim.net/2.7/getting-started.html.

[33] Shalla's blacklists, 2015, http://www.shallalist.de.

[34] Alexa the Web Information Company, 2017, http://www.alexa.com/.

[35] Dga families, 2015, http://data.netlab.360.com/dga/.

[36] ODPnn- Open Directory Project, 2015, http://www.dmoz.org/.

Hindawi
Wireless Communications and Mobile Computing
Volume 2022, Article ID 5383526, 15 pages
https://doi.org/10.1155/2022/5383526

Research Article

Multi-UAV Cooperative Assisted RSU Data Acquisition Strategy considering Coverage Quality

Xiaoyu Du,[1] Qicheng Guo,[2] Yanyu Zhang,[3] Yinyin Li,[2] and Yi Zhou[3]

[1]*School of Computer and Information Engineering, Henan University, Henan, China*
[2]*Henan Engineering Laboratory of Spatial Information Processing, Henan University, Henan, China*
[3]*International Joint Research Laboratory for Cooperative Vehicular Networks of Henan, Henan University, Henan, China*

Correspondence should be addressed to Yanyu Zhang; zyy@henu.edu.cn

Received 26 October 2021; Revised 9 March 2022; Accepted 26 March 2022; Published 25 April 2022

Academic Editor: Farhan Ullah

The multiple Unmanned Aerial Vehicle (multi-UAV) assisted roadside unit (RSU) data acquisition problem considering the coverage quality is a multiobjective optimization problem, which is a NP-hard problem. Heuristic and hyperheuristic algorithms are effective to solve problems of this type. These algorithms can find the optimal or suboptimal solution in a reasonable time. However, such algorithms still have the problems of low convergence accuracy, slow convergence speed, and being easy to fall into the local optimal solution. In this paper, firstly, according to the specific problem scenarios of roadside unit data collection, minimum cost and maximum coverage models based on task cost and coverage quality are established. Then, to solve the optimization model, combined with the update characteristics of the gray wolf optimization algorithm (GWO) and the whale optimization algorithm (WOA), a hybrid weighted gray wolf and whale optimization algorithm (HWGWOA) is proposed. Finally, to verify the effectiveness of the proposed algorithm, extensive simulation experiments are conducted under four different task acquisition scenarios, and the results are compared with those of genetic algorithm (GA), GWO, and WOA. Simulation results show that the algorithm proposed in this paper not only can get lower task cost and higher coverage quality but also has faster convergence speed and better robustness. Specifically, in terms of task cost, the HWGWOA is about 9.54% lower than the GA, about 7.31% lower than the GWO, and about 5.8% lower than the WOA. In terms of coverage, the HWGWOA is up to about 27.87% higher than the GA, about 15.19% higher than the GWO, and about 9.86% higher than the WOA. Therefore, the algorithm is more suitable for large-scale optimization problems.

1. Introduction

With the development of artificial intelligence, intelligent transportation has become an important research field. In this field, it is crucial to collect road and traffic data. Currently, it mainly relies on roadside units (RSUs) to collect and transmit data to data center. However, in some remote areas, poor areas, or some special areas, data collection and transmission have big challenges [1].

In recent years, unmanned aerial vehicles (UAVs) have been widely used in military and civilian fields because of their high flexibility, low risk, low cost, and easy deployment [2]. At the same time, UAVs are widely used in the field of intelligent transportation, and they play an important role in traffic detection, road patrol, data collection, emergency communications, traffic accident evidence collection, target tracking, and transportation [3]. Compared with traditional mobile sensors, UAVs have faster moving speed, wider deployment range and longer working hours, so they are more suitable for performing various tasks [4–6]. UAV-assisted RSUs have become an effective method of data collection, which have greatly improved the efficiency of data collection [7].

Currently, most UAVs are powered by batteries and cannot complete large-scale tasks independently due to energy consumption constraints. Therefore, it is becoming more and more common for multiple UAVs to perform tasks cooperatively. Collaborative planning is an important way to improve the efficiency of UAVs [8]. At present, most algorithms about UAV task assignment and path planning

optimize the following indicators given the number of UAV, such as (1) optimizing the task completion time under the premise of the given number of drones, (2) optimizing the task completion energy consumption under the premise of the given number of drones, and (3) weighing the energy consumption under the premise of the given number of drones and time cost. However, in fact, the optimal number of UAVs to complete tasks is unknown. The optimal number of UAVs is unknown. Assuming there are enough UAVs, it is important to find the best number of UAVs for a given time limit and task set.

In addition, for large-scale data collection scenarios, it will take a long time to collect data from RSUs, and the number of employed UAVs will inevitably increase, which will result in high collection cost. Therefore, in fact, under the constraints of energy consumption and time, as the collection task increases, we cannot collect all RSU data. At this time, the data collection problem is transformed into a sweep coverage problem. At present, for the sweep coverage problem, the coverage rate is generally expressed by the ratio of the number of covered target points to the total number of target points, which is not reasonable in the problem of RSU data collection. In the RSU data collection problem, the RSUs deployed in different locations often collect road and traffic data with different data size and importance at the same time. Therefore, nodes with different importance need different data collection frequency. For example, it is necessary to collect more important and complex data information from RSUs deployed near scenic spots, urban arterial road intersections, and near stations. The RSUs deployed on remote trails carry less important and less data information. To this end, this paper proposes a data collection model based on coverage quality while optimizing time and energy consumption. We define this problem as a minimum cost and maximum coverage problem.

In this paper, the problem of multi-UAV cooperatively assisted roadside unit data acquisition considering coverage quality is regarded as the problem of minimum cost and maximum coverage. We need to dispatch a certain number of UAVs to collect data from RSUs in the target area to achieve the greatest coverage quality with the smallest task cost. This problem is a NP-hard problem, which is an extension of the traveling salesman problem. In order to solve this problem, this paper proposes a hybrid weighted gray wolf whale algorithm with the minimum cost and maximum coverage as the optimization objectives under the constraints of the task and environment.

The main contributions of this article are as follows:

(i) We propose a multi-UAV assisted RSU data collection model that considers the coverage quality, that is, the minimum cost and maximum coverage model. We considered the different importance of different roadside units, assigned weights to the roadside units, and redefined the task coverage. A more suitable coverage calculation model is constructed

(ii) We modeled the problem of multi-UAV assisted RSU data collection. An optimization objective is established to balance task cost and coverage quality. Make the optimization goal more in line with the actual task requirements of the problem. A hybrid weighted gray wolf whale optimization algorithm is proposed to solve the proposed problem and optimize the multi-UAV collaborative mission planning scheme

(iii) This paper simulates mission scenarios of different scales by changing the location and number of roadside units and conducts sufficient simulation and comparison experiments to verify the effectiveness and superiority of the algorithm proposed in this paper. The experimental results show that under different scales of task scenarios, the proposed algorithm achieves lower task cost and higher coverage and has better algorithm stability coverage

The remainder of this paper is organized as follows. Section 2 summarizes the related work. Section 3 describes the requirements and constraints of the problem, explains the meaning of each symbol, and establishes a mathematical model for a specific problem. Section 4 focuses on the algorithm proposed in this paper. Section 5 verifies the effectiveness and superiority of the algorithm through extensive simulations. Finally, Section 6 concludes the paper and proposes some future research direction in this field.

2. Related Work

At present, there are many papers about UAV mission planning. In this section, we will review the literature on cooperative task assignment and path planning for multi-UAVs.

Multi-UAV cooperative task assignment is a typical multiple traveling salesman problem (MTSP), which is a typical NP-hard problem. Many algorithms have been proposed for this problem such as branch and bound method, linear programming, dynamic programming, method based on Voronoi diagram [9], fuzzy logic [10], and differential evolution algorithm [11]. However, when the scale of the problem increases, the computation time will increase exponentially, and the efficiency is low. Therefore, scholars turn to intelligent methods and begin to develop approximate algorithms and heuristic algorithms such as auction algorithm [12, 13], genetic algorithm [14–17], simulated annealing algorithm [18, 19], ant colony algorithm [20–22], particle swarm algorithm [23, 24], and fruit fly optimization algorithm [25]. However, these algorithms were proposed for specific problems, and their universality is poor.

UAV task planning is a problem that finds the optimal path with the minimum cost to complete tasks. These path planning problems are usually solved based on one or several optimization criteria, such as time optimization [3, 6, 15, 18], energy optimization [14, 20], time and energy mix optimization [13, 22, 25–27], and hybrid optimization based on coverage [28]. In terms of time optimization, in Reference [3], a time first immune clonal selection algorithm with optimization modification was proposed to solve the task assignment problem of road patrol. The immune clonal selection algorithm was used to obtain the best sequence of

task points, and the time first method was used to divide the sequence of task points. The optimal UAV path was further optimized and modified. Reference [6] solved the problem of path planning for multiple UAVs collecting data from RSUs, and its goal was to find the best time path for multiple UAVs. An improved evolutionary method based on genetic algorithm (GA) and harmony search (HS) was used to solve the problem. Reference [15] pointed out that in the task allocation problem, it is crucial to determine the number of UAVs and find the mission path of each UAV. Based on this idea, the author proposes a collaborative optimization algorithm that combines genetic algorithm and clustering algorithm to solve the task assignment and path planning problems of multiple UAVs for multiple tasks and can find the best UAV when the task time constraints are met. In Reference [18], an effective task allocation and route planning method was proposed to solve the problem of vehicle planning. This method balanced the tasks between UAVs and optimized the task time. According to the number of UAVs, virtual nodes were added to the original model of the vehicle routing problem (VRP), so it is easier to form a solution suitable for the heuristic algorithm. The concept of a universal distance matrix was proposed, which transformed time constraints into space constraints and simplified the planning model. On this basis, a swap judgment simulated annealing (SJSA) algorithm was proposed to improve the generation efficiency of feasible neighbor solutions. In terms of energy optimization, in [14], in order to optimize the UAV energy, the authors describe the UAV path planning problem as a traveling salesman problem. A genetic algorithm is proposed to solve the optimization problem to minimize the energy consumption of the UAV to complete the task. Reference [20] introduced an energy minimization problem of UAV-assisted MEC system and proposed an algorithm based on the ant colony system (ACS) to obtain a high-quality near-optimal solution to this problem, in terms of time and energy mix optimization.

Reference [13] proposed a method based on auction algorithm to allocate dynamic tasks to UAVs, and designed a multilayer cost calculation method considering constraints such as UAV number, time threshold, fuel cost and driving danger to solve the task assignment problem of multi-UAV system. Reference [25] proposed a method of finding the best flight path for UAV to successfully complete the inspection work in oilfield. Firstly, a novel task assignment method was proposed, which included initial task assignment and task assignment with changing tasks to determine the initial task sequence of each UAV, and quickly reschedule the task sequence after the task changes. Then, an improved fruit fly optimization algorithm (ORPFOA) was proposed to solve the path planning problem in the initial task sequence and the new task sequence after task change. In [26], for the solution of task assignment problem, four objectives are simultaneously optimized, namely, maximizing the number of tasks successfully assigned, maximizing task execution benefit, minimizing resource cost and minimizing time cost. A multi-UAV task assignment method based on clone selection algorithm is proposed. In [27], the authors comprehensively consider the problems of minimizing resource consumption and maximizing task revenue during UAV task assignment. On the basis of considering constraints and multiobjective problems, the brute force allocation algorithm, constrained optimization evolutionary algorithm, particle swarm optimization algorithm, and greedy algorithm combined with constrained evolutionary algorithm in the process of UAV task allocation are improved and optimized. And analyze the performance and conclusions of the above four algorithms under the limited UAV task assignment scheme. In terms of coverage-based hybrid optimization, in order to solve the scanning coverage problem in forest fire warning and monitoring, Reference [7] considered the minimum time maximum coverage (MTMC) problem of maximum coverage. The authors propose a heuristic Weighted Targets Sweep Coverage (WTSC) algorithm considering target weights and UAV performance constraints to find the optimal path.

Reference [28] considers finding the optimal path for the UAV to maximize its coverage in the designated area under the time constraints and path feasibility. The problem is modeled as an Epsilon-constraint optimization in which coverage function has to be maximized, considering the constraints on the length and the smoothness of the path. For this purpose, a new genetic path planning algorithm with adaptive operator selection is proposed to solve such a complicated constrained optimization problem. In recent years, autonomous underwater vehicles (UAVs) have been widely used to assist in information collection in ocean development and exploration. In [29], the authors embedded a biologically inspired neural network (BINN) into a self-organizing map (SOM) neural network and divided the tasks into two layers: task assignment and path planning. Utilize BINN to update the weights of SOM winners to realize path planning and efficient navigation of AUVs. Aiming at the problem of information collection in harsh underwater environment, Reference [30] proposed a heterogeneous AUV auxiliary information collection system; the AUV path with low time complexity was obtained by particle swarm algorithm; Additionally, a two-stage joint optimization algorithm based on Lyapunov optimization is constructed to strike a trade-off between energy efficiency and system queue backlog iteratively. In [31], the author considering both the realistic complex underwater acoustic environment and the AUVs energy consumptiona limited service M/G/1 vacation queueing model is constructed for describing and optimizing the age of information(AoI) of the Internet of underwater things (IoUT). Also, a low-computational algorithm is proposed for adaptively adjusting the upper limit of the queuing length formulated and reducing the peak AoI under energy constraints. In order to ensure the efficient operation of UAV, an intelligent mechanism was developed in Reference [32], which considered two main factors, energy consumption and operation time of UAV. Then, three complementary schemes, energy aware UAV (EAUS), delay aware UAV (DAUS), and fair exchange UAV (FTUs), were proposed. These solutions were optimized as linear integer problems (LIP). EAUS solution aims to reduce the energy consumption of UAV, while DAUS solution aims to shorten the operation time of UAV. However, FTUs is a trade-off between energy consumption and task time

As mentioned in Reference [32], for different task type, complexity, constraints and other factors, the optimization objectives of multi-UAV task assignment are different such as minimizing mission time, minimizing energy, and minimizing composite indicator of time and energy. In order to more clearly compare the work done in the existing literature, Table 1 lists the key information of the related literature. In this paper, we study the scan coverage problem of multi-UAV assisted RSU data acquisition. According to the number of UAVs, the task cost and coverage quality are considered comprehensively to find an optimal scheme that can maximize coverage quality and minimize task cost simultaneously. We conclude it as minimum cost maximum coverage model with variable number of UAVs.

3. Problem Formulation and Mathematical Model

A complex urban environment including urban, suburban, and rural areas is considered in this paper. According to the needs of intelligent transportation, it is supposed that several RSUs are deployed in the urban environment to collect road environment and traffic information. In the problem of multi-UAV collaborative assistance RSU data collection, when the number of RSUs is large, it is often impossible to collect data from all RSUs due to the timeliness of data and limited energy of UAVs. Therefore, this paper proposes a minimum cost and maximum coverage model to solve the problem of scanning and coverage. Due to the different locations of RSUs, the importance and size of the data collected by them are different. Therefore, this paper assigns different weight value, a positive integer between one and five, to each RSU according to its importance. The schematic diagram of a multi-UAV cooperatively assisted RSU for data acquisition is depicted in Figure 1.

The problem we considered in this paper can be modeled as a triplet $\{R, U, C\}$, where $R = \{R_1, R_2, \cdots, R_N\}$ is the set of RSUs that are deployed along roads. Each element R_i can also be described as a triplet $\{P_i, D_i, W_i\}$. Symbol P_i is the position coordinates of the i^{th} RSU, D_i is the data size collected by the i^{th} RSU, and W_i is the weight value of the i^{th} RSU. The set of UAVs that are deployed in base station is described by set $U = (U_1, U_2, \cdots, U_K)$. Each element U_j can be described by the same quadruple $\{v, s, L_{\max}, E_{\max}\}$, which means that all UAVs have same flight speed v, transmission speed s, maximum flight distance $L_{\max}$, and energy threshold $E_{\max}$. Symbol C represents the constraints in task assignment. The number of UAVs selected to accomplish the task is k, and the data collection path of the j^{th} UAV is represented as $X_j = [B, R_a, \cdots, R_b, B]$. This problem can be described as a multiple traveling salesman problem. The main symbols and their definitions used in this article are listed in Table 2.

The problem presented above is designing a reasonable scheme of task allocation and path planning for multi-UAVs to collect data from RSUs based on the number, location, data size and weight value of RSUs. To solve this problem, the constraints we considered in this paper are as follows: Firstly, the energy consumption and total flight distance of each UAV to accomplish its tasks cannot exceed its maximum values. Secondly, the number of UAVs used should not exceed the total number of UAVs stay in base station, and each RSU can only be visited by one UAV at most. In addition, UAV should start flying from the base station and finally return to it after finishing data acquisition. These constraints can be expressed as follows:

$$\begin{aligned} E^j &\le E_{\max} (j = 1, 2, \cdots, k), \\ L_j &\le L_{\max} (j = 1, 2, \cdots, k), \\ k &\le K, \\ X_1 \cap X_2 \cap \cdots \cap X_k &= B. \end{aligned} \tag{1}$$

In this paper, a mathematical model is established with the objective of optimizing the minimum cost and maximum coverage. Assume that k UAVs are dispatched from the base station to accomplish data collection tasks. When the last UAV returned to base station after finishing data collection, the task is considered as completed. The mission time is defined as the time interval between the take-off time of the first UAV and the return time of the last UAV. Energy consumption is the total energy consumption of k UAVs to accomplish data collection tasks. Coverage is defined as the total weight ratio of RSUs collected by UAVs to all RSUs.

The mission time T^j includes flight time T_f^j and data collection time T_c^j which is described in

$$T^j = T_f^j + T_c^j. \tag{2}$$

The flight time T_f^j and data collection time T_c^j are, respectively, determined by

$$T_f^j = \frac{L_j}{v}, \tag{3}$$

$$T_c^j = \frac{C_{\text{total}}^j}{s}. \tag{4}$$

The flying distance L_j and total data size C_j are calculated using

$$L_j = \sum D_{X_j}, \tag{5}$$

$$C_j = \sum C_{X_j}. \tag{6}$$

The total energy consumption of UAVs to accomplish tasks includes flight energy consumption, hovering energy consumption, and data transmission energy consumption. Compared with flight energy consumption and hovering energy consumption, data transmission energy consumption is negligible. Therefore, the total energy consumption of UAV U_j is expressed as follows:

$$E_j = E_f^j + E_h^j. \tag{7}$$

Table 1: The key information of the related literature.

Reference	Application field	Optimization objective	Algorithm of UAVs	Number type	Overlay
[3]	Road patrol	Time	Immune clonal selection algorithm (ICSA) and time-priority method	Fixed	All
[6]	RSU data collection	Time	Genetic algorithm (GA) and harmony search (HS)	Fixed	All
[15]	Task planning	Time	GA and cluster algorithm	Variable	All
[18]	Task planning	Time	Swap-and-judge simulated annealing (SJSA)	Fixed	All
[14]	Monitoring wildfires in remote areas	Energy	Hybrid gray wolf optimization (HGWO)	Fixed	All
[20]	Data collection in mobile edge computing	Energy	Ant colony system (ACS)	Fixed	All
[22]	Reconnaissance task allocation	Time and energy	Grouping ant colony optimization algorithm (GACO)	Fixed	All
[25]	Oilfield inspection	Time	An improved fruit fly optimization algorithm (ORPFOA)	Fixed	All
[26]	Task allocation	Time and energy	Clone selection algorithm (CSA)	Fixed	All
[27]	Task allocation	Energy and revenue	Violence allocation algorithm; constraint optimization evolutionary algorithm; PSO algorithm; greedy algorithm combined with a constraint evolutionary algorithm	Fixed	All
[7]	Forest fire early warning and monitoring	Time and coverage	Heuristic algorithm weighted targets sweep coverage (WTSC)	Fixed	Partial
[28]	Coverage-based path planning (CBPP) problem	Coverage rate	Genetic algorithm with adaptive operator selection	Fixed	Partial
In this paper	RSU data collection	Time, energy, and coverage	Hybrid weighted gray wolf and whale optimization algorithm (HWGWOA)	Variable	Partial

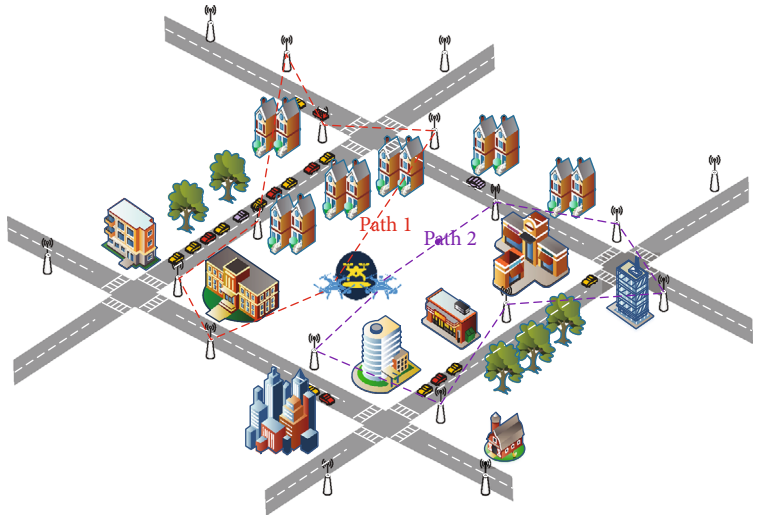

Figure 1: Multi-UAV cooperatively assisted RSUs for data collection.

Table 2: Symbols and their definitions used in this paper.

Parameters	Definition
N	Number of RSUs
K	Number of UAV base stations
k	Number of UAVs selected
$B(x_B, y_B)$	Base station coordinates
$R_i(x_i, y_i)$	Coordinates of the RSU R_i
C_i	Size of data collected by RSU R_i
D_{ij}	Distance from RSU R_i to RSU R_j
$L_{\max}$	Maximum flying distance of UAV
$E_{\max}$	Energy consumption threshold of UAV
v	Flying speed of UAV
s	Data transmission rate of UAV
$X_j = [B, R_a, \cdots, R_b, B]$	Data collection path of UAV U_j
T_f^j	Flight time of UAV U_j
T_c^j	Data collection time of UAV U_j
T^j	Task time of UAV U_j
L_j	Flying distance of UAV U_j
C_{total}^j	Size of data collected by UAV U_j
E_f^j	Flight energy consumption of UAV U_j
E_h^j	Hovering energy consumption of UAV U_j
E^j	Task energy consumption of UAV U_j
P_f	Flying power of UAV U_j
P_h	Hovering power of UAV U_j
W_i	Weight of RSU R_i
F	Task cost
W	Coverage quality
P	Coverage

The calculation of flight energy consumption and hovering energy consumption is as follows:

$$\begin{aligned} E_f^j &= L_j \times P_f, \\ E_h^j &= T_c^j \times P_h. \end{aligned} \tag{8}$$

The flight power P_f and hovering power P_h are specific parameters of UAV, which can be found in its handbook.

In this paper, the optimization objective is the weighted sum of maximum task time and total task energy consumption, which is expressed as follows:

$$F = \gamma \sum_{j=1}^{k} E_j + (1-\gamma) \max \left[T^1, T^2, \cdots, T^{k-1}, T^k \right]. \tag{9}$$

Here, $\gamma \in [0, 1]$ is the weight coefficient reflecting the importance of task energy consumption in the entire data collection task.

In this paper, the problem we considered is a problem of incomplete coverage, which means that not all RSUs must be visited by UAVs, However, due to the large number of UAV in this scenario. Therefore, the coverage ratio is another important optimization indicator, which is calculated as follows:

$$P = \frac{W}{\sum_{i=1}^{N} W_i}. \tag{10}$$

The coverage quality W can be calculated by

$$W = \sum_{i=1}^{N} (X_i W_i). \tag{11}$$

Here, X_i is a binary variable, which is determined by

$$X_i = \begin{cases} 1, \text{The UAV passes by the } R_i, \\ 0, \text{other}. \end{cases} \tag{12}$$

The main goal of this paper is to achieve maximum coverage with minimal task energy consumption in the shortest task time. When the weights of all RSUs are known, the total weight is a constant. Therefore, the coverage ratio can be substituted by the coverage quality; then, the optimization objectives are minimizing F and maximizing the coverage quality W simultaneously. This problem is a typical multiobjective optimization problem.

To transform the multiobjective optimization problem to a single objective optimization problem, a utility function Y as described in (13) is proposed to represent the total benefit of the task.

$$Y = \lambda F - (1-\lambda) W. \tag{13}$$

Here, $\lambda \in [0, 1]$ is a weight coefficient, which reflects the importance of the task cost in the entire data collection task, and its value will be given in the simulation experiment part. Finally, the optimization problem in this paper is written as

$$\begin{aligned} &\min (Y) \\ &\text{S.t.} \\ &C_1 : E^j \le E_{\max} (j = 1, 2, \cdots, k) \\ &C_2 : L_j \le L_{\max} (j = 1, 2, \cdots, k) \\ &C_3 : k \le K \\ &C_4 : X_1 \cap X_2 \cap \cdots \cap X_k = B. \end{aligned} \tag{14}$$

Constraint C_1 ensures that each UAV has enough energy to complete its missions. Constraint C_2 ensures that the flight distance of each UAV does not exceed its maximum flight distance. Constraint C_3 ensures that the number of

UAVs selected does not exceed the number of UAVs in the base station. Constraint C_4 ensures that the data of each RSU is collected by only one UAV.

The solution of multi-UAV coassisted RSU data collection is the grouping and combination sorting of some RSUs in the target area, so the problem is a combinatorial optimization problem. Combinatorial optimization problems are NP-hard problems. When the problem become large, it is difficult to find the optimal solution in a short time. In addition, the strong coupling of multi-UAV collaborative task assignment also increases the difficulty of solving the problem. Therefore, an effective solution for multi-UAV coassisted RSU data collection is to design heuristic or hyperheuristic algorithms to find the optimal solution or suboptimal solution in a reasonable time.

4. Algorithm Design

In order to solve the problems of slow convergence speed, low convergence accuracy, and being easy to fall into local optimal solution of bionic learning algorithm in solving combinatorial optimization problems, in this paper, we propose an improved hybrid weighted gray wolf and whale optimization algorithm to optimize the task assignment scheme of multiple UAVs. Firstly, the grey wolf optimization algorithm (GWO) [33] is improved and further mixed with the whale optimization algorithm (WOA) [34], which is called hybrid weighted grey wolf and whale optimization algorithm (HWGWOA). The specific improvement ideas of the algorithm are as follows.

(a) Tent map initialization

Bionic learning algorithm uses random initialization to generate initial population, each individual in the population is a feasible solution, and then the solution is updated to the optimal solution or suboptimal solution step by step through iteration. It can be seen that the quality of the initial solution will greatly affect the convergence speed and final results of the algorithm. However, random initialization can't guarantee the diversity and ergodicity of the initial solution, especially when the population size is small; it will lead to uneven distribution of the initial solution, which is not conducive to the updating and optimization process of the algorithm.

In order to ensure the uniformity and diversity of the initial feasible solution in the solution space, a tent map [35] is used to initialize the population. The chaotic sequence has the characteristics of inner randomness, ergodicity, and boundedness, but the ergodic uniformity of chaotic sequence generated by different maps is different, which will have different effects on the optimization speed of the algorithm. At present, most of the research uses the chaotic sequence generated by logistic mapping. However, the uniformity of the chaotic sequence generated by logistic mapping is poor, and most of the values are in the interval [0, 0.1] and [0.9, 1] [36]. Tent mapping has a simple structure, better ergodic uniformity, and faster iteration speed, and the chaotic sequences generated by it are evenly distributed in [0, 1]. Therefore, in this paper, tent mapping is selected to initialize the population. The mathematical expression of tent mapping is

$$x(n+1) = \begin{cases} \dfrac{x_n}{a}\, x_n \in [0, a), \\ \dfrac{1 - x_n}{(1-a)} x_n \in [a, 1]. \end{cases} \tag{15}$$

(b) Weighted update mechanism

The GWO algorithm uses the three solutions, alpha (α), beta (β), and delta (δ), with the highest fitness value to guide other individuals to update towards the optimal solution. In the original GWO algorithm, the guidance strength of the three best solutions is the same, which will make the algorithm easily fall into the local optimal solution area. In order to increase the diversity and randomness of the updates, we use the weighted update mechanism. Each update randomly generates three weight coefficients added to the three solutions.

$$\begin{cases} D_\alpha = |C_1 X_\alpha - X_t| \\ D_\beta = |C_2 X_\beta - X_t|, \\ D_\delta = |C_3 X_\delta - X_t| \end{cases} \tag{16}$$

$$\begin{cases} X_1 = X_\alpha - A_1 \cdot D_\alpha \\ X_2 = X_\beta - A_2 \cdot D_\beta. \\ X_3 = X_\delta - A_3 \cdot D_\delta \end{cases} \tag{17}$$

$$X_{t+1} = \frac{(J_1 X_1 + J_2 X_2 + J_3 X_3)}{3}, \tag{18}$$

where equations (16) and (17) define the update direction and step length of other individuals in the wolf pack towards α, β, and δ. J_1, J_2, and J_3 are weight coefficients, and they are calculated by

$$J_1 = \frac{j_1}{(j_1 + j_2 + j_3)}, \tag{19}$$

$$J_2 = \frac{j_2}{(j_1 + j_2 + j_3)}, \tag{20}$$

$$J_3 = \frac{j_3}{(j_1 + j_2 + j_3)}, \tag{21}$$

where j_1, j_2, and j_3 are random numbers of $[0, 1]$.

(c) Hybrid spiral renewal mechanism

In this paper, we propose a new hybrid algorithm composed of the improved GWO algorithm and WOA. In this hybrid algorithm, the WOA is adopted at the exploration stage due to its good global search ability, which is achieved by its logarithmic spiral update. In addition, the location of the best solution found by the GWO algorithm is replaced by the location of the whale. The

Input: R,U,C
Output: Y,X^*
1. Initialize the population:$X = (X_1, X_2,\cdots,X_m)$;
2. Initialize the parameter: a,A,C,l,T , $p,t = 0$;
3. Calculate the fitness of each search agent;
4. $X_t^* = X_\alpha$ =the best search agent;
5. X_β =the Second best search agent;
6. X_δ = the Third best search agent;
7. **While** $(t < T)$
8. **For** (every search member)
9. Update a,A,C,l,T and p;
10. **If1**$(|A| \le 1)$
11. **If2**$(p < 0.5)$
12. Update the position of the current search agent by the Equation (24);
13. **Else if2**$(p \ge 0.5)$
14. Update the position of the present search agent by the Equations (25);
15. **End if2**
16. **Else if1**$(|A| > 1)$
17. Select a random search agent X_{rand}
18. Update the position of the current search agent by the Equation (26);
19. **End if1**
20. **End for**
21. Calculate the fitness of each search agent;
22. Update X^*, X_α,X_β and X_δ ;
23. t = t +1;
24. **End while**
25. Return X^* ;

Algorithm 1: HWGWOA.

location of the whale is the same as that of the gray wolf, but it can quickly move to the optimal solution. The WOA guides the wolves to converge to the optimal solution, and reduce the calculation time.

In a word, combining the best characteristics of GWO algorithm and WOA makes the probability of finding the global optimal solution higher, and the algorithm stagnation or falling into local optimization is avoided. The HWGWOA combines the advantages of the GWO algorithm at the exploitation stage and the WOA at the exploration stage to obtain the global optimal solution. The mathematical model of HWGWOA is as follows:

According to the hierarchical system, the GWO algorithm preserves three solutions with the highest fitness value in each iteration, which are named α, β, and δ, respectively. In order to improve the convergence performance of the GWO algorithm, the spiral update equation of the WOA is used to update the positions of alpha, beta, and delta as described by

$$\begin{cases} D_\alpha = |C_1 \cdot X_\alpha - Q| \\ D_\beta = \left|C_2 \cdot X_\beta - Q\right|, \\ D_\delta = |C_3 \cdot X_\delta - Q| \end{cases} \tag{22}$$

$$Q = \mathrm{X}_t + D' e^{bl} \cos(2\pi l), \tag{23}$$

where $D' = |X_t^* - X_t|$ denotes the distance from an individual to the prey, b is a constant that defines the shape of the logarithmic helix, and l is a random number in [-1, 1].

To sum up, the updating mechanism of HWGWOA is described by (24)–(31).

$$X_{t+1} = X_t^* - A \cdot D|\mathrm{A}| \le 1P < 0.5, \tag{24}$$

$$X_{t+1} = \frac{(J_1X_1 + J_2X_2 + J_3X_3)}{3}|A| \le 1p \ge 0.5, \tag{25}$$

$$X_{t+1} = X_{\text{rand}} - A \cdot D_{\text{rand}}|\mathrm{A}| > 1, \tag{26}$$

where

$$D = |C \cdot X_t^* - X_t|, \tag{27}$$

$$A = 2 \times a \cdot r_1 - a, \tag{28}$$

$$C = 2 \times r_2, \tag{29}$$

$$a = 2 \times \cos\left(\frac{\pi}{2} \times \frac{t}{T}\right), \tag{30}$$

$$D_{\text{rand}} = |C \cdot X_{\text{rand}} - X_t|, \tag{31}$$

where t is the current number of iterations, T is the maximum number of iterations, p,r_1,r_2 are random numbers in [0, 1], X_t is the current position of a individual, and X_t^* is the optimal solution of the current iteration.

Table 3: The main parameters symbols in this paper.

λ		0.1	0.3	0.5	0.7	0.9
$N = 30$	Task cost coverage rate	45.96 0.90	42.70 0.97	43.80 0.93	43.65 0.95	43.84 0.89
$N = 50$	Task cost coverage rate	63.70 0.93	57.36 0.83	53.94 0.91	55.64 0.92	60.20 0.88
$N = 70$	Task cost coverage rate	80.93 0.77	77.52 0.79	70.51 0.79	75.73 0.72	77.95 0.69
$N = 100$	Task cost coverage rate	95.65 0.68	91.95 0.72	87.10 0.76	82.53 0.78	94.96 0.69

Table 4: Task cost and coverage rate under different scenarios.

RSU number	UAV number	Total weight	Task cost	Coverage rate
30	2	78	51.33	0.86
	3		42.81	0.93
	4		43.80	0.94
	5		45.98	0.97
50	2	127	68.17	0.79
	3		63.01	0.84
	4		53.94	0.91
	5		57.47	0.93
70	2	180	91.88	0.67
	3		78.97	0.72
	4		70.51	0.80
	5		72.83	0.86
100	2	226	117.86	0.64
	3		96.87	0.69
	4		87.10	0.73
	5		79.92	0.78

In the whole iterative process, by controlling the parameters of a, A, C, l, and p, the algorithm makes full global search at the early stage and accelerates convergence at the later stage. The pseudocode of the HWGWOA is shown in Algorithm 1.

In the HWGWOA, we set the number of populations as N, taking one iteration as an example. N calculations are needed to initialize the population, calculate the fitness of each individual, and update the individual position. The first three individuals selected by us need $3N - 3$ calculations at most. The update parameter is constant time, and the calculation in the iterative process is serial. Therefore, the time complexity of the algorithm is $O(N)$.

5. Simulation and Result Analysis

In this section, simulation results are provided to evaluate the performance of the HWGWOA. Specifically, we compare the HWGWOA with the genetic algorithm (GA) [17], GWO [37], and WOA [38]. As a classical algorithm to solve TSP and MTSP, the GA has good stability. GWO algorithm and WOA, as two bionic learning algorithms proposed in recent years, show good performance in solving optimization problems and are also widely used in various optimization problems. All simulations in this section are carried out in MATLAB. All experimental data are rounded to 2 decimal places. The detailed experimental results are as follows.

(A) Simulation model

The parameters in the simulation are set as follows. We consider a 10 km Ã-10 km urban area and randomly deploy multiple RSUs. Four different scenarios are chosen for simulation experiments, whose number of RSUs is set to 30, 50, 70, and 100, respectively. The total number of UAVs in the base station is 5. The base station location of UAV is $B(1, 1)$. It is assumed that the configuration of each UAV is the same; that is, the UAV flies at a constant speed of 60 km/h when performing tasks, and the data transmission speed of UAV is 1.5 mbps/s.

(B) HWGWOA performance evaluation

Here, we study the influence of system parameters on the performance of HWGWOA. In order to achieve the goal of

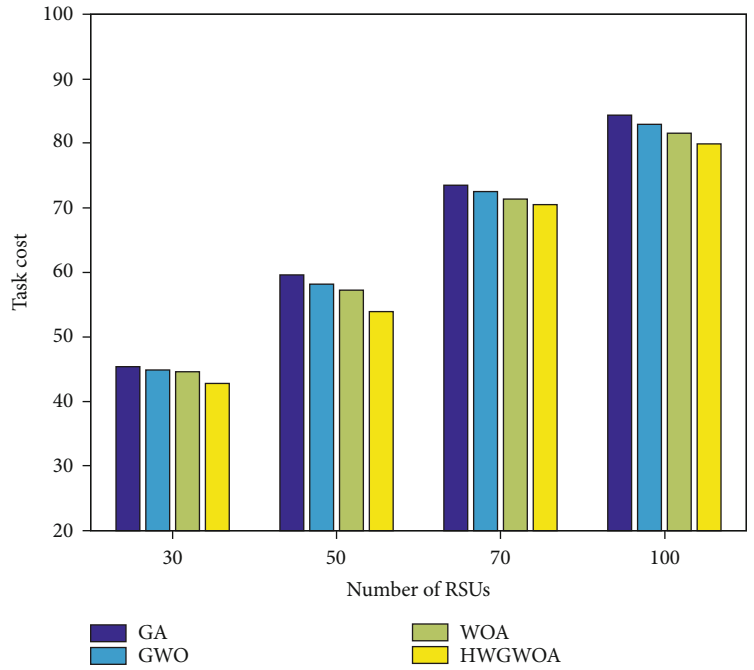

Figure 2: Task cost under different numbers of RSUs.

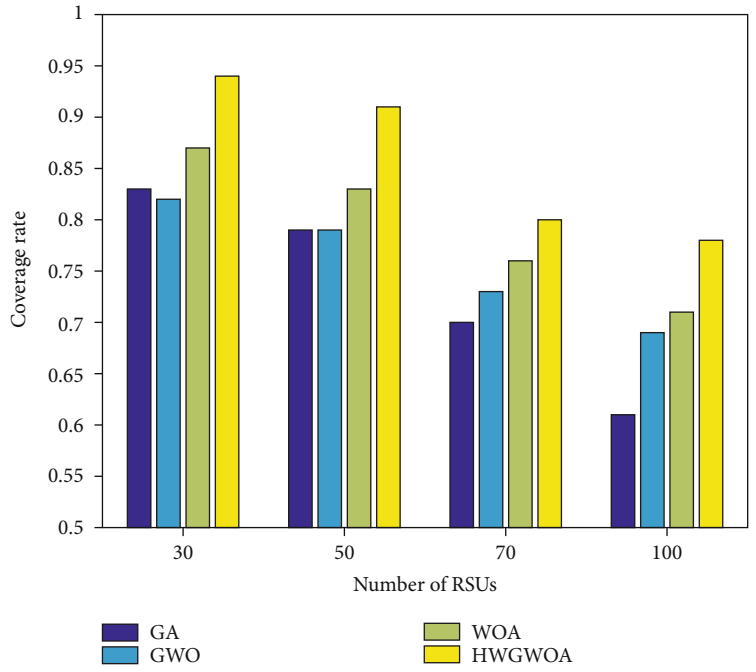

Figure 3: Coverage rate under different numbers of RSUs.

minimum cost and maximum coverage, the weight of task cost and coverage quality should be considered in task planning. Here, we assign equal weights to task time and task energy consumption in task cost; that is, γ in formula (9) is fixed at 0.5.

In formula (13), we use the adjustment parameter γ to balance the weight between task cost and coverage quality. We adjust it from 0.1 to 0.9 and set the number of UAVs to 4 for simulation. Algorithm 1 shows the change of task cost and coverage rate with parameter γ when the number of RSUs is 30, 50, 70, and 100, respectively. Because the algorithm uses random initialization, in order to better show the convergence effect, this paper uses the average of 30 convergence results as the convergence value.

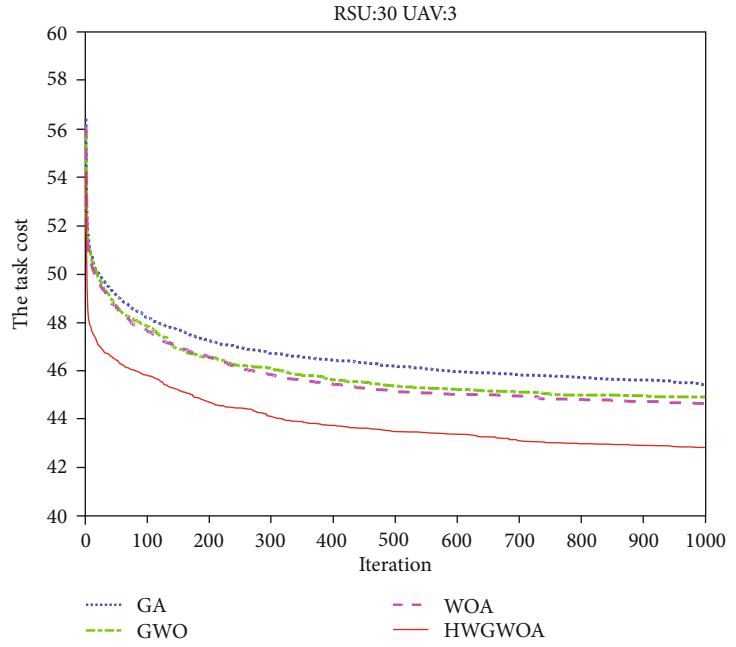

(a)

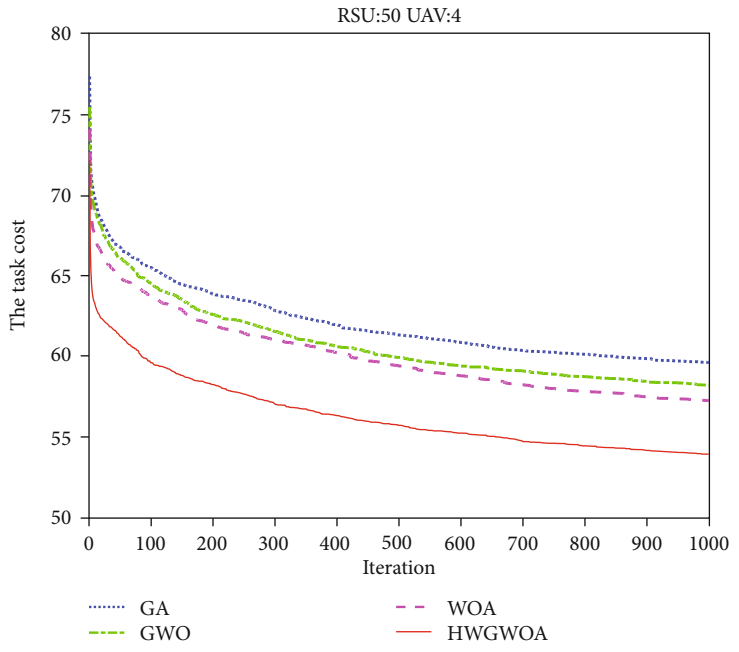

(b)

Figure 4: Continued.

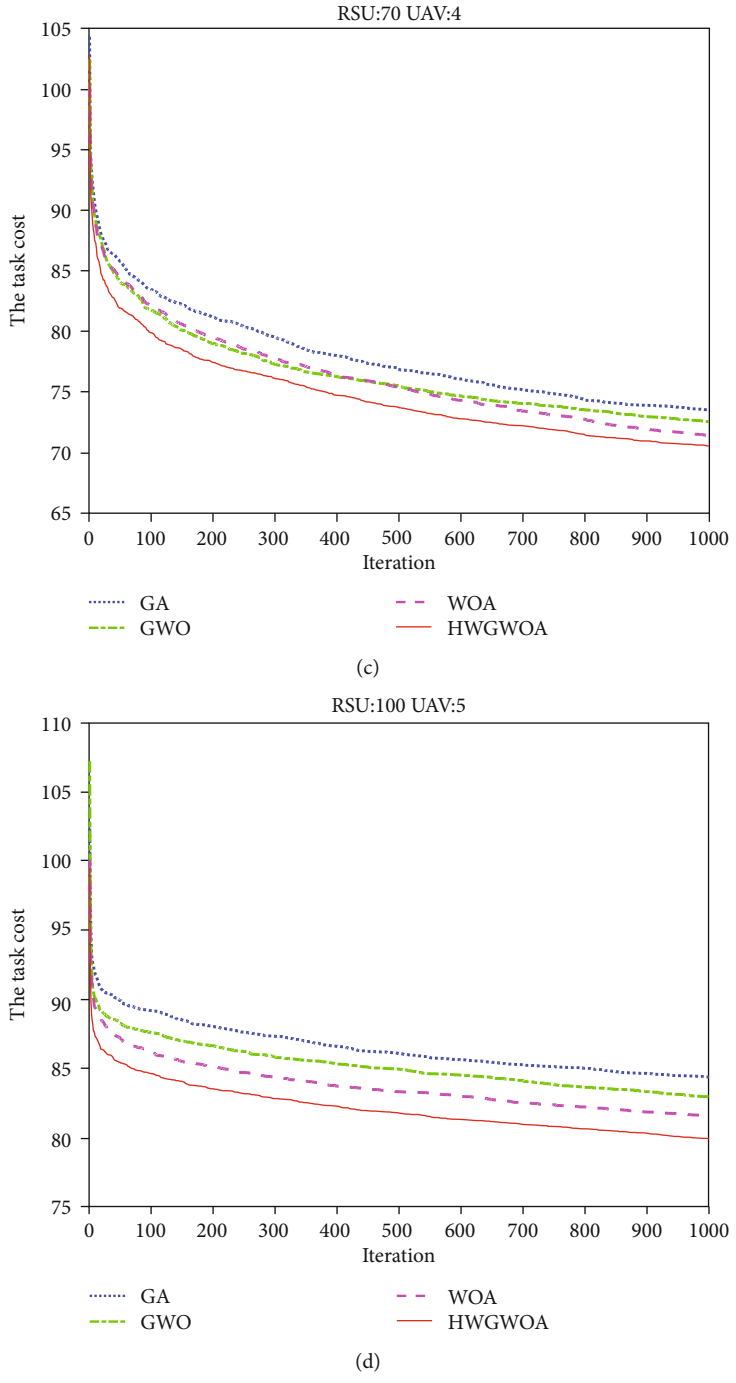

Figure 4: Convergence results of the four algorithms.

Simulation results show that the algorithm is better when γ is between 0.3 and 0.7, as shown in Table 3; we can get lower acquisition cost and higher coverage quality.

Then, we investigate the optimal number of UAVs with different numbers of RSUs. When the parameter γ is set to 0.5, that is, the task cost and the coverage quality weight are equal, the change of task cost and coverage rate with the number of RSUs and UAVs is tested. The number of UAVs is changed from 2 to 5, and the numbers of RSUs are 30, 50, 70, and 100, respectively. Similarly, the average of 30 convergence results is used as the convergence value. The total cost of each case is shown in Table 4.

It can be seen from Algorithm 1 that when the number of RSUs is 30 and the number of UAVs is 3, the total cost is the smallest and the coverage rate is high. When two UAVs are selected, each UAV needs to collect more RSUs, which makes the task cost maximum. Due to the constraint of energy consumption, the path will ignore more nodes, resulting in lower coverage rate. However, when there are more UAVs, individual UAVs will collect less RSUs and

Table 5: Stability comparison of the four algorithms.

		GA	GWO	WOA	HWGWOA
Scene 1	Worst	47.82	47.40	47.81	45.58
	Best	44.40	43.73	43.83	41.90
	Mean	45.41	44.89	44.62	42.81
	Std	0.77	1.02	0.99	0.84
Scene 2	Worst	61.46	62.17	60.56	55.71
	Best	57.92	56.25	54.93	51.82
	Mean	59.62	58.19	57.26	53.94
	Std	0.96	1.36	1.51	1.04
Scene 3	Worst	76.25	76.41	75.89	74.49
	Best	70.95	69.23	67.36	67.51
	Mean	73.51	72.53	71.37	70.51
	Std	1.43	2.14	2.10	1.69
Scene 4	Worst	87.29	85.93	84.45	82.41
	Best	81.70	78.96	78.87	77.68
	Mean	84.37	82.95	81.57	79.92
	Std	1.38	1.58	1.49	1.18

return to the base station, which greatly increases the energy consumption, resulting in higher task cost, but lower coverage rate. Similarly, when the number of RSUs is 50 and the number of UAVs is 4, the minimum task cost and high coverage rate will be obtained. When the number of RSUs is 70 and the number of UAVs is 4, the mission cost is the lowest and the coverage rate is higher. When the number of RSUs is 100 and the number of UAVs is 5, the mission cost is the lowest and the coverage rate is the highest. Therefore, with the increase in the number of tasks, increasing the number of UAVs appropriately can get lower task cost and higher coverage.

(C) Algorithm convergence comparison

In order to verify the performance of the algorithm, this paper compares the task cost and coverage of genetic algorithm, gray wolf optimization algorithm, and whale optimization algorithm for multi-UAV coassisted RSU data collection. The convergence of the four algorithms in 1000 iterations was tested in the following four scenarios: (1) 30 RSUs and 3 UAVs, (2) 50 RSUs and 4 UAVs, (3) 70 RSUs and 4 UAVs, and (4) 100 RSUs and 5 UAVs. Similarly, the average value of 30 simulations of the algorithm is used as the convergence result. The task cost comparison is shown in Figure 2, and the coverage comparison is shown in Figure 3.

As shown in Figures 2 and 3, HWGWOA achieves lower task cost and higher coverage in the above four scenarios. Specifically, as for task cost, HWGWOA is 9.54% lower than the genetic algorithm, 7.31% lower than the gray wolf algorithm, and 5.8% lower than the whale algorithm; in terms of coverage, HWGWOA is 27.87% higher than the genetic algorithm, 15.19% higher than the gray wolf algorithm, and 9.86% higher than the whale algorithm. In a word, HWGWOA has low task cost compared with the other three algorithms, and it can get more coverage. When the number of RSUs increases, this advantage is more obvious. In order to more intuitively compare the convergence speed and convergence results of the four algorithms, the convergence trends of task cost of the four algorithms in four scenarios are shown in Figure 4.

As shown in Figure 4, in the four scenarios, the HWGWOA acquires a lower task cost and a faster convergence speed. When the task scale is small, this advantage is more obvious. As the task scale increases, it becomes more difficult to solve the problem, and the advantage of the HWGWOA decreases a little.

(D) Stability comparison of four algorithms

Robustness is an important index to evaluate the performance of this kind random search algorithm. Therefore, the robustness of four algorithms is tested in this section. To this end, each algorithm runs for 30 times, and the optimal solution, the worst solution, the average solution, and the variance of the task cost are recorded as shown in Table 5.

As shown in Table 4, the convergence accuracy of genetic algorithm is the worst, but the variance is small, that is, the robustness of the algorithm is good; the convergence accuracy and stability of gray wolf optimization algorithm and whale optimization algorithm are general; HWGWOA is better than the gray wolf optimization algorithm and whale optimization algorithm in convergence accuracy and robustness. When the task scale is small, the robustness is slightly worse than that of the genetic algorithm; with the task size increasing, the robustness of HWGWOA is better when the number of RSUs reaches 100 with the increase in modulus. It can be seen that HWGWOA has better convergence speed and accuracy than the other three algorithms in solving the data acquisition problem of multi-UAV coassisted RSU, and it also has better algorithm robustness, which is more suitable for solving large-scale optimization problems.

6. Conclusion and Further Work

This paper investigated the data acquisition of multi-UAV coassisted RSU in a large-scale scene. First of all, according to the physical constraints and collaborative constraints of UAV, considering the two factors of mission cost and mission coverage quality, a maximum cost minimum coverage model was proposed to seek the solution to obtain the maximum coverage benefit under the premise of minimum mission cost. Then, the HWGWOA was proposed for UAV mission planning. Finally, the HWGWOA was compared with the genetic algorithm, gray wolf optimization algorithm, and whale optimization algorithm. The experimental results show that the HWGWOA has faster convergence speed, better stability, and higher convergence accuracy, and it is more suitable for large-scale optimization problems. In the future work, we are committed to further research from the following aspects: on the one hand, we will solve the real-time replanning problem of multi-UAV cooperative task planning according to the actual constraints; on the other hand, we will consider the multi-UAV cooperative task planning problem under rechargeable conditions.

Data Availability

The raw/processed data required to reproduce these findings cannot be shared at this time as the data also forms part of an ongoing study.

Additional Points

This article is a further expansion based on conference papers. Conference papers consider a smaller task environment and fewer roadside units. In the conference papers, the task distribution and path planning schemes are mainly formulated according to the task set to realize the complete collection of roadside unit data. On this basis, this article considers more realistic large-scale scenarios. In a large-scale data collection scenario, it will take a long time to collect data from all roadside units. Therefore, the number of drones selected will inevitably increase, which will result in high collection costs. In actual scenarios, there are energy consumption and time constraints. As the collection tasks increase, we cannot collect all roadside unit data. At this time, we need to perform partial collection, and the problem is transformed into a scan coverage problem, that is, an incomplete coverage problem. At present, for the scan coverage problem, the coverage rate is generally expressed by the ratio of the number of target points covered to the total number of target points. This is not reasonable in the data collection problem of the roadside unit. In the problem of roadside unit data collection, roadside units deployed in different locations often collect road and traffic information of different data sizes and different degrees of importance in the same time period. This leads to different data collection needs for each node. For example, roadside units deployed near scenic spots, urban main road intersections, near stations, etc., will collect more important and complex data information. On the contrary, a roadside unit deployed on a remote trail will carry less important and less data information. Therefore, this paper proposes a data collection model based on coverage quality while optimizing time and energy consumption. We define it as the minimum cost and maximum coverage problem.

Conflicts of Interest

The authors declare that they have no conflicts of interest.

Acknowledgments

This work was supported by the National Natural Science Foundation of China (61701170), Science and Technology Development Plan of Henan Province (202102210327, 212102210412), and Special Project for Key R&D and Promotion of Science and Technology Department of Henan Province (222102210052, 222102210007, and 222102210062).

References

[1] L. Zhang, C. Huan, R. Wu, and D. Roy, "Joint data collection and fusion using mobile sink in heterogeneous wireless sensor networks," *IEEE Sensors Journal*, vol. 21, no. 2, pp. 2364–2376, 2021.

[2] C. Xu, X. Liao, J. Tan, H. Ye, and H. Lu, "Recent research progress of unmanned aerial vehicle regulation policies and technologies in urban low altitude," *IEEE Access*, vol. 8, pp. 74175–74194, 2020.

[3] L. Cheng, L. Zhong, S. Tian, and J. Xing, "Task assignment algorithm for road patrol by multiple UAVs with multiple bases and rechargeable endurance," *IEEE Access*, vol. 7, pp. 144381–144397, 2019.

[4] P. Sun, A. Boukerche, and Y. Tao, "Theoretical analysis of the area coverage in a UAV-based wireless sensor network," in *2017 13th International Conference on Distributed Computing in Sensor Systems (DCOSS)*, pp. 117–120, Ottawa, ON, Canada, 2017.

[5] Y. Zhao, Z. Zheng, and Y. Liu, "Survey on computational-intelligence-based UAV path planning," *Knowledge-Based Systems*, vol. 158, pp. 54–64, 2018.

[6] C. Yin, Z. Xiao, X. Cao, X. Xi, P. Yang, and D. Wu, "Offline and online search: UAV multi-objective path planning under dynamic urban environment," *IEEE Internet of Things Journal*, vol. 5, no. 2, pp. 546–558, 2017.

[7] J. Li, Y. Xiong, J. She, and M. Wu, "A path planning method for sweep coverage with multiple UAVs," *IEEE Internet of Things Journal*, vol. 7, no. 9, pp. 8967–8978, 2020.

[8] W. Wang, L. Feng, T. Zheng, and Y. Liu, "The sustainability of ecotourism stakeholders in ecologically fragile areas: implications for cleaner production," *Journal of Cleaner Production*, vol. 279, article 123606, 2021.

[9] Y. Wang, X. Wen, Z. Hu et al., "Multi-UAV collaborative data collection for IoT devices powered by battery," in *In 2020 IEEE Wireless Communications and Networking Conference (WCNC)*, Seoul, Korea (South), 2020.

[10] S. Trigui, O. Cheikhrouhou, A. Koubaa, U. Baroudi, and H. Youssef, "FL-MTSP: a fuzzy logic approach to solve the multi-objective multiple traveling salesman problem for multi-robot systems," *Soft Computing*, vol. 21, no. 24, pp. 7351–7362, 2017.

[11] M. Mi, X. Huifeng, Z. Ming, and G. Yu, "An improved differential evolution algorithm for TSP problem," in *2010 International Conference on Intelligent Computation Technology and Automation*, pp. 544–547, Changsha, China, 2010.

[12] X. Duan, H. Liu, H. Tang, Q. Cai, F. Zhang, and X. Han, "A novel hybrid auction algorithm for multi-UAVs dynamic task assignment," *IEEE Access*, vol. 8, pp. 86207–86222, 2020.

[13] Q. Cheng, D. Yin, J. Yang, and L. Shen, "An auction-based multiple constraints task allocation algorithm for multi-UAV system," in *2016 International Conference on Cybernetics, Robotics and Control (CRC)*, Hong Kong, China, 2016.

[14] S. M. S. Poudel and S. Moh, "Hybrid path planning for efficient data collection in UAV-aided WSNs for emergency applications," *Sensors*, vol. 21, no. 8, p. 2839, 2021.

[15] Y. Ma, H. Zhang, Y. Zhang, R. Gao, Z. Xu, and J. Yang, "Coordinated optimization algorithm combining GA with cluster for multi-UAVs to multi-tasks task assignment and path planning," in *2019 IEEE 15th International Conference on Control and Automation (ICCA)*, pp. 1026–1031, Edinburgh, UK, 2019.

[16] X. A. Yang, S. A. Zhu, A. Xx, G. A. Wei, and B. Bp, "A hybrid algorithm based on MOSFLA and GA for multi-UAVs plant protection task assignment and sequencing optimization," *Applied Soft Computing*, vol. 96, no. 4, article 106623, 2020.

[17] F. Ye, J. Chen, Y. Tian, and T. Jiang, "Cooperative multiple task assignment of heterogeneous UAVs using a modified genetic algorithm with multi-type-gene chromosome encoding strategy," *Journal of Intelligent and Robotic Systems*, vol. 100, no. 2, pp. 615–627, 2020.

[18] L. Huo, J. Zhu, G. Wu, and Z. Li, "A novel simulated annealing based strategy for balanced UAV task assignment and path planning," *Sensors*, vol. 20, no. 17, p. 4769, 2020.

[19] P. Stodola, K. Michenka, J. Nohel, and M. Rybansk, "Hybrid algorithm based on ant colony optimization and simulated annealing applied to the dynamic traveling salesman problem," *Entropy*, vol. 22, no. 8, p. 884, 2020.

[20] H. Xiao, Z. Hu, K. Yang, Y. Du, and D. Chen, "An energy-aware joint routing and task allocation algorithm in MEC systems assisted by multiple UAVs," in *2020 International Wireless Communications and Mobile Computing (IWCMC)*, pp. 1654–1659, Limassol, Cyprus, 2020.

[21] M. Wang, T. Ma, G. Li, X. Zhai, and S. Qiao, "Ant colony optimization with an improved pheromone model for solving MTSP with capacity and time window constraint," *IEEE Access*, vol. 8, pp. 106872–106879, 2020.

[22] L. Lu and T. Yue, "Mission-oriented ant-team ACO for min-max MTSP," in *2017 International Conference on Information, Communication and Engineering (ICICE)*, pp. 522–525, Xiamen China, 2017.

[23] X. Hou, Z. Ren, J. Wang, S. Zheng, and H. Zhang, "Latency and reliability oriented collaborative optimization for multi-UAV aided mobile edge computing system," in *IEEE INFOCOM 2020-IEEE Conference on Computer Communications Workshops (INFOCOM WKSHPS)*, pp. 150–156, Toronto, ON, Canada, 2020.

[24] X. Chen, Y. Liu, L. Yin, and L. Qi, "Cooperative task assignment and track planning for multi-UAV attack mobile targets," *Journal of Intelligent and Robotic Systems*, vol. 100, no. 3, pp. 1383–1400, 2020.

[25] K. Li, F. Ge, Y. Han, Y. Wang, and W. Xu, "Path planning of multiple UAVs with online changing tasks by an ORPFOA algorithm," *Engineering Applications of Artificial Intelligence*, vol. 94, article 103807, 2020.

[26] X. Zhang and X. Chen, "UAV task allocation based on clone selection algorithm," *Wireless Communications and Mobile Computing*, vol. 2021, Article ID 5518927, 9 pages, 2021.

[27] X. Zhang and X. Chen, "Solving "limited" task allocation problem for UAVs based on optimization algorithms," *Wireless Communications and Mobile Computing*, vol. 2021, Article ID 5530454, 14 pages, 2021.

[28] S. M. Ahmadi, H. Kebriaei, and H. Moradi, "Constrained coverage path planning: evolutionary and classical approaches," *Robotica*, vol. 36, no. 6, pp. 904–924, 2018.

[29] D. Zhu, X. Cao, B. Sun, and C. Luo, "Biologically inspired self-organizing map applied to task assignment and path planning of an AUV system," *IEEE Transactions on Cognitive and Developmental Systems*, vol. 10, no. 2, pp. 304–313, 2018.

[30] Z. Fang, J. Wang, J. Du, X. Hou, Y. Ren, and Z. Han, "Stochastic optimization aided energy-efficient information collection in internet of underwater things networks," *IEEE Internet of Things Journal*, vol. 9, no. 3, pp. 1775–1789, 2022.

[31] Z. Fang, J. Wang, C. Jiang, Q. Zhang, and Y. Ren, "AoI-inspired collaborative information collection for AUV-assisted Internet of underwater things," *IEEE Internet of Things Journal*, vol. 8, no. 19, pp. 14559–14571, 2021.

[32] N. Motlagh, M. Bagaa, and T. Taleb, "Energy and delay aware task assignment mechanism for UAV-based IoT platform," *IEEE Internet of Things Journal*, vol. 6, no. 4, pp. 6523–6536, 2019.

[33] A. Sm, B. Smm, and A. Al, "Grey wolf optimizer," *Advances in Engineering Software*, vol. 69, pp. 46–61, 2014.

[34] S. Mirjalili and A. Lewis, "The whale optimization algorithm," *Advances in Engineering Software*, vol. 95, pp. 51–67, 2016.

[35] X. Yi, "Hash function based on chaotic tent maps," *IEEE Transactions on Circuits and Systems II: Express Briefs*, vol. 52, no. 6, pp. 354–357, 2005.

[36] X. U. Chenhua, L. I. Chengxian, Y. U. Xin, and Q. Huang, "Improved grey wolf optimization algorithm based on chaotic Cat mapping and Gaussian mutation," *Computer Engineering and Applications*, vol. 53, no. 4, pp. 1–9, 2017.

[37] B. V. Natesha, N. Kumar Sharma, S. Domanal, and R. M. Reddy Guddeti, "GWOTS: greywolf optimization based task scheduling at the green cloud data center," in *2018 14th International Conference on Semantics, Knowledge and Grids (SKG)*, pp. 181–187, Guangzhou, China, 2018.

[38] X. Chen, L. Cheng, C. Liu et al., "A WOA-based optimization approach for task scheduling in cloud computing systems," *IEEE Systems Journal*, vol. 14, no. 3, pp. 3117–3128, 2020.

Hindawi
Wireless Communications and Mobile Computing
Volume 2022, Article ID 1194899, 26 pages
https://doi.org/10.1155/2022/1194899

Research Article

Detection and Blockchain-Based Collaborative Mitigation of Internet of Things Botnets

Syed Muhammad Sajjad,[1] Muhammad Rafiq Mufti,[2] Muhammad Yousaf,[1] Waqar Aslam,[3] Reem Alshahrani,[4] Nadhem Nemri,[5] Humaira Afzal,[6] Muhammad Asghar Khan,[7] and Chien-Ming Chen[8]

[1]*Riphah Institute of Systems Engineering, Riphah International University, Islamabad 45320, Pakistan*
[2]*Department of Computer Science, COMSATS University Islambad, Vehari Campus, 61100, Pakistan*
[3]*Department of Computer Science & Information Technology, The Islamia University of Bahawalpur, 63100, Pakistan*
[4]*Department of Computer Science, College of Computers and Information Technology, Taif University, P.O.Box 11099, Taif 21944, Saudi Arabia*
[5]*Department of Information Systems, College of Science and Arts at Mahayil, King Khalid University, Muhayel Aseer, Saudi Arabia*
[6]*Department of Computer Science, Bahauddin Zakariya University, Multan 60822, Pakistan*
[7]*Hamdard Institute of Engineering & Technology, Islamabad, Pakistan*
[8]*College of Computer Science and Technology, Shandong University of Science and Technology, Shandong, China*

Correspondence should be addressed to Chien-Ming Chen; chienmingchen@ieee.org

Received 5 February 2022; Revised 22 March 2022; Accepted 30 March 2022; Published 20 April 2022

Academic Editor: Farhan Ullah

DDoS (distributed denial of service) attacks have drastically effected the functioning of Internet-based services in recent years. Following the release of the Mirai botnet source code on GitHub, the scope of these exploitations has grown. The attackers have been able to construct and launch variations of the Mirai botnet thanks to the open-sourcing of the Mirai code. These variants make the signature-based detection of these attacks challenging. Moreover, DDoS attacks are typically detected and mitigated reactively, making DDoS mitigation solutions very expensive. This paper presents a proactive IoT botnet detection system that detects the anomalies in the behavior of the IoT device and mitigates the DDoS botnet exploitation at the source end, which makes our proposal a low-cost solution. Further, this paper uses a collaborative trust relationship-based threat intelligence-sharing mechanism to prevent other IoT devices from being compromised by the detected botnet. The researchers have evaluated the collaborative threat intelligence sharing mechanism using Ethereum Virtual Machine and Hyperledger. The performance of our proposed system can detect 97% of the Mirai botnet attack activities. Furthermore, our collaborative threat intelligence sharing mechanism based on the Ethereum Virtual Machine showed more scalability.

1. Introduction

Due to the advancements in microelectromechanical systems (MEMS), wireless technologies, microservices, and the Internet, IoT has evolved rapidly in recent times, anything connected to the Internet, a ubiquitous device, for example, a heart monitor or health monitoring sensors implanted in a person or biochip transponders implanted in animals in a form [1]. The ample space of IP address due to IPv6 is one of the essential factors in the massive development of the Internet of Things [2]. IoT applications can be found in energy, transportation, health care, building management, cattle farms, and agriculture.

Other than trend-setters, architects, sellers, and clients, IoT has too pulled into consideration of assailants. These IoT devices are generally set up with fewer security controls. This inborn imperfection has made the IoT millions of insecure devices [3]. The more significant volume of the Web of

Things makes its assault surface more noteworthy [4, 5]. Time to showcase, low-cost thought, and the need for related security regulations have empowered vendors to make less secure gadgets. Security specialists have, numerous times, issued notices concerning the utilization of these less ensured gadgets [6].

Numerous hosts and autonomous systems attacked GitHub with a 1.35 Tbps attack in February 2018 [7]. In May 2018, malware infecting particular network-attached storage devices and home routers was identified as "VPNFilter." This malware has affected around 500,000 home routers worldwide [8–10]. The exploitation of these insecure IoT devices for initiating well-coordinated Distributed Denial of Service (DDoS) was attacked by Mirai malware in October 2016. Such kinds of attacks affect user trust in adopting the IoT paradigm. After the Mirai malware source code release, many Mirai malware variants were authored by black hat hackers.

Traditional detection and mitigation of DDoS are carried out at the destination of the attack. However, enterprises are deploying costly and complicated solutions for DDoS protection to continue their core business processes. Therefore, there is a limitation in detecting and mitigating DDoS at the destination end.

1.1. Research Motivation. Collaborative security is a technique that is characterized by many vital features, including "collective responsibility" and "think globally, act locally" [11]. Different players, manufacturers, and vendors should collaborate by sharing attack knowledge to provide proactive detection and real-time mitigation of attacks. They also have a significant role in the mitigation and prevention of botnets. They are well placed to identify malicious activities produced by infected systems and subsequently separate them from the network to safeguard the system. However, detecting and stopping a single source of DDoS attack traffic is not sufficient.

This paper presents detection and a collaborative mitigation system for the Mirai IoT type of malware. The main contributions of this paper are the following:

(i) Based on the performed Mirai malware analysis, this paper presented a model for detecting the attempts of device compromise and subsequent installation of the malware binaries on it

(ii) This research proposed a mitigation mechanism that prevents a device from becoming a part of the Mirai type of botnets

(iii) This paper also proposed a collaborative mitigation mechanism for threat intelligence sharing among trusted peers. This paper used smart contracts and blockchain-based methodologies for trust establishment and collaboration that helped implement the proactive defense mechanism against the IoT botnets

The remaining of the paper is structured as follows. Section 2 discusses the existing state of the art. Section 3 is about the threat model, and it includes an analysis of the complete functionality of Mirai malware, command and control server, its scanning for vulnerable devices as potential bot targets, and malware loading process on these vulnerable devices. Section 4 elaborates on the particulars of the proposed detection system. Section 5 contains the specifics of the anticipated collaborative mitigation system. Implementation and deployment specifications are presented in Section 6. Section 7 provides results and analysis of both detection and mitigation systems. Finally, Section 8 concludes the paper.

1.2. Significance of Work. Significance and potential benefits of this work are the following:

(i) IoT malware attack can be detected at its source end

(ii) Timely informing the network administrator of the compromised device during the attack

(iii) Availability of a mechanism for sharing the attacker information with the peers in a proactive way

(iv) Significant addition in the enhancement of the security and sustainability of the global Internet

(v) Significant addition in the enhancement of the consumer trust on the Internet of Things

2. Related Work

In recent times, IoT security has been a popular area of research. This study divided the related work section into two subsections for a focused discussion. The first subsection discusses the approaches related to IoT botnet detection, and the second subsection discusses the collaborative mitigation approaches and their limitations.

2.1. IoT Botnet Detection. Due to diverse reasons, from comparatively fewer computing capabilities to the pressure on the market, there has been a trend to ship and deploy the IoT devices and applications with less secure security controls. Security researchers in academia [12] and industry [13, 14] have been identifying the severe risks associated with this trend of negligence in IoT security [15].

There have been numerous honeypot-based IoT botnet detection efforts. Pa et al. [16] proposed the IoT honeypot. Another attempt in this regard is [17]. These are low-interaction honeypots, an emulated package that provides the attacker with a limited level of interaction and is of little use for the practical deployments in the IoT devices.

Numan et al. discussed that DDoS mitigation solutions at the service provider's end have many business advantages for Internet service providers. In this way, not only ISPs can safeguard themselves from DDoS attacks, but they also can offer DDoS mitigation protection to their customers, leading to secure and reliable Internet services [18]. However, these solutions are costly and protect DDoS at its destination end rather than the source end. Therefore, ISP-based DDoS detection and mitigation solutions that block the CNC during the IoT Botnet propagation stage before the launch of

actual DDoS are more effective. Therefore, there is a need for such kinds of solutions.

There have been some efforts on the DDoS preventive techniques in the Internet of Things [19]. For example, Dao et al. proposed to install Smart filters at the edge of the attack source or destination. A central controller is deployed, performing coordination among the smart filters. The main controller restricts each smart filter by adopting suitable parameters into its self-organizing map module, built on the attacking behavior. However, the proposed solution fails to define how to identify the source of the attack. Moreover, the complexity of the proposed method made it unsuitable for smart home and smart office scenarios.

An access control mechanism, Manufacturer Usage Description (MUD) enables functional correctness to devices [20, 21]. MUD profiles are available on MUD servers openly. The MUD profile consists of private consumer information. Therefore, there is a chance of leakage of the consumer's data.

Furthermore, a compromised device might direct toward an illegitimate or corrupted profile as the MUD's DHCP and LLDP methods do not authenticate the device. MUD standard suggests the use of an X.509 extension. However, most Internet of Things home gateways and WiFi access routers do not possess X.509 certification. The deployment of the proposed MUD solution is based and dependent on the manufacturer of the devices. The implementation of the defense solution must not be dependent on the manufacturer. Consumers and users must be capable of deploying the defense solution independently.

Heimdal is an intrusion detection solution based on the principle of whitelisting aimed at the IoT devices [22]. It can operate on gateway routers and offer protection to all the devices behind the gateway router. It is continually applied on every device present in the network. Although the whitelisting-based mechanism proposed in Heimdal produces good results, the limitation of this approach is its reliance on VirusTotal, which would hinder the detection of zero-day malware.

A collaborative defense scheme to confront Mirai is proposed by [23]. The authors deployed a white Mirai, which expels the Mirai malware and blocks the communication ports in case of a Mirai attack. Although collaborative defense mechanisms are more productive, yet these solutions have shortcomings. The limitation of this scheme is that it only defeats the original Mirai malware. Furthermore, the Mirai variant may use other ports and vulnerabilities. Therefore, there is a need for a collaborative defense scheme to detect any Internet of Things malware.

A SIEM-based system for the accurate identification of malicious activities in the Internet of Things is proposed [24]. The authors discuss vulnerabilities presented in IoT devices. The detection of malicious activities in IoT devices is detected using SIEM. However, SIEM deployment for IoT devices in the smart home scenario is costly and not cost-effective. Moreover, the integrity of the security events generated by SIEM is critical. Its alteration would lead to the generation of false alarms. Also, a centralized design for detecting abnormalities in IoT systems creates a single point of failure and attack.

An e-MUD for IoT botnets prevention on home WiFi routers is presented in [25]. As MUD does not consider identifying and patching vulnerabilities present in the device before the issuance of the MUD profile, a device can be compromised even in the presence of the Manufacturer Usage Description profile by exploiting either the configuration vulnerabilities or firmware vulnerabilities present in the device. E-MUD presents an evaluation study of the Manufacturer Usage Description (MUD), identifies its weaknesses, and proposed enhancements in its architecture. It proposed a mechanism for identifying and eliminating the configuration vulnerabilities before creating the MUD profile for a device to minimize the attack surface. The authors adopt the OWASP firmware testing methodology for discovering vulnerabilities in the firmware of WiFi home routers. The device is allowed to request the MUD profile only if the identified firmware vulnerabilities are low. A Usage, Communication and Access Monitoring Based Botnets Detection System for IoT is proposed in [26] . The proposed solution has three main components, i.e., descriptor, monitor, and comparator. Descriptor defines device usage, communication, and access policies. Monitor observes the current state of device usage, communication, and access. Anomalies are detected by the comparator. Results show that the proposed detection system successfully detects Mirai IoT malware.

2.2. Collaborative Mitigation Approaches. The faith that sharing security attack evidence amongst systems would enhance the general protective position of the public is gaining popularity. For example, during the post-Morris Worm attack, the government of the US made CERT. Similarly, PDD-63 made ISACs help fight the perceived cyber threats [27]. Gordon et al. assessed the state of attacker information sharing and presented an economic incentive-based prototype that broke down the managerial expense [28]. This effort was then extended by Gal-Or et al. by utilizing game theory to assess the demand-side consequences happening underneath the existing sharing model [29]. The two works lay the foundation for understanding the advantages of sharing. In particular, sharing gives expected benefits to security and cost savings [30].

The most promising cyber threat intelligence standards in the market today are the Trusted Automated Exchange of Indicator Information (TAXII) [31] and Structured Threat Information Expression (STIX) [32]. STIX and TAXII are open community efforts that are continually developing. The MITRE Corporation initially served on behalf and under the sponsorship of the US Homeland Security Department as the creator and moderator of both the STIX and TAXII communities. The US Homeland Security Department, in 2015, moved STIX and TAXII for further development to the OASIS Cyber Threat Intelligence Technical Committee (OASIS CTI TC). Today, STIX and TAXII are widely discussed in the community.

Moreover, they have already incorporated many platforms and tools, making them a de facto standard for threat sharing to achieve collaborative mitigation. The main drawback of the TAXII STIX combination is its inability to establish trust between the receiver and the sender of the threat

data. Trust establishment between the peers before threat information sharing is one of the main requirements for threat data sharing to achieve successful collaborative mitigation.

Fidelis Barncat [33] is a threat intelligence database for sharing attacker information. It offers a tight security package that automates, correlates, orchestrates, and integrates metadata from across the network, endpoint, and trickery defenses to help the user swiftly detect, chase, and respond with accuracy to threats. There are privacy issues in the threat feed of Fidelis Barncat. The feed contains private information about the victim. The data generated during the decompilation of the virus includes victim server info: FTP hosts, FTP passwords, usernames, IPs, and passwords of the victim organization. In addition, the threat data contains an attack pattern and hashes. This situation leads to a none GDPR compliant environment. None GDPR compliance may harm the sender of the threat feed [34].

Such issues hamper the user's trust in sharing threat data to achieve collaborative mitigation. The reasons of lack of coordinated efforts in threat intelligence sharing are listed below:

(i) Privacy and secrecy of security posture of the victim [35]

(ii) Tradecraft on victim data by attacker [36, 37]

(iii) Lack of structure and context of the shared data [38]

(iv) The nonexistence of pertinent records [39]

(v) Lack of motivations [40]

Altogether, these points of interest create a climate where people and organizations are reluctant to share threat data. If sharing takes place, the realities are uncovered so that the moment noteworthiness gets to be far-fetched. Unfortunately, this ends in a worldview where conceivably fundamental focuses that can halt dangers frequently, by no implies, reach the imminent peers in time.

The transparency and security features provided by the blockchain can enhance cybersecurity issues. They can connect devices in a decentralized manner employing digital signatures.

This decentralized establishment reduces the chance of attack initialization from a central point for the attacker. Once an assault happens, the information concerning the occurrence can be unnoticed, jumbled, and complex. However, blockchain can proficiently outline what takes place.

During the recent years, few research initiatives have aimed for a reliable framework that considers the issues occurring during threat sharing [41–47]. This has led to blockchain-based approaches, but still none is comprehensive enough.

3. Threat Model

Recent past cyber-attacks demonstrate that susceptibilities present in IoT devices are exploited for initiating DDoS. After compromising the IP cameras, DVRs, and WiFi access routers, Mirai malware launches nine different types of attacks: UDP flood, SYN flood, ACK flood, TCP stomp flood, Valve source engine specific flood, GRE IP flood, GRE Ethernet flood, HTTP flood, and DNS water torturing. Figure 1 shows the infection process of Mirai malware, and Figure 2 elaborates on the details of the analysis of the functionality flow of the Mirai botnets. Scanner server is responsible for scanning vulnerable devices, brute-forcing the device password, and reporting them to loader server.

The command and control server collaborates with human operators, allowing them to govern the botnets, connected to a database, and provisions three kinds of performers, each permitted to execute different procedures: admin, user, and bot. In addition, the command and control server runs two services, rental services on port 101 and master services listening on port 23.

3.1. Mirai Malware Components. Mirai bot operates on compromised and infected devices. It has three submodules, namely, "scanner," "killer," and "attacker." The "scanner" module is responsible for scanning for new vulnerable devices and finding any weak device, directing the scan result to the "reporting server." The "killer" module is in charge of finding and killing other malware running on the compromised machine. The 'Attacker' component performs the actual DDoS attack; it receives the attack command from the command and control server. On execution, the bot deletes itself, rewrites function pointers, changes code execution and process name, and connects to the CNC server. The reporting server receives scan results of vulnerable devices from the scanner server and newly compromised devices (bots) and forwards them to the loader server. The loader server transfers the Mirai malware binaries to susceptible devices, making them bots, consequently making them part of the botnet.

3.2. Mirai Malware Functionality. The Mirai CNC initially scans several IP addresses to discover susceptible devices. In the second phase, the pool of the Internet Protocol (IP) addresses of the susceptible devices are transferred to the loader server, which loads the Mirai malware on the reported vulnerable IoT devices for making bots. Malware is a malicious program that is implemented on infested devices. As a next step, malware eliminates itself from the infected machine, altering its surname to a random value. Afterwards, it attempts to shelter itself from any rival malware by a background killer process, which destroys competing worms that ultimately belong to the same device. It also prevents everybody from breaking using additional conventional means, such as Telnet, SSH, or HTTP. The main objective of this action is to extend the attack perspective of every device, making sure the complete readiness of all its computational means for the attack. As a final point, it drives into the main lead implementation phase. This round establishes a connection with the CNC server and keeps it active, waiting for attack instructions. In case it receives an attack command, the bot accomplishes the attack. Next, the bot must complete a domain resolution to connect to the reporting server or main command and control server

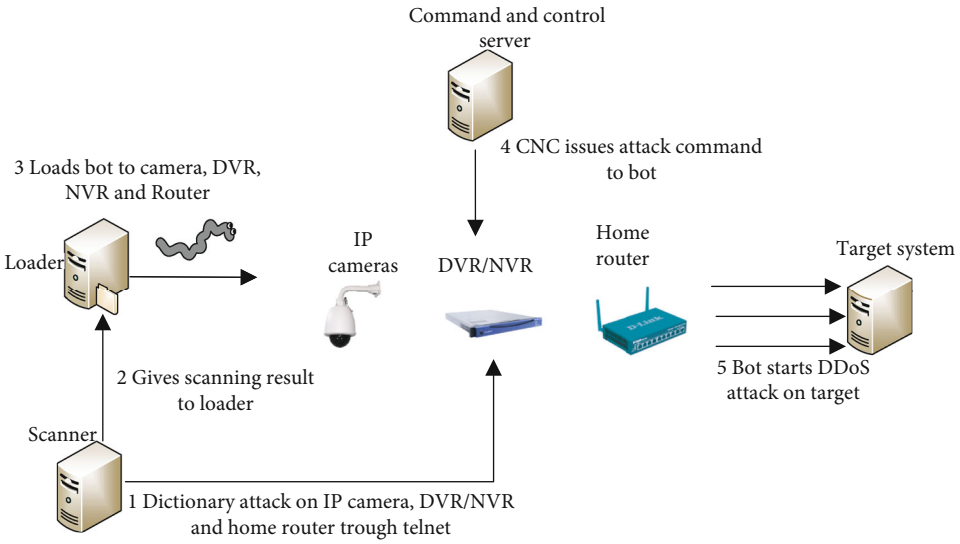

Figure 1: Compromising and exploiting IoT devices for launching DDoS attack.

by getting the corresponding IP address. The process-wise functionality of Mirai malware is given below:

(1) Mirai scanner scans for vulnerable devices

(2) Mirai scanner pass on scans results to loader server

(3) Loader server loads Mirai malware on vulnerable devices

(4) Vulnerable devices act as a bot after Mirai malware is loaded on it

(5) The bot then kills its competitor

(6) The bot starts scanning for more vulnerable devices

(7) It reports new bots to the loader server

(8) The CNC issues the attack commands

(9) Bot initiates DDoS attacks on the destination

4. The Proposed IoT Botnet Detection System

IoT devices are typically run on specific applications and constitute a network generally termed as a stub network. These devices have well-defined access, communication, and usage. Furthermore, the network administrator these devices are deployed has full authorized access to these devices. Let us consider installing a temperature sensor to pick up the room temperature and transfer the sensed information to the database system to comprehend this concept. In this case, the sensing temperature of the room is the usage of the IoT device, sending sensed data to the database machine is the predefined communication of the IoT device, and the network administrator of the network in which these IoT devices are part has authorized access to these devices. This research proposes a botnet detection solution for the IoT based on the above-explained principle. The proposed botnet detection solution is presented in Figure 3.

The suggested detection technique has a policy descriptor that refers to the device's predefined policies for access, communication, and usage. Another component is the policy monitor, whose first job is to observe the present state of access on the device, communication of the device, and device usage. The comparator matches the current access, communication, and usage with predefined access, communication, and usage policies. If immediate access to the device, communication pattern of the device, and usage of the device fit according to the predefined rules, the behavior is called normal. If there is a disparity, the behavior is called attack behavior. The attack classifier categorizes attack behavior as one of the following violations: access policy, communication policy, and usage policy. The access, communication, and usage monitor report these violations of the predefined policies. At this point, the botnet detection scheme produces alarms to network administrators.

4.1. System Model. In the proposed botnet detection system, a B number of nodes are in the network. The number of nodes present in a local network is presented as $B = \{b_0, b_1, b_2 \cdots \cdots b_n\}$. A node b_0 observes its neighbouring nodes. The neighbours of b_0 is a set of nodes having one-hop contact with node b_0 and are represented as $N_b(b_0) = \{b_1, b_2 \cdots \cdots b_n\}$. Every node b_i possesses different attributes. The set of attributes of the node b_i can be denoted as $A_{b_i} = \{a_1 \cdots \cdots a_m\}$. The node b_0 observes the activity of the node b_i by observing its attributes. If node b_0 observes its neighbouring nodes $N_i(b_0) = \{b_1 \cdots \cdots b_n\}$, it stores the set of the corresponding attribute vectors $A_{N_b(b_0)} = \{a_{b_1} \cdots \cdots a_{b_m}\}$. This can be represented in matrix form as follows.

$$A_{N_b(b_o)} = \begin{pmatrix} a_{b_{11}} & a_{b_{12}} & \cdots & a_{b_{1m}} \\ a_{b_{21}} & a_{b_{22}} & \cdots & a_{b_{2m}} \\ \vdots & \vdots & \vdots & \vdots \\ a_{b_{n1}} & a_{b_{n2}} & \cdots & a_{b_{nm}} \end{pmatrix}. \quad (1)$$

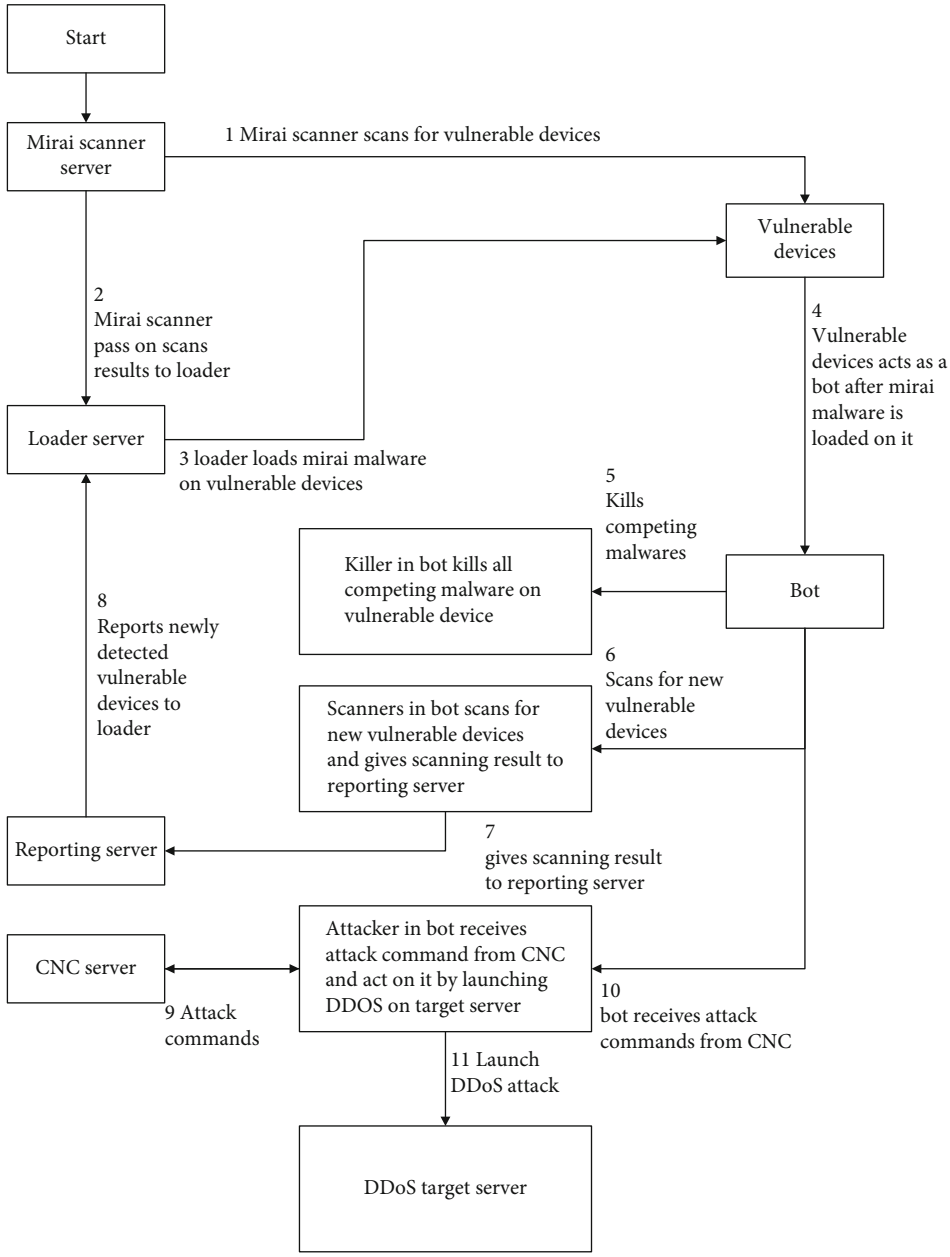

Figure 2: Analysis of functionality flow of Mirai.

More precisely, the attributes of any node include access policy access_{b_0}, communication policy com_{b_0}, and usage policy usg_{b_0}. These are generic attributes and can be of homogenious and hetrogenious setup. The set of defined access attributes vector ADb_0 can be represented in matrix form as follows.

$$AccessD_{N_b(b_o)} = \begin{pmatrix} accessD_{b_{11}} & \cdots & accessD_{b_{1m}} \\ accessD_{b_{21}} & \cdots & accessD_{b_{2m}} \\ \vdots & \vdots & \vdots \\ accessD_{b_{n1}} & \cdots & accessD_{b_{nm}} \end{pmatrix}. \quad (2)$$

The set of current access attributes vector AccessCb_0 can be represented in matrix form as follows.

$$AccessC_{N_b(b_o)} = \begin{pmatrix} accessC_{b_{11}} & \cdots & accessC_{b_{1m}} \\ accessC_{b_{21}} & \cdots & accessC_{b_{2m}} \\ \vdots & \vdots & \vdots \\ accessC_{b_{n1}} & \cdots & accessC_{b_{nm}} \end{pmatrix}. \quad (3)$$

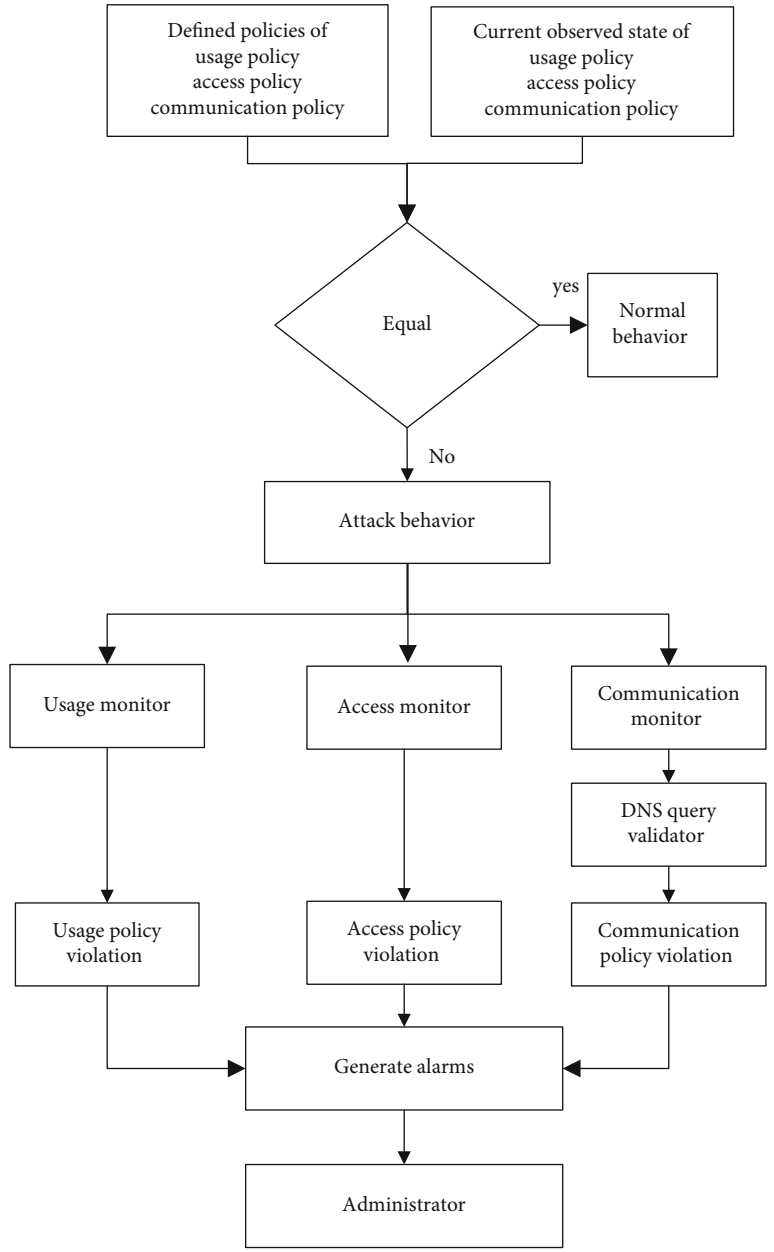

FIGURE 3: The flow of the proposed IoT botnets detection system.

The set of defined communication attributes vector com D_{b_0} can be represented in matrix form as follows.

$$ComD_{N_b(b_o)} = \begin{pmatrix} comD_{b_{11}} & comD_{b_{12}} & \cdots & comD_{b_{1m}} \\ comD_{b_{21}} & comD_{b_{22}} & \cdots & comD_{b_{2m}} \\ \vdots & \vdots & \vdots & \vdots \\ comD_{b_{n1}} & comD_{b_{n2}} & \cdots & comD_{b_{nm}} \end{pmatrix}. \tag{4}$$

The set of current communication attributes vector com C_{b_0} can be represented in matrix form as follows.

$$ComC_{N_b(b_o)} = \begin{pmatrix} comC_{b_{11}} & comC_{b_{12}} & \cdots & comC_{b_{1m}} \\ comC_{b_{21}} & comC_{b_{22}} & \cdots & comC_{b_{2m}} \\ \vdots & \vdots & \vdots & \vdots \\ comC_{b_{n1}} & comC_{b_{n2}} & \cdots & comC_{b_{nm}} \end{pmatrix}. \tag{5}$$

4.2. Detection of Access Policy Violation. Let AccessCb_i is the current access control attribute of the node b_i observed by its neighbouring nodes $N_i(b_i) = \{b_1 \cdots \cdots b_n\}$ during time interval t and AccessDb_i is the Access control of node b_i in the defined access policy. At any instant t, if the current access control AccessCb_i is the same as AccessDb_i defined in policies, node access control behaviour is normal. Mathematically

$$AccessCb_i == AccessDb_i \begin{pmatrix} accessC_{b_{11}} & accessC_{b_{12}} & \cdots & accessC_{b_{1m}} \\ accessC_{b_{21}} & accessC_{b_{22}} & \cdots & accessC_{b_{2m}} \\ \vdots & \vdots & \vdots & \vdots \\ accessC_{b_{n1}} & accessC_{b_{n2}} & \cdots & accessC_{b_{nm}} \end{pmatrix} == \begin{pmatrix} accessD_{b_{11}} & accessD_{b_{12}} & \cdots & accessD_{b_{1m}} \\ accessD_{b_{21}} & accessD_{b_{22}} & \cdots & accessD_{b_{2m}} \\ \vdots & \vdots & \vdots & \vdots \\ accessD_{b_{n1}} & accessD_{b_{n2}} & \cdots & accessD_{b_{nm}} \end{pmatrix}. \tag{6}$$

For any node b_i, if both AccessCb_i and AccessDb_i are not equal, then the behaviour is termed as access policy violation. Mathematically

$$\text{AccessCb}_i \neq \text{AccessCb}_i \begin{pmatrix} accessC_{b_{11}} & accessC_{b_{12}} & \cdots & accessC_{b_{1m}} \\ accessC_{b_{21}} & accessC_{b_{22}} & \cdots & accessC_{b_{2m}} \\ \vdots & \vdots & \vdots & \vdots \\ accessC_{b_{n1}} & accessC_{b_{n2}} & \cdots & accessC_{b_{nm}} \end{pmatrix} \neq \begin{pmatrix} accessD_{b_{11}} & accessD_{b_{12}} & \cdots & accessD_{b_{1m}} \\ accessD_{b_{21}} & accessD_{b_{22}} & \cdots & accessD_{b_{2m}} \\ \vdots & \vdots & \vdots & \vdots \\ accessD_{b_{n1}} & accessD_{b_{n2}} & \cdots & accessD_{b_{nm}} \end{pmatrix}. \tag{7}$$

The detection system generates an alarm and sends it to the network administrator.

4.3. Detection of Communication Policy Violation. Let comCb_i is the current communication attribute of the node b_i observed by its neighbouring nodes $N_i(b_0) = \{b_1 \cdots \cdots b_n\}$ during time interval t and comDb_i is the communication attribute of the node b_i in the defined communication policy. At any instant t, if the current communication policy comCb_i is the same as comDb_i defined in policies, node communication is normal. Mathematically

$$comCb_i == comDb_i \begin{pmatrix} comC_{b_{11}} & comC_{b_{12}} & \cdots & comC_{b_{1m}} \\ comC_{b_{21}} & comC_{b_{22}} & \cdots & comC_{b_{2m}} \\ \vdots & \vdots & \vdots & \vdots \\ comC_{b_{n1}} & comC_{b_{n2}} & \cdots & comC_{b_{nm}} \end{pmatrix} == \begin{pmatrix} comD_{b_{11}} & comD_{b_{12}} & \cdots & comD_{b_{1m}} \\ comD_{b_{21}} & comD_{b_{22}} & \cdots & comD_{b_{2m}} \\ \vdots & \vdots & \vdots & \vdots \\ comD_{b_{n1}} & comD_{b_{n2}} & \cdots & comD_{b_{nm}} \end{pmatrix}. \tag{8}$$

For any node b_i, if both comCb_i and comDb_i are not equal, then the behavior is termed as communication policy violation. Mathematically

$$comCb_i \neq comDb_i \begin{pmatrix} comC_{b_{11}} & comC_{b_{12}} & \cdots & comC_{b_{1m}} \\ comC_{b_{21}} & comC_{b_{22}} & \cdots & comC_{b_{2m}} \\ \vdots & \vdots & \vdots & \vdots \\ comC_{b_{n1}} & comC_{b_{n2}} & \cdots & comC_{b_{nm}} \end{pmatrix} \neq \begin{pmatrix} comD_{b_{11}} & comD_{b_{12}} & \cdots & comD_{b_{1m}} \\ comD_{b_{21}} & comD_{b_{22}} & \cdots & comD_{b_{2m}} \\ \vdots & \vdots & \vdots & \vdots \\ comD_{b_{n1}} & comD_{b_{n2}} & \cdots & comD_{b_{nm}} \end{pmatrix}. \tag{9}$$

The detection system generates an alarm and sends it to the network administrator.

4.4. Detection of Usage Policy Violation. Let usgCb_i is the current usage attribute of the node b_i observed by its neighbouring nodes $N_i(b_0) = \{b_1 \cdots \cdots b_n\}$ during time interval t and usgDb_i is the usage attribute of the node b_i in the defined usage policy. At any instant t, if the current usage

policy usgCb_i is same as usgDb_i defined in policies, node usage is normal. Mathematically

$$\text{usgCb}_i == \text{usgDb}_i \begin{pmatrix} \text{usgC}_{b_{11}} & \text{usgC}_{b_{12}} & \cdots & \text{usgC}_{b_{1m}} \\ \text{usgC}_{b_{21}} & \text{usgC}_{b_{22}} & \cdots & \text{usgC}_{b_{2m}} \\ \vdots & \vdots & \vdots & \vdots \\ \text{usgC}_{b_{n1}} & \text{usgC}_{b_{n2}} & \cdots & \text{usgC}_{b_{nm}} \end{pmatrix}$$
$$== \begin{pmatrix} \text{usgD}_{b_{11}} & \text{usgD}_{b_{12}} & \cdots & \text{usgD}_{b_{1m}} \\ \text{usgD}_{b_{21}} & \text{usgD}_{b_{22}} & \cdots & \text{usgD}_{b_{2m}} \\ \vdots & \vdots & \vdots & \vdots \\ \text{usgD}_{b_{n1}} & \text{usgD}_{b_{n2}} & \cdots & \text{usgD}_{b_{nm}} \end{pmatrix}. \tag{10}$$

For any node b_i, if both usgCb_i and usgDb_i are not equal, then the behaviour is termed as usage policy violation. Mathematically

$$\text{comCb}_i \neq \text{comDb}_i \begin{pmatrix} \text{usgC}_{b_{11}} & \text{usgC}_{b_{12}} & \cdots & \text{usgC}_{b_{1m}} \\ \text{usgC}_{b_{21}} & \text{usgC}_{b_{22}} & \cdots & \text{usgC}_{b_{2m}} \\ \vdots & \vdots & \vdots & \vdots \\ \text{usgC}_{b_{n1}} & \text{usgC}_{b_{n2}} & \cdots & \text{usgC}_{b_{nm}} \end{pmatrix}$$
$$\neq \begin{pmatrix} \text{usgD}_{b_{11}} & \text{usgD}_{b_{12}} & \cdots & \text{usgD}_{b_{1m}} \\ \text{usgD}_{b_{21}} & \text{usgD}_{b_{22}} & \cdots & \text{usgD}_{b_{2m}} \\ \vdots & \vdots & \vdots & \vdots \\ \text{usgD}_{b_{n1}} & \text{usgD}_{b_{n2}} & \cdots & \text{usgD}_{b_{nm}} \end{pmatrix}. \tag{11}$$

The detection system generates an alarm and sends it to the network administrator.

4.5. Explicit Notification of Device Health State to Network Administrator. The detection system periodically reports the health status of devices to the network administrator. If the network administrator does not get an explicit notification from the detection system, they assume that all the devices in the network are either under attack or have been compromised. In that case, it reboots all the devices in the network.

4.6. Local Mitigation Actions. The detection system initializes the local mitigator. Then, it performs the following three main tasks.

(i) Change device credentials: The attacker gets access to the device by successfully brute-forcing the device login credentials. The local mitigator changes the device login credentials and informs the network administrator about the new access credentials as a first defensive measure

(ii) Block attacker domain and IPs address access to devices: Local mitigator blocks access of the identified "command and control" server's domain and IPs to devices in the network

(iii) Reboot the device: The Internet of Things malware resides in volatile memory. Rebooting the device would remove the malware from the device. Instead, the local mitigator reboots the infected devices to abolish Mirai from devices

5. Proposed Collaborative IoT Botnets Mitigation System

The proposed collaborative mitigation system is depicted in Figures 4 and 5. Table 1 illustrates the mathematical notations used in the collaborative mitigation system. In the suggested collaborative mitigation technique, members in the blockchain-based smart contract agree to share attacker information to the members present in the smart contract through its peer mitigator. Every member of the smart contract has its detection system deployed at its premises responsible for detecting the abnormal activities defined in Section 4. After getting attacker evidence from the used detection system, every fellow takes defensive actions via its local mitigator.

If one of the members of the smart contract is an Internet service provider, it also safeguards its customers by blocking access to attacker domains and IPs on their network. In case the CNC server is using the internet connection from one of the smart contract signatory Internet service providers, the Internet service provider takes action and blocks command and control server IP addresses, leading to the prevention of the source of the attack provides proactive defense against IoT botnets. Next are the stages of the anticipated collaborative mitigation system.

As a first step, a smart contract is formed. This smart contract confines every contributing member to share invader info with the fellow of the smart contract in case of an attack on IoT devices deployed within their network. This smart contract is joined by various enterprises of IoT devices capable of comprehensive threat intelligence abilities.

Figure 6 explains the smart contract management stack. Initially, the like-minded vendors form a consortium. The consortium management unit, responsible for managing the consortium, executes the smart contract operation. First, the public-private key pairs would be generated by registration with the certificate authority and certificates from trusted CAs (certificate authorities). In the next phase of the stack, the block is generated, leading to blockchain formation.

Suppose an attack is launched on IoT devices deployed by any members. In that case, the proposed botnet detection

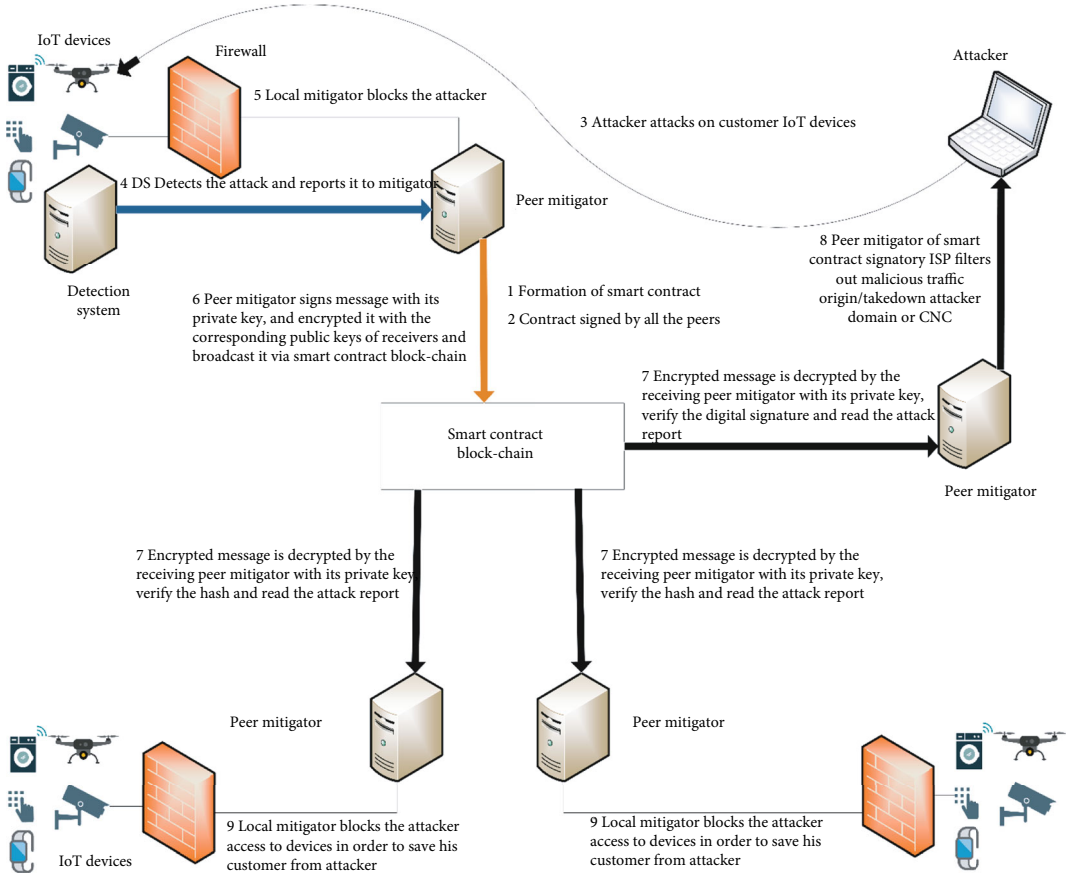

Figure 4: Functionality flow of the proposed collaborative mitigation system.

system becomes aware of the attack based on the violation of the defined policies and reports it to the peer mitigator.

The peer mitigator signs it as $E(SP_rK(T_x)) = ST_x$.

The peer mitigator encrypts with group public key or with public keys as $E(RP_pK(ST_x)) = EST_x$.

The peer mitigator decrypts this transaction with his/her private key as $D(RP_rK(EST_x)) = ST_x$.

The peer mitigator then validates the digital signature of the sender by decrypting the message with either the public keys of the or group public key as $D(SP_PK(ST_x)) = T_x$.

Upon receiving attacker information, local mitigators block the attacker access at receiving members end to the network through firewall policies. In the attacker's case, the IP addresses pole belongs to one of the smart contract signatory ISP; the ISP filters out attack traffic by taking down the CNC server and blocking allocated public IPs.

6. Deployment and Implementation

This unit details the implementation and deployment of the Mirai botnet attack setup, proposed detection, and collaborative mitigation system. This research established the lab setup for deploying and implementing the proposed solution, as depicted in Figure 7.

6.1. Deployment of Mirai Setup. This study set up the Mirai CNC server (IP address is 192.168.2.11 and domain name "cnc.sajjad.local.") from its source code [48], having a database, loader, and scanner server "192.168.2.12." A DNS server "IP address 192.168.2.53" is established to resolve the domain queries made by the devices, two WiFi home routers as IoT devices. A system (IP address 192.168.2.141) is also set up as a DDoS destination target system. The IP addresses of the two WiFi home routers are 192.168.2.71 and 192.168.2.72, respectively. In the initial stage, a scanner server starts scanning for compromised devices. The scan results are reported to the loader server. The binaries of the Mirai malware are loaded on the compromised WiFi home Router by the loader server.

6.2. Implementation of Suggested IoT Botnet Detection System. For the implementation of the detection, OSSIM [49] is used. This research first defined the standard policies for the access on the device, communication of the device, and usage of the device for both WiFi access routers. Sample predefined rules are presented in Table 2. At that point, these predefined policies are implemented in the form of OSSIM rules. Those rules were then included in the native rules of Suricata IDS present in the OSSIM. In the attack, the suggested botnet detection system produced alarms. Mitigator started actions required for local mitigation and subsequently initialized collaborative mitigation procedures.

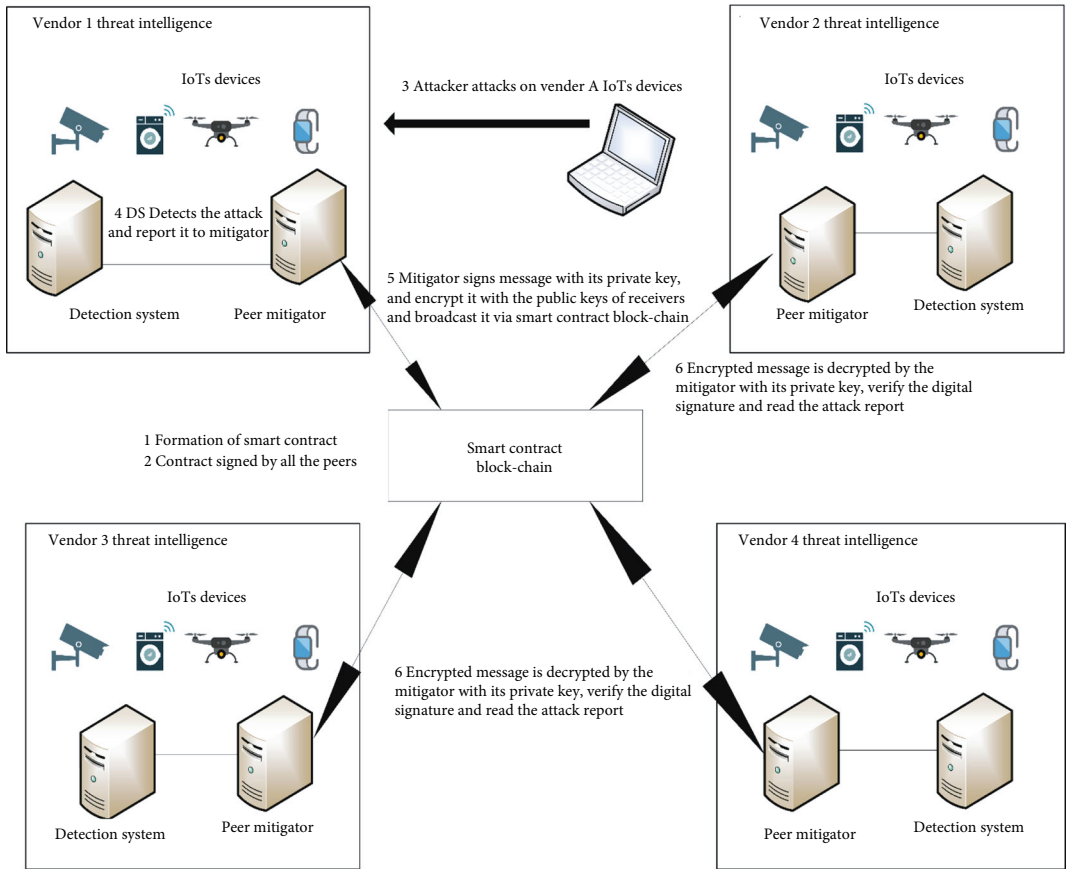

Figure 5: Functionality flow of the collaborative mitigation system between different vendors.

Table 1: Used mathematical notations.

Notation	Description
Tx	Transaction
STx	Transaction with signature
$ESTx$	An encrypted transaction with a signature
$DSTx$	A decrypted transaction with a signature
SP_rK	Private key of the sender
SP_pK	Public key of the sender
RP_rK	Private key of the receiver or group private key
RP_pK	Public key of the receiver or group public key

6.3. Implementation of Proposed Collaborative Mitigation System. The proposed mitigation system consists of two parts, namely, local mitigator and peer mitigator. This study implemented a local mitigator by implementing a software module. It then executes necessary administrative commands to perform the following three tasks.

(i) Change device credentials: An attacker could compromise the device by successfully brute-forcing the device's login credentials. Therefore, the local mitigator changes the device login credentials and informs the network administrator about the new access credentials as a first defensive measure

(ii) Block attacker access to devices: The detection system provides the identified command and control server's domain name and IP addresses to the local mitigator. The local mitigator automatically updates firewall rules for blocking the attacker access to the previously compromised devices in the local network

(iii) Reboot the device: As Mirai malware resides in the volatile memory, rebooting the device can remove the malware from the device. For example, local mitigator reboots the infected devices to remove Mirai from devices

The collaborative mitigation system uses Hyperledger and Ethereum [50, 51]. Attack information, including attacker domain and IP addresses, is shared with the participants of the smart contract. Figure 8 illustrates the operational flow of a smart contract. Initially, a smart contract is compiled using an online solidity browser [52]. Then, the variables returned by Web3 [53] are executed in the geth terminal [53].

7. Results and Analysis

This section includes the results and analysis of both detection and mitigation systems.

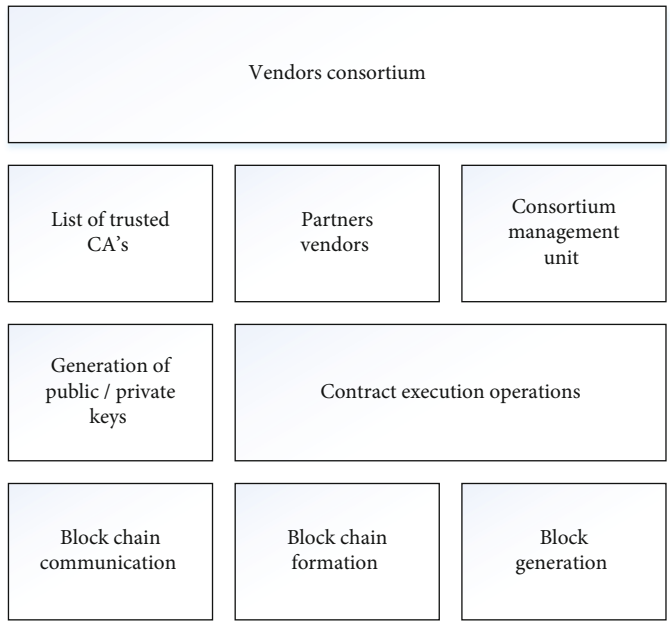

Figure 6: Smart contract management stack.

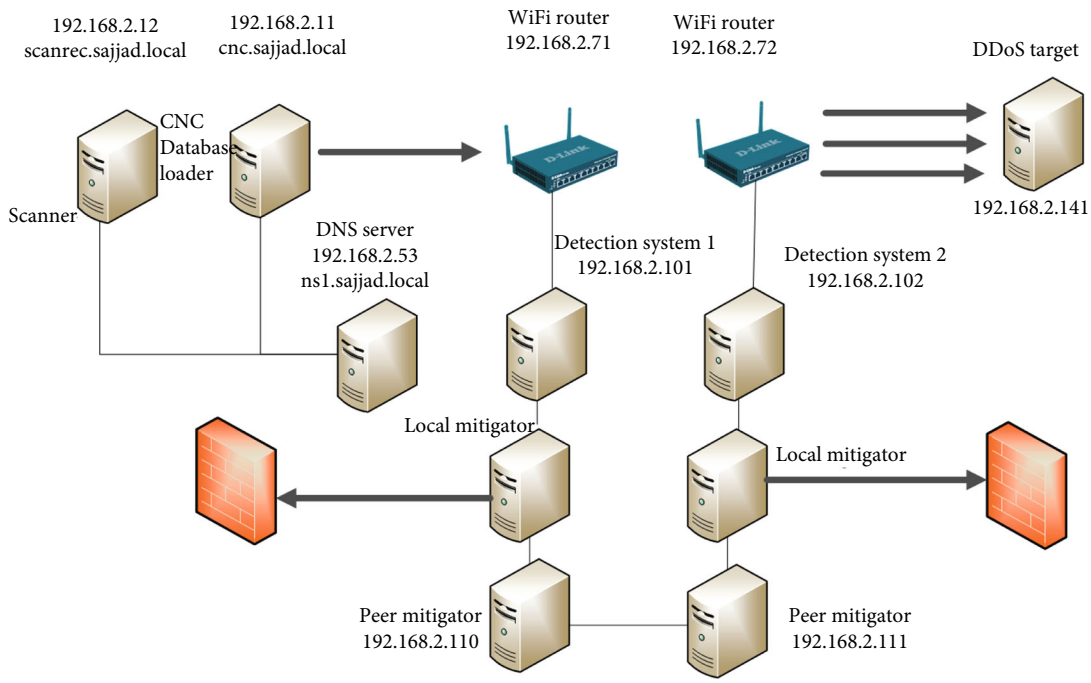

Figure 7: Topology of the deployed lab setup.

Table 2: Example of defined policies for a device.

Policy	Definition
Policy for accessing device	Administrate access allowed from 192.168.20.201
Policy for device communication	Communicate with 192.168.2.201
Policy for device usage	Collection of permitted commands

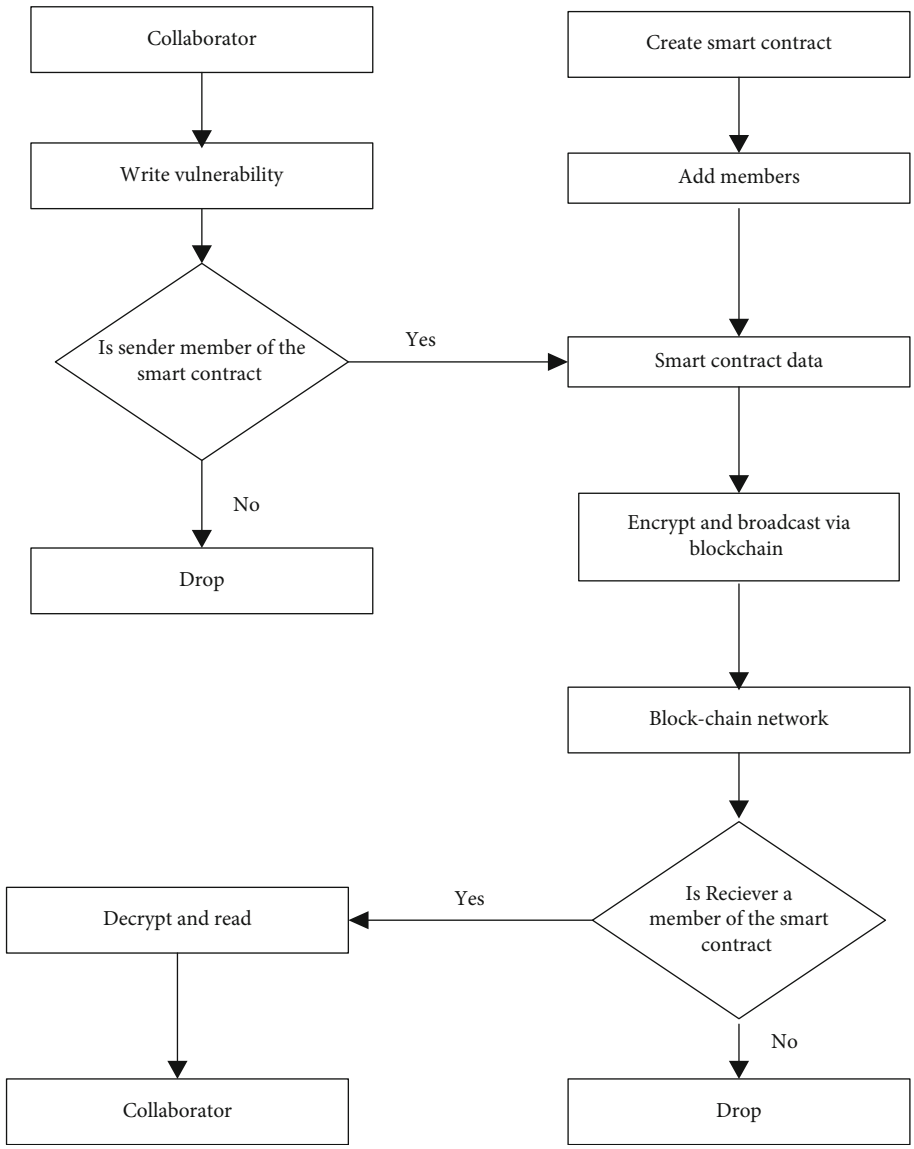

Figure 8: Operational flow of smart contract.

7.1. Results and Analysis of Detection System. The process of compromising the devices entails the following six steps.

(1) Compromising the initial login access of the device by the attacker

(2) Getting access to the device shell

(3) Connection establishment with CNC

(4) Getting malware from CNC

(5) Malware execution on the compromised device

(6) A compromised device acting as a bot

Table 2 depicts the defined policies for a device. The proposed botnet detection system produces alarms at each step of the device compromise if there is a violation of predefined policies. Table 3 describes the plotting of the alarms generated by the proposed botnet detection system during each stage of the device compromise. A thorough study of the packets taken by the proposed botnet detection system during every step of the device compromise is carried out in the subsequent subsections.

7.1.1. Compromising the Initial Login Access of the Device by the Attacker. As a first step, CNC attempts to access the target device through login. The traffic packets transferred between the CNC server and the target device are captured during this process. The CNC server succeeded in getting access to the target using the username root and default password device, as shown in Figure 9.

7.1.2. Getting Access to the Device Shell. After successfully logging into the target device, the CNC servers' next job is to get into the BusyBox of the compromised device. The packet captured during the attempt of the CNC server to access the BusyBox of compromised is shown in Figure 10.

Table 3: Alarms generated at every step of making a device bot.

Alarm	Steps
Violation of access policy	Compromising the initial login access
	Getting access to the device shell
Communication policy violation	Connection establishment with CNC
	Getting malware from CNC
Usage policy violation	Command execution in BusyBox
	A compromised device acting as bot

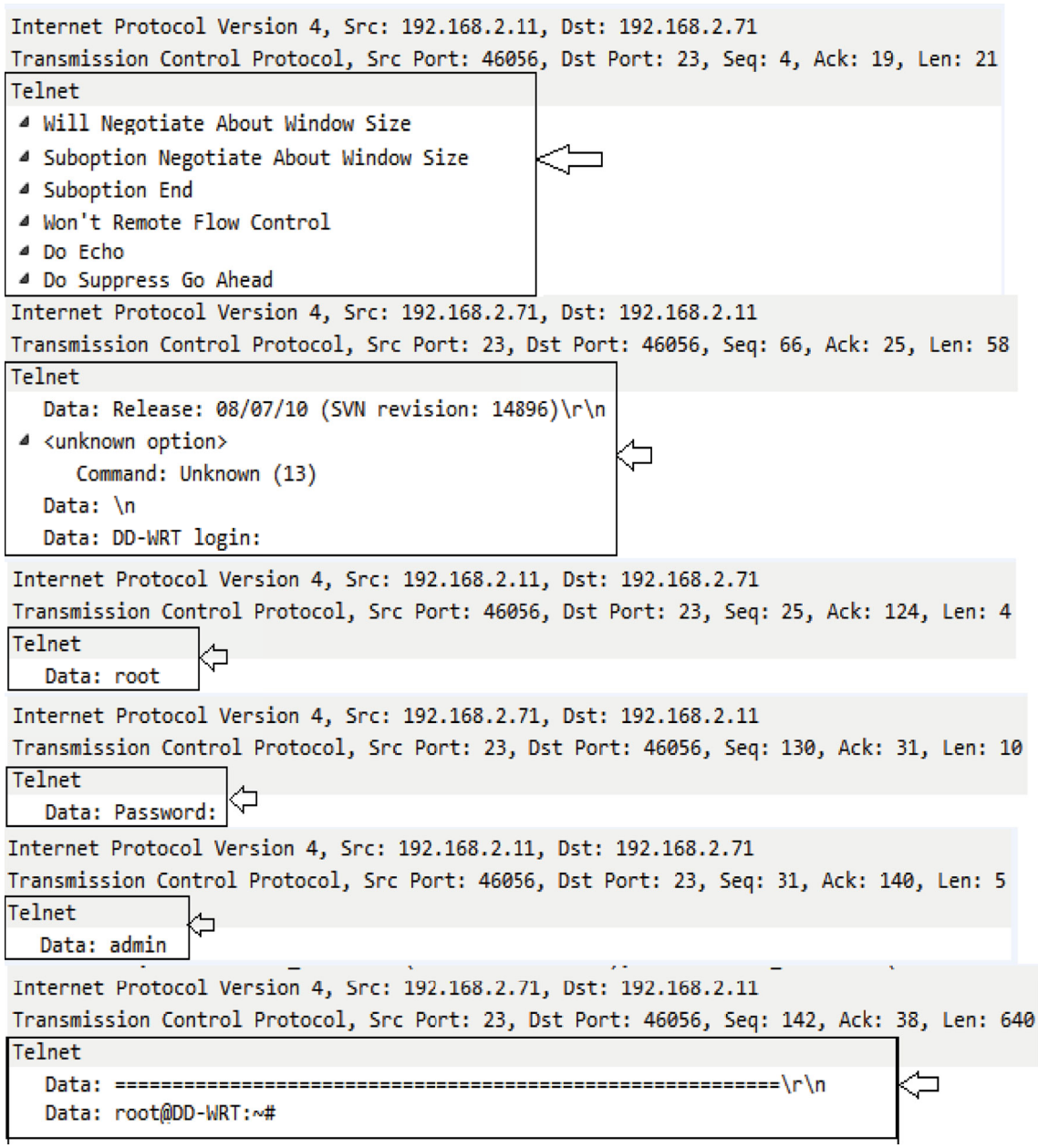

Figure 9: Packets taken by botnet detection system during attacker efforts of compromising the initial login access of the device.

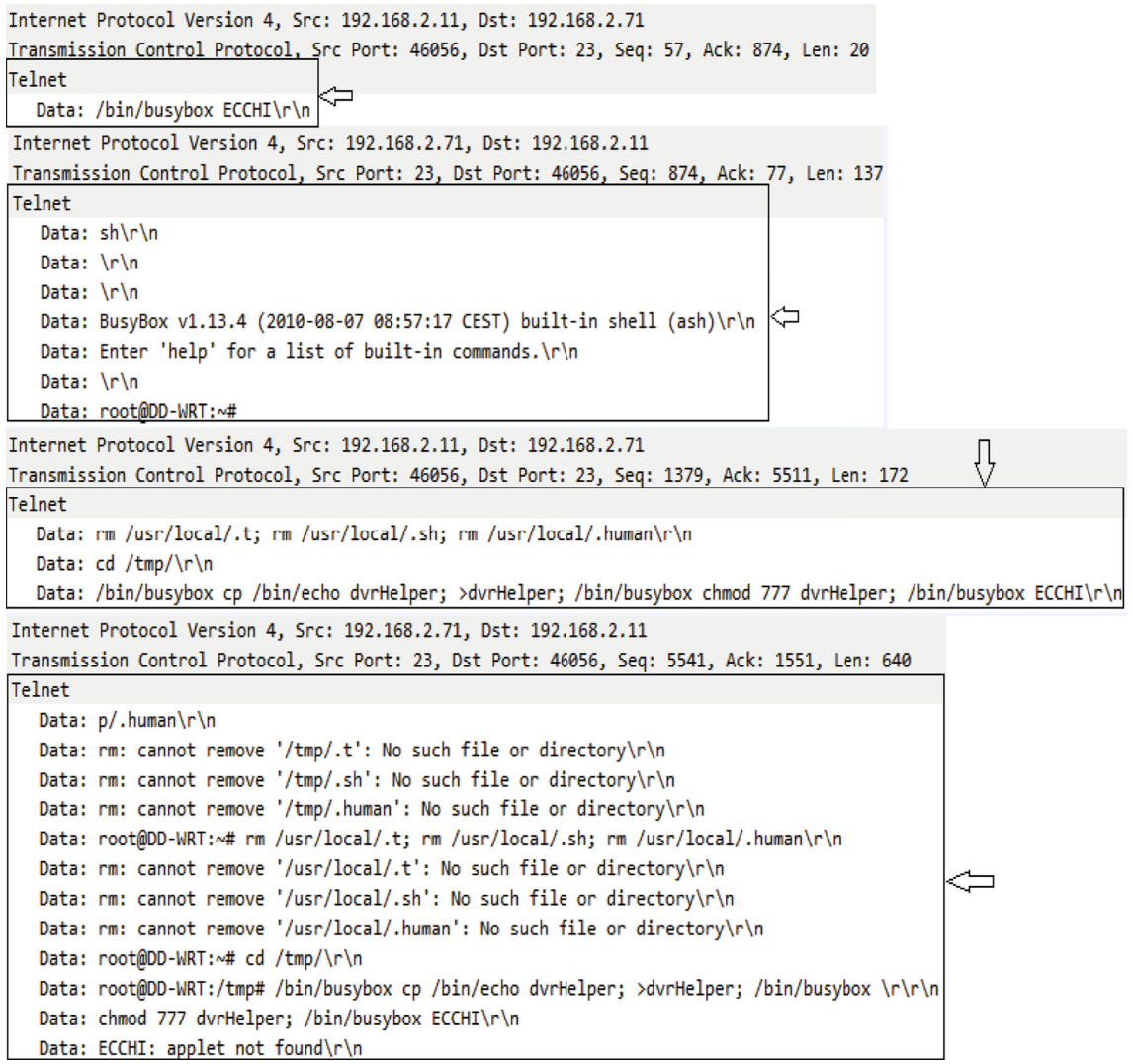

Figure 10: Packets taken by botnet detection system during attackers getting access of the device shell.

7.1.3. Connection Establishment with CNC. After getting access to the BusyBox, the CNC server directs the compromised device to the web server having Mirai malware binaries. The packets are swapped between the CNC server, and the target device is shown in Figure 11.

7.1.4. Getting Malware from CNC. After a successful connection establishment, the Mirai binaries are downloaded. The packets captured during this process are shown in Figure 12.

7.1.5. Malware Execution on the Compromised Device. The CNC server executes the downloaded Mirai binaries attack in this step, as shown in Figure 13.

7.1.6. Compromised Device Acting as a Bot. After getting access and making the target device a bot, the CNC starts the scan process to find the vulnerabilities in other devices to make them part of the bot.

7.1.7. Mapping between Predefined Policies and Alarms Generated by the Proposed IoT Botnet Detection System. Table 2 demonstrates the predefined usage, communication, and access policies. The mapping between violations of predefined policies and the alarms generated by the proposed IoT botnet detection system is depicted in Table 3. Access to devices by the CNC and its shell (BusyBox) is the abuse of the predefined policy for accessing the device. Device communication with CNC Server for downloading Mirai malware binaries is the abuse of the predefined communication policy. Finally, implementation of Mirai malware on the device and the compromised device acting as the bot is the abuse of the predefined policy for usage.

7.1.8. Alarms Generated against Each Attacked Host. In the lab setup, two WiFi access routers having DD-WRT firmware are deployed as vulnerable devices. The command and control server attacks these two devices during the experiment. This research draw alarms generated against each attacked device, as shown in Figure 14. Three hundred sixty alarms are made during the attack on the WiFi access router having IP 192.168.2.71. The number of generated alarms is 280 when the router having IP 192.168.2.72 is attacked.

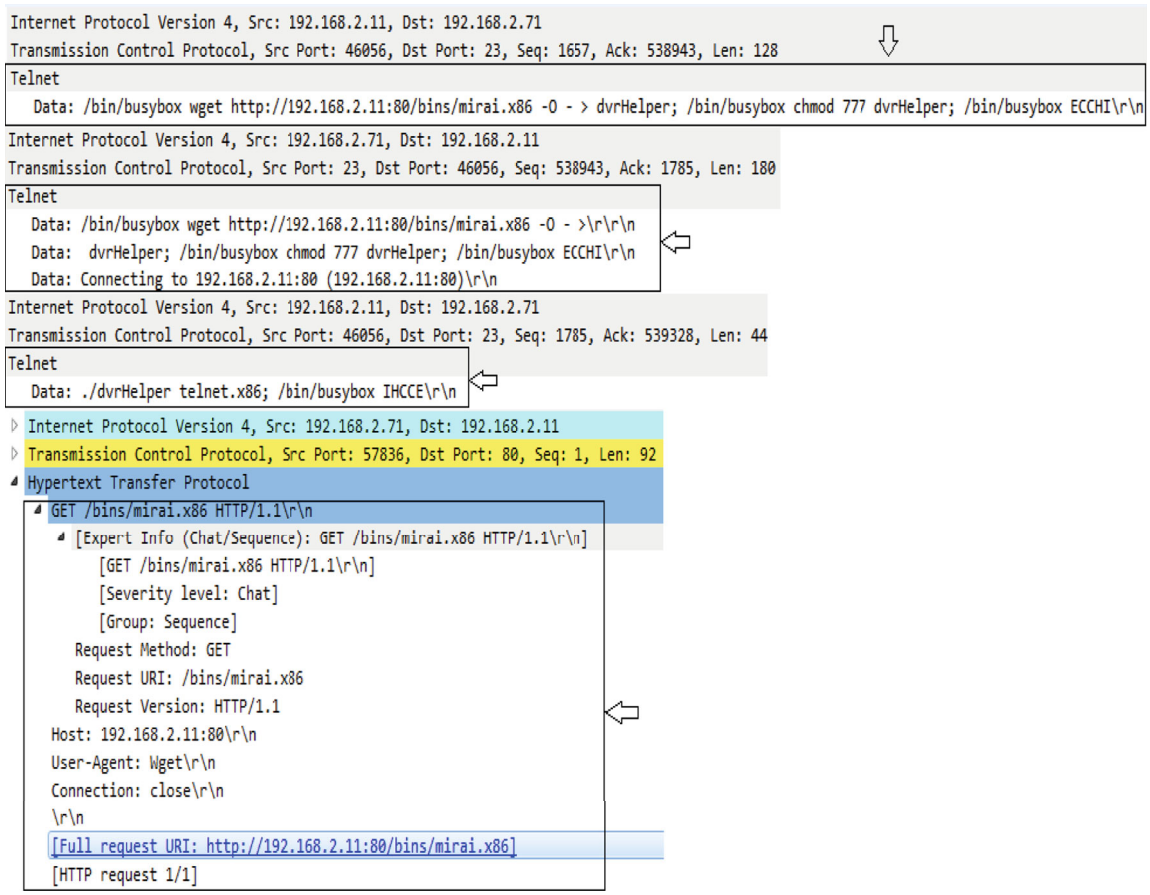

Figure 11: Packets taken by the botnet detection system during Bot Plea of establishing connection with CNC to download malware binaries.

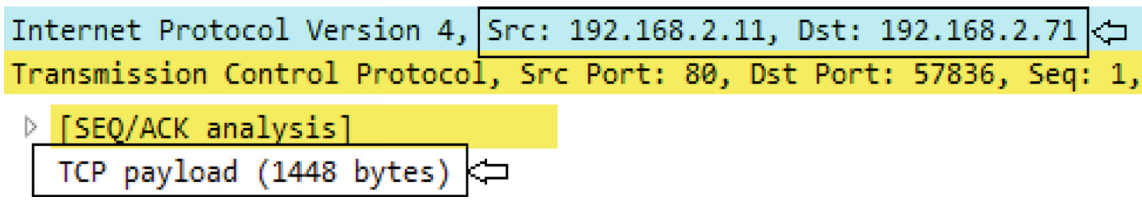

Figure 12: Packets taken by the botnet detection system during bot acknowledging download of malware binaries.

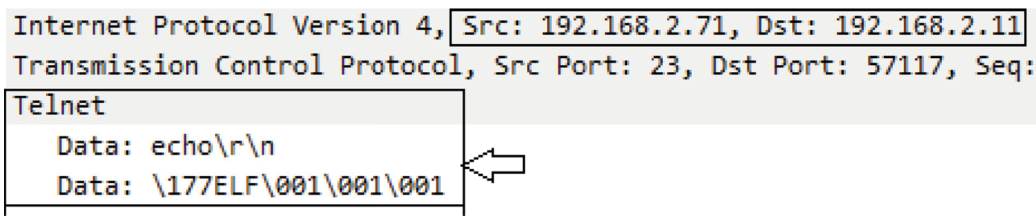

Figure 13: Packets taken by the botnet detection system during the execution of the malware binaries downloaded earlier.

7.1.9. Alarms Generated by Each Attacker Host. The command and control server (192.168.2.11) and scanner (192.168.2.12) are primarily the attacker hosts. In addition, two WiFi access routers, after becoming bots, act as the scanner. Alarms generated against each attacking host are shown in Figure 15. The figure depicts that the detection system generates around 540 alerts if the attacker is the command and control server. The number of generated alerts is 150, 110, and 105 in case attacker, WiFi access router 1 has IP address 192.168.2.71, WiFi access router 2 has IP address 192.168.2.72, and scanner server has IP address 192.168.2.12.

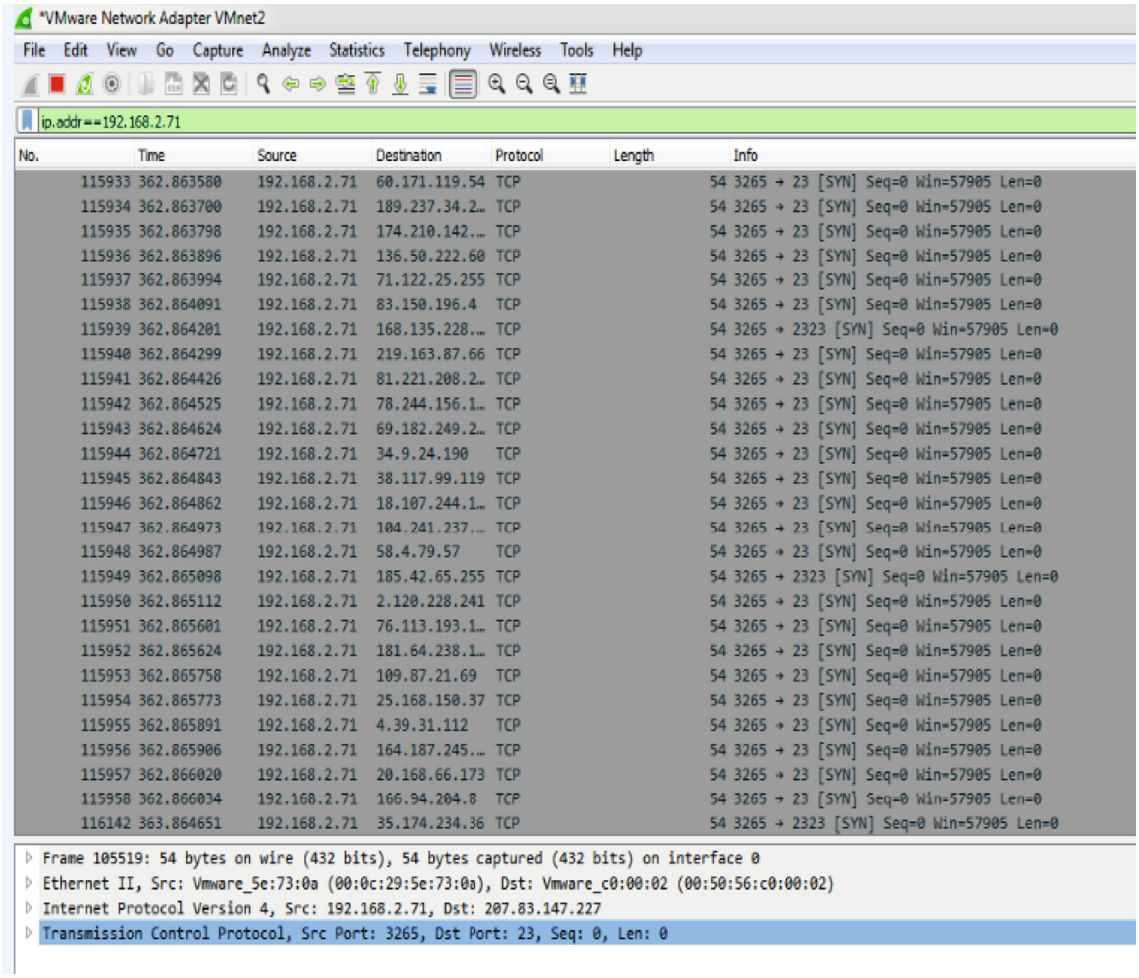

Figure 14: Packets taken by the botnet detection system during compromised device acting as bot.

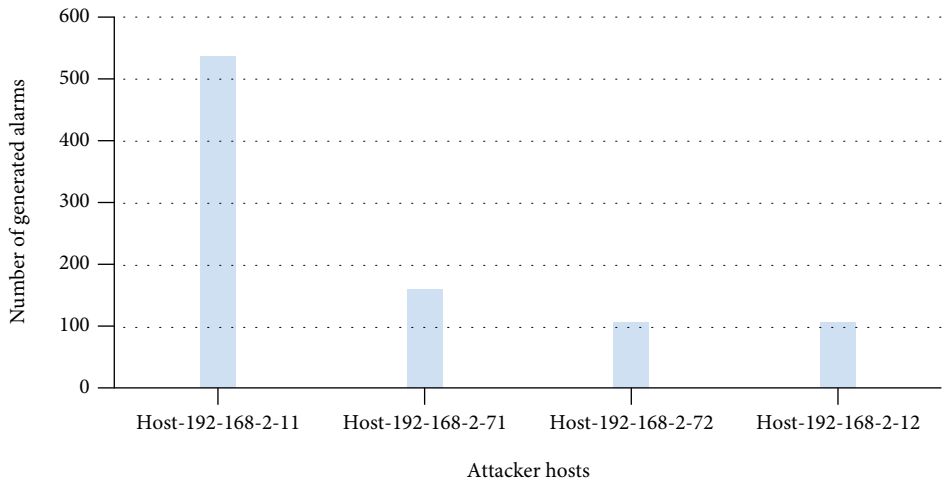

Figure 15: Alarms generated by each attacking host.

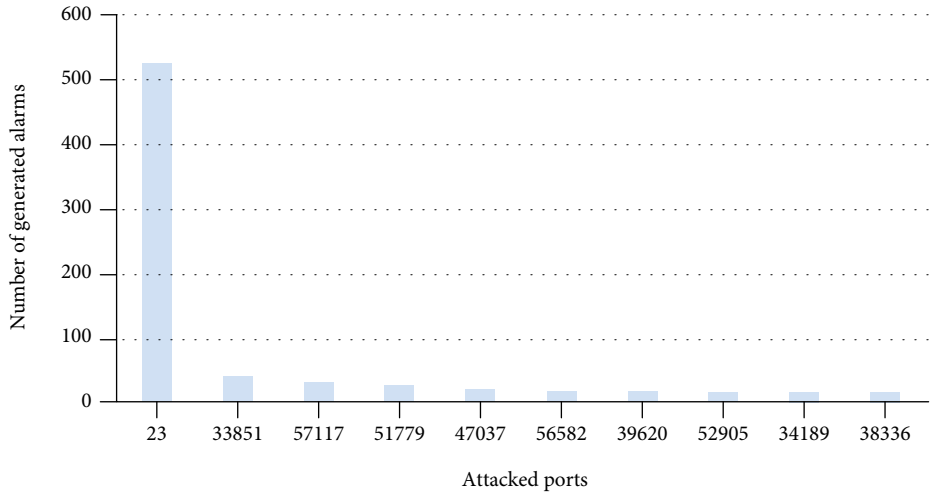

Figure 16: Alarms generated against each attacked port.

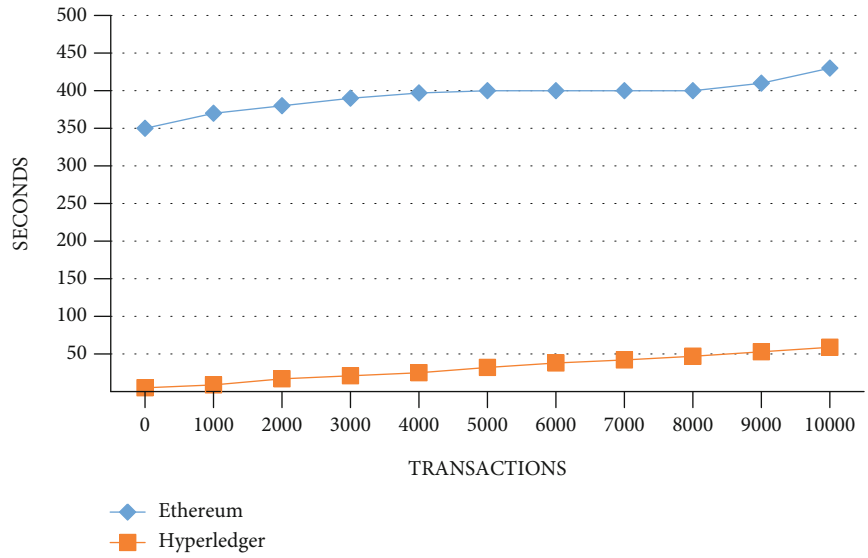

Figure 17: Throughput of the proposed collaborative mitigation system.

7.1.10. Alarms Generated against Each Attacked Port. During the attack process, the attacker tries to gain access to the WiFi access router by scanning different ports of the target bot. The number of alarms generated against different ports is shown in Figure 16. It shows that the detection system against telnet access generates around 520 alerts.

7.2. Results and Analysis of Mitigation. The local mitigator changes the device login credentials and informs the network administrator about the new access credentials as a first defensive measure. The detection system provides the identified command and control server's domain name, i.e., cnc.sajjad.local, and IP addresses, i.e., 192.168.2.11, to the local mitigator. The local mitigator automatically updates firewall rules for blocking the attacker access to the previously compromised devices in the local network. As Mirai malware resides in the volatile memory, rebooting the device can remove the malware from the device. Local mitigator reboots the infected devices to remove Mirai from devices. The collaborative mitigator writes the attacker IP addresses and the attacked ports to the smart contract and shares them with the member of the smart contract. This information is received by all the members of the smart contract. The local mitigator of each member blocks the access of the attacker IP address and the attacked ports. After the mitigation steps, this research again launched the attack on the WiFi access router from the Mirai scanner. Mirai scanner (scanrec.sajjad.local having IP 192.168.2.12) cannot compromise WiFi access routers as attacker access on the WiFi access router is blocked by the firewall. The peer mitigator of any organization takes the proactive defense steps. The peer mitigator of any vendor or peer Internet service provider safeguards the users or customers of the vendors or Internet service provider from becoming part of the IoT botnets.

Similarly, the proactive defense steps taken by the attacker organization, vendor, or Internet service provider

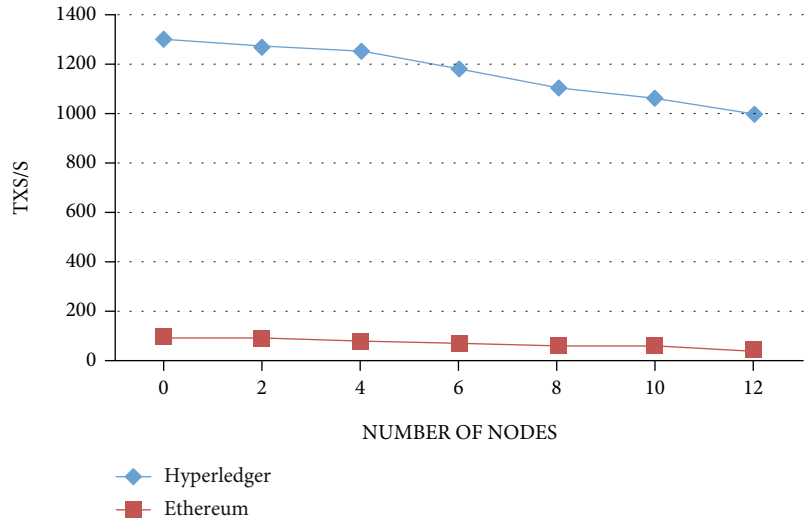

Figure 18: Scalability of the proposed collaborative mitigation system.

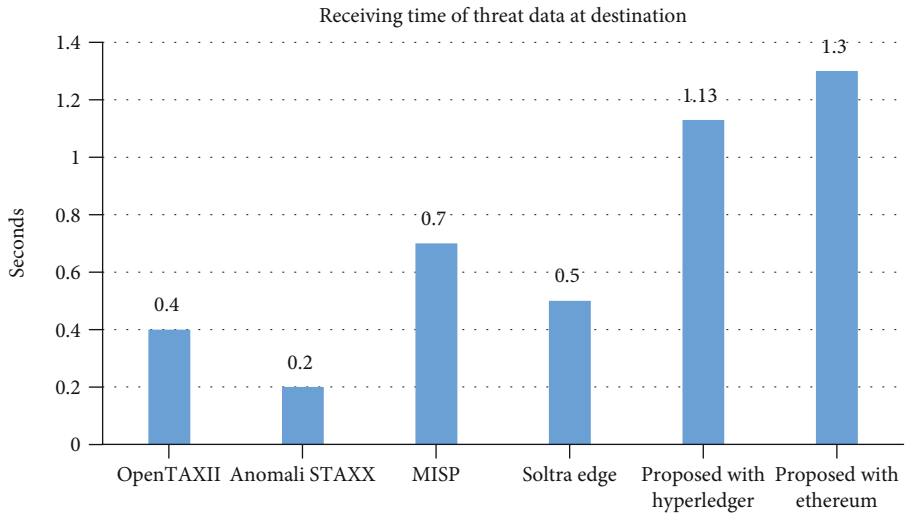

Figure 19: Delay caused by the encryption overhead.

completely stop the source of the attack. In this way, smart contract and blockchain-based collaborative mitigation provide a means of proactive defense to all the members of the smart contract without members experiencing the attack themselves. The actions taken by the collaborative mitigator of the attacker vendor or Internet service provider completely stop the attack source.

7.2.1. Throughput. The measurement of the per second transactions is called throughput. Figure 17 elaborates the throughput of the proposed system. Due to the complexity and difficulty of the Ethereum's consensus protocol "proof of work," the initial transaction occurred after 360 seconds. Contrary to this, in Hyperledger, the initial transaction occurred after 7 seconds.

7.2.2. Scalability. Figure 18 shows the scalability evaluation of the collaborative mitigation. Hyperledger is less scalable than Ethereum. Nevertheless, it is also eminent that transactions per second also declined with the number of peer nodes.

7.2.3. Latency. As shown in Figure 17, the occurrence of the first transaction is at 350 seconds. Due to the higher difficulty level of Ethereum's "proof of work" consensus algorithm, 10,000 transactions occurred in 440 seconds. In Hyperledger's case, an initial transaction happens at around 4 seconds, while 10000 transactions occur in 440 seconds.

7.2.4. Performance Discussion. Ethereum Casper, an improved version of the Ethereum consensus protocol, was launched in May 2018 [54]. Version 2 of the said protocol utilizing a "proof of stake" based improved consensus mechanism is expected to resolve the issues present in Ethereum [55]. This release targets enhanced scalability and performance. These improvements would probably solve performance issues at Ethereum.

Table 4: List of threat exchange protocols and their formats.

S#	Protocol	Format
1	"Common Intrusion Detection Framework (CIDF)" [62]	"Common Intrusion Specification Language (CISL) Messages" [63]
2	Real-time Inter-network Defense (RID) [64]	"Incident Object Description Exchange Format (IODEF)" [65–67]
3	XEP-0268 Incident Handling [68–71]	Incident Object Description Exchange Format (IODEF)
4	"Intrusion Detection Exchange Protocol (IDXP)" [72]	"The Intrusion Detection Message Exchange Format (IDMEF)" [73, 74]
5	Simple Mail Transfer Protocol (SMTP) [75]	Common Announcement Interchange Format (CAIF), Abuse Reporting Format(ARF) [76]
6	CEE Log Transport (CLT) [77]	Command Event Expression (CEE) [78]
7	Syslog Protocol [79]	Syslog [80]

Table 5: Description of evaluation criteria.

S. no	Level	Score
1	Low	5
2	Medium	10
3	High	15
4	Very high	20

7.2.5. Encryption Overhead. By default, blockchain does not include data encryption. In the proposed collaborative mitigation system, the peer mitigator in the proposed collaborative mitigation system sends the signed transaction by encrypting it with the receiver public keys one by one. This process causes an extra encryption overhead at the sender side and additionally may cause delays. Figure 19 depicts the comparison of the time taken by the arrival of threat data at the receiver end in a proposed scheme with OpenTAXII [56], Anomali STAXX [57], MISP [58], and Soltra Edge [59]. The proposed scheme implementation with Ethereum takes the most time compared to the proposed scheme implementation with Hyperledger and other threat data-sharing platforms. The symmetric group encryption key can be used to avoid the encryption overhead on the sender side.

7.3. Comparative Analysis. There are numerous threat exchange protocols. Each protocol has a specific exchange format. An exchange protocol is a set of rules describing how network devices across a computer network can be interconnected to create a channel for transmitting data through exchange formats [60, 61]. Table 4 describes some of the threat exchange protocols and their formats.

7.3.1. Evaluation Parameter and Criteria. The exchange protocols are assessed on the following twelve parameters:

(1) Confidentiality

(2) Nonrepudiation

(3) Authenticity

(4) Trust

(5) Integrity

(6) Reliable message transport

(7) Scalability

(8) Product based on standard

The confidentiality principle defines the capacity to safeguard sensitive information from exposure to unauthorized parties. The authenticity defines the ability to assess if the exchanging parties are really whom they have claimed to be and therefore use authentication mechanisms. The potential to secure data from unauthorized parties' alteration or deletion is defined by the integrity. If the transmission of a threat data uses a guaranteed delivery to prevent duplicate messages and message loss, an exchange protocol uses "reliable message transport." The ability to manage various network sizes is defined by the metric of "scalability." Ensuring that the sender and receiver cannot deny the transmission and receiving of data is termed nonrepudiation.

The sender and receiver should have a trusting relationship with each other. The recipient of the threat data should authenticate the origins of the received data and verify the correctness of the received data and the sender. Thus the threat sharing platform should have a mechanism that should provide correctness of the received data.

7.3.2. Evaluation Results. The following sections discuss the evaluation results. Table 5 presents the numerical evaluation criteria.

(1)Confidentiality. Figure 20 depicts the comparison of the confidentiality of the CTI platforms to the proposed mechanism. CIDF offers a matchmaking service with the help of which CIDF components use authenticated and secured communications between CIDF components. The matchmaker service also acts as a certificate authority (CA).

Therefore, the confidentiality, integrity, and authentication capabilities of the CIDF are great. RID utilizes XML encryption to offer confidentiality in the "IODEF' and "IODEF-RID" [132] systems, based on the iodef: restriction attribute. To provide confidentiality, IDXP uses TLS' underlying BEEP protection profile with the "TLS DHE DSS WITH 3DES EDE CBC SHA" cipher suite. XMPP employs TLS to guarantee privacy and confidentiality, making the

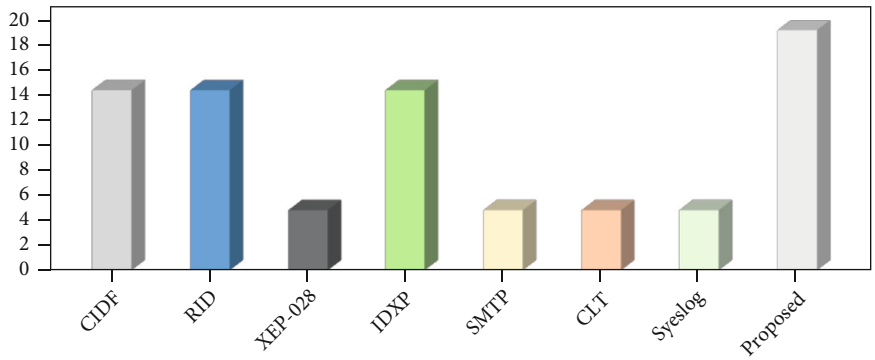

Figure 20: Data confidentiality in Information Sharing Platform concerning proposed blockchain platform.

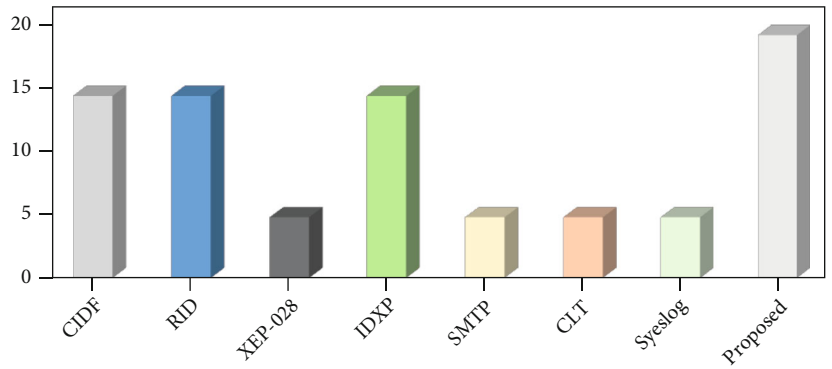

Figure 21: Nonrepudiation in Information Sharing Platform with respect to proposed blockchain platform.

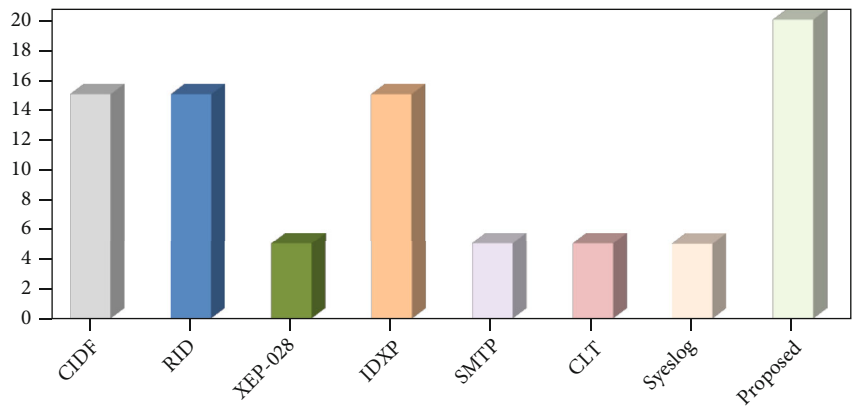

Figure 22: Authentication process in Information Sharing Platform with respect to proposed blockchain platform.

confidentiality services and capabilities of XMPP and XEP-0268 strong enough. SMTP does not include the usage of any technique to guarantee protection. The potential for secrecy is, therefore, low in SMTP. To counter security event disclosure, CLT and Syslog RFC 5424 use TLS; thus, the confidentiality capacity is high. In the proposed blockchain-based threat information sharing, encrypting the digitally signed transaction with the receiver's public keys provides a high level of confidentiality.

(2)Nonrepudiation. As trust in CIDF is high due to origin authentication provided by Generalized Intrusion Detection Objects (GIDO) messages exchanged between CIDF-compliant components, nonrepudiation is high. As RID, CLT, and Syslog (RFC 5425) have high trust due to TLS based authentication and authorization, it has high nonrepudiation. XEP-0268 has low nonrepudiation as sharing incident reports with trusted peers is optional. IDXP has high nonrepudiation due to high trust as it employs a BEEP security profile. A user cannot deny a transaction as its private key signs in the proposed blockchain-based threat information sharing. Figure 21 demonstrates the comparison of the nonrepudiation property of the CTI platforms regarding the proposed mechanism.

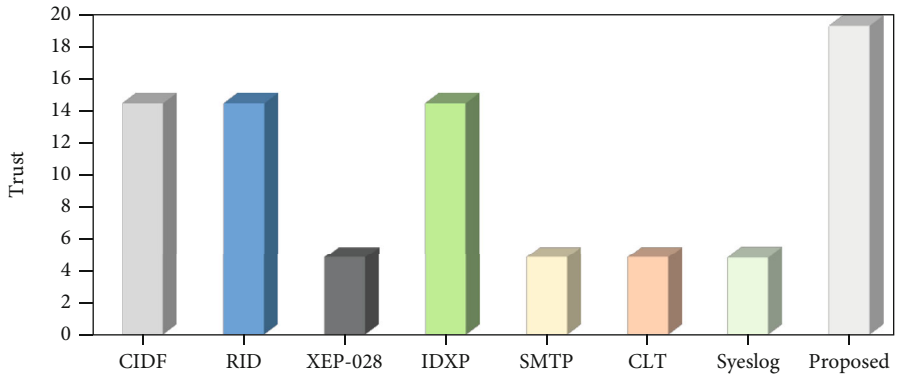

Figure 23: Trust in Information Sharing Platform with respect to proposed blockchain platforms.

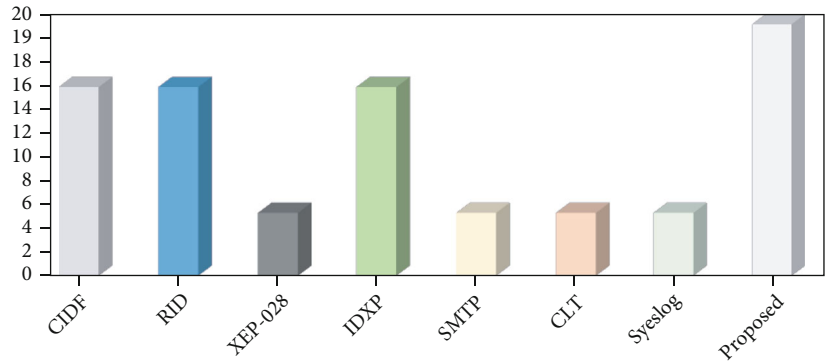

Figure 24: Data Integrity in Information Sharing Platform with respect to proposed blockchain platform.

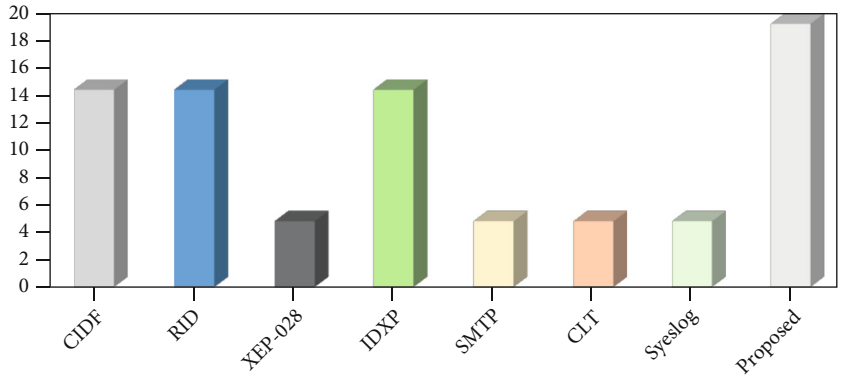

Figure 25: Reliable message transportation in Information Sharing Platform with respect to proposed blockchain platform.

(3)Authenticity. Figure 22 shows the comparison of the authenticity of the CTI platforms to the proposed mechanism. To authenticate the sender of the RID message, RID utilizes digital signatures on the hash of the RID message with an X.509v3 certificate provided by the trusted authority. XEP-0268 is XMPP-based. The authentication capabilities of XEP-0268 are considered to be strong because XMPP uses the "Simple Authentication and Security Layer (SASL)" for peer authentication. IDXP provides mutual authentication by employing the public-key certificates of the TLS security profile of underlying BEEP protocol. Syslog RFC 5425 also uses mutually authenticated channels with cryptographic algorithms and protocols commonly deployed. As CLT is Syslog RFC 5424, the CLT has the same features as Syslog RFC 5424. The authentication capacity of the "RID, IDXP, CLT, and Syslog RFC 5425" exchange protocols is high. The SMTP exchange protocols cannot verify that the declared sender is the message-sending peer, so the SMTP authentication functionality is low. IDXP utilizes the underlying BEEP protection profile of TLS with the "TLS DHE DSS WITH 3DES EDE CBC SHA" cipher suite to provide high authentication capabilities. In the proposed

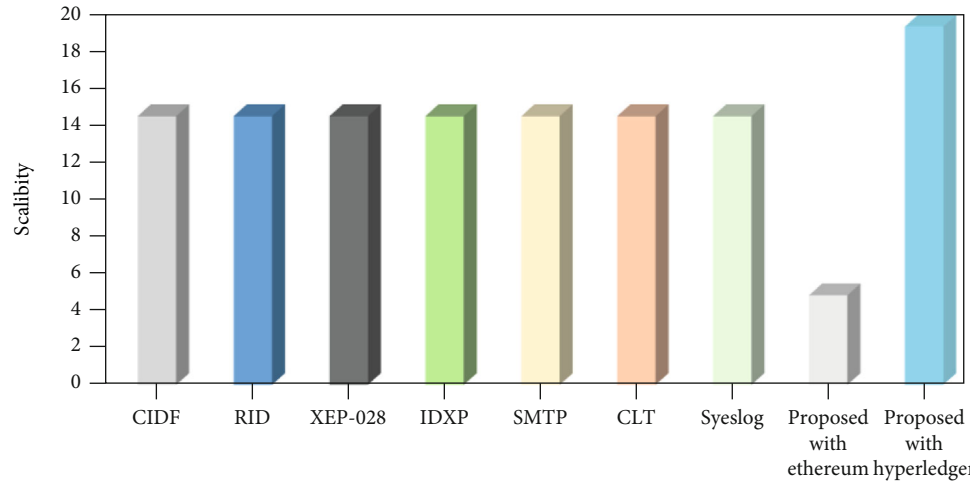

Figure 26: Scalability in Information Sharing Platform with respect to proposed blockchain platform.

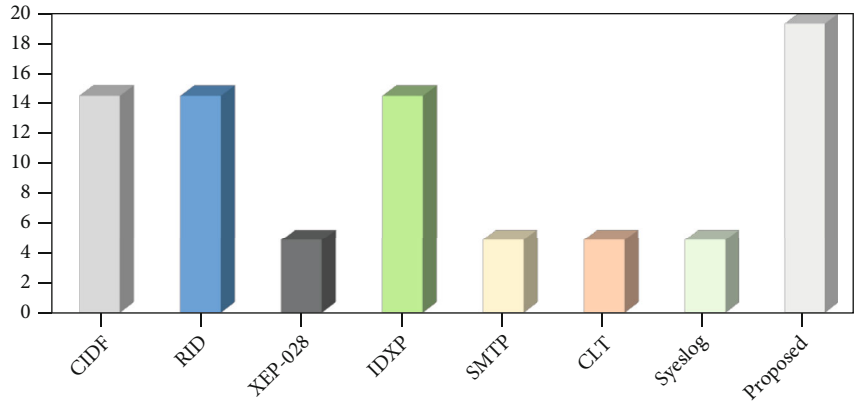

Figure 27: Practical application of Information Sharing Platform with respect to proposed blockchain platform.

blockchain-based mechanism, the user sends a digital signature (encryption with its private key) to the data, ensuring user and data authentication.

(4)Trust. Trust in CIDF is high due to origin authentication provided by Generalized Intrusion Detection Objects (GIDO) messages exchanged between CIDF-compliant components. RID, CLT, and Syslog (RFC 5425) have high trust due to TLS-based authentication and authorization. XEP-0268 has low trust as sharing incident reports with trusted peers is optional. IDXP has high trust as it employs a BEEP security profile. A BEEP security profile is used to establish trust between end-to-end peers of the IDXP. In the proposed blockchain-based solution, trust is established via the smart contract.

Additionally, each transaction contains the hash of the previous transaction forming the data origin authentication. Moreover, the sender encrypts the data with its private key before sending it to the receiver. Figure 23 elaborates the comparison of the trust of the CTI platforms with respect to the proposed mechanism.

(5)Integrity. Figure 24 depicts the comparison of the integrity of the CTI platforms with respect to the proposed mechanism. The integrity of messages sent over the network is tackled using authentication methods. The "RID, XEP-0268, IDXP, CTL and Syslog RFC 5424" TLS-based protocols support message integrity by using TLS message authentication, TLS security profile of BEEP, or SASL profile members. The capacity of "RID, XEP-0368, IDXP, CTL, and Syslog RFC 5424" TLS-based exchange protocols to maintain the integrity of the transmitted message is high. On the other hand, SMTP does not have any mechanisms to guarantee integrity, and thus, the integrity capacity is low. In the proposed blockchain-based threat, information sharing digital signature of the receiver and hashes of the transaction provides temper proof integrity.

(6)Reliable Message Transport. Figure 25 demonstrates the comparison of the reliable message transport of the CTI platforms regarding the proposed mechanism. Reliable CIDF messaging over UDP is the default transport layer protocol for CIDF messages. However, CIDF also uses (i) the message layer directly over UDP without acknowledgement

and retransmission, (ii) message layer of the CIDF with acknowledgement and retransmission through UDP, and (iii) the CIDF message layer explicitly over TCP. "RID, XEP-0268, and IDXP" include the use of connection-oriented protocols and therefore use TCP. SMTP is independent of the specific transmission protocol, but a stable, organized data stream channel is necessary. Hence, the ability of a reliable message transport of the protocols "CIDF, RID, XEP-0268, IDXP, SMTP, CLT, and Syslog RFC 5425" is high. In the proposed blockchain-based mechanism, the receiver sends an acknowledgement message upon receiving the information. Secondly, the consensus algorithm does not allow the duplication or replay of the actual message.

(7)Scalability. The scalability of "CIDF, IDXP, XEP-0268, SMTP, CLT, and Syslog" is high. RID's capacity to support various network sizes is low; hence, it does not scale up to the mark. The EVM implementation of the suggested threat data sharing scheme is more scalable as compared to Hyperledger. Figure 26 shows the comparison of the scalability of the CTI platforms with respect to the proposed mechanism.

(8)Practical Application (Product Based on Standard). CIDF was not meant to be a standard impacting the commercial marketplace. There are no practical applications that allow CIDF, CTL, and XEP-0268 since CIDF was a research project and the work on CEE and XEP-0268 is currently stopped. The availability of practical applications is, therefore, low. Some implementations that use RID and IDXP are available, so the practical application is average. Most businesses use SMTP and Syslog, and thus, the realistic implementation of these two is robust. The practical applicability of blockchain-based information sharing is high since the platform is readily deployed. Figure 27 shows the comparison of the practical application of the CTI platforms with respect to the proposed mechanism.

8. Conclusion

In this paper, the functionality of Mirai malware was analyzed in detail. This research proposed detection and collaborative mitigation system. The detection system detects the abnormal behavior of the device based on the violation of the defined policies by the device. The local mitigator blocked the command and control server access to the WiFi access router, blocked the attacked ports, and rebooted the device. The collaborative mitigator sends the attack detection report to the peer mitigators. Peer mitigators block the attacker's access to their network. The attacker was unable to compromise the device after the mitigation actions. A collaborative mitigator provides a means of proactive defense to all the members of the smart contract.

Results show that the proposed detection and mitigation system detects Mirai malware and mitigates it successfully. Results demonstrate that the proposed detection system successfully detects each offensive step of the attacker and gives a 97 percent detection rate. Collaborative mitigation system implementation with "Hyperledger" offers a high-throughput and a more negligible latency due to its consensus algorithm's lesser complexity than its implementation in "Ethereum Virtual Machine." Ethereum "proof of work" complexity is greater than the Hyperledger. Contrary, its implementation in "Ethereum Virtual Machine" exhibits great scalability compared to its implementation in "Hyperledger."

Data Availability

All data generated or analyzed during this study are included in this published article.

Conflicts of Interest

The authors declare that they have no conflicts of interest to report regarding the present study.

Acknowledgments

The authors extend their appreciation to the Deanship of Scientific Research at King Khalid University for funding this work under grant number (RGP2/71/43) and Taif University Researchers Supporting Project number (TURSP-2020/346), Taif University, Taif, Saudi Arabia.

References

[1] C.-M. Chen, S. Liu, S. A. Chaudhry, Y.-C. Chen, and M. A. Khan, "A lightweight and robust user authentication protocol with user anonymity for IoT-based healthcare," *CMES-Computer Modeling in Engineering & Sciences*, vol. 131, no. 1, pp. 307–329, 2022.

[2] A. Mihovska and M. Sarkar, "Smart connectivity for internet of things (IoT) applications," in *In New advances in the Internet of things*, pp. 105–118, Springer, Cham, 2018.

[3] R. Pannananda, D. Botheju, L. Silva, and T. Sandaru, "Internet of Things security (IoT sec) challenges, current status, trends and architecture," in *2nd International Conference on Library and Information Management*, University of Kelaniya, Sri Lanka, 2017.

[4] S. M. Sajjad and M. Yousaf, "Security analysis of Internet of Things adaptation layer," *Science International*, vol. 28, no. 4, pp. 3311–3317, 2016.

[5] S. M. Sajjad and M. Yousaf, "Security analysis of IEEE 802.15.4 MAC in the context of Internet of Things (IoT)," in *IEEE Conference on Information Assurance and Cyber Security (CIACS)*, pp. 9–14, Rawalpindi, Pakistan, 2014.

[6] M. A. J. Jamali, B. Bahrami, A. Heidari, P. Allahverdizadeh, and F. Nourozi, "The IoT Landscape," in *Towards the Internet of Things*, pp. 1–6, EAI/Springer Innovations in Communication and Computing Series, 2018.

[7] L. H. Neuman, *GitHub Survived the Biggest DDoS Attack Ever Recorded*, Wired, 2018.

[8] D. Goodin, *VPNFilter Malware Infecting 500,000 Devices Is Worse than We Thought*, ARS Technica, 2018.

[9] J. Scott and D. Spaniel, "Rise of the machines: the DYN attack was just a practice run," in *Institute for Critical Infrastructure Technology (ICIT)*, pp. 1–62, CreateSpace Independent Publishing Platform, 2016.

[10] S. Hilton, *Dyn Analysis Summary of Friday, October 21 Attack*, Dyn Blog, 2016, https://dyn.com/blog/dyn-analysis-summary-of-friday-october-21-attack.

[11] O. Kolkman, *Introducing Collaborative Security, Our Approach to Internet Security Issues*, Internet Society, 2015.

[12] S. M. Sajjad, S. H. Bouk, and M. Yousaf, "Neighbor node trust based intrusion detection system for WSN," *Procedia Computer Science*, vol. 63, pp. 183–188, 2015.

[13] M. A. Khan, "A provable and privacy-preserving authentication scheme for UAV-enabled intelligent transportation systems," *IEEE Transactions on Industrial Informatics*, vol. 18, no. 5, pp. 3416–3425, 2022.

[14] M. A. Khan, H. Shah, S. U. Rehman et al., "Securing internet of drones with identity-based proxy Signcryption," *IEEE Access*, vol. 9, pp. 89133–89142, 2021.

[15] A. S. Yahaya, N. Javaid, S. Ullah et al., "A secure and efficient energy trading model using blockchain for a 5G-deployed smart community," *Wireless Communications and Mobile Computing*, vol. 2022, Article ID 6953125, 27 pages, 2022.

[16] Y. M. P. Pa, S. Suzuki, K. Yoshioka, T. Matsumoto, T. Kasama, and C. Rossow, "IoTPot: analyzing the rise of IoT compromises," *9th USENIX Workshop on Offensive Technologies (WOOT 15)*, 2015.

[17] T. Luo, Z. Xu, X. Jin, Y. Jia, and X. Ouyang, *Iotcandyjar: Towards an Intelligent-Interaction Honeypot for IoT Devices*, Black Hat, 2017.

[18] S. Newman, "Service providers: the gatekeepers of internet security," *Network Security*, vol. 2017, no. 5, pp. 5–7, 2017.

[19] N. N. Dao, T. V. Phan, J. Kim, T. Bauschert, and S. Cho, "Securing heterogeneous IoT with intelligent DDoS attack behavior learning," *IEEE Systems Journal*, pp. 1–10, 2021.

[20] E. Lear, R. Droms, and D. Romascanu, "Manufacturer usage description specification," *Internet Engineering Task Force, RFC*, vol. 8520, 2019.

[21] E. Lear and B. Weis, "Slinging MUD: manufacturer usage descriptions: how the network can protect things," in *In IEEE International Conference on Selected Topics in Mobile Wireless Networking (MoWNeT)*, pp. 1–6, Cairo, Egypt, 2016.

[22] J. Habibi, D. Midi, A. Mudgerikar, and E. Bertino, "Heimdall: mitigating the internet of insecure things," *IEEE Internet of Things Journal*, vol. 4, no. 4, pp. 968–978, 2017.

[23] C. Cao, L. Guan, P. Liu, N. Gao, J. Lin, and J. Xiang, "Hey, you, keep away from my device: remotely implanting a virus expeller to defeat Mirai on IoT devices," 2017, https://arxiv.org/abs/1706.05779.

[24] D. D. López, M. B. Uribe, C. S. Cely et al., "Shielding IoT against cyber-attacks: an event-based approach using SIEM," *Wireless Communications and Mobile Computing*, vol. 2018, 18 pages, 2018.

[25] S. M. Sajjad, M. Yousaf, H. Afzal, and M. R. Mufti, "eMUD: enhanced manufacturer usage description for IoT botnets prevention on home WiFi routers," *IEEE Access*, vol. 8, pp. 164200–164213, 2020.

[26] S. M. Sajjad and M. Yousaf, "UCAM: usage, communication and access monitoring based detection system for IoT botnets," in *2018 17th IEEE International Conference On Trust, Security And Privacy In Computing And Communications/12th IEEE International Conference On Big Data Science And Engineering (TrustCom/BigDataSE)*, pp. 1547–1550, New York, NY, USA, 2018.

[27] *CSIRT Frequently Asked Questions (FAQ)*, Software Engineering Institute, Carnegie Mellon University, 2017, https://resources.sei.cmu.edu.

[28] L. Gordon, M. Loeb, and W. Lucyshyn, "Sharing information on computer systems security: an economic analysis," *Journal of Accounting and Public Policy*, vol. 22, no. 6, pp. 461–485, 2003.

[29] E. Gal-Or and A. Chose, "The economic incentives for sharing security information," *Information Systems Research*, vol. 16, no. 2, pp. 186–208, 2005.

[30] *Executive Order 13636: Improving Critical Infrastructure Cybersecurity*, Department of Homeland Security Integrated Task Force, Incentives Study, 2013.

[31] J. Connolly, D. Mark, and S. Charles, *The Trusted Automated Exchange of Indicator Information (TAXII)*, The MITRE Corporation, 2014.

[32] S. Barnum, *Standardizing Cyber Threat Intelligence Information with Structured Threat Information Expression (Stix)*, The Mitre Corporation, 2012.

[33] Fidelis barncathttps://fidelissecurity.com/.

[34] A. Albakri, E. Boiten, and R. De Lemos, "Sharing cyber threat intelligence under the general data protection regulation," in *In the Annual Privacy Forum*, pp. 28–41, Springer, Cham, 2019.

[35] M. O'Reirdan, "U.S. anti-bot code of conduct (ABC) for Internet service providers (ISPs): barrier and metric consideration," *The Communications Security, Reliability and Interoperability Council, Working Group 7: Botnet Remediation, Final Report*, 2013.

[36] C. Johnson, L. Badger, D. Waltermire, J. Snyder, and C. Skorupka, *Guide to Cyber Threat Information Sharing*, NIST Special Publication 800, 2016.

[37] P. Cichonski, T. Millar, T. Grance, and K. Scarfone, *Computer Security Incident Handling Guide-Recommendations of the National Institute of Standards and Technology*, NIST Special Publication, 2012.

[38] S. Laube and R. B. Ohme, "Strategic aspects of cyber risk information sharing," *ACM Computing Surveys*, vol. 50, no. 5, pp. 1–36, 2018.

[39] T. Moore, R. Clayton, and R. Anderson, "The economics of online crime," *Journal of Economic Perspectives*, vol. 23, no. 3, pp. 3–20, 2009.

[40] J. Milletary, *Citadel Trojan Malware Analysis*, Dell SecureWorks, 2012.

[41] W. Li, Y. Wang, J. Li, and M. H. Au, "Towards blockchained challenge-based collaborative intrusion detection," in *In International Conference on Applied Cryptography and Network Security*, pp. 122–139, Springer, Cham, 2019.

[42] N. Alexopoulos, E. Vasilomanolakis, S. L. Roux, S. Rowe, and M. Mühlhäuser, "TRIDEnT: building decentralized incentives for collaborative security," 2019, https://arxiv.org/abs/1905.03571.

[43] T. Salman, R. Jain, and L. Gupta, "Probabilistic blockchains: a blockchain paradigm for collaborative decision-making," in *In 9th IEEE Annual Ubiquitous Computing, Electronics and Mobile Communication Conference (UEMCON)*, pp. 457–465, New York, NY, USA, 2018.

[44] D. B. Rawat, L. Njilla, K. Kwiat, and C. Kamhoua, "iShare: blockchain-based privacy-aware multi-agent information sharing games for cybersecurity," in *In IEEE International*

Conference on Computing, Networking and Communications (ICNC), pp. 425–431, Maui, HI, USA, 2018.

[45] A. Adebayo, D. B. Rawat, L. Njilla, and C. A. Kamhoua, "Blockchain-enabled information sharing framework for cybersecurity," *Blockchain for Distributed Systems Security*, pp. 143–158, 2019.

[46] Y. Pu, J. Luo, C. Hu et al., "Two secure privacy-preserving data aggregation schemes for IoT," *Wireless Communications and Mobile Computing*, vol. 2019, 11 pages, 2019.

[47] Y. Zhang, D. He, and K. K. R. Choo, "BaDS: blockchain-based architecture for data sharing with ABS and CP-ABE in IoT," *Wireless Communications and Mobile Computing*, vol. 2018, 9 pages, 2018.

[48] Mirai Source Codehttps://github.com/jgamblin/Mirai-Source-Code.

[49] Open Source Security Information and Event Managementhttps://www.alienvault.com/products/ossim.

[50] Hyper Ledgerhttps://www.hyperledger.org.

[51] V. Buterin, *A Next-Generation Smart Contract and Decentralized Application Platform*, White paper, 2014, https://github.com/ethereum/wiki/wiki/White-Paper.

[52] Remix Solidity Browserhttp://cdetr.io/browser-solidity/.

[53] Web3, Ethereum JavaScript APIhttps://web3js.readthedocs.io/en/1.0/.

[54] V. Buterin and V. Griffith, *Casper the Friendly Finality Gadget*, 2017, https://arxiv.org/abs/1710.09437.

[55] R. Danny and L. Chih-Cheng, *Hybrid Casper FFG*https://eips.ethereum.org/EIPS/eip-1011.

[56] OpenTAXII, *Stable Release*https://opentaxii.readthedocs.io/en/stable/.

[57] Anomli STAXXhttps://www.anomali.com/resources/staxx.

[58] C. Wagner, A. Dulaunoy, G. Wagener, and A. Iklody, "Misp: the design and implementation of a collaborative threat intelligence sharing platform," *2016 ACM on Workshop on Information Sharing and Collaborative Security*, pp. 49–56, 2016.

[59] N. C. Soltra, *Soltra Edge*, 2018, http://www.soltra.com/en.

[60] J. Postel, *Internet Protocol*, RFC 791 (Standard), IETF, 1981.

[61] M. Kerrisk, *The Linux Programming Interface: A Linux and UNIX System Programming Handbook*, No Starch Press, 2010.

[62] B. Tung, *Common Intrusion Detection Framework*http://gost.isi.edu/cidf/.

[63] D. Schnackenberg, K. Djahandari, and D. Sterne, "Infrastructure for intrusion detection and response," in *DARPA Information Survivability Conference and Exposition, DISCEX '00*, vol. 2, pp. 3–11, 2000.

[64] K. Moriarty, *Real-time inter-network defense(RID)*, Internet Engineering Task Force (IETF), RFC 6545, 2012, https://tools.ietf.org/html/rfc6545.

[65] R. Danyliw, *The Incident Object Description Exchange Format Version 2*, Internet Engineering Task Force (IETF), RFC 7970, 2016, https://tools.ietf.org/html/rfc7970.

[66] B. Trammell, *Transport of Real-time Inter-network Defense (RID) Messages over HTTP/TLS*, Internet Engineering Task Force (IETF), RFC 6546, 2012, https://www.rfc-editor.org/rfc/rfc6546.

[67] P. Kampanakis and M. Suzuki, *Incident Object Description Exchange Format Usage Guidance*, Internet Engineering Task Force (IETF), RFC 8274, 2017, https://tools.ietf.org/html/rfc8274.

[68] P. Saint-Andre, *Extensible messaging and presence protocol (xmpp): Core*, Internet Engineering Task Force (IETF), RFC 6120, 2011, https://tools.ietf.org/html/rfc6120.

[69] P. Saint-Andre, *Extensible Messaging and Presence Protocol (XMPP): Instant Messaging and Presence*, Internet Engineering Task Force (IETF), RFC 6121, 2011, https://tools.ietf.org/html/rfc6121.

[70] P. Saint-Andre, *Extensible Messaging and Presence Protocol (XMPP): AddressFormat*, Internet Engineering Task Force (IETF), RFC 7622, 2015, https://tools.ietf.org/html/rfc7622.

[71] P. Saint-Andre, *Use of Transport Layer Security (TLS) in the Extensible Messaging and Presence Protocol (XMPP)*, Internet Engineering Task Force (IETF), RFC 7590, 2015, https://tools.ietf.org/html/rfc7590.

[72] B. Feinstein and G. Matthews, "The Intrusion Detection Exchange Protocol (IDXP)," Internet Engineering Task Force (IETF), RFC 4767, 2007, https://tools.ietf.org/html/rfc4767.

[73] H. Debar, D. Curry, and B. Feinstein, *The Intrusion Detection Message Exchange Format (IDMEF)*, Internet Engineering Task Force (IETF), RFC 4765, 2007, https://tools.ietf.org/html/rfc4765.

[74] T. Buchheim, M. Erlinger, B. Feinstein et al., "Implementing the intrusion detection exchange protocol," in *Seventeen Annaul Computer Security Applications Conference (ACSAC)*, pp. 32–41, 2001.

[75] J. Klensin, *Simple Mail Transfer Protocol*, Internet Engineering Task Force (IETF), RFC 5321, 2008, https://tools.ietf.org/html/rfc5321.

[76] Y. Shafranovich, J. Levine, and M. Kucherawy, *An Extensible Format for Email Feedback Reports*, Internet Engineering Task Force (IETF), RFC 5965, 2010, https://datatracker.ietf.org/doc/rfc6650/.

[77] *CEE Log Transport (CLT) Specification*, The MITRE Corporation, 2012, https://cee.mitre.org/language/1.0-beta1/clt.html.

[78] *Common Event Expression*, The MITRE Corporation, 2013, https://cee.mitre.org/.

[79] R. Gerhards, *The syslog protocol*, Internet Engineering Task Force (IETF), RFC 5424, 2009, https://tools.ietf.org/html/rfc5424.

[80] F. Miao, Y. Ma, and J. Salowey, *Transport layer security (TLS) transport mapping for syslog*, Internet Engineering Task Force (IETF), RFC 5425, 2009, https://tools.ietf.org/html/rfc5425.

Hindawi
Wireless Communications and Mobile Computing
Volume 2022, Article ID 7336279, 8 pages
https://doi.org/10.1155/2022/7336279

Research Article

Certificate-Based Signature Scheme for Industrial Internet of Things Using Hyperelliptic Curve Cryptography

Insaf Ullah,[1] Ali Alkhalifah,[2] Maha M. Althobaiti,[3] Fahd N. Al-Wesabi,[4] Anwer Mustafa Hilal,[5] Muhammad Asghar Khan,[1] and Jimmy Ming-Tai Wu[6]

[1]*Hamdard University Karachi, Islamabad Campus, Islamabad 44000, Pakistan*
[2]*Department of Information Technology, College of Computer, Qassim University, Buraydah 51452, Saudi Arabia*
[3]*Department of Computer Science, College of Computing and Information Technology, Taif University, P.O. Box 11099, Taif 21944, Saudi Arabia*
[4]*Department of Computer Science, College of Science & Art, King Khalid University, Abha, Saudi Arabia*
[5]*Department of Computer and Self Development, Preparatory Year Deanship, Prince Sattam Bin Abdulaziz University, AlKharj, Saudi Arabia*
[6]*College of Computer Science and Technology, Shandong University of Science and Technology, Shandong, China*

Correspondence should be addressed to Jimmy Ming-Tai Wu; wmt@wmt35.idv.tw

Received 27 October 2021; Revised 9 December 2021; Accepted 3 January 2022; Published 8 February 2022

Academic Editor: Zahid Khan

The Industrial Internet of Things (IIoT) is a technology that uses the Internet of Things (IoT) infrastructure to sense, process, and communicate real-time events in the industrial system to cut down on unnecessary operating costs and to speed up industrial automation of internal and external working processes. Since the IIoT system inherits the same cyber-physical vulnerabilities that the IoT system already encounters, it requires additional work to address security concerns owing to its heterogeneous nature. As a result, an efficient security mechanism is essential to protect against various and unknown cyber-attacks. In this article, we propose a certificate-based signature scheme based on hyperelliptic curve cryptography (HECC), with the aim of improving security while reducing computational and communication costs in the IIoT environment. The proposed scheme outperforms existing schemes in terms of both computational and communication costs, as well as offering better security.

1. Introduction

The term "Industrial Internet of Things" (IIoT) refers to the use of Internet of Things (IoT) devices and infrastructure to collect and communicate real-time events in industrial systems in order to reduce human efforts and operational costs while also improving manufacturing and industrial processes [1]. Chemical factories, for example, are a good example of industrial processes since they include highly sensitive processes that require real-time communication between machines and other entities [2]. One of the advanced tiers of networking design, termed Fifth Generation (5G) mobile networks, appears to give a worthy communication in the digital words of IIoT [3]. The International Data Corporation (IDC) report that globally 70% of companies spend $1.2 billion on 5G connectivity management solutions. When 5G and IIoT (5G-IIoT) are combined, a rapid, intelligent, and ubiquitous communication system emerges [4]. Additionally, 5G mobile networks support a cutting-edge technology known as cloud computing [5], which ensures the storage, processing, analysis, and exchange of data generated by IIoT devices. A traditional cloud computing paradigm, on the other hand, is incapable of effectively managing data directly. Because the sensor has limited resources, it will be unable to process the complicated intelligent algorithms. A mobile edge node with extra attributes of powerful processing and storage capacity will be employed to overcome this challenge. In Figure 1, collaborative technologies such as 5G, cloud server (CS), edge computing (EC), and bluetooth low energy (BLE) are used to create an infrastructure for an IIoT environment.

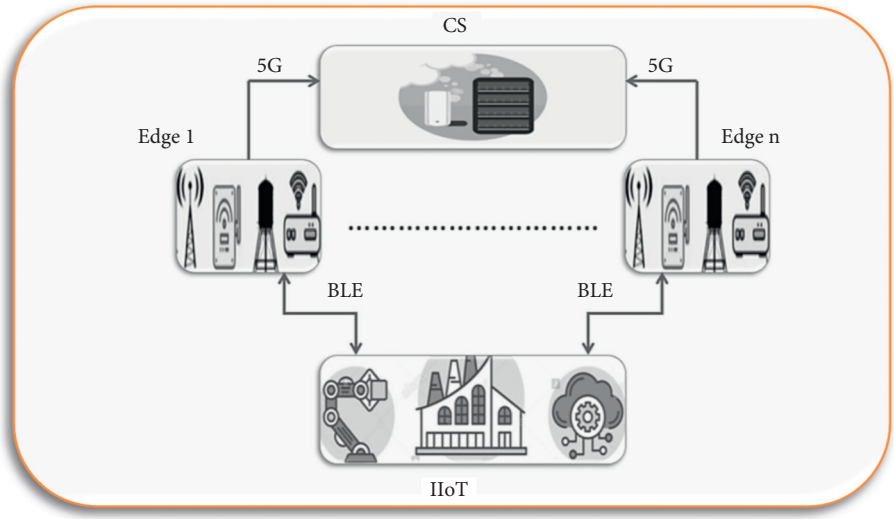

Figure 1: A collaborative technology architecture for IIoT.

However, in an IIoT setting, a malicious sensor can put the entire network at risk, necessitating the use of a robust authentication mechanism [6]. For the purpose of ensuring integrity and authenticity, the digital signature procedure is used [7]. Digital signatures are public key cryptographic primitives (PKCP), which are classified into three categories: public key environment (PKE), identity-based environment (IBE), and certificateless environment (CE). In the cryptography/information security field, PKE has got a lot of attention. It does, however, have severe flaws in terms of certificate management and revocations. Then, when a trusted agent (TA) or organization receives the participant identification, IBE removes certificate management and revocation concerns, and a trusted agent (TA) or organization creates the private key for participating devices. The secret key was provided with participants through a dedicated link by TA. However, if TA so desires, it will provide the opponent with the private key, so that he or she may generate a real signature of the participants. The CE resolves the issue of participant signature forgery in IBE by eliminating the process of private key generation from the TA and having the TA produce the partial private key (PPK) for the participating users, which is then shared with participants via a dedicated link. Sharing PPK with participants, on the other hand, necessitates a dedicated link with participants, which is a major concern in CE.

The certificate-based environment (CBE) is an enhanced version of PKCP that overcomes the limitations of PKE, IBE, and CE by removing the need for certificate management and revocations, as well as a dedicated link for exchanging private key and PPK with participants. The CBE is a hybrid of PKE and IBE in which the participant sends his identification to the TA, who subsequently generates a certificate using his private key and public parameters, as well as the participant's identity. Furthermore, instead of utilizing a dedicated link, TA provides the certificate to that user, and the participants create their private and public keys. PKCP security and efficiency are usually determined by mathematical parameters. Because it substitutes elliptic curve (EPC) with an extra package of low key and parameter size, the mathematical aspects of hyperelliptic curve (HPEC) have received increased attention when creating protocols for resource hungry environments [8]. As we all know, bilinear pairing is worse than EPC and RSA; thus, we can conclude that HPEC is the best option for building a scheme for the IIoT environment. As a result, using collaborative technologies such as 5G, cloud computing, and edge computing, we introduced a new intelligent certificate-based signature for IIoT in this article. The following are the study's key contributions:

(i) We propose a HECC-based certificate-based signature scheme for IIoT security, which improves security while having a small key size.

(ii) We introduce an edge computing architecture for IIoT that uses BLE to directly access data from IIoT devices and transmits it to a cloud server through a 5G wireless link.

(iii) We use the random oracle model (ROM) to undertake a formal security analysis of the proposed scheme, ensuring that it is secure against type 1 and type 2 adversaries.

(iv) We compare the computation and communication costs of the proposed scheme to some of the existing schemes, demonstrating that our scheme is more efficient.

The organization of the article is set out as follows. The related work on certificate-based signature schemes is presented in Section 2. We go through the network model in Section 3, which also includes network and threat models. In Section 4, the proposed model and algorithm are defined. Section 5, on the other hand, provides the proposed scheme's security analysis. In addition, we discuss performance analysis in Section 6. The conclusion is presented in Section 7.

2. Related Works

The major security measures rely on cryptographic concepts to ensure authenticity, confidentiality, and integrity. A well-designed data security strategy may greatly reduce the likelihood of data being compromised. Kang et al. [9] presented a certificate-based signature with the help of pairings on elliptic curves, and its security analysis is provided by utilizing the random oracle model. Then, Li et al. [10], analyzed the presented scheme in [9], and they say that it is suffering from key replacement attack. Furthermore, they proposed an enhanced certificate-based signature with the use of lower length operations. However, the scheme presented in [9, 10] will definitely suffer by higher computational cost due to expensive pairing operations. To avoid such limitations, Liu et al. [11] presented a new certificate-based signature by not entertaining the expensive operations of bilinear pairing. However, it can still be affected by exponential operations when we consider today's resource hungry IoT devices. Also, Zhang [12] stated that the scheme presented in [11] is suffering from certain security flaws and proposed new approach with the help of pairing operations. Ming and Wang [13] presented a new certificate-based signature by not entertaining the expensive operations of bilinear pairing. Li et al. [14] presented a new certificate-based signature by entertaining the expensive operations of bilinear pairing that can be suffered from greater computational operations. In 2013, Li et al. [15] proved that the scheme used in [13] is not secure from malicious certifier, and they further proposed a low processing time-oriented certificate-based signature. Lu and Li [16] presented a certificate-based signature by entertaining the expensive operations of bilinear pairing. Zhang et al. [17] presented a certificate-based signature by not entertaining the expensive operations of bilinear pairing. Li et al. [18] contributed a key-insulated certificate-based signature; however, Lu et al. [19] proved that the scheme of [18] is not secure from malicious certifier. Also, the proposed certificate-based signature is with improved nature. Lu and Li [20] presented a certificate-based signature by entertaining the expensive operations of bilinear pairing.

3. Network Model

The proposed scheme's network model comprised of four entities, as shown in Figure 2: certificate authority (CA), edge node, cloud server, IIoT devices, and data users. The following is the role of each entity:

(i) Certificate authority (CA): this entity can function as a trusted third party, creating system parameters for the whole network as well as certificates for IIoT devices and data users.

(ii) Cloud server (CS): this entity may be used to store data generated by IIoT devices and data users in a big resource-oriented database.

(iii) IIoT devices: these devices are responsible to generate data from different machines and send it to the edge node using BLE.

(iv) Edge node: this node will be responsible for producing certificate-based signatures on IIoT data after it obtains a certificate from a CA and generates his public and private key.

(v) Data users: data users are responsible for validating the received certificate-based signature from IIoT devices after receiving a certificate from a CA and creating his public and private key.

4. Proposed Certificate-Based Signature Scheme

Here, we first provide the symbols used in the proposed scheme, as given in Table 1; then, the proposed scheme is defined in detail in the phases that follow [21]:

Setup: suppose $\mathcal{O}$ is the given HECC security parameter with size of 80 bits. Then, CA performs the following steps for generating master secrete key ($\mathcal{Q}$), public key (δ), and global parameter set (σ).

(i) CA select $\mathcal{Q}$ randomly, where $1 \le \mathcal{Q} \le n$

(ii) It computes $\delta = \mathcal{Q}.\mathcal{D}$ and selects h^o and h^p as hash functions

(iii) Make $\sigma = \{n, \mathcal{O}, h^o, h^p, \delta, \mathcal{D}\}$ and get available in a network publicly

Key generation: given σ, an actor with identity (ID^a) select $\mathcal{U}^a$ randomly, where $1 \le \mathcal{U}^a \le n$ and compute $\mathcal{V}^a = \mathcal{U}^a.\mathcal{D}$. Then, an actor with identity (ID^a) set $\mathcal{U}^a$ as his private key and $\mathcal{V}^a$ as his public key.

Certificate generation: an actor with identity (ID^a) send ($\mathcal{V}^a, \mathrm{ID}^a$) to CA. Then, select $\mathcal{W}^a$ randomly, where $1 \le \mathcal{W}^a \le n$, compute $\mathcal{X}^a = \mathcal{W}^a.\mathcal{D}$, and compute $\mathcal{C}^a = \mathcal{W}^a + \mathcal{Q}.\ h^o\ (\mathrm{ID}^a, \mathcal{V}^a)$. Finally, CA dispatched $\mathcal{C}\mathrm{ert}^a = (\mathcal{C}^a, \mathcal{X}^a)$ to an actor with ID^a.

Signature generation: a sender can generate signature $(\mathcal{Z}, \mathcal{S})$ utilizing the following steps

(i) It selects $\mathcal{G}$ randomly, where $1 \le \mathcal{G} \le n$ and computes $\mathcal{N} = \mathcal{X}^s + \mathcal{G}.\mathcal{D}$

(ii) Compute $\mathcal{Z} = h^p\,(\mathcal{V}^s, \mathrm{ID}^s, \delta)$ and $\mathcal{S} = \mathcal{G} + \mathcal{U}^s.\mathcal{Z} + \mathcal{C}^s$

(iii) Send $(\mathcal{Z}, \mathcal{S})$ to receiver

Signature verifications: a receiver can verify the signature $(\mathcal{Z}, \mathcal{S})$ utilizing $\mathcal{S}.\mathcal{D} = \mathcal{N} + \delta.h^o\,(\mathrm{ID}^s, \mathcal{V}^s) + h^p\,(\mathcal{V}^s, \mathrm{ID}^s, \delta).\mathcal{V}^s$.

(i) Correctness

A receiver can verify the signature $(\mathcal{Z}, \mathcal{S})$ utilizing the following computations:

$\mathcal{S}.\mathcal{D} = \mathcal{G} + \mathcal{U}^s.\mathcal{Z} + \mathcal{C}^s.\mathcal{D} = \mathcal{G} + \mathcal{W}^s + \mathcal{Q}.h^o\,(\mathrm{ID}^s, \mathcal{V}^s) + \mathcal{U}^s.h^p \quad (\mathcal{V}^s, \mathrm{ID}^s, \delta).\mathcal{D} = \mathcal{G}.\mathcal{D} + \mathcal{W}^s.\mathcal{D} + \mathcal{Q}.\mathcal{D}.h^o\,(\mathrm{ID}^s, \mathcal{V}^s) + \mathcal{U}^s.\mathcal{D}.h^p\,(\mathcal{V}^s, \mathrm{ID}^s, \delta) \quad (\mathcal{G}.\mathcal{D} + \mathcal{X}^s +$

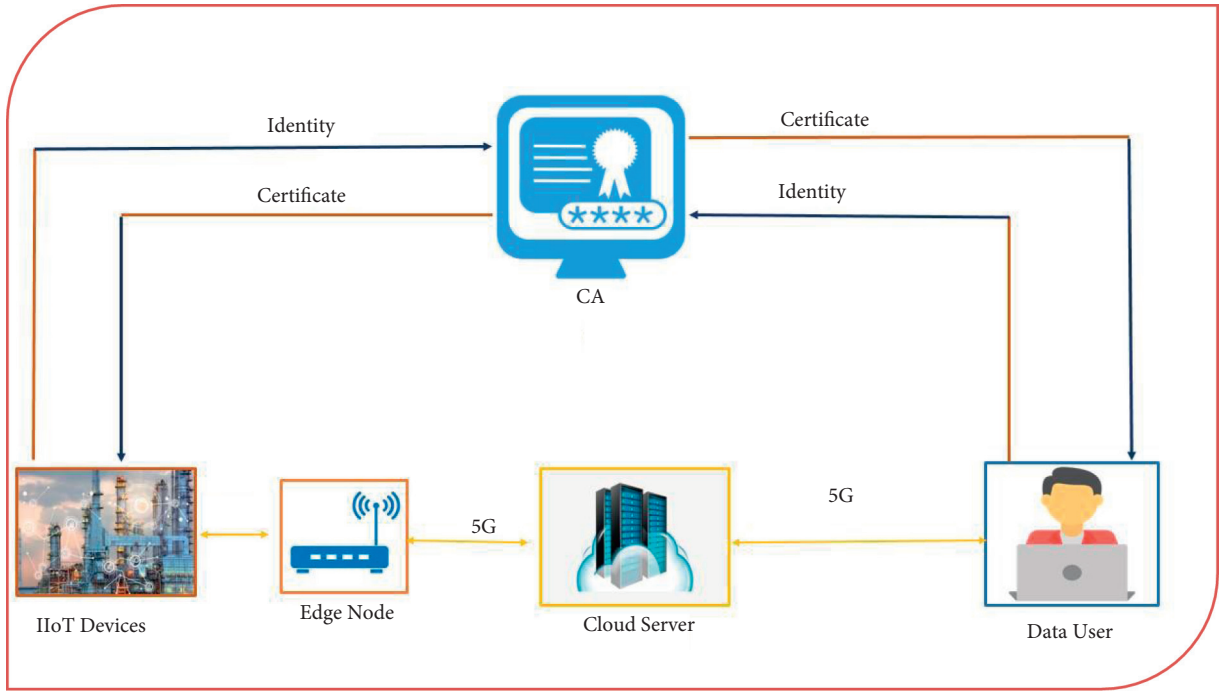

Figure 2: Network model of the proposed scheme.

Table 1: Symbols used in the proposed scheme.

No.	Symbol	Descriptions
1	$\mathcal{Q}$	Master secret key of CA which is picked from hyperelliptic curve finite field
2	δ	Master public key of CA which is the combination of $\mathcal{Q}$ and $\mathcal{D}$
3	$\mathcal{D}$	Devisor of hyperelliptic curve
4	h^o and h^p	These are two hash functions of a same nature and with same properties
5	$\mathcal{O}$	It is the selected security parameter from hyperelliptic curve
6	n	It is a finite number with range of 80 bits
7	$\mathcal{C}\text{ert}^s = (\mathcal{C}^s, \mathcal{X}^s)$	It show certificate of sender
8	$\mathcal{C}\text{ert}^r = (\mathcal{C}^r, \mathcal{X}^r)$	It show certificate of receiver
9	$\mathcal{V}^s$	It show the public key of sender
10	$\mathcal{V}^r$	It show the public key of receiver
11	$\mathcal{U}^s$	It show the private key of sender
12	$\mathcal{U}^r$	It show the private key of receiver
13	ID^s	It show the identity of sender
14	ID^r	It show the identity of receiver
15	$\mathfrak{f}^1$	A symbol used to represent type 1 adversary
16	$\mathfrak{f}^2$	A symbol used to represent type 2 adversary
17	$\mathcal{C}$	The symbol of a facilitator for type 1 and type 2 adversaries

$\delta.h^o(\text{ID}^s, \mathcal{V}^s) + \mathcal{V}^s h^p(\mathcal{V}^s, \text{ID}^s, \delta)) = \mathcal{N} + \delta.h^o \quad (\text{ID}^s, \mathcal{V}^s) + h^p(\mathcal{V}^s, \text{ID}^s, \delta).\mathcal{V}^s$.

5. Security Analysis

Here, the security analysis is totally based on the hardiness of the hyperelliptic curve discrete logarithm problem (HECDLP) that can be defined as follows: suppose $A = B.\mathcal{D}$, where $1 \le B \le n$, so finding B is said to be HECDLP. This section comprises the following two games that are playing for defending of our scheme signature against two types of adversaries, e.g., type 1 ($\mathfrak{f}^1$) and type 2 ($\mathfrak{f}^2$). Here, $\mathcal{C}$ acts as a facilitator for these adversaries. So, $\mathfrak{f}^1$ is the outsider attacker whose capability is to replace the user public key for generating the forge signature; furthermore, it is not capable to access the private key of CA. Moreover, $\mathfrak{f}^2$ is the insider attacker whose capability is to access CA private key, and it is not capable to replace user public key.

Game 1: in this game, by performing maximum number of queries (Q), using ROM, $\mathfrak{f}^1$ can forge our scheme signature with the help of $\mathcal{C}$, when it is to solve HECDLP utilizing the following advantages:

$$\text{Success}^{\mathfrak{f}^1} \geq \frac{1}{Q}\left(1-\frac{1}{Q}\right)^{Q}\xi, \tag{1}$$

where ξ represents the $\mathfrak{f}^1$ success advantages key generation, h^o (.), h^p (.), private key generation, certificate generation, and signature generation, respectively. The results of these queries include in the lists $\mathscr{L}^{\text{KG}}$ $\mathscr{L}^{h^0}$, $\mathscr{L}^{h^p}$ $\mathscr{L}^{\text{PKG}}$, $\mathscr{L}^{cg}$, and $\mathscr{L}^{\text{sig}}$. Also, $\mathscr{C}$ perform the following steps for generating master secrete key ($\mathscr{Q}$), public key (δ), and global parameter set (σ).

Proof. The instance $\Upsilon = \beta$ of HECDLP is given to $\mathfrak{f}^1$; then, $\mathfrak{f}^1$ make the queries such as

(i) It selects $\mathscr{Q}$ randomly, where $1 \leq \mathscr{Q} \leq n$ and gives it to $\mathfrak{f}^1$

(ii) It computes $\delta = \mathscr{Q}.\mathscr{D}$ and selects h^o and h^p as hash functions

(iii) Make $\sigma = \{n, \mathscr{O}, h^o, h^p, \delta, \mathscr{D}\}$ and get available in a network publicly

(iv) It also picks the index $\mathscr{J}$, where $1 \leq \mathscr{J} \leq h^p$ (.)

So, we discuss the queries in the following steps with their results.

Key generation query (.): $\mathfrak{f}^1$ sends ID^g $(1 \leq g \leq \text{KG})$ to key generation oracle (.), where KG represents the maximum number query. $\mathscr{C}$ includes the outputs in $\mathscr{L}^{\text{KG}}$. To reply, $\mathscr{C}$ look for $(\text{ID}^g, \mathscr{V}^g, \mathscr{U}^g)$ in $\mathscr{L}^{\text{KG}}$; if it exists, then $\mathscr{C}$ send $\mathscr{V}^g$ to $\mathfrak{f}^1$; otherwise, it performs the following steps.

(i) If $\mathscr{J} \neq g$, then it selects $\mathscr{U}^g$ randomly, where $1 \leq \mathscr{U}^g \leq n$ and compute $\mathscr{V}^g = \mathscr{U}^g.\mathscr{D}$

(ii) If $\mathscr{J} = g$, it sets $\mathscr{V}^g = \beta.\mathscr{D}$.

h^o (.): $\mathfrak{f}^1$ sends this query; to reply, $\mathscr{C}$ look for $(\text{ID}^g, \mathscr{V}^g, f)$ in $\mathscr{L}^{h^0}$; if it exists, then $\mathscr{C}$ send f to $\mathfrak{f}^1$. Otherwise, $\mathscr{C}$ select f randomly, send f to $\mathfrak{f}^1$, and store $(\text{ID}^g, \mathscr{V}^g, f)$ in $\mathscr{L}^{h^0}$.

h^p (.): $\mathfrak{f}^1$ sends this query; to reply, $\mathscr{C}$ look for $(\text{ID}^g, \mathscr{V}^g, \delta, h)$ in $\mathscr{L}^{h^p}$; if it exists, then $\mathscr{C}$ send h to $\mathfrak{f}^1$. Otherwise, $\mathscr{C}$ select h randomly, send h to $\mathfrak{f}^1$, and store $(\text{ID}^g, \mathscr{V}^g, \delta, h)$ in $\mathscr{L}^{h^0}$.

Private key generation query (.): $\mathfrak{f}^1$ send ID^g; to reply, $\mathscr{C}$ perform the following steps:

(i) If $\mathscr{J} \neq g$, $\mathscr{C}$ look for $(\text{ID}^g, \mathscr{V}^g, \mathscr{U}^g)$ in $\mathscr{L}^{\text{PKG}}$; if it exists, then $\mathscr{C}$ send $\mathscr{U}^g$ to $\mathfrak{f}^1$

(ii) If $\mathscr{J} = g$, then it selects $\mathscr{U}^g$ randomly, send $\mathscr{U}^g$ to $\mathfrak{f}^1$, and includes $(\text{ID}^g, \mathscr{V}^g, \mathscr{U}^g)$ in $\mathscr{L}^{\text{PKG}}$

Signature generation query (.): $\mathfrak{f}^1$ sends ID^g; in reply, $\mathscr{C}$ runs key generation query (.), private key generation query (.), h^o (.), and h^p (.) oracles. $\mathscr{C}$ perform the following steps.

(i) If $\mathscr{J} \neq g$, $\mathscr{C}$ runs certificate generation oracle (.) and run signature generation oracle (.); then, $\mathscr{C}$ send the resultant value to $\mathfrak{f}^1$

(ii) If $\mathscr{J} = g$, then it selects $\phi^{\mathscr{J}}, f^{\mathscr{J}}, \varrho^{\mathscr{J}}$, and $\mathscr{C}^{\mathscr{J}}$ randomly, and set $\mathscr{N}^{\mathscr{J}} = \mathscr{X}^{\mathscr{J}} + \Upsilon$, $f^{\mathscr{J}} = h^o(\text{ID}^{\mathscr{J}}, \mathscr{V}^{\mathscr{J}})$, and $\varrho^{\mathscr{J}} = h^p(\mathscr{V}^{\mathscr{J}}, \text{ID}^{\mathscr{J}}, \delta)$

Forgery: when we take Forking lemma [21] in account, $\mathscr{C}$ can output two signature that are $(\mathscr{X}^*, \mathscr{S}^*)$ and $(\mathscr{X}^{**}, \mathscr{S}^{**})$, and we have the following computations:

$$\begin{aligned}
\mathscr{S}^*.\mathscr{D} &= \mathscr{X}^{\mathscr{J}} + Y + \delta.f^{\mathscr{J}} + \varrho^{\mathscr{J}}.\mathscr{V}^{\mathscr{J}},\\
\mathscr{S}^{**}.\mathscr{D} &= \mathscr{X}^{\mathscr{J}} + Y + \delta.f^{\mathscr{J}} + \varrho^{\mathscr{J}}.\mathscr{V}^{\mathscr{J}}\\
\mathscr{S}^*.\mathscr{D} - \mathscr{S}^{**}.\mathscr{D} &= \mathscr{X}^{\mathscr{J}} + Y^* + \delta.f^{\mathscr{J}} + \varrho^{\mathscr{J}}.\mathscr{V}^{\mathscr{J}}\\
&\quad - \mathscr{X}^{\mathscr{J}} - Y^{**}\\
-\delta.f^{\mathscr{J}} - \varrho^{\mathscr{J}}.\mathscr{V}^{\mathscr{J}} &= \mathscr{S}^*.\mathscr{D} - \mathscr{S}^{**}.\mathscr{D} = Y^* - Y^{**}\\
&= \mathscr{S}^*.\mathscr{D} - \mathscr{S}^{**}.\mathscr{D}\\
&= \beta.\mathscr{D}^* - \beta.\mathscr{D}^{**} = (\mathscr{S}^* - \mathscr{S}^{**}).\mathscr{D}\\
&= \beta.(\mathscr{D}^* - \mathscr{D}^{**}) = \beta = \frac{(\mathscr{S}^* - \mathscr{S}^{**}).\mathscr{D}}{(\mathscr{D}^* - \mathscr{D}^{**})}.
\end{aligned} \tag{2}$$

Probability analysis: here, we define the following events:

(i) $\mathscr{E}^1$: during execution of this game, $\mathscr{C}$ is not abandon

(ii) $\mathscr{E}^2$: $\mathfrak{f}^1$ is succeeded

(iii) $\mathscr{E}^3$: target identity is supposed to forge the proposed scheme signature

So, $(\mathscr{E}^1) \geq (1 - (1/Q))^Q$, $(\mathscr{E}^1, \mathscr{E}^2) = \xi$, and $(\mathscr{E}^1, \mathscr{E}^3, \mathscr{E}^2) = 1/Q$. Therefore,

$$\text{Success}^{\mathfrak{f}^1} \geq \frac{1}{Q}\left(1-\frac{1}{Q}\right)^{Q}\xi, \tag{3}$$

where ξ represents the $\mathfrak{f}^1$ success advantages.

Game 2: in this game, by performing maximum number of queries (Q), using ROM, $\mathfrak{f}^2$ can forge our scheme signature with the help of $\mathscr{C}$, when it solves HECDLP utilizing the following advantages:

$$\text{Success}^{\mathfrak{f}^1} \geq \frac{1}{Q}\left(1-\frac{1}{Q}\right)^{Q}\xi, \tag{4}$$

where ξ represents the $\mathfrak{f}^2$ success advantages. □

Proof:. The instance $\Upsilon = \beta.\mathscr{D}$ of HECDLP is given to $\mathfrak{f}^2$; then, $\mathfrak{f}^2$ make the queries such as key generation, h^o (.), h^p (.), private key generation, and signature generation, respectively. Also, $\mathscr{C}$ perform the following steps for generating master secrete key ($\mathscr{Q}$), public key (δ), and global parameter set (σ). Then, $\mathscr{C}$ give all these parameters to $\mathfrak{f}^2$.

The proof is same like a game 1. □

Table 2: Major operations of proposed and existing schemes.

Schemes	Signature	Verification	Total
Lu and Li [16]	6EPL	2EPL + 3P	8EPL + 3P
Li et al. [18]	4EPL	4P	4EPL + 4P
Lu et al. [19]	5EPL	1EPL + 4P	6EPL + 4P
Lu and Li [20]	9EPL	1EPL + 4P	10EPL + 4P
Proposed scheme	2 HM	3 HM	5 HM

Table 3: Computational cost comparisons of the proposed scheme and existing method on the bases of mile seconds.

Schemes	Signature	Verification	Total
Lu and Li [16]	$6 * 1.25 = 7.5$	$2 * 1.25 + 3 * 14.90 = 47.2$	$8 * 1.25 + 3 * 14.90 = 54.7$
Li et al. [18]	$4 * 1.25 = 5$	$4 * 14.90 = 59.6$	$4 * 1.25 + 4 * 14.90 = 64.4$
Lu et al. [19]	$5 * 1.25 = 6.25$	$1 * 1.25 + 4 * 14.90 = 60.85$	$6 * 1.25 + 4 * 14.90 = 67.1$
Lu and Li [20]	$9 * 1.25 = 11.25$	$1 * 1.25 + 4 * 14.90 = 60.85$	$10 * 1.25 + 4 * 14.90 = 72.1$
Proposed scheme	$2 * 0.48 = 0.96$	$3 * 0.48 = 1.44$	$5 * 0.48 = 2.4$

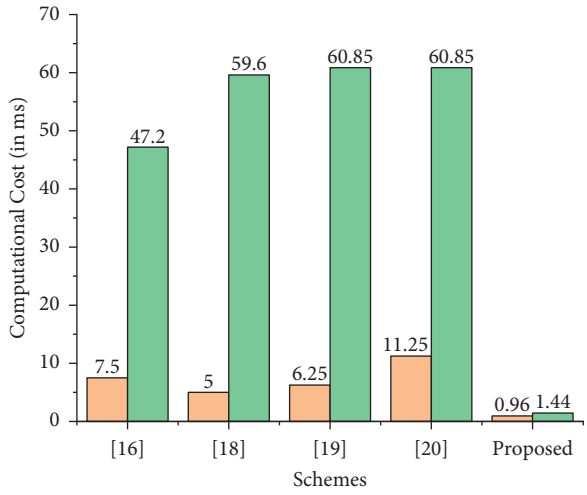

Figure 3: Computational cost comparison.

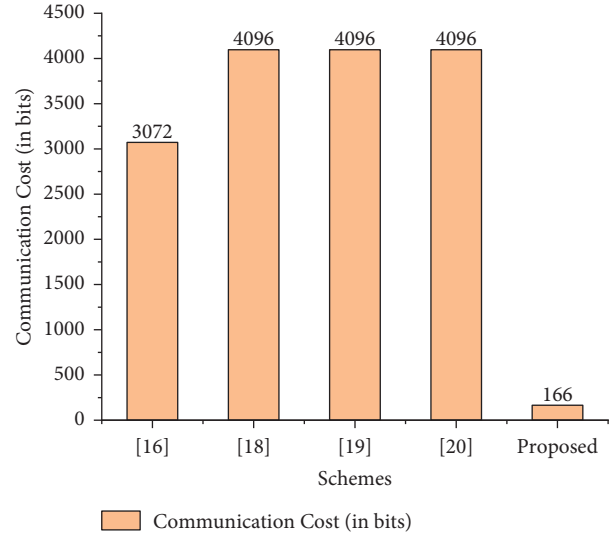

Figure 4: Communication cost comparison.

Table 4: Communication overhead comparisons of the proposed scheme and existing method on the bases of bits.

Schemes	Signature size	Signature size in bits
Lu and Li [16]	$3\|G\|$	$3 * 1024 = 3072$
Li et al. [18]	$4\|G\|$	$4 * 1024 = 4096$
Lu et al. [19]	$4\|G\|$	$4 * 1024 = 4096$
Lu and Li [20]	$4\|G\|$	$4 * 1024 = 4096$
Proposed scheme	$2\|n\|$	$2 * 80 = 160$

6. Performance Analysis

In this section, we provide details about computational and communication costs of the proposed scheme with its counterpart schemes.

6.1. Computational Cost. Here, we first provide major operations such as exponential (EPL), bilinear pairing (P), and hyperelliptic curve divisor multiplications (HM) in proposed certificate-based signature scheme and the other approaches such as by Lu and Li [16], Li et al. [18], Lu et al. [19], and Lu and Li [20], respectively, as given in Table 2. Then, we consider the time taken by each major operations from [1], in which EPL consumes 1.25 ms, P takes 14.90 ms, and HM utilizes 0.48 ms, respectively [22, 23]. So, on the bases of above-discussed consuming time of major operations, we make the comparisons of proposed certificate-based signature scheme and the other approaches such as by Lu and Li [16], Li et al. [18], Lu et al. [19], and Lu and Li [20], as given in Table 3. Thus, the clearer improvement in computational cost can be seen from Table 3 and Figure 3, and it means our scheme consumes less time during computational processing.

6.2. Communication Cost. Here, we provide the parameter considered for communication overhead bilinear pairing group (G) and hyperelliptic curve (n) in proposed certificate-

based signature scheme and the other approaches such as by Lu and Li [16], Li et al. [18], Lu et al. [19], and Lu and Li [20], respectively, as given in Table 3. Then, we consider the bits consumed by each parameter, in which G consumes 1024 bits and n take 80 bits. So, on the bases of above-discussed consuming bits by each parameter, we make the comparisons of proposed certificate-based signature scheme and the other approaches such as by Lu and Li [16], Li et al. [18], Lu et al. [19], and Lu and Li [20], as given in Table 4. Thus, the clearer improvement in computational communication overhead can be seen from Table 4 and Figure 4, which authenticates that our scheme ingests less bits during communications.

7. Conclusion

The Industrial Internet of Things (IIoT) has recently gained popularity for industrial applications. IIoT systems are vulnerable to a variety of cyber-attacks due to the wireless and widespread connectivity of IoT sensors and devices. Certificate-based signature methods are a better solution than other cryptographic schemes for solving the IIoT's security demands in terms of offering resilience to such attacks. As a result, certificate-based IIoT signature mechanisms are proposed in this study. We employed HECC, which is similar to RSA, bilinear pairing, and ECC, but has a smaller key size. After performing a comparison study, we found that our scheme outperforms its equivalent schemes in terms of computation and communication costs. In addition, the proposed scheme improves security against both known and unknown attacks.

Data Availability

The data generated or analyzed during this study are included within the article.

Conflicts of Interest

The authors declare that they have no conflicts of interest.

Acknowledgments

The authors extend their appreciation to the Deanship of Scientific Research at King Khalid University for funding this work (RGP 2/209/42). The authors deeply acknowledge Taif University, Taif, Saudi Arabia, for supporting this research through Taif University Researchers Supporting Project Number (TURSP-2020/328).

References

[1] P. Lade, R. Ghosh, and S. Srinivasan, "Manufacturing analytics and industrial Internet of Things," *IEEE Intelligent Systems*, vol. 32, no. 3, pp. 74–79, 2017.

[2] T. Kumar, E. Harjula, M. Ejaz, and A. Manzo, "BlockEdge: blockchain-edge framework for industrial IoT networks," *IEEE Access*, vol. 8, pp. 154166–154185, 2020.

[3] T. K. Ahmad, M. Liyanage, J. Okwuibe, M. Ylianttila, and A. Gurtov, "Overview of 5G security challenges and solutions," *IEEE Communication and Standards Magazine*, vol. 2, no. 1, pp. 36–43, 2018.

[4] H. Rahimi, A. Zibaeenejad, and A. A. Safavi, "A novel IoT architecture based on 5G-IoT and next generation technologies," in *Proceedings of the 2018 IEEE 9th Annual Information Technology, Electronics and Mobile Communication Conference (IEMCON)*, pp. 81–88, Vancouver, BC, 2018.

[5] H. Wang, W. Jia, A. Liu, and M. Xie, "MTES: an intelligent trust evaluation scheme in sensor-cloud-enabled industrial Internet of Things," *IEEE Transactions on Industrial Informatics*, vol. 16, no. 3, pp. 2054–2062, 2020.

[6] M. Kumar, H. Kumar Verma, and G. Sikka, "A secure data transmission protocol for cloud-assisted edge-Internet of Things environment," *Transactions on Emerging Telecommunications Technologies*, 2020.

[7] M. A. Khan, I. M. Qureshi, I. Ullah, S. Khan, F. Khanzada, and F. Noor, "An efficient and provably secure certificateless blind signature scheme for flying ad-hoc network based on multi-access edge computing," *Electronics*, vol. 9, no. 1, p. 30, 2019.

[8] M. A. Khan, I. Ullah, and N. Kumar, "An efficient and secure certificate-based access control and key agreement scheme for flying ad hoc networks," *IEEE Transactions on Vehicular Technology*, vol. 70, 2021.

[9] B. G. Kang, J. H. Park, and S. G. Hahn, "A certificate-based signature scheme," in *in Topics in Cryptology-CT-RSA 2004*, T. Okamoto, Ed., vol. 2964, Springer, Heidelberg, Germany, 2004, Lecture Notes in Computer Science.

[10] J. Li, X. Huang, Y. Mu, W. Susilo, and Q. Wu, "Certificate-based signature: security model and efficient construction in public key Infrastructure," *Lecture Notes in Computer Science*, Vol. 4582, Springer, , Heidelberg, Germany, 2007.

[11] J. K. Liu, J. Baek, W. Susilo, and J. Zhou, "Certificate-based signature schemes without pairings or random oracles," in *in Information Security. ISC 2008*, T. C. Wu, C. L. Lei, V. Rijmen, and D. T. Lee, Eds., vol. 5222, Springer, Heidelberg, Germany, 2008, Lecture Notes in Computer Science.

[12] J. Zhang, "On the security of a certificate-based signature scheme and its improvement with pairings," in *Proceedings of the International Conference of Information Security Practice and Experience*, pp. 47–58, 2009.

[13] Y. Ming and Y. Wang, "Efficient certificate-based signature scheme," *IAS*, vol. 2, pp. 87–90, 2009.

[14] J. Li, X. Huang, Y. Mu, W. Susilo, and Q. Wu, "Constructions of certificate-based signature secure against key replacement attacks," *Journal of Computer Security*, vol. 18, no. 3, pp. 421–449, 2010.

[15] J. Li, Z. Wang, and Y. Zhang, "Provably secure certificate-based signature scheme without pairings," *Information Science*, vol. 233, pp. 313–320, 2013.

[16] Y. Lu and J. Li, "Improved certificate-based signature scheme without random oracles," *IET Information Security*, vol. 10, no. 2, pp. 80–86, 2016.

[17] Y. Zhang, J. Li, Z. Wang, and W. Yao, "A new efficient certificate-based signature scheme," *Chinese Journal of Electronics*, vol. 24, no. 4, pp. 776–782, 2015.

[18] J. Li, H. Du, and Y. Zhang, "Certificate-based key-insulated signature in the standard model," *Computer Journal*, vol. 59, no. 7, pp. 1028–1039, 2016.

[19] Y. Lu, J. Li, and J. Shen, "Weakness and improvement of a certificatebased key-insulated signature in the standard model," *Computer Journal*, vol. 60, no. 12, pp. 1729–1744, 2017.

[20] Y. Lu and J. Li, "A forward-secure certificate-based signature scheme with enhanced security in the standard model," *KSII*

Transactions on Internet and Information System, vol. 13, no. 3, pp. 1502–1522, 2019.

[21] G. K. Verma, N. Kumar, P. Gope, B. B. Singh, and H. Singh, "SCBS: a short certificate-based signature scheme with efficient aggregation for industrial-internet-of-things environment," *IEEE Internet of Things Journal*, vol. 8, no. 11, pp. 9305–9316, 2021.

[22] I. Ullah, N. U. Amin, M. A. Khan, H. Khattak, and S. Kumari, "An efficient and provable secure certificate-based combined signature, encryption and signcryption scheme for Internet of Things (IoT) in mobile health (M-Health) system," *Journal of Medical Systems*, vol. 45, p. 4, 2021.

[23] M. A. Khan et al., "A provable and privacy-preserving authentication scheme for UAV-enabled intelligent transportation systems," *IEEE Transactions on Industrial Informatics*, vol. 18, no. 5, pp. 3416–3425, 2022.

Hindawi
Wireless Communications and Mobile Computing
Volume 2022, Article ID 5432023, 11 pages
https://doi.org/10.1155/2022/5432023

Research Article

Connectivity of Drones in FANETs Using Biologically Inspired Dragonfly Algorithm (DA) through Machine Learning

Shahzad Hameed,[1] Qurratul-Ain Minhas,[1] Sheeraz Ahmad,[2] Fasee Ullah,[3] Arshad Khan,[4] Atif Khan,[5] M. Irfan Uddin,[6] and Qiaozhi Hua[7]

[1]*Department of Electronics, Quaid-i-Azam University, Islamabad, Pakistan*
[2]*Department of Computer Science, Iqra National University, Peshawar, Pakistan*
[3]*Department of Computer Science, Sarhad University of Science and Information Technology, Peshawar, Pakistan*
[4]*Institute of Computer Sciences and Information Technology, The University of Agriculture Peshawar, Peshawar, Pakistan*
[5]*Department of Computer Science, Islamia College Peshawar, Peshawar, Pakistan*
[6]*Institute of Computing, Kohat University of Science and Technology, Kohat, Pakistan*
[7]*Computer School, Hubei University of Arts and Science, Xiangyang 441000, China*

Correspondence should be addressed to Qiaozhi Hua; 11722@hbuas.edu.cn

Received 10 October 2021; Revised 28 December 2021; Accepted 10 January 2022; Published 28 January 2022

Academic Editor: Zahid Khan

Flying Ad hoc Network (FANET) presents various challenges during communication due to the dynamic nature of network and ever-changing topology. Owing to high mobility, it is difficult to ensure a well-connected network and link stability. Thus, flying nodes have a higher chance of becoming disconnected from the network. In order to overcome these discrepancies, this work provides a well-connected network, reducing the number of isolated nodes in FANETs utilizing the depth of machine learning by taking inspiration from biology. Every biological species is innately intelligent and has strong learning ability. Moreover, they can also learn from existing active events and can take decision based on previous experience. There may be some unusual events such as attack of predator or when it may become isolated from the rest of the community. This ability helps them to maintain connectivity and concentrate on target. In this work, we take inspiration from dragonflies, which provide novel swarming behaviors of dynamic swarming and static swarming. The nodes in FANETs learn from the dragonflies and use this learning to search for a neighbor, ensuring connectivity. Moreover, to avoid collision and establish larger coverage area, they employ separation and alignment. In case a drone is isolated, it strives to become part of the network using machine learning (ML) via the dragonfly algorithm (DA). The proposed scheme results in larger coverage area with reduced number of isolated drones. This improves the connectivity in FANETs adding to the network intelligence via learning through DA, allowing communication despite the complexity of mobility and dynamic network topology.

1. Introduction

UAV (unmanned aerial vehicle) is an aircraft without a human pilot onboard which is popularly known as flying drone. They are equipped with a variety of additional equipment such as cameras, global positioning systems (GPSs), GPS-guided missiles, navigation systems, and sensors. They have ultra-stable flight and can hover and perform different acrobatics in the air. Their versatility is what truly makes them popular. Multiple drones are connected directly or through intermediate nodes in FANETs. These drones act as wireless relay in ad hoc networks, which provide coverage of wirelessly connected devices. Formation of small drones are now being introducing in military expeditions, civilian applications, disaster management, forest fire detection, agricultural management, border surveillance, and

telecommunications [1]. FANETs can be used as mobile radio stations or WLAN transmitters in regions lacking infrastructure [2–12].

Connectivity of a network is of utmost importance in critical fields involving uncertain flying driving units in FANETs. If a drone is destroyed by an enemy, it is important to offload data wirelessly to other neighboring drones. Therefore, FANETs can address predisaster and postdisaster calamity in real-time applications. Drones in the predisaster situation, collect the location information of all vulnerable zones and update that information periodically such as occurrence of disaster. This can measure the destroyed area for rescue operation. It can strengthen respond ability to the end user. Moreover, drones deployed on the postdisaster situation can help to establish necessary communication service. Application of FANETs in calamity situation is shown in Figure 1.

Previously, traditional approaches were adopted to analyze the performance of FANET to model the connectivity. The performances of the biological inspired algorithms are important development to capture the scalability and reliability patterns of wireless ad hoc networks. We therefore propose a machine-learning-based DA algorithm for connectivity of the drones in FANETs. Quick deployment of small flying drones is similar to dragonfly's behavior. Instead of food, the drones are searching for neighbors to enable wireless communication network. The choice of dragonfly technique comes into inspiration due to their light weight, rapid flying adjustment and finding neighbors within a communication range. They are able to maintain mobility, reduce isolation, and search for target consistently. Unpredictable FANETs scenario needs to organize crucial flight factors of altitude, speed, direction, etc. Organizing flying drones is a key challenge to establish a wireless network, and we attempt to make it possible through social inspiration behavior of dragonfly. To the best of our knowledge, the proposed work is the first solution for connectivity in the field of FANETs using machine learning. Our proposed scheme is valid for ad hoc applications and other wireless development technologies.

The rest of the paper is constructed as follows: Section 2 briefly explains the existing work. Section 3 presents the proposed working architecture of the dragonfly algorithm. The simulation results of the proposed work are presented in Section 4. Finally, the conclusion of this paper is presented in Section 5.

2. Related Work

FANETs are sparsely connected networks because of low density and high mobility of nodes. This causes fluctuation of link, loss of connectivity, and performance degradation. In He et al.'s study [13], the concepts of relay chain and relay tree are presented. When nodes are unable to establish connection with existing infrastructures on the ground, they can still communicate through other nodes. In Rautu et al.'s study [14], air-to-ground communication is investigated to overcome the loss of connectivity. The results showed that network stay connected when node replacement is performed. Optimal replacement of flying drone is a challenging task during flight missions. However, it is not feasible to replace the drones in an existing network. Replacing a drone is not a simple task due to ever-changing location information.

In Zhao et al.'s study [15], emergency communication system is established with the help of UAVs which relies on the mesh network with the objective to ensure connectivity between ground station and UAV. Yu et al. [16] developed UAVNet framework and established flying wireless mesh network. These studies focused on infrastructure-based ad hoc networks which is not the case of pure ad hoc network and may influence the quality of communication due to interference and time delay. Oubbati et al.'s study [17], an algorithm that considers change in network topology was constructed with an assumption that UAVs have full knowledge of the location of devices. It is investigated that optimal movement of UAVs can improve the connectivity of ad hoc networks.

In Cicek et al.'s study [18], semicentralized framework is proposed to establish ad hoc communication between UAVs under the conserving centralized organization. In this research, movement planning and reliability are addressed with the structure of multiple groups. This requires a governing framework including control and motion planning. This can utilize the UAVs to play the role of gateway to connect the groups to the base station (BS) and communicate further. This framework presents improved performance as compared to purely centralized base framework. However, certain data transfer route through ground BS still exists which can cause network partition due to failure of BS. This failure can isolate a group of UAVs from the rest of the network. Popescu et al. [19] present the use of UAV as relay to support wireless sensor network and guaranteed the delivery of data generated by wireless nodes on the ground. As a feature of mobility, the significance of possible isolated drone is not studied in most research works. There is a need of intra-network connectivity for transmitting information with recently employed drone.

Many problems in networking can take inspiration from the biological world for its solution. Biological world demonstrates the algorithms which propose different models of networking behavior for optimal solutions. Unlike conventional networks, the study of swarm organizing helps to develop the idea from the natural world in the research field. There are several swarming techniques studied in which the researchers tried to figure out the principles of interaction between the individuals. The study that mimics the behavior of individuals and yields to social intelligence is called swarm intelligence (SI) [20]. It deals with the artificial implementation or simulation because there is no centralized unit to control and guide the individuals. The basic principles between some of them can easily simulate the social behavior of the entire population.

Ant colony optimization (ACO) is the first SI technique which simulates the social intelligence of ants [21]. Based on the natural ability of pheromone, each ant in this algorithm draws its own path from nest to food with the help of pheromone. Another popular SI model is particle swarm optimization (PSO) algorithm [22], which mimics the foraging and navigation behavior of flocking birds. It is based on three rules of interaction between birds:

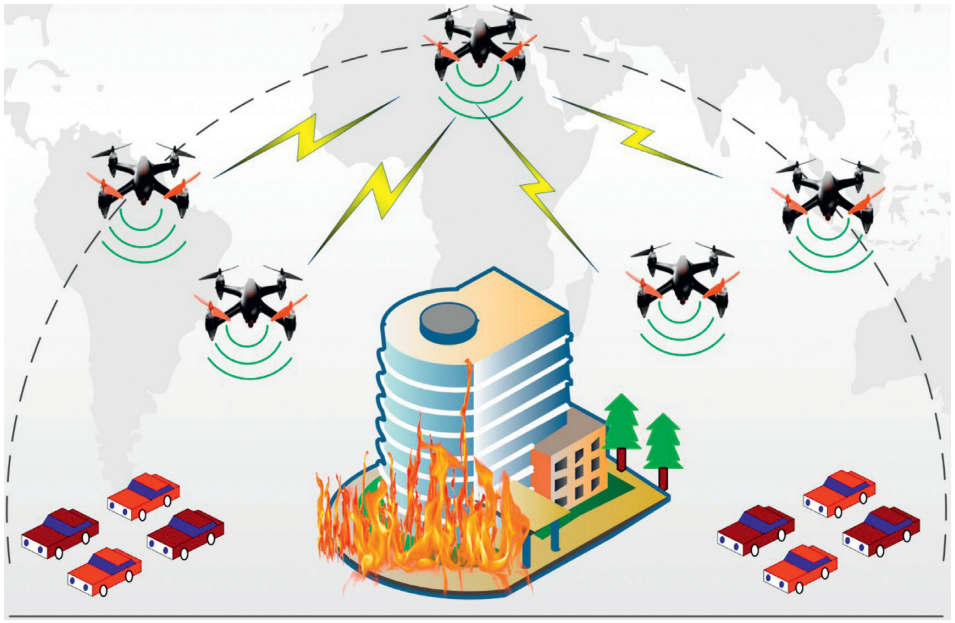

Figure 1: FANETs in calamity situation.

(i) Fly and maintain their direction towards current direction

(ii) Best food location obtained so far

(iii) Best food swam found so far

These rules help each individual towards the optimal solution and swarm simultaneously. Artificial bee colony (ABC) is another recent and well-regarded SI-based algorithm [23], mimicking the social behavior of honey bees when foraging nectar. In this algorithm, bees are categorized in three different ways:

(i) The employed bee

(ii) Onlooker bee

(iii) Scout bee

Implementations of PSO [24, 25], ABC [26, 27], and ACO [28, 29] have been applied in different problems to improve the existing algorithms. However these optimization techniques do not obtain static and dynamic swarming behaviors. DA is a recent development in swarm optimization which improved the diversity of solutions and caused exploration algorithms to become effective. The exploration and exploitation of DA are mainly determined by five primitive principles and significant research applications of DA in applied sciences have been conducted. For example, image processing [30–32], machine learning [33–35], wireless and network [36, 37], cooperative diversity [38, 39], etc. However, no study is discussed in literature for connectivity in ad hoc networks to simulate the individual and apply social intelligence of dragonfly swarming.

Social behaviours of animals derived in Boids of Reynolds swarm intelligence introduced three primitive principles of separation, alignment, and cohesion [40]. Dragonfly algorithm [41] is an extension of Boids with the novel objectives of static and dynamic swarming behavior of dragonflies. Therefore, no scientific procedures were made use of the objective that maintaining high-performance connectivity in FANETs. However, insufficient work cited to provide and maintain network connectivity. Moreover, literature has numerous SI algorithms for applied sciences; however, there is no study found to analyze the DA for FANETs. We summarize our contribution for this research and describe as follows:

(i) Biological species are innately intelligent, and they have strong learning ability. Instead of searching for food as in biological species, the proposed learning-based approach supports the isolated drones to search for a neighbor to ensure connectivity.

(ii) To construct a valid solution, our proposed work follows the nature-inspired flying principles of DA through machine learning.

(iii) When a drone is isolated, it flies in a random flight termed as levy flight. This situation opts an important feature in learning contribution.

(iv) Only isolated drone should go for levy flight to search for possible neighbor while learning helps them to become early finding of neighbors. The rest of the drones retain the mobility as per DA rules.

(v) Learning supports the isolated drone to move to the direction experienced in its last isolation.

(vi) Connectivity is a key challenge in dynamic topology network. However, when a drone is isolated during flight mission, it strives to become a part of the network.

(vii) Maximum numbers of drones stay connected using DA to ensue connectivity in minimum number of iterations.

2.1. Machine Learning. Machine learning (ML) offers computer systems to learn with minimal human intervention and teach a machine how to learn and find better solution from practice. Basically, ML is an application of artificial intelligence (AI) and comprises on data analytics technique. This technique not only educates computer systems to do what comes naturally to human individuals but also biological species. This strategy permits computers to learn autonomously or assistance and adjust actions accordingly. Algorithms based on ML employing computational techniques to "learn" information directly without depending on a defined equation as a model. The learning process commence with different observations such as paradigm, direct behavior, experience, or command. Such actions have been learnt from regular practice. The iterative feature of ML is significant; however, as models are discovered to fresh data, they are intelligent to autonomously adjust. They learn from computations that have been done earlier and able to generate efficient and frequent judgments to improve accuracy.

3. The Proposed Dragonfly Algorithm (DA) Using Machine Learning

Dragonfly algorithm is an emerging SI algorithm which mimics the behavior of dragonflies. Logically, DA divides the search process into two phases, namely exploration phase and exploitation phase. Dragonflies get into small groups in exploitation phase which enable them to forage over different areas to find their food repeatedly, whereas they form a group of large number in exploration phase when migrating to a certain direction to one destination. The pentagon representation of the basic concept of DA consists of five primitive principles as shown in Figure 2. These are vital in finding the weights solution with the following classifications:

(i) Separation
(ii) Alignment
(iii) Cohesion
(iv) Attraction to food
(v) Distraction from enemy

Due to natural leaning and intelligent decisions capability, our work assumes that the dragonflies in a swarm are similar to drone in a FANET. The search range of the dragonfly defines the communication range of drone with potential to allow accurate area marking and unambiguous identification of drones. Based on learning, the search agent feature of the dragonfly assists in identification of neighbors within the predefined range of each dragonfly. The quick deployment of drones inspired from DA and establishing small groups in static swarming may assist in situations to fly over disaster areas. Furthermore, subswarm or interaction of few drones within a network marks the presence of another subgroup in the existing network which aims the property of static swarming. Flying drones need to remain separated from each other in a defined range to avoid collision. Similarly, alignment in FANETs can control the flying speed and direction which ensures data transfer reliably. Finally, cohesion brings each drone to try to move to the center of swarm for the best position to achieve better connectivity. Hence, DA is the only algorithm that fulfils the requirements to establish FANETs through ML and simultaneously search for neighbors to ensure connectivity.

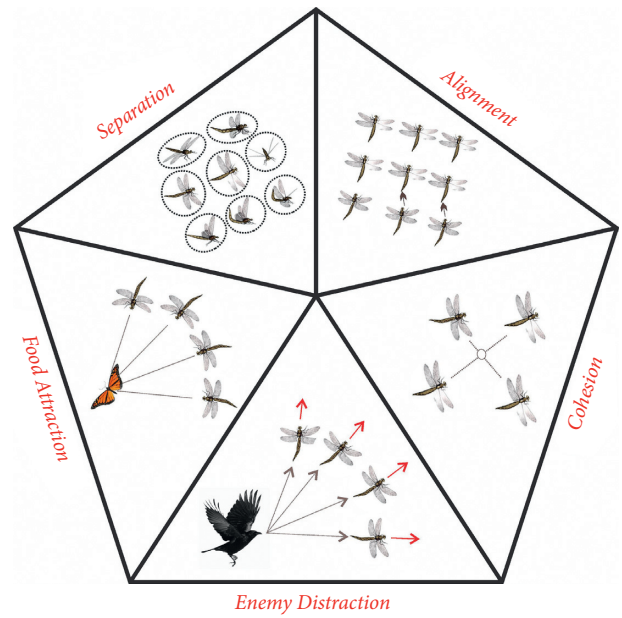

Figure 2: Primitive principles of DA.

3.1. System Model. Our system model details the features of dragonfly through ML in FANETs. This aims to provide efficient neighboring search solution and connectivity. Assuming similar mobility behavior of drones (i.e., speed and range), proper neighbor selection ensures the connectivity in a network. The drones are deployed randomly and connected within a fixed communication range "R" at the distance "d," whereas each drone is equipped with ad hoc communication capability. Each drone tries to sustain connectivity within the vicinity; however, due to scarcity of network, some drones are isolated and listed outside the communication range of other drones as shown in Figure 3.

The maximum step size ($\text{Delta}_{\text{max}}$) is defined for all the drones, and it is based on network dimension. This step size determines the mobility of the drone towards the partial network for joining or rejoining during flight operations. On the contrary, isolated drones are those drones that have no neighbors within their communication range. These drones need to survive and randomly search for possible neighbors by adopting levy flight. To become a part of a connected network, this can force the isolated drone to search for neighbors. Thus to recognize drone as isolated, ML supports the drone to opt efficient decision based on previous experience and obtain neighboring solution. Only those drones opt for random flights which have no neighbor. The rest of the drones retain the mobility as per DA rules.

Stability and control are much more complex for flying drones, which can move freely in three-dimensional space as compared to static or vehicular networks. At present, there is an increased need to establish a

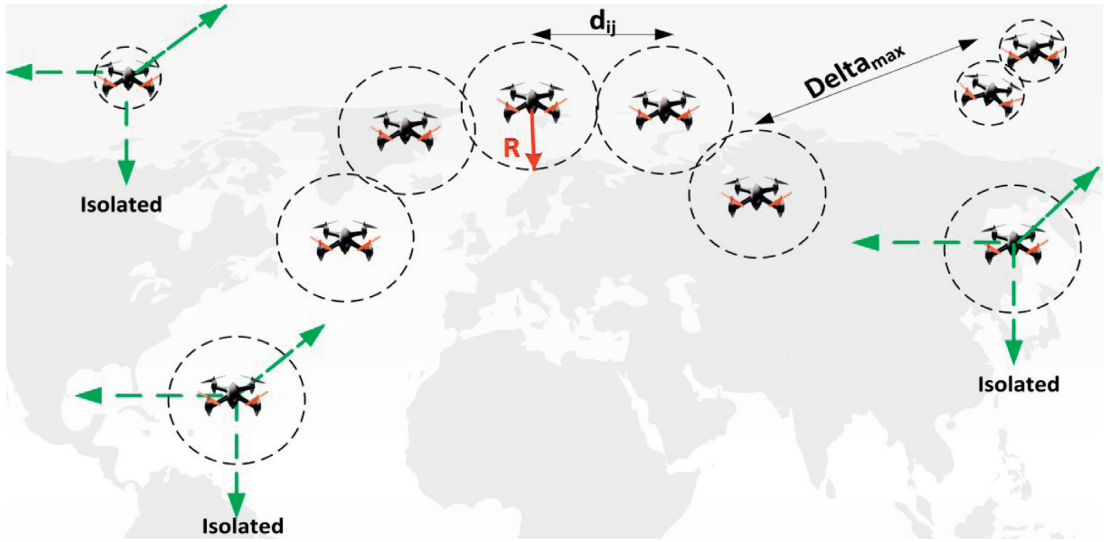

Figure 3: Schematic diagram of the system model.

mechanism which could define the collaborative steps among the uncertain movement of drones for its applicability in the FANETs.

3.2. Mathematical Model. This section details the mathematical modeling of proposed scheme. In this scheme, every drone can sense its communication range to determine any possible neighbor drones. The separation rule ensures to maintain a minimum distance between drones when they are closer to each other or to move towards a drone when located far away. The key separation among flying drones helps in avoiding collision by maintaining a minimum distance between the drones. Mathematically separation can be expressed as

$$S^i = -\sum_{j=1}^{k} p^i - p^j, \tag{1}$$

where S^i is the gap between the drones defined for ith drone, p^i is the current position of drone, and p^j is the position for jth point in the neighbor. The variable k is defined as the number of neighbors situated within the communication range of ith drone.

The ith drone moves with an average velocity which depends on the speed of other drones whether it is in searching mode or connecting mode. The flying movement of drones is matched in velocity to other nearby drones. This average velocity refers to the particles not exceeding in speed from other neighbors in a unit space. The tendency of an individual to match its velocity with neighboring drones can be mathematically calculated as

$$v^i = \frac{1}{k}\sum_{j=1}^{k} v^j, \tag{2}$$

where v^j is the velocity of jth neighbor for ith drone.

Every drone in FANETs obtaining the proposed architecture tends to move to the center of radius for the best position to achieve better results. In other words, the cohesion step refers to the drone towards the center point of space that contains other drones close to its position. The tendency of an individual to move toward the center of mass of neighboring drones can be mathematically calculated as

$$C^i = \frac{1}{k}\sum_{j=1}^{k}\left(p^j - kp^i\right), \tag{3}$$

where p^i is the position of ith drone, k is the number of neighbourhood, and p^j shows the position of jth neighboring individual. Whenever a drone is isolated, it strives to move to find neighboring drone within the communication range to ensure connectivity. Let $d_{ij}(t)$ be the Euclidean distance at time t between position p^i and position p^j and is given as

$$d_{ij}(t) = \sqrt{\left(x^j - x^i\right)^2 + \left(y^j - y^i\right)^2}. \tag{4}$$

In view of the aforementioned mathematical model, the disciplinary instructions are assumed for drone operation in the flying zone. Thus, a newly linkedup drone in a swarm learns to follow these primitive rules to maintain the network connectivity and conserve its resources. As long as the drone is connected, cooperation among the drones would be sustainable which prolongs the network life.

The drone attaining at least one neighboring solution learns to update its positions by a couple of defined vectors, that is, velocity step vector (ΔQ^i) and position vector (Q^i) according to the following mathematical expressions:

$$\Delta Q^i(t+1) = sS^i + \hat{v}v^i + cC^i + fF^i + eE^i + w\Delta Q^i(t), \tag{5}$$

where $\Delta Q^i(t+1)$ is a step vector which is a movement of drone at the next time step $t+1$. The product sS^i shows separation weight and separation of ith individual respectively. Similarly, $\hat{v}$ is velocity weight, v^i is the velocity of ith individual, c is cohesion weight, C^i is the cohesion of ith individual, f is food factor, F^i is the food source of ith individual, e is the attacker factor, E^i is the location of enemy of ith individual, w denotes the weight of inertia, and t is the

iteration number. The point of vector position is computed afterward by the step vector:

$$Q^i(t+1) = Q^i(t) + \Delta Q^i(t+1), \tag{6}$$

where $Q^i(t+1)$ is a position vector at next time $t+1$. The different explanative and exploratory natures can be obtained during flight such as separation, velocity, cohesion, food, and enemy attacker factors $s, \widehat{v}, c, f,$ and e. Finally, the position of a drone having no neighboring solution updates its position using the following mathematical function:

$$Q^i(t+1) = Q^i(t) + \zeta Q^i(t), \tag{7}$$

where ζ is the levy flight and is calculated as follows [42]:

$$\zeta = 0.01 * \frac{r_1}{|r_2|^{(1/\beta)}} * \sigma, \tag{8}$$

where r_1 and r_2 denote the two random numbers in [0, 1], β is assumed constant, and σ is computed as follows:

$$\sigma = \left(\frac{\Gamma(1+\beta)sin(\pi\beta/2)}{\Gamma(1+\beta/2)2^{(\beta-1/2)}\beta}\right)^{(1/\beta)}, \tag{9}$$

where $\Gamma(x) = (x-1)!$. Solo flight reduces the lifetime of a drone and disrupts connectivity. This mathematical expression assists in learning the nearest neighbor when there is no neighbor and drone is isolated.

In order to ensure connectivity in a large area, every drone in FANET acts as relay for transfer of information to the other drones and/or base station. A link is established between nodes i and j such that $j \in k | d_{ij} < R$. As soon as these individuals are the members of a group, they maintain minimal separation and contribute to the connectivity of the entire network. If a drone is isolated, the connectivity is compromised for that particular region. Moreover, along with task-oriented sensors, drones are also equipped with GPS, radar mechanism, and height sensors. Frequent topology changes with drones leaving or joining the network is often another complex challenge in FANETs. This situation benefits from machine learning to accomplish communication in a highly dynamic topology network. In order to achieve maximum connected drones in entire flying network, we present a solution for connectivity problem. After performing primitive principles of natural species such as separation, alignment, and cohesion, it is now possible to achieve better communication path by maintaining link between drones so they can share data easily. Mathematical expression for improved path stability is given as follows:

$$\mu = \max(k_n), \tag{10}$$

where greater μ presents better connection opportunity. In the above discussion, it is established that drones do not remain isolated when following the devised strategy. Iteratively, isolated drones become a part of the swarm by using levy flight and cover larger area with maximum connectivity and minimize the isolated drones accordingly. In this learning scheme, the maximum number of flying drones stay connected in the network in minimum iteration and reduces the isolated drones during flight. Hence, neighboring solution minimizes the isolated drones adaptively, which are preserved till the period of network communication.

The factor range index is taken into account when measuring the connectivity between drones. The connectivity decreases with increase in the distance and subsequently drone is not able to communicate with any of the other drones. Range index allows selection of appropriate drone for communication path stability. This can be modeled as follows:

$$\eta^i = \frac{\propto^i}{\max_{\forall j}\left(d_{ij}(t)\right)}, \tag{11}$$

where η^i is the range index of ith individual that decreases with an increase in distance and α is a constant $0 < \propto^i \leq 1$.

In order to determine the suitability of a drone for relaying as part of the swarm, a fitness function is considered which summarizes a single figure of merit. It shows a given design solution to achieve connectivity. The fitness is devised so that the number of isolated drones in the network is reduced and can be calculated as follows:

$$\lambda^i(t) = k^i(t) + \frac{\gamma^i(t)}{d_{iB}(t)}, \tag{12}$$

where λ^i is the fitness value of ith drone, k^i is the number of neighbors of ith drone at any given time t, γ^i is the remaining energy of ith flying drone, and $d_{iB}(t)$ is the distance of the ith drone from the BS at time t. The distance from BS is incorporated to accommodate the drones which may not have a neighbor but are within transmission range of BS. These drones are not isolated drones, rather these drones are a great option for relaying data of other flying drones to the BS.

The pseudo code for the proposed solution is given in Algorithm 1. Considerable stages for the proposed scheme are detailed as follows: Lines 1 to 4 show the basic network initialization. Here, the number of drones is initialized with random deployment. Solution set for the drones is initialized in certain restricted boundaries. Furthermore, communication range for each drone remains the same, and step vector is initialized for necessary flight operation. Lines 5 to 12 show the computation and update stage. On the basis of initial deployment, each drone computes the position values and available neighboring solutions within an assigned communication range. Different weights such as $s, \widehat{v}, c, f, e,$ and w are updated in this stage. Distances are calculated between the drones and BS. $S, v, C, F,$ and E are also computed in this stage. Thus drone should update the position values and neighbouring solution using first three primitive flight rules. In this course of action, each isolated drone learns to locate neighbors and update action of practice accordingly. Lines 13 to 22 show the proposed neighboring solution for isolated drones. If at least one neighbor is available within the drone vicinity, it should retain the flight as per DA principle. However, if there is no neighbor, it should go to opt learning and update their position using levy flight to search for possible neighbor. ML supports the isolated drone to move to the direction experienced in its last isolation. Hence, isolated drone count is reduced adaptively.

Proposed DA algorithm using machine learning
(1) Initialize the random position of drones (flying nodes)
(2) Initialize the communication range and step size for all drone
(3) **for** iteration 1 to max
(4) Compute the position values of all the drones based on mobility
(5) Determine the nodes in the communication range of each nodes
(6) Determine learning stack to the isolated nodes
(7) Compute the neighboring solution
(8) Compute the network parameters by Equations (1) to Equation (4)
(9) Update the position values
(10) Update the neighboring solution
(11) Update learning solution
(12) **if** (a drone has at least one neighboring drone)
(13) Learn velocity vector by Equation (5)
(14) Learn position vector by Equation (6)
(15) **else**
(16) Declare the node as isolated
(17) Calculate the isolated drones
(18) Update position of isolated drone by flying randomly by Equation (7)
(19) Update the neighboring connectivity by Equation (8) to Equation (10)
(20) **end if**
(21) Check and correct the new positions by Equation (12)
(22) **end for**
(23) Determine average network connectivity based on the isolated node count

Algorithm 1: Pseudo code for the proposed solution.

4. Simulation and Results

Simulations are conducted to evaluate the performance of the proposed scheme. In this section, the performance of the proposed scheme is tested using MATLAB simulator. This evaluation observes the effects of flight of drones, its connectivity and reduction of isolated drones using DA technique for machine learning. Basic set of parameters used for simulations are presented in Table 1.

Initial network deployment of nodes is shown in Figure 4. In this model, DA technique is implemented for learning in the proposed scheme. Network is initialized using DA principles such as random deployment of nodes, set the define parameters to maintain separation, velocity, and cohesion. Flight of the nodes experiences the course of actions during iterations, and they are based on learning. However, the wireless communication range for a node in a grid of 100 m^3 is set to 20 m for 10 homogeneous nodes. During flight, the network nodes detect their neighbors within 20 m communication range. There are six nodes shown isolated in an initial deployment of network, that is, 4, 5, 6, 7, 8, and 9. It can be seen that there is no neighbor within 20 m communication range for these nodes while rest of the nodes having at least one neighbor within their vicinity. If neighbor is found by a node, it will retain the mobility under DA principle; however, if there is no neighbor in the node vicinity, it will consider isolated and opt ML to flies in a levy flight. This can help the node to search for prospective neighbors. This search is repeated iteratively till a neighboring solution is found. If there is at least one neighboring solution for an isolated node, it will update its defined vectors of velocity step vector and position

Table 1: Simulation parameters.

Parameters	Values
Number of nodes	10
Network area	10 m^3
Node flight	Random
Channel type	Wireless channel
Communication range	20 m
Maximum iteration	25
Antenna model	Omni antenna
Upper bound	100
Lower bound	0

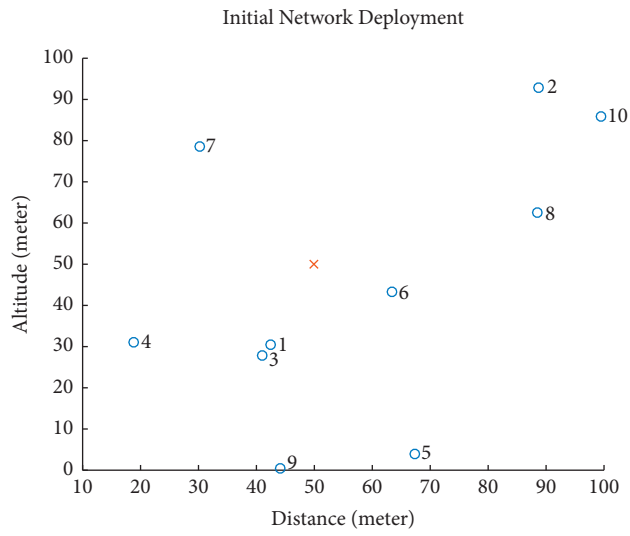

Figure 4: Initial network deployment.

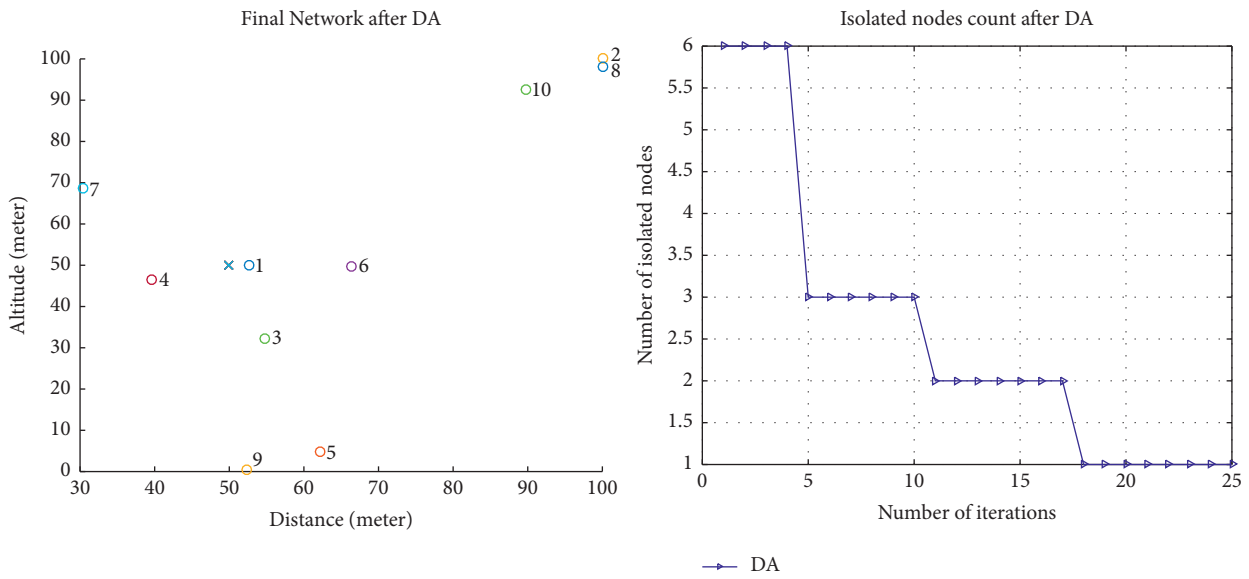

Figure 5: Final network after DA.

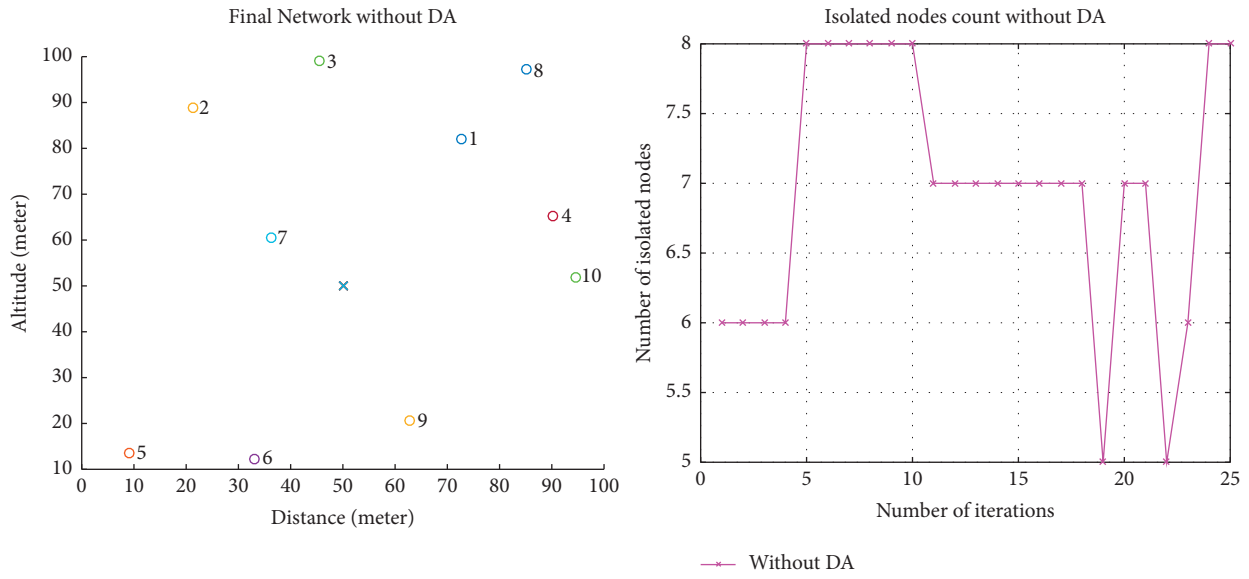

Figure 6: Final network without DA.

step vector according to Equations (5) and (6), respectively. Since the nodes are dynamic and gain experience due to repeatedly finding neighboring solutions. Such type of action helps the existing isolated node to learn for next term of isolation. This aims to update the node position efficiently in future course of actions. Those drones having no neighbor will have to update its position according to Equation (7).

When the simulation begins, three important flight factors of separation, velocity, and cohesion are performed for sustainable network operation. To avoid collision, the distance between the nodes is maintained. They shall also match the velocity to its neighboring nodes and maintain cohesion among these nodes. All nodes which become a part of this disciplinary behavior create a group for future cooperation. It is important that members of the group must be in the neighboring communication range. DA aims the group of nodes plays to a key role in selecting a networking architecture for effective performance. As soon as a neighboring solution exists for a node, the network becomes connected. Furthermore, as explained, there are two important vectors of DA such as velocity step vector and position vector are incorporated to store and update position of those nodes having at least one neighboring node. They are now able to update their positions by adding the step vectors to the position vectors as given in Equation (6). Keep knowing the updated vectors of all nodes; this work enables us to simulate the next iteration based on the existing node position as well as the learning performs levy

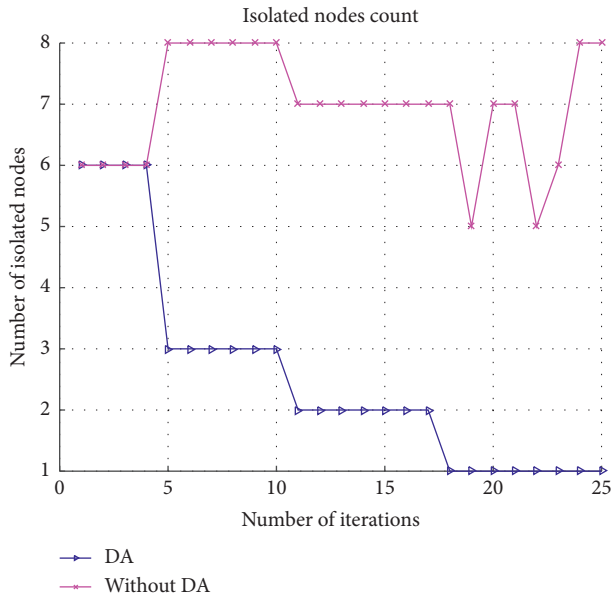

Figure 7: Comparison result with and without DA.

flight of nodes who is finding the solo flying in an entire network. Thus, a node in a dynamic topology network may be isolated and reduce network efficiency especially in high mobility FANETs.

Graphical representation of isolated nodes count after DA results the significance of DA through ML. The result of the final network after DA is shown in Figure 5. Although there are six nodes isolated in initial deployment, they become a part of cooperative nodes. This reduces the isolated node count significantly. It can be seen that after the completion of course of iterations, only one node is isolated, that is, Node 7. This improvement is achieved due to DA technique as well as previous experiences of isolated nodes during action of isolation using ML. Moreover, all the other nodes have one or more than one neighbors and consider connected to each other and/or BS. Hence maximum number of nodes stay connected using DA to ensue connectivity in minimum number of iterations. Based on learning-based finding neighbors, this scheme works to reduce the time, provides the best finding neighboring solution, maintains node's connectivity, and updates the flying positing of the drone. This scheme reduces the spatial complexities of possible isolated drones.

Significance of DA algorithm for proposed scheme is compared without DA algorithm. The result of isolated count without DA is shown in Figure 6. This view results the importance of DA algorithm for dynamic network. As mentioned earlier that there are six nodes isolated at the start of network deployment. The plot of isolated node count without DA shows that isolated node counts are not sufficiently reduced as compared to DA. Higher number of node isolated during course of iterations and found no learning and discipline to force an isolated node to become a part of cooperative nodes. Consequently, only Node 4 and Node 10, which is lying exist within the vicinity of each other, while the rest of the nodes are isolated. The significance of DA can be gauged from its implementation and comparison. This challenging problem of FANET is overcome by inspiring the biological nature of DA and especially the learning-based levy flight.

Significance of DA for ML is clearly viewed in the comparison result of isolated node count with and without DA which is shown in Figure 7. Simulations are performed iteratively and results are obtained for isolated node count. Now it can be clearly seen that isolated nodes count started with six isolated nodes for both the schemes. However, after course of iterations, DA reduced the isolated nodes in best way due to learning. Consequently, it overcomes the connectivity problem of FANETs by reducing the isolated nodes which improves the communication area. On the contrary, without DA scheme where there is no learning exists, maximum nodes stay isolated which reduces the network performance. Hence, neighboring solution minimizes the isolated nodes adaptively, which are preserved till the period of network communication.

5. Conclusion

In this paper, we have attempted to design a well-connected FANET via biological inspired learning. The rapid mobility of drones leads to drone isolation in FANETs which is a main challenge for FANETs. We present a scheme to minimize the number of isolated drones. This scheme is based on biologically inspired technique of DA using the depth of machine learning. Thus, connectivity is achieved by choosing the primitive principles of DA and ML. The preference to DA especially for FANETs is due to the novel SI behavior of dragonflies namely static swarming and dynamic swarming. Social behavior of DA is investigated in this paper, and an ML-based solution is proposed to find the efficient neighboring solution of the drones isolated during the flight mission. In this scheme, maximum number of flying drones stay connected in the network by effective learning in minimum iterations and reduces the isolated drones during flight. Hence, neighboring solution minimizes the isolated drones adaptively, which are preserved till the period of network communication. Furthermore, adopting the concept of biological step walk for neighbor searching overcomes the energy issue in the FANETs. We propose a fitness function for drones situated within the communication range which assists in the proposed learning scheme. Simulation results show that our proposed fitness function maximizes the network stability period, improves connectivity for routing, and updates the flying positioning of drones. Thus the proposed scheme benefits from the intelligence of machine learning and strategic learning of dragonfly to reduce energy consumption and ensure network connectivity.

Data Availability

Data of simulation code are available and provided in the supplementary materials in attachment separately.

Conflicts of Interest

The authors declare that there are no conflicts of interest regarding the publication of this paper.

Acknowledgments

This work was supported by the Hubei Natural Science Foundation under grant 2021CFB156.

Supplementary Materials

The supplementary material contains only simulation code of the proposed methodology assisted to generate results as mentioned in this paper. . (*Supplementary Materials*)

References

[1] A. Bujari, C. E. Palazzi, and D. Ronzani, "FANET application scenarios and mobility models," in *Proceedings of the 3rd Workshop on Micro Aerial Vehicle Networks, Systems, and Applications*, pp. 43–46, Niagara Falls, NY, USA, June 2017.

[2] A. Srivastava and J. Prakash, "Future FANET with application and enabling techniques: anatomization and sustainability issues," *Computer Science Review*, vol. 39, Article ID 100359, 2021.

[3] L. Tan, K. Yu, N. Shi, C. Yang, W. Wei, and H. Lu, "Towards secure and privacy-preserving data sharing for Covid-19 medical records: a blockchain-empowered approach," *IEEE Transactions on Network Science and Engineering*, vol. 9, 2021.

[4] C. Wu, Z. Liu, D. Zhang, T. Yoshinaga, and Y. Ji, "Spatial intelligence toward trustworthy vehicular IoT," *IEEE Communications Magazine*, vol. 56, no. 10, pp. 22–27, 2018.

[5] D. Liu, Y. Xu, J. Wang et al., "Self-organizing relay selection in UAV communication networks: a matching game perspective," *IEEE Wireless Communications*, vol. 26, no. 6, pp. 102–110, 2019.

[6] X. Chen, C. Wu, T. Chen et al., "Age of information aware radio resource management in vehicular networks: a proactive deep reinforcement learning perspective," *IEEE Transactions on Wireless Communications*, vol. 19, no. 4, pp. 2268–2281, 2020.

[7] T. Guo, K. Yu, M. Aloqaily, and S. Wan, "Constructing a prior-dependent graph for data clustering and dimension reduction in the edge of AIoT," *Future Generation Computer Systems*, vol. 128, pp. 381–394, 2022.

[8] C. Feng, K. Yu, A. Bashir et al., "Efficient and secure data sharing for 5G flying drones: a blockchain-enabled approach," *IEEE Network*, vol. 35, no. 1, pp. 130–137, 2021.

[9] D. Wang, Y. He, K. Yu, G. Srivastava, L. Nie, and R. Zhang, "Delay sensitive secure NOMA transmission for hierarchical HAP-LAP medical-care IoT networks," *IEEE Transactions on Industrial Informatics*, 2021.

[10] K.-W. Chiang, G.-J. Tsai, Y.-H. Li, and N. El-Sheimy, "Development of LiDAR-based UAV system for environment reconstruction," *IEEE Geoscience and Remote Sensing Letters*, vol. 14, no. 10, pp. 1790–1794, 2017.

[11] L. Yang, K. Yu, X. Simon, C. Chakraborty, Y. Lu, and T. Guo, "An intelligent trust cloud management method for secure clustering in 5G enabled internet of medical things," *IEEE Transactions on Industrial Informatics*, vol. 1, 2021.

[12] Z. Guo, K. Yu, A. Jolfaei, F. Ding, and N. Zhang, "Fuz-spam: label smoothing-based fuzzy detection of spammers in internet of things," *IEEE Transactions on Fuzzy Systems*, 2021.

[13] X. He, W. Yu, H. Xu et al., "Towards 3D deployment of UAV base stations in uneven terrain," in *Proceedings of the 2018 27th International Conference on Computer Communication and Networks (ICCCN)*, pp. 1–9, IEEE, Hangzhou, China, August 2018.

[14] D. Rautu, R. Dhaou, and E. Chaput, "Maintaining a permanent connectivity between nodes of an air-to-ground communication network," in *Proceedings of the 2017 13th International Wireless Communications and Mobile Computing Conference (IWCMC)*, pp. 681–686, IEEE, Valencia, Spain, June 2017.

[15] N. Zhao, W. Lu, M. Sheng et al., "UAV-assisted emergency networks in disasters," *IEEE Wireless Communications*, vol. 26, no. 1, pp. 45–51, 2019.

[16] K. Yu, L. Tan, C. Yang, J. J. P. C. Rodrigues, and T. Sato, "A blockchain-based shamir's threshold cryptography scheme for data protection in industrial internet of things settings," *IEEE Internet of Things Journal*, 2021.

[17] O. S. Oubbati, N. Chaib, A. Lakas, P. Lorenz, and A. Rachedi, "UAV-assisted supporting services connectivity in urban VANETs," *IEEE Transactions on Vehicular Technology*, vol. 68, no. 4, pp. 3944–3951, 2019.

[18] Cicek, C. Tugrul, H. Gultekin, B. Tavli, and H. Yanikomeroglu, "UAV base station location optimization for next generation wireless networks: overview and future research directions," in *Proceedings of the 2019 1st International Conference on Unmanned Vehicle Systems-Oman (UVS)*, pp. 1–6, IEEE, Muscat, Oman, February 2019.

[19] D. Popescu, F. Stoican, Stamatescu, O. Chenaru, and L. Ichim, "A survey of collaborative UAV-WSN systems for efficient monitoring," *Sensors*, vol. 19, no. 21, Article ID 4690, 2019.

[20] A. Chakraborty and A. K. Kar, "Swarm intelligence: a review of algorithms," *Nature-Inspired Computing and Optimization*, vol. 10, pp. 475–494, 2017.

[21] S.. Ahmed, "Nature inspired optimization techniques, A review for FANETs," *Sukkur IBA Journal of Emerging Technologies*, vol. 3, no. 2, pp. 40–58, 2020.

[22] S. Sengupta, S. Basak, and R. A. Peters, "Particle Swarm Optimization: a survey of historical and recent developments with hybridization perspectives," *Machine Learning and Knowledge Extraction*, vol. 1, no. 1, pp. 157–191, 2019.

[23] S. Aslan, "A comparative study between artificial bee colony (ABC) algorithm and its variants on big data optimization," *Memetic Computing*, vol. 12, no. 2, pp. 129–150, 2020.

[24] D. Wang, D. Tan, and L. Liu, "Particle swarm optimization algorithm: an overview," *Soft Computing*, vol. 22, no. 2, pp. 387–408, 2018.

[25] M. S. Kiran, "Particle swarm optimization with a new update mechanism," *Applied Soft Computing*, vol. 60, pp. 670–678, 2017.

[26] J. C. Bansal, A. Gopal, and A. K. Nagar, "Stability analysis of artificial bee colony optimization algorithm," *Swarm and evolutionary computation*, vol. 41, pp. 9–19, 2018.

[27] J. Li, D. Lu, G. Zhang, J. Tian, and Y. Pang, "Post-disaster unmanned aerial Vehicle base station deployment method based on artificial bee colony algorithm," *IEEE Access*, vol. 7, pp. 168327–168336, 2019.

[28] D. Karaboga, B. Gorkemli, C. Ozturk, and N. Karaboga, "A comprehensive survey: artificial bee colony (ABC) algorithm and applications," *Artificial Intelligence Review*, vol. 42, no. 1, pp. 21–57, 2014.

[29] M. Dorigo and T. Stützle, "Ant colony optimization: overview and recent advances," *Handbook of Metaheuristics*, vol. 146, pp. 311–351, 2019.

[30] F. Ding, G. Zhu, Y. Li, X. Zhang, P. K. Atrey, and S. Lyu, "Anti-forensics for face swapping videos via adversarial training," *IEEE Transactions on Multimedia*, 2021.

[31] F. Ding, K. Yu, Z. Gu, X. Li, and Y. Shi, "Anti-forensics for face swapping videos via adversarial training," *IEEE Transactions on Intelligent Transportation Systems*, 2021.

[32] B. Hemamalini and V. Nagarajan, "Wavelet transform and pixel strength-based robust watermarking using dragonflyoptimization," *Multimedia Tools and Applications*, vol. 79, no. 13-14, pp. 8727–8746, 2020.

[33] A. Tharwat, T. Gabel, and A. E. Hassanien, "Parameter optimization of support vector machine using dragonfly algorithm," in *Proceedings of the International Conference on Advanced Intelligent Systems and Informatics 2017*, pp. 309–319, Springer, Cham, Switzerland, August 2017.

[34] K. Yu, L. Tan, S. Mumtaz et al., "Securing critical infrastructures: deep-learning-based threat detection in IIoT," *IEEE Communications Magazine*, vol. 59, no. 10, pp. 76–82, 2021.

[35] C. Feng, B. Liu, K. Yu, S. K. Goudos, and S. Wan, "Blockchain-empowered decentralized horizontal federated learning for 5G-enabled UAVs," *IEEE Transactions on Industrial Informatics*, 2021.

[36] L. Tan, K. Yu, L. Lin et al., "Speech emotion recognition enhanced traffic efficiency solution for autonomous vehicles in a 5G-enabled space-air-ground integrated intelligent transportation system," *IEEE Transactions on Intelligent Transportation Systems*, vol. 99, 2021.

[37] C. Feng, B. Liu, Z. Guo, K. Yu, and Z. Qin, "Blockchain-based cross-domain authentication for intelligent 5 g-enabled internet of drones," *IEEE Internet of Things Journal*, 2021.

[38] S. Hameed, S. Alyahya, Q.-A. Minhas et al., "Link and loss aware GW-COOP routing protocol for FANETs," *IEEE Access*, vol. 9, pp. 110544–110557, 2021.

[39] S. Hameed, Q.-A. Minhas, S. Ahmed et al., "An improved iBAT-COOP protocol for cooperative diversity in FANETs," *Computers, Materials & Continua*, vol. 67, no. 2, pp. 2527–2546, 2021.

[40] C. W. Reynolds, "Flocks, herds and schools: a distributed behavioral model," *ACM SIGGRAPH Computer Graphics*, vol. 21, no. 4, pp. 25–34, 1987.

[41] S. Mirjalili, "Dragonfly algorithm: a new meta-heuristic optimization technique for solving single-objective, discrete, and multi-objective problems," *Neural Computing & Applications*, vol. 27, no. 4, pp. 1053–1073, 2016.

[42] X.-S. Yang, *Nature-inspired Metaheuristic Algorithms*, Luniver press, London, UK, 2010.